CANADIAN THESES ON MICROFICHE

THÈSES CANADIENNES SUR MICROFICHE

National Library of Canada
Collections Development Branch

Canadian Theses on
Microfiche Service

Ottawa, Canada
K1A 0N4

Bibliothèque nationale du Canada
Direction du développement des collections

Service des thèses canadiennes
sur microfiche

NOTICE

The quality of this microfiche is heavily dependent upon the quality of the original thesis submitted for microfilming. Every effort has been made to ensure the highest quality of reproduction possible.

If pages are missing, contact the university which granted the degree.

Some pages may have indistinct print especially if the original pages were typed with a poor typewriter ribbon or if the university sent us an inferior photocopy.

Previously copyrighted materials (journal articles, published tests, etc.) are not filmed.

Reproduction in full or in part of this film is governed by the Canadian Copyright Act, R.S.C. 1970, c. C-30. Please read the authorization forms which accompany this thesis.

AVIS

La qualité de cette microfiche dépend grandement de la qualité de la thèse soumise au microfilmage. Nous avons tout fait pour assurer une qualité supérieure de reproduction.

S'il manque des pages, veuillez communiquer avec l'université qui a conféré le grade.

La qualité d'impression de certaines pages peut laisser à désirer, surtout si les pages originales ont été dactylographiées à l'aide d'un ruban usé ou si l'université nous a fait parvenir une photocopie de qualité inférieure.

Les documents qui font déjà l'objet d'un droit d'auteur (articles de revue, examens publiés, etc.) ne sont pas microfilmés.

La reproduction, même partielle, de ce microfilm est soumise à la Loi canadienne sur le droit d'auteur, SRC 1970, c. C-30. Veuillez prendre connaissance des formules d'autorisation qui accompagnent cette thèse.

THIS DISSERTATION
HAS BEEN MICROFILMED
EXACTLY AS RECEIVED

LA THÈSE A ÉTÉ
MICROFILMÉE TELLE QUE
NOUS L'AVONS REÇUE

Canada

NL 339 (r. 85/09)

0-315-19458-8

National Library of Canada
Canadian Theses Division
Ottawa, Canada
K1A 0N4

Bibliothèque nationale du Canada
Division des thèses canadiennes

67366

PERMISSION TO MICROFILM — AUTORISATION DE MICROFILMER

• Please print or type — Écrire en lettres moulées ou dactylographier

Full Name of Author — Nom complet de l'auteur

MUHAMMAD ABDUL WAHAB

Date of Birth — Date de naissance	Country of Birth — Lieu de naissance
19 TH APRIL, 1952	BANGLADESH

Permanent Address — Résidence fixe

C/O. DR. MUHAMMAD A. SATTAR.
PROFESSOR, DEPT. OF CHEMISTRY
RAJSHAHI UNIVERSITY, RAJSHAHI, BANGLADESH.

Title of Thesis — Titre de la thèse

MODEL ANALYSIS OF FATIGUE LIFE ESTIMATION OF WELDED STRUCTURES.

University — Université

UNIVERSITY OF ALBERTA

Degree for which thesis was presented — Grade pour lequel cette thèse fut présentée

Ph.D.

Year this degree conferred — Année d'obtention de ce grade	Name of Supervisor — Nom du directeur de thèse
1984	DR. M.G. FAULKNER

Permission is hereby granted to the NATIONAL LIBRARY OF CANADA to microfilm this thesis and to lend or sell copies of the film.

The author reserves other publication rights, and neither the thesis nor extensive extracts from it may be printed or otherwise reproduced without the author's written permission.

L'autorisation est, par la présente, accordée à la BIBLIOTHÈQUE NATIONALE DU CANADA de microfilmer cette thèse et de prêter ou de vendre des exemplaires du film.

L'auteur se réserve les autres droits de publication; ni la thèse ni de longs extraits de celle-ci ne doivent être imprimés ou autrement reproduits sans l'autorisation écrite de l'auteur.

Date	Signature
July 19, 1984	M. A. Wahab.

THE UNIVERSITY OF ALBERTA

MODEL ANALYSIS OF FATIGUE LIFE ESTIMATION OF WELDED STRUCTURES

by

MUHAMMAD A. WAHAB

(C)

A THESIS

SUBMITTED TO THE FACULTY OF GRADUATE STUDIES AND RESEARCH

IN PARTIAL FULFILMENT OF THE REQUIREMENTS FOR THE DEGREE

OF DOCTOR OF PHILOSOPHY

DEPARTMENT OF MECHANICAL ENGINEERING

EDMONTON, ALBERTA

FALL 1984

THE UNIVERSITY OF ALBERTA

RELEASE FORM

NAME OF AUTHOR MUHAMMAD A. WAHAB

TITLE OF THESIS MODEL ANALYSIS OF FATIGUE LIFE ESTIMATION OF WELDED STRUCTURES

DEGREE FOR WHICH THESIS WAS PRESENTED DOCTOR OF PHILOSOPHY

YEAR THIS DEGREE GRANTED FALL 1984

Permission is hereby granted to THE UNIVERSITY OF ALBERTA LIBRARY to reproduce single copies of this thesis and to lend or sell such copies for private, scholarly or scientific research purposes only.

The author reserves other publication rights, and neither the thesis nor extensive extracts from it may be printed or otherwise reproduced without the author's written permission.

(SIGNED) M. A. Wahab

PERMANENT ADDRESS:

C/O: Dr. Muhammad A. Sattar
Department of Chemistry
Rajshahi Univ., Bangladesh.

DATED ....July 19th., 1984.

THE UNIVERSITY OF ALBERTA

FACULTY OF GRADUATE STUDIES AND RESEARCH

The undersigned certify that they have read, and recommend to the Faculty of Graduate Studies and Research, for acceptance, a thesis entitled MODEL ANALYSIS OF FATIGUE LIFE ESTIMATION OF WELDED STRUCTURES submitted by MUHAMMAD A. WAHAB in partial fulfilment of the requirements for the degree of DOCTOR OF PHILOSOPHY in APPLIED MECHANICS.

Gary Faulkner

Supervisor

External Examiner

Date...July 10, 1984.....

ABSTRACT

This study includes both an experimental and theoretical analysis of the effect of residual stresses on the fatigue life of butt-welded low-alloy steel structures. The purpose is to develop a more complete method to estimate the total fatigue life of a weldment.

To theoretically calculate the total fatigue life the process was considered as a combination of crack initiation and crack propagation lives. The initiation portion was based on an extension of the local-strain fatigue life initiation model to accomodate the effect of residual and mean stresses. To determine the local notch-root stress-strain condition more accurately a relationship between the fatigue notch and stress concentration factors was developed. Using elastic superposition and modifying Neuber's equation, which relates nominal stress-strain to local notch-root stress-strain residual stresses at the weld-toe were simulated. This analysis allows a more complete estimation of crack initiation life.

For the theoretical analysis of fatigue crack propagation life Forman's equation with an appropriate combination effective stress ratio, axial and bending stresses along with residual stress effects was considered. To incorporate the residual stress distribution at the weld-toe a theoretical expression which correlates closely with experimentally determined distributions was developed. Unlike previous investigations this analysis allows the

study of the combined effects of axial loading, bending stresses and residual stresses on the fatigue crack propagation life to be considered. With this theoretical model the total fatigue life can be predicted using basic material properties and the loading history including any surface treatment. To test the suitability of this analysis it was applied to welds with mechanically and thermally induced surface stresses. The residual stresses due to various treatments (annealing, tensile preloading, glass and steel shot peening, single and multiple point hammer peening and stress peening) were used to theoretically predict the total fatigue life.

The more complete theoretical analysis of the total fatigue life was compared to the experimental results for all the treated and untreated welded specimens. The results show very good agreement; the variations in applied stress for a given fatigue life were between four to 15% for all the treatments listed above.

ACKNOWLEDGEMENT

The author gratefully acknowledges the active interest, invaluable encouragement and the guidance given to him by his thesis supervisors Dr. D.G.Bellow and Dr. M.G.Faulkner, professors of Mechanical Engineering during the research and preparation of this thesis. Working with them was the most memorable experience which the author will always cherish.

A very special thanks are owed to Dr. B.M.Patchet, professor of Mineral Engineering for his valuable suggestions and encouragements and for allowing the author to use his Welding Research Laboratory facilities. The author is indebted to Dr. F.H.Vitovec, professor of Mechanical Engineering for much assistance which the author received during the research. The author also wishes to express his sincere appreciation for the enthusiastic support and suggestions of the professors of Mechanical Engineering.

Acknowledgements are also due to Mr.T.Villet, Mr.J.Foy, Mr.A.Muir, Mr.B.Ceiling, Mr.T.Nord, Mr.M.Schubert and Mr.C.Bechtel for their assistances in mechanical testing and for helping the author build the experimental setups. The author is gratefully indebted to the fellow graduate students for their valuable assistances.

The financial support of the National Research Council of Canada under the research grants NSERC A2705, NSERC A7514 and the Department of Mechanical Engineering of the University of Alberta are acknowledged with gratitude.

The author is deeply indebted to his parents for their understanding, patience and optimism.

Table of Contents

Chapter		Page
1.	INTRODUCTION AND HISTORICAL REVIEW	1
	1.1 BACKGROUND	1
	1.2 Origin And Nature Of Residual Stresses In Welded Joints	3
	1.3 Previous Investigations On The Effect Of Residual Stresses On Fatigue Behaviour Of Welded Structures	7
	1.4 Redistribution Of Residual Stresses By Mechanical And Thermal Means	12
	1.4.1 Introduction	12
	1.4.2 Shot-peening	12
	1.4.3 Stress Peening	14
	1.4.4 Tensile Preloading	15
	1.4.5 Post-Weld Thermal Treatments	16
	1.5 The Specific Problems And Objectives	18
2.	THEORETICAL ANALYSIS	20
	2.1 Theoretical Approach To Fatigue Analysis	20
	2.1.1 Theory Of Crack Initiation	21
	2.1.2 Notch Simulation And Local Plasticity	23
	2.1.3 Theoretical Stress Concentration Factor	28
	2.1.4 Fatigue Notch Factor	29
	2.1.5 Cyclic Stress-Strain Curve And Hysteresis Loops	33
	2.1.6 Local Strain Analysis With Residual Stresses	36
	2.1.7 Strain-Life Relation	44
	2.1.8 Cumulative Fatigue Damage Analysis	45

2.2 Fatigue Crack Propagation Life For A Weld 48

2.3 Method Of Analysis For Fatigue Life 59

3. EXPERIMENTAL PROGRAM 62

3.1 Scope Of The Experimental Investigation 62

3.2 Determination Of Material Properties 63

3.2.1 Tensile Test 64

3.2.2 Cyclic Strain-Controlled Test 64

3.2.3 Cyclic Relaxation Test Of Mean Stress 69

3.3 Experiments On Welded Structures 74

3.3.1 Preparation Of High Cycle Fatigue Specimen 74

3.3.2 Generation Of Compressive Residual Stress By Mechanical And Thermal Treatment 77

3.3.3 High Cycle Fatigue Testing Of Welded specimen 80

3.4 Measurement Of Residual Stress 81

3.5 Hardness Test 82

4. RESULTS AND DISCUSSION 85

4.1 Introduction 85

4.2 Experimental Results 85

4.2.1 Properties Of Columbium-50 Steel Material 85

4.2.2 Results Of Smooth Specimen Fatigue Behaviour 93

4.2.3 Cyclic Mean Stress Relaxation 98

4.3 Experimental Verification Of The Welding Residual Stresses 105

4.3.1 Introduction 105

4.3.2 Distribution Of Welding Residual Stresses 106

4.3.3 Surface Compressive Stress Measurements Of Treated Welded Specimens 115

4.4 Fatigue Testing, Methods Of Stress Relief And Their Effectiveness 122

4.5 Theoretical Results, Correlations With Experiments And Discussion 138

4.5.1 Introduction 138

4.5.2 Predictions Of Total Fatigue Life And Experimental Results 140

4.5.3 Observations On The Total Life Model 161

5. MODEL PREDICTIONS FOR CRACK INITIATION AND CRACK PROPAGATION 163

5.1 Introduction 163

5.2 Influence Of Residual Stresses, Stress Relieving And Stress Ratios On Fatigue Life 163

5.3 Results Of Theoretical Study From The Crack Propagation Model 170

6. CONCLUSIONS & RECOMMENDATIONS FOR FUTURE WORK 183

6.1 Conclusions 183

6.2 Recommendations For Future Work 187

REFERENCES 189

7. APPENDIX A 200

7.1 Introduction: Calibration Of X-ray Diffraction Stress Measurements 200

7.1.1 Calibration Of X-ray Stress Measurements 200

7.1.2 Measurements Of Stresses In Steel Parts By X-ray Diffraction 201

7.1.3 Measurements Of Residual Stresses By The Blind-Hole Drilling Technique 204

7.1.4 Stress Measurements By Sectioning 207

7.1.5 Stress Measurements By A Strain Gauging 210

7.1.6 Plastic Strain Measurements By Strain Gauging 212

7.1.7 Plastic Strain Measurements Using An Extensometer 212

8. APPENDIX B 213

8.1 Cyclic Hardening And Softening Behaviour Of Constant Strain Amplitude Tests 213

9. APPENDIX C 216

9.1 Cyclic Stress-Strain Properties From Micro-Hardness Measurements 216

10. APPENDIX D 218

10.1 Tables Of Experimental Data 218

List of Figures

Figure		Page
1.1	Origin of residual stress during heating and cooling	6
1.2	Typical residual stress distribution in welded plates without fixed ends (a) longitudinal and (b) transverse directions	6
2.1	Elastic-plastic stress-strain field at the notch root	25
2.2	Geometrical parameters for transverse butt-weld	25
2.3	Fatigue notch factor & elastic stress concentration factor as a function of weld toe root radius	32
2.4	Tips of hysteresis loop and points on cyclic stress - strain curve	35
2.5	Notch-root stress and strain, $S_{end} > S_{min}$	37
2.6	Notch-root stress and strain, $S_{end} = S_{min}$	37
2.7	Simulation of residual stress at the weld toe by elastic superposition and Neuber's rule (Eq.(5))	43
2.8	Distribution of residual stress at the weld toe	55
2.9	Fatigue crack closure concepts (plastically induced crack closure)	55
2.10	Computational procedure for total fatigue life analysis	62
3.1	Specimen geometry for tensile test	67
3.2	Specimen geometry for cylindrical specimen	67
3.3	Stable hysteresis loop for fully reversed condition	68
3.4	Cyclic stress-strain curve drawn through stable hysteresis loop tips	69
3.5	Local (notch-root) hysteresis loop subsequent to first cycle under zero to tension fatigue loading of welded structures	70

Figure		Page
3.6	Block sequence of the mean stress relaxation tests on the base material	73
3.7	High cycle fatigue specimens	76
3.8	Bending stress jig	76
3.9	Typical locations of fatigue crack initiation in a butt-weld	84
4.1	The cyclic and monotonic stress-strain curves for Columbium-50 steel base material	90
4.2	Determination of static strength coefficient and strain hardening exponent from true plastic strain and true plastic stress	91
4.3	Determination of cyclic strength coefficient and cyclic strain hardening exponent from plastic strain and stress amplitudes measured from hysteresis loops	92
4.4	Fatigue properties from total strain amplitudes and reversals to failure using smooth specimens fully reversed strain controlled tests	96
4.5	Fatigue strength coefficient from stress amplitudes and reversals to failure using smooth specinmens strain-controlled tests	97
4.6	Mean stress relaxation tests using three mean strains and constant strain amplitude	101
4.7	Mean stress relaxation tests for constant mean strain and three strain amplitudes	102
4.8	Normalized mean stress relaxation behavour of Columbium-50 steel	103
4.9	Relaxation exponent (k) as a function of modulus of elasticity,transition strain and plastic strain amplitude	104
4.10	General residual stress distribution near the weld toe of Columbium-50 / Oxweld #36 butt-weld	109

Figure		Page
4.11	Distribution of residual stresses after fatigue cycling	110
4.12	Measurement of residual stress along the thickness on the middle of the width of the specimen	111
4.13	Measurement of residual stress through the thickness on the end along the width of the specimen	112
4.14	Measurement of stress across the thickness of the parent material	113
4.15	Measurement of surface stresses of base metal by Sectioning method	114
4.16	Change of residual stress pattern after preloading	117
4.17	Change of residual stress pattern after preloading	118
4.18	Change of residual stress pattern after preloading	119
4.19	Introduction of compressive peening stresses by various mechanical / thermal methods	120
4.20	Introduction of compressive stresses by stress-peening	121
4.21	Experimental fatigue tests results of parent material, single point hammer peened, tensile preloaded and untreated welded specimens.	126
4.22	Experimental fatigue tests results of annealed and multiple point hammer peened specimens	127
4.23	Experimental fatigue tests results of glass peened, steel shot peened and stress peened specimens	128
4.24	Percentage improvement in fatigue strength and difference in induced stress	129

Figure		Page
4.25	Knoop hardness values vs. depth of work hardening of glass and steel shot peened specimens	131
4.26	Knoop hardness values vs. depth of work hardening for multiple and single point hammer peening	132
4.27	Knoop hardness values vs. depth of work hardening for two cases of stress-peening	133
4.28	Depth of work hardening and Almen strip intensity vs induced compressive residual stresses by various methods.	134
4.29	Hardness on the surface across the weld, the HAZ and the base matal	136
4.30	Hardness readings across the thickness of untreated weld and glass shot peened specimens	137
4.31	Experimental results and theoretical predictions of as-welded specimens	144
4.32	Experimental results and theoretical predictions for crack initiation, crack propagation and total fatigue lives of the butt-welded joints	145
4.33	Experimental results and theoretical predictions for annealed specimens	148
4.34	Experimental results and theoretical predictions for tensile preloaded specimens	149
4.35	Experimental results and theoretical predictions of glass shot peened specimens	150
4.36	Experimental results and theoretical predictions of steel shot peened specimens	151
4.37	Experimental results and theoretical predictions of single point hammer peened specimens	153
4.38	Experimental results and theoretical predictions of multiple point hammer peened specimens	154

Figure		Page
4.39	Experimental results and theoretical predictions of stress-peened specimens	155
4.40	Experimental results of untreated weld and theoretical predictions of all cases of mechanical / thermal treatments.	158
4.41	Experimental results of untreated weld and theoretical predictions using the HAZ and the weld metal properties	159
4.42	Percentage of total life needed to initiate a crack for the base, the weld and the HAZ materials	160
5.1	Theoretical predictions showing the influence of stress ratios and stress relieving for the total fatigue life of butt-welded joints	165
5.2	Theoretical predictions showing the influence of stress ratios and stress relieving for the crack initiation life of butt-welded specimens	166
5.3	Modified Goodman diagram showing the as-welded and stress-relieved conditions	168
5.4	Theoretical predictions showing the percentage of total life needed for initiaton of a crack for three stress ratios in as-welded and stress-relieved conditions	169
5.5	Theoretical predictions of crack propagation life and a half crack length	173
5.6	Calculated value of the range of stress intensity factor and the rate of crack propagation	174
5.7	Calculated value of the range of stress intensity factor and the rate of crack propagation	175
5.8	Calculated value of the residual stress intensity factor and the rate of crack propagation	176

Figure		Page
5.9	Calculated value of the residual stress intensity factor and the rate of crack propagation	177
5.10	Calculated value of the range of stress intensity factor and the residual stress intensity factor	178
5.11	Calculated value of the range of stress intensity factor and the residual stress intensity factor.	179
5.12	Calculated value of the range of stress intensity factor and the rate of crack propagation for as-welded, stress-relieved and induced compressive residual stress	181
5.13	Enlarged view of Figure 5.12 showing the effect of stress relieving and induced compressive stress as a function of the range of stress intensity factor and the rate of crack propagation	182
A.1	"Thomas method B" X-ray diffraction stress measurements	202
A.2	Rectangular rosette for residual stress measurement	206
A.3	Sectioning of Columbium-50 base material	209
A.4	Sectioning of annealed specimen	209
A.5	Strain gauge and X-ray stress measurements	210
A.6	Calibration of X-ray stress measurements vs. other methods	211
B.1	Cyclic hardening and softening behaviour for constant amplitude and fully reversed strain-controlled tests on Columbium-50 smooth specimen	215

List of Tables

Table		Page
1	Mechanical properties of base, weld and HAZ materials for Columbium-50 steel/ Oxweld # 36 Weld metal / HAZ metal	86
2	Cyclic and fatigue properties of base, weld and HAZ materials for Columbium-50 steel / Oxweld # 36 Weld metal / HAZ metal	87
3	Experimental results for low-cycle fatigue strain control tests of Columbium-50 steel base metal (fully reversed case)	95
4	Adjusted material properties ("weld-parent" interface material properties taken as average of the weld and parent material properties)	143
5	Test data for mean stress relaxation tests (constant strain amplitude but variable mean strain)	219
6	Test data for mean stress relaxation tests for constant mean strain but variable strain amplitudes	220
7	Cyclic hardening and softening behaviour for constant amplitude fully-reversed strain-controlled tests on the base metal of Columbium-50 steel	221
8	Improvements in fatigue strength vs. amount of induced stress & Induced stress vs. depth of work-hardening and Almen strip intensity	222
9	Theoretical stress concentration factor K_t and fatigue notch factor K_f as a function of weld toe root radius r.	223
10	Peterson's material value and assumed crack growth rate constants for materials at the crack initiation site.	224
11	Chemical composition of the base metal and welding electrodes	225

GLOSSARY OF SYMBOLS

A = Parameter depending on weld geometry

a = Half crack length

a_i, a_f, a_{th} = Initial ,final and threshold crack length

b = Fatigue strength exponent

c = Fatigue ductility exponent

C_n = Neuber's hyperbola

C, C_R = Crack growth rate material constants

C_f = Crack opening factor

$C_f(R=0)$ = Crack opening factor for zero to tension loading

$C_f(R)$ = Crack opening factor for any stress ratio

$D_{i,t}$ = Total damage due to elastic or plastic and mean stress per reversal

$\Delta\epsilon_p/2, \Delta\epsilon_e/2, \Delta\epsilon/2$= Plastic, elastic and total strain amplitude

$\epsilon_{tr}, \epsilon_t$ = Transition and total strain

$\Delta\epsilon, \epsilon$ = Local strain range, local strain

$\Delta e, e$ = Nominal strain range, nominal strain

e_{max} = Maximum nominal strain per cycle

ϵ_{end} = Local strain at the end of cycle

$\epsilon_{r,i}$ = Local residual strain prior to cyclic loading

ϵ_{unload} = Local strain due to unloading

E = Modulus of Elasticity

ϵ_f, σ_f = True strain and stress at fracture

ϵ_f', σ_f' = Fatigue ductility and strength coefficients

K,K′=Monotonic and cyclic strength coefficient

ΔK = Range of stress intensity factor

K_{op} = Crack opening stress intensity factor

K_{max}, K_{min} = Maximum and minimum stress intensity factor

ΔK_{th} = Range of threshold stress intensity factor

ΔK_{eff} = Range of effective stress intensity factor

K_f = Fatigue notch factor (fatigue strength reduction factor)

$K_t, K\varepsilon, K\sigma$ = Elastic, strain and stress concentration factor

k = Relaxation exponent

K_R = Residual stress intensity factor

m = Crack propagation exponent material constant

n, n' = Monotonic and cyclic strain hardening exponent

N_I, N_P, N_T = Fatigue crack initiation, propagation and total life

$2N_f, 2N_{tr}, 2N$ = Reversal to failure, transition fatigue life and reversal

R = Nominal stress ratio, (S_{min}/S_{max})

R_{eff} = Fracture mechanics effective stress ratio

r, t, ϕ, θ = Weld toe root radius, weld plate thickness, edge preparation angle and flank angle of weld

S_y = Tensile yield strength

S_u = Ultimate tensile strength

$S, \Delta S$ = Nominal stress, nominal stress range

S_{end} = Nominal stress at the end of cycle

S_{max}, S_{min} = Maximum and minimum nominal stress

S_m = Nominal mean stress

W = Width of the specimen

Y = Geometric correction factor for weld, function of crack length and specimen geometry

ρ^* = Peterson's material constant

$\sigma_{r,i}$ = Initial residual stress at the weld toe

σ_r = Residual stress at the weld toe

$\sigma_{r,s}$ = Local residual stress subsequent to cyclic loading

σ_0 = Local mean stress

$\sigma_{0,i}$ = Initial mean stress

$\sigma_{0,2N}$ = Mean stress at reversal 2N

$\sigma, \Delta\sigma, \Delta\sigma/2$ = Local stress, stress range and stress amplitude

σ'_y = Cyclic yield stress

σ_{unload} = Local stress range due to unloading

1. INTRODUCTION AND HISTORICAL REVIEW

1.1 BACKGROUND

The development of residual stresses in welded construction is intrinsic to the welding process. This can be extremely important in determining the behaviour of a structure under static and dynamic loads. In the welding process high residual stresses are inevitably set up and often cannot be entirely removed by a post-welding heat treatment. The increased use of welding as a joining technique accentuates the need for a thorough investigation of the problems of relating the influence of residual stresses to the fatigue behaviour of welded structures. The presence of these "locked-in" stresses frequently threatens the reliability of structures. Recent work has tended to show that residual stresses are not always to blame, even though, in certain circumstances they certainly may have a detrimental effect.

The role of residual stresses in fatigue performance is still not fully understood (Puchner 1963, Ross 1950, Hebrant & others 1957, Dugdale 1959, Gurney 1979). Many investigators contend that residual stresses do not have any significant influence. They base their opinions on comparisons of specimens heat-treated after welding to those in the as-welded condition. These tests have proved inconclusive; the stress relieving sometimes increased the fatigue limit while either being entirely ineffective or

slightly negative in other cases.

Ross(1950), for example, stated that residual stresses can be ignored in the case of good welds while Hebrant(1957) suggested that residual stresses have little effect on fatigue behaviour as compared with the effect of weld geometry. On the other hand, Dugdale (1959) demonstrated the existence of a substantial residual stress effect in small notched specimens. If this were true, one might expect that residual stresses could affect the fatigue behaviour of welded joints in which flaws or sharp cracks exist. However, there is a great deal of information in the literature which contradicts this view (Munse,1964).

The above comments cannot however, be taken as proof that residual stresses do not markedly affect fatigue life as many of these studies ignored the changes in material properties caused by stress relieving. Furthermore, especially with pulsating tensile stresses, it is known that residual stresses are redistributed during testing (Buhler & Buchholtz 1933, Horger 1945).

The investigation of the effect of residual stresses requires the study of two phenomena and their mutual interaction. These are; the influence of residual stresses on the endurance and fatigue limits, and the influence of stresses induced by loading on the magnitude of the residual stresses. Various researchers (Gurney 1977,1979, Higashida & others 1978, Chang & Lawrence 1981, Lawrence & others 1981, Harrison 1981) have found that residual stresses exert some

influence on the fatigue limit, the degree depending upon the kind of external loading. If the residual stresses are of the same sign as the stresses due to loading they affect the fatigue limit only slightly; residual tensile stresses reduce the fatigue life while compressive ones increase it. In general, the intent of this work is to predict or at least determine the influence of residual stresses on the fatigue life of welded structures, in particular butt-welded steel joints.

In the following sections the origin and nature of residual stresses in butt-welded joints are discussed along with a brief literature review that outlines the previous work on the fatigue behaviour of welded structures. Redistribution and introduction of residual stresses are discussed for several types of mechanical surface and thermal treatments. These methods are used to study both experimentally and theoretically the effect of residual stresses on the fatigue life of butt-welded structures.

1.2 Origin And Nature Of Residual Stresses In Welded Joints

Residual stresses, or stresses existing in a member in the absence of any external load, are caused by local yielding in an otherwise elastic body, e.g., at a notch root or by non-uniform plastic deformation. By definition they are self-equilibrating and thus for most welded structures they are confined to the neighbourhood of the welds. Residual stresses are associated with the fusion welding

process which cause distortion after the welding process. Conditions of restraint limit distortions but impose large local strains in the welded joints giving rise to higher residual stresses and a greatly increased risk of failure. Conversely, low restraint does not inhibit the local contractions which result in larger displacements or distortions and a lower level of residual stresses (Parlane 1981).

Residual stresses in welded components arise from the localized shrinkage associated with the cooling down of the hot weld metal which is restrained either internally or externally by the cold section of the fabrication surrounding the weldment. It has been shown by Weck (1947) that this principle is universal. Residual stresses can only be produced by those processes which involve a definite or permanent alteration of at least part of the body, so that an incompatible state of deformation would exist for a stress free state. The usual way in which this redistribution occurs, without involving cutting and joining, is by plastic flow.

During welding severe thermal stresses may arise because the temperature distribution in the body will be far from uniform. These thermal stresses can produce large plastic deformations. When the body is hot, a compatible system will exist between the plastic and thermal deformations, but on cooling, the thermal strains disappear while plastic deformations remain. These plastic

deformations will not by themselves satisfy the compatibility conditions so that a residual stress distribution is formed.

To better understand the process, consider the behaviour of an element of material. This is illustrated in Fig.1.1 (Parlane 1981) which shows a typical thermal / stress cycle for an element of material whose yield strength in tension and compression decreases with temperature. If the cycle starts at room temperature (RT),O, the initial thermal expansion is restrained by surrounding cold material, thus generating elastic compressive stresses until the yield strength is reached at position A. Further increases in temperature result in plastic strains which occur following the compressive yielding curve, AB. On cooling, the initial response is once again elastic, but opposite in sign to the heating cycle, until the tensile yield strength is achieved at position C. Cooling back to room temperature then follows the tensile yield strength curve, generating residual stresses at room temperature (position D). This figure also shows that the magnitude of residual stress is a function of the temperature difference experienced. In the case considered, any temperature rise exceeding "T" will always generate residual stresses equal to yield, whereas, at lower temperatures the shrinkage strains are not sufficient to reach the tensile yield limit. As a result, the residual stresses are less than the yield stress.

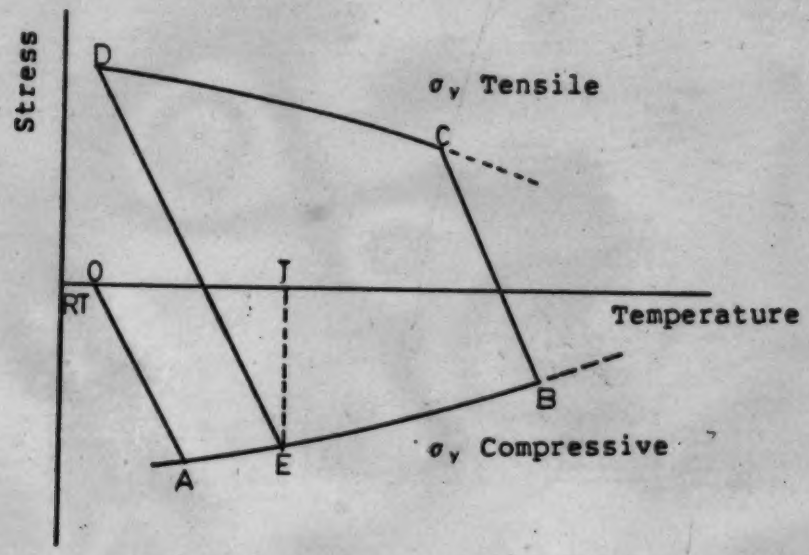

Figure 1.1 Origin of residual stress during heating and cooling.

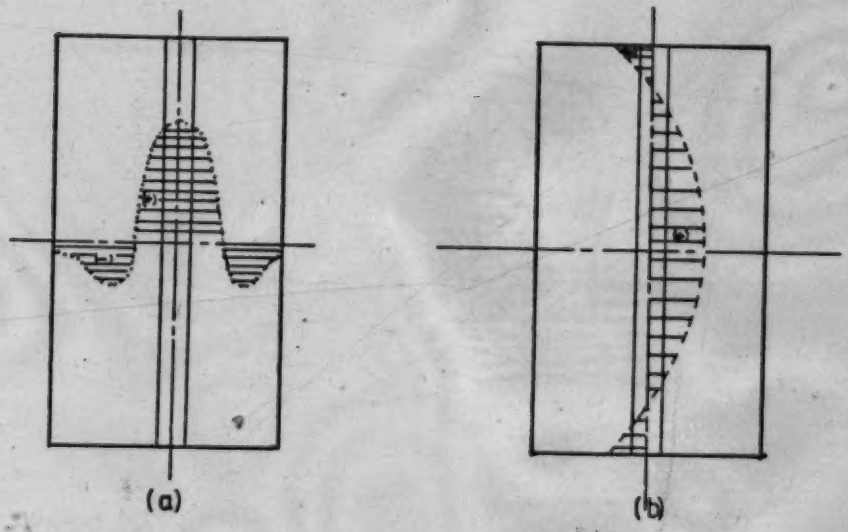

Figure 1.2 Typical residual stress distribution in welded plates without fixed ends: (a) longitudinal and (b) transverse directions.

1.3 Previous Investigations On The Effect Of Residual Stresses On Fatigue Behaviour Of Welded Structures

The influence of residual stress on the fatigue life of welded steel joints have been studied by numerous researchers. In order to investigate the effect of fatigue the original stress distribution after welding should be known. Under normal circumstances the residual stress distribution in the vicinity of a butt-welded joint can be described with reference to Fig.1.2 (see for example: Gurney 1979, Gurney & Maddox 1973, Munse 1964, Pollard & Cover 1972, Harrison 1965,1981, Parker 1957, Tall 1964). In the direction parallel to the weld, the weld and the parent material immediately adjacent to it are subjected to a high tensile stress which is balanced by a compressive stress at points further away from the weld. The entire stress system reduces to zero at the plate edge. Transverse to the weld the residual stresses are tensile near the centre of the width and compressive near the plate ends (Fig.1.2b). Superimposed on this residual stress pattern is the dynamic loading. Early investigators (Gurney 1973, Pollard & Cover 1972, Harrison 1965, Parker 1957, Tall 1964) observed the effect of residual stresses when they found that the fatigue strength in as-welded butt joints (not stress-relieved) was less than that in the stress-relieved ones (pulsating tension tests). It was observed that under this loading stress relief produces a small increase in fatigue strength. However, it was also found that if the thermal stress relief

was incorrectly carried out, a large decrease in strength could result (Gurney 1960). Moroever, the improvement in fatigue resistance by stress relief was found to be less effective in low cycle fatigue ranges.

Harrison (1981) showed that the effect of residual stress on fatigue behaviour depended to a large extent on the applied stress ratio, $R=S_{min} / S_{max}$. When the applied stress range was purely tensile the residual stress had little effect but if the stress cycle passed through zero they became more damaging; the larger the compressive components the more harmful. He concluded that stress relief would be beneficial near the endurance limit and under alternating loading.

None of the investigations cited above used any analytical models which could estimate the fatigue life in a welded specimen or completely predict the influence of residual stresses. Dowling (1979) studied the notched member fatigue life predictions and considered the general notched specimen but not welded structures in particular. Mattos (1976) studied the crack initiation life of welded joints but he did not consider the effect of residual stresses and the influence of effective stress ratio. Burk (1978) extended the model suggested by Mattos (1976) for estimating the crack initiation life and applied it to estimate the residual stress influence on fatigue crack initiation life of welds. He treated the influence of residual stresses on weld fatigue life by the use of the damage integral together

with the "set-up cycle" model which establishes a mean stress. This in turn allowed the mean stress relaxation in the prediction of fatigue life.

Several authors including Harrison (1968), Maddox (1975), McHenry & others (1979), Frank (1979), and Zettlemoyer (1976) used fracture mechanics concept to predict the fatigue behaviour of mild steel specimens. It was hypothesized that welds are fabricated with small, crack-like defects at the weld toe (Signes & others 1967) and therefore the crack initiation life was assumed to be short or non-existent. Signes & others (1967) mentioned that the morphology of some of the defects is such that they constitute sharp notches, the root radius of which may be less than 0.0001 inch (0.00254mm). These notches are situated at the maximum stress concentration due to weld geometry and fatigue cracking appeared to initiate from these defects. Their work has shown that there is a high probability that every weld will contain a number of defects which will be sufficiently sharp to bring about the maximum possible stress concentration.

For analysis it is convenient to divide the total fatigue life into initiation and propagation phases. An investigation by Burk & Lawrence (1977) and Lawrence (1973) using ASTM A36 butt-welds showed that a significant portion of fatigue life was spent in initiating a 0.01 inch (0.254mm) fatigue crack at the weld toe. In addition, unrealistically small values of initial crack length (a_i)

(below the threshold crack length a_{th}) would be required, especially in the long life regime, to account for the total fatigue life on the basis of propagation alone. The effect of weld geometry, material properties, stress level and initial flaw size were considered. Differences in weld geometry were found to influence the fatigue crack propagation life by as much as a factor of three while material properties and initial flaw size could have an even larger effect.

Mattos (1976) studied the crack initiation life (N_I) of ASTM A36 butt-welds (simulated) and considered the influence of base metal material properties, weld geometry and simulated residual stress on fatigue life. The weld geometry was found to influence the initiation life and was similar to the influence of geometry on the propagation life (N_P) in butt or fillet welds (Maddox 1975, Harrison 1968, Frank 1979, Burk & Lawrence 1977, Mattos 1976, Lawrence 1973). Mattos also found that different weld materials had affected the length of the crack initiation and propagation phases of the total fatigue life when an initial crack length (a_i) of 0.01 inch (0.254mm) was assumed. Mattos also considered the influence of residual stress on crack initiation life and found that residual stresses had no effect on the initiation life of a weld for lives of less than 10^6 cycles. Subsequently, Lomacky & others (1975), Smith & others (1977) and El Haddad & others (1980) considered the crack initiation and propagation lives in an analysis of butt-weld

fatigue life. Generally an elastic-plastic fracture mechanics solution for fatigue cracks initiating from weld toes was introduced. It accounted for the propagation of very short cracks by the introduction of an effective crack length. Considerations were also given to the effect of mean stress, and a residual stress adjustment was made on the assumption that the maximum stress at the notch root is equal to the yield stress.

To study the propagation portion of the failure the crack growth rate constant in Paris' crack growth equation (C) as well as the strain-life fatigue properties of the Heat-affected-zone (HAZ) and the weld-metal (WM) in butt-welds were considered by numerous researchers (Maddox 1972, Kapadia & Imhoff 1976, Parry & others 1972a, 1972b). The crack growth rate in the HAZ and WM in high strength and low alloy mild steels showed a wide range of scattering in comparison to the base metal behaviour. Higashida (1976) determined the strain-life fatigue properties of the HAZ and the WM of ASTM A36 and A514 grade F steels. The cyclic strain properties of WM and HAZ were found to differ significantly from the base metal properties, especially at lives $>10^4$ cycles, but were shown to vary systematically with hardness. The relaxation rates of mean stress, an important material property which governs the influence of residual stress on fatigue life, was also found to be significantly different from that of the base metal.

1.4 Redistribution Of Residual Stresses By Mechanical And Thermal Means

1.4.1 Introduction

This section describes the various means available to introduce beneficial surface compressive stresses by mechanical and thermal means with the goal of improving the fatigue life of butt-welded joints. Also described are how the various treatments were employed and reported improvements or disadvantages are mentioned.

1.4.2 Shot-peening

The resistance to fatigue of metal components is influenced by (i) surface finish, (ii) residual stresses, (iii) and the structure of the surface layer. Shot peening modifies the above factors and can contribute considerably to the improvement of the fatigue life of components in service.

It is recognized that surface compressive stresses due to peening usually improves the fatigue properties of welded steel components (Almen & Black 1963, Brine & others 1968, Gurney 1968, Knight 1976, Sanders 1972). Gurney (1968,1979) and Knight (1976) have also reported that peening was beneficial for fillet welded specimens. Guerrera (1966) reported that the fatigue life in pulsating tension was improved approximately 25 percent above that of the untreated weld. Baron & Brine (1965) obtained a 35 percent

improvement for C-Mn steels. Kenyon & others (1966) obtained a 50 percent improvement by adding an extra bead by using an argon torch and mild steel filler rod. In this way, the weld profile blended smoothly with the plate and the notch at the toe was eliminated. A similar procedure was obtained by Kanazawa & others (1970) on medium strength steel. They obtained an increase of approximately 35 percent. Chadwick (1971) reported improvements of 40 percent by explosively peening maraging steel. Horger & Neifert (1944,1945) mentioned various investigations by the previous researchers who found considerable improvement by shot-peening processes. It was found that for structures subjected to large number of cycles of lower stress level peening gave a better fatigue life.

Faulkner & Bellow (1972) studied the improvement on the fatigue life of butt-welded medium strength steel (Columbium-60 Steel). They compared the improvements obtained by grinding the weld bead flush and by steel shot-peening the weld. Four forms of peening processes were employed in this study; air-blasted glass beads, steel shot, multiple point hammer, and a single point hammer. They obtained a 45 percent improvement of the fatigue strength by steel shot peening. The results showed that multiple point hammer peening gave the greatest improvement (65%) but at fatigue lives higher than 10^6 cycles, the steel shot, multiple points and single point hammer peening processes gave nearly the same improvement. In general, it was shown

that the effectiveness of the peening is dependent on the depth of cold working of the surface layer.

Niku-Lari (1983a,1983b) found that the depth of the plastically deformed layer is the greatest in a soft material (approximately 0.8mm). For a material with a high surface hardness the maximum residual compressive stress is situated below the surface, while for material with a low hardness number the maximum stress is situated at the surface. He concluded that the residual stresses due to shot peening change during the external loading of the component, particularly at high operating temperatures.

The variations in the effect of peening are at least in part due to variation in peening intensity. In general, an optimum peening condition should be based on a combination of the residual stress pattern, the distortion, and the surface roughness.

1.4.3 Stress Peening

'Stress-peening' consists of peening a part while it is statically loaded in the direction in which it is to be loaded in service. The elastic limit of the surface metal increases by strain hardening (plastic yielding) that occurs during the stress peening.

Polmear (1980) carried out extensive investigations of the effect of surface peening on the fatigue characteristic of aluminium alloy specimens having load carrying fillet welds to see if the improved performance reported for

butt-welded components was also observed. He tested peened and unpeened batches of specimens with transverse and longitudinal fillet welds over wide stress ranges involving high tensile preload and high cyclic loads. Peening of the welded region was carried out with a needle gun either before or after the application of preload. Polmear showed that peening was beneficial under most conditions, most notably when peening was carried out after preloading. Peening after the application of a preload caused a notable increase (approximately 60% higher than ordinary peened specimens) in fatigue resistance over a wide range of preloads and levels of cyclic stress. Peening before the application of a preload increased the fatigue resistance at most stress levels although the effects were less than those recorded if preloading was carried out before peening.

1.4.4 Tensile Preloading

A fundamental principle of elastic-plastic deformation theory is that it is only possible to redistribute elastic stresses by decreasing the plastic deformation. Thus, the occurance of a certain amount of plastic deformation results in a corresponding reduction in the overall total elastic stress. This plastic stress occurs at points where the pre-existing elastic stresses were closest to the yield point of the material i.e. at highly stressed regions. By the application of a continuously increasing static load of less than the yield strength of the material, the effect of

applied load and the pre-existing elastic strains produces plastic deformation. In the welded structures the effect of the initial residual stress field and the applied tensile force causes plastic deformation in regions of peak stress. The conversion of elastic strain to plastic strain produces a compressive stress field at the weld toe which upon unloading cause an uneven stress distribtion.

In the case of butt-welded specimens the tensile preloading causes a compressive residual stress. Firstly, due to a stress concentration at the weld toe, loading the specimen to below the yield stress of the net section causes the material at the weld toe to become plastic and undergo large non-recoverable plastic strains. The material near the weld toe becomes permanently strained while the total section remains elastic. Upon unloading, the material becomes compressed as the specimen returns to its original shape (or nearly so) as the load is returned to zero. The weld toe then contains a compressive residual stress .

1.4.5 Post-Weld Thermal Treatments

Thermal stress-relieving is the process of uniform heating of a component to a suitable temperature, holding it at this temperature for a predetermined period of time, then uniformly cooling it. Stress-relief heat treatment is usually performed below the lower critical range to avoid changes in grain sizes. The lower critical point A_1 temperature in considered at 1290°F (700°C). In the

annealing -relief, recrystallization and grain growth occur during the reheating of the metal. The percentage reduction of residual stresses is dependent on steel type, composition or yield strength. The closer the temperature to the critical or recrystallization temperature the more effective it is in the removal of residual stresses.

Parker (1957) studied the mechanical properties of mild steel at elevated temperatures. He found that at 1020°F (550°C) an initial stress of 12000 psi (83 MPa) and 5000 psi (38 Mpa) each dropped to less than half of their initial value in about two hours. He also found that stress relaxation by creep may contribute substantially to the stress relieving process. A large part of the improvement produced by thermal stress relieving may be a combination of metallurgical changes and relaxation of welding residual stresses.

De Garmo (1952), Greene & Holzbarr (1946), McKinsey (1954), and Jelm & Herres (1946) all found that thermal stress-relieving improved the mechanical properties and fatigue life of carbon-steel weldments by relaxation of residual stresses. Nedoseka (1974), Vinokurov (1967), Fried Lima (1971) and Gruzd (1972) found that the annealing temperature makes it possible to reduce residual stresses up to a 50 percent. They concluded that the effectiveness of a particular method depends on numerous factors such as the physical and mechanical properties of the material, the initial residual stresses, the geometry of the weld toe, the

type of stresses, the type of the treatment and the type of the joint. Pollard & Cover (1972) found that for transverse butt-welded specimen improvement in fatigue strength of 14 to 32 percent have been obtained by stress-relief annealing.

1.5 The Specific Problems And Objectives

The welding process is complex and therefore in the prediction of the fatigue life of welded structures, many variables must be considered: geometry of the weld, methods of welding, variable material properties of HAZ, WM and BM, and distribution of the residual stresses. To this time, most of the studies carried out on the fatigue life of welded joints were of experimental nature. Various cases of mechanical and thermal treatment of welds showed improvement in fatigue life but no clear explanations were given for their improvement. A complete study is needed to show how the various material properties and post-weld treatment affect the fatigue life of welded joints.

The influence of the residual stress on the fatigue life of welded joints is not fully understood at the present time. Possible reasons may be due to the limitations of the methods for their determination, the absence of a complete analytical method to predict their influence and their changes throughout the fatigue life. Most experimental studies considered the initial residual stresses present before the fatigue cycling and did not show the changes that occur during fatigue cycling. The influence of the variables

(cyclic and fatigue material properties, magnitude and sense of initial residual stress, applied stress amplitudes, etc) which affect the relaxation of the residual stresses have been controversial. This may be mainly because of the absence of a unified model to explain the effect of these variables. This study intends to discuss the effects of the redistribution of residual stresses in the fatigue of butt-welded joints , the methods of stress relief and their efficacy, and experimental and theoretical studies to predict the total fatigue life of a welded component as the sum total of crack initiation and crack propagation lives.

2. THEORETICAL ANALYSIS

2.1 Theoretical Approach To Fatigue Analysis

The traditional approach to the analysis of fatigue of notched structures has been based on the classical "stress cycle to failure (S-N)" curve. The "S-N" curve is determined experimentally. As an alternate to this approach developments using concepts from fracture mechanics and low-cycle fatigue are used for analysis of fatigue phenomena. However, as yet no unified approach has been developed. Independent estimates of the fatigue crack initiation can be based on the "strain-life" properties and cumulative fatigue damage while the fatigue crack propagation life can be based on fracture mechanics concepts (Topper & Conle 1972, Mattos & Lawrence 1977, and Morrow & Socie 1981.)

The low-cycle fatigue concept for the estimation of crack initiation life considers the basic material properties and overall stress-strain analysis relating local and nominal stress-strain condition. "Local stress-strain analysis" simulates the notch-root stress-strain which determines the change in the initial residual stress pattern upon loading. The simulation of the actual effect of residual stress at the weld toe, cyclic and fatigue material properties and the damage accumulation model determine the crack initiation life. The crack propagation model considers the effect of axial and bending stresses along with residual

stress effects. The crack propagation model uses Forman's equation with appropriate combination of effective stress ratio, loading histories and the crack opening concepts under constant amplitude loading. Combination of crack initiation and crack propagation lives determines the total fatigue life and are described in the following sections.

2.1.1 Theory Of Crack Initiation

The rationale behind the theoretical approach to crack initiation assumes that the most highly strained region can be represented by a filament of material whose mechanical response is similar to that of a smooth fatigue specimen. Topper & others (1969) proposed that the fatigue crack initiation of a notched member can be considered to occur by the rupture of this filament of material. Under an appropriate control the smooth specimen can be used to reproduce the stress-strain history of the filament and the life of the smooth specimen can be taken as the crack initiation life.

The use of the above model requires information regarding the material properties and the stress-strain history of the most highly strained region (notch-root). To obtain an accurate prediction the properties obtained from these smooth specimen tests must be correlated with the local conditions at the most highly strained region.

Estimation of crack initiation life in a welded specimen requires the following information as summarized by

Topper & others (1969):

(i) A mechanical stress analysis that relates the nominal and local (notch-root) stresses and strains.

(ii) Knowledge of notch-root cyclic stress-strain behaviour.

(iii) The "strain-life" fatigue properties of the notch-root material.

(iv) A damage accumulation model for which the parameters may be determined from simple material tests and which will predict the fatigue crack initiation life.

It is often considered that the fatigue crack initiation portion in welds is eliminated by the existence of crack-like defects in the form of impurities, slag, or other non-metallic inclusions present at the toe of the weld or in the HAZ material (Signes & others 1967). These assumptions may not be justified mainly because it is unlikely that all welds are defective. Even for sharp notches, a period of crack initiation is required before a fatigue crack starts to propagate (Jack & Price 1970, 1972).

In contrast with the case of fatigue crack propagation there exist no adequate analytical models for estimating the fatigue crack initiation life in weldments which include the effect of residual stresses, cyclic hardening and softening conditions. Although the fatigue crack propagation estimates can provide a lower bound to the total fatigue life, omissions of the crack initiation life can lead to an

underestimation of the total fatigue life. This is especially true in the high cycle fatigue life regime where the crack initiation portion occupies a considerable portion of the total life.

The crack initiation life is assumed to end when the cumulative damage is satisfied. In order to calculate the damage it is necessary to model the highly stressed region (weld toe in this case). This is done using the notch simulation and local plasticity concepts developed by Neuber(1961). This Chapter will outline the material properties and calculations necessary for the prediction of crack initiation and crack propagation lives.

2.1.2 Notch Simulation And Local Plasticity

Theoretical and experimental studies of stress and strain concentrations around discontinuities have been limited to certain geometric shapes mainly in the elastic region. For notched members which have yielded at the notch root there exists no simple stress-strain relationship. When the plastic strains occur at the notch the stress concentrations start to decrease. In this case, the notch must be viewed as causing a strain as well as a stress concentration. After yielding the strain concentration factor K_ϵ increases while the stress concentration factor K_σ decreases. In this way the fatigue phenomena of metals can be accounted for by using the basis of loss of energy due to plasticity. The presence of stress raisers magnifies the

effect of plasticity and reduces the fatigue life (Stowell 1968). Several analytical approaches exist to address the problem of relating nominal stress-strain to local (at the weld-toe) stress-strain behaviour (Stowell 1950, Hardrath & Ohman 1951, Irwin 1960, Neuber 1961, Dixon & Straunigan 1964 and Huang 1972). Of these, Neuber's formulation has gained more popularity because of its simplicity.

The fraction of life spent in initiation versus propagation for a particular material is a function of the gross stress level and notch sharpness. Figure 2.1 shows the elastic and plastic zones at a notch root. Remote from the notch the nominal cyclic stress-strain behaviour is given by ΔS and Δe. If no cyclic plasticity occurs at the notch root, then

$$\Delta S \leq \Delta \sigma'_{y,} / K_t$$

where

$\Delta \sigma'_{y,}$ is the cyclic yield stress range and

K_t is the theoretical stress concentration factor.

Neuber (1946) showed that for elastic behaviour the stress at a point distance "x" ahead of the notch is approximately

$$\sigma = K_t \, S(\rho/(\rho+4x))^{1/2}$$

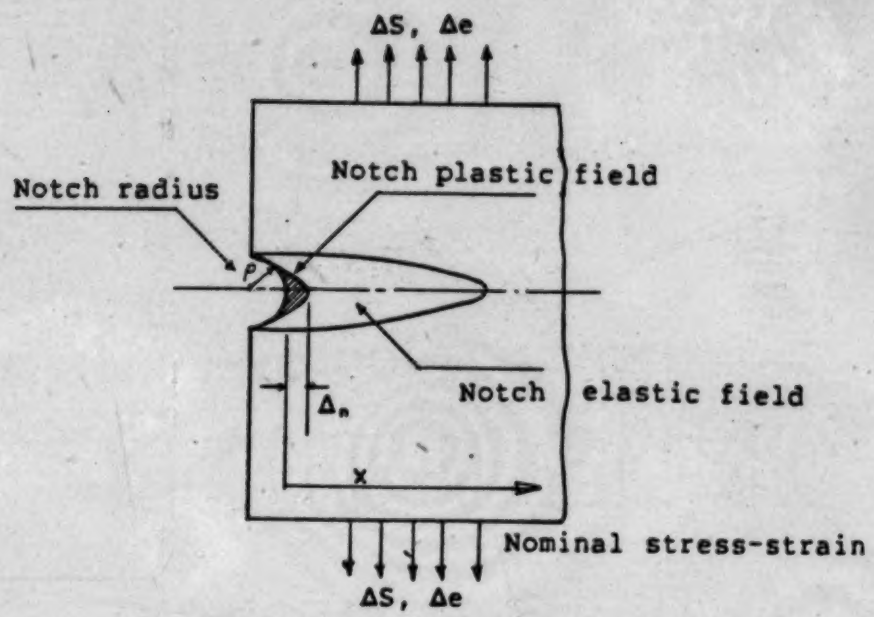

Figure 2.1 Elastic-plastic stress-strain field at the notch root.

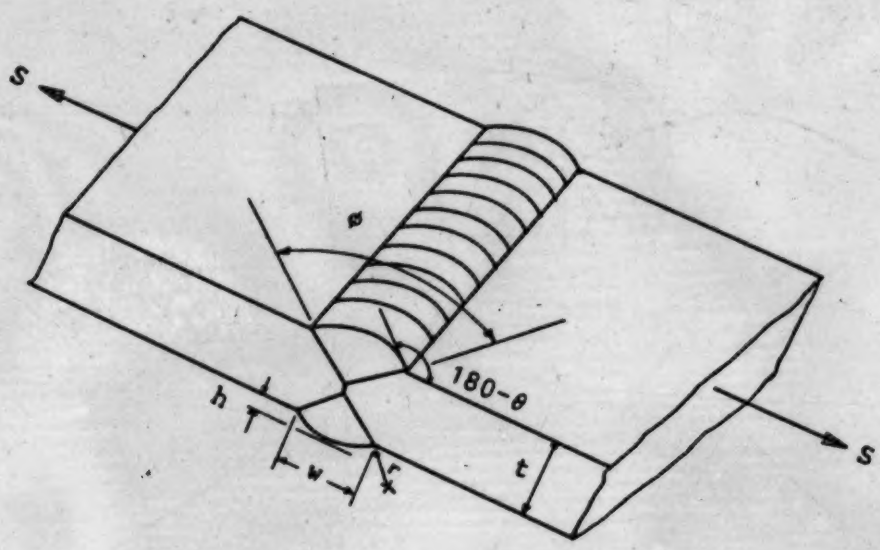

Figure 2.2 Geometrical parameters for transverse butt-weld.

However, if ΔS is sufficiently large, then cyclic plasticity occurs at a depth of Δ_n which can be estimated by substituting the cyclic yield stress range $\Delta\sigma'_y$, for σ in the above equation at "x" equal to Δ_n.

$$\Delta_n = \rho(\mu^2-1)/4$$

where

$$\mu = K_t \, \Delta S/\Delta\sigma'_y.$$

But for any linear or nonlinear elastic material Neuber (1961) stated that the elastic stress concentration factor K_t is equal to the geometric mean value of the actual stress concentration factor $K\sigma$ and the actual strain concentration factor $K\epsilon$, that is:

$$K_t = (K\sigma \; K\epsilon)^{1/2} \qquad (1)$$

and this will apply at any point a distance "x" ahead of the notch root. Equation (1) can be used to estimate the crack initiation life of a structure. In this case, it is necessary to relate local stresses and strains at the notch root to the nominal stresses and strains. From the above equations and using definitions of $K\sigma$, $K\epsilon$ Hammouda & others (1979) showed that

$$K_t^2 = (\Delta\sigma \; \Delta\epsilon)E \; / \; \Delta S^2 \qquad (2)$$

where

$\Delta\sigma$, $\Delta\epsilon$ = Local stress and strain ranges at the notch

root,

ΔS, Δe = Nominal stress and strain ranges remote from the notch root.

Topper & others (1969) extended Neuber's hypothesis, Eq.(1) to fatigue loading, particularly in the low and intermediate life ranges where local yielding can occur. For cyclic loading, K_f, the fatigue notch factor was substituted for K_t and Eq.(1) can be rewritten as:

$$K_f = (K\sigma\ K\epsilon)^{1/2}. \qquad (3)$$

When $K\sigma$ and $K\epsilon$ were written in terms of the ranges of stress and strain,

$$K_f = (\Delta\sigma\ \Delta\epsilon/\Delta S\ \Delta e)^{1/2}.$$

Neuber's rule is used to account for plastic action so K_f is defined as a constant which is different from K_t only as a result of size effects. For large radius notches, K_f is nearly equal to K_t and for sharp notches K_t is conservative and K_f can be used in preference to K_t.

Substituting the elastic modulus E into the above equation yields the following:

$$K_f(\Delta S\ \Delta e\ E)^{1/2} = (\Delta\sigma\ \Delta\epsilon\ E)^{1/2}. \qquad (4)$$

Under conditions of nominal elastic cyclic loading

$$\Delta S = E\ \Delta e$$

that is, when elastic conditions are assumed for the bulk of

the weld or notched member away from the critical location (weld-toe), Eq.(4) can be written as:

$$K_f^2 \, \Delta S^2/E = \Delta\sigma \, \Delta\epsilon. \qquad (5)$$

Equation (5) (Neuber-Topper) can also be obtained by substituting K_f for K_t in Eq.(2). The curves given by $K_f^2 \Delta S^2/E = C_n$ is called Neuber's rectangular hyperbola.

Equation (5) relates the nominal stress-strain behaviour to the local notch-root (weld-toe) stress-strain behaviour. It also predicts the notched behaviour from smooth specimen fatigue data provided K_f is known. For smooth specimens that were forced to undergo the stress-strain behaviour imposed by Eq.(5) Topper & others (1969) found that the fatigue life of the smooth specimen may be used to estimate the initiation life of the notched specimen. Equation (4) then relates the local $\Delta\sigma \, \Delta\epsilon$ product to the nominal $\Delta S \, \Delta e$.

Equation (5) assumes that the state of stress at the notch is uniaxial as in the smooth specimen. It also assumed that the stress gradient in the notched region is small so that the plastic zone is large relative to the diameter of the smooth specimen.

2.1.3 Theoretical Stress Concentration Factor

The elastic stress concentration factor K_t is generally available for simple geometries such as holes, ellipses, grooves etc (Peterson 1974). For the case of a butt-welded

specimen the geometry is not obvious. For this case, Lawrence (1973) approximated the weld reinforcement by a segment of a circle as shown in the Fig.2.2. He specified the weld geometry by using the flank angle θ and edge preparation angle ϕ and established a relationship between them and the ratios of h/w and w/t. Although θ and ϕ completely describe the external or macro geometry, the stress concentration factor is also a function of the microgeometry at the weld toe. A variable radius at the weld toe "r" was used to represent this microgeometry by Mattos & Lawrence (1977). They determined the elastic stress concentration factor K_t for selected butt-welded geometries by using an elastic finite element method. The K_t may be described by the following equation,

$$K_t = 1 + A\sqrt{t/r} \qquad (6)$$

where the parameter "A" depends on weld macrogeometry.

2.1.4 Fatigue Notch Factor

It is also necessary to find K_f (see Eq.(5)) for use in Neuber's theory (Neuber 1961). The fatigue notch factor K_f is determined by taking the ratio of unnotched to notched fatigue strength at some finite life. Hardness and notch size are important factors in determining the effectiveness of notches under cyclic loading. To account for the above conditions several equations relating the fatigue strength reduction factor K_f and the elastic stress concentration

factor K_t have been proposed. The formulas for K_f obtained by Neuber (1958), Peterson (1959), El Haddad & others (1979) and Tanaka & others (1981) are frequently used. McEvily & Gregor (1977) and recently Mura & Tanaka (1981) reviewed the ability of those equations in various special circumstances to predict K_f and proposed that Neuber's Equation (1958) can be used in most general cases but none of them produce consistent results.

Neuber's equation (1958) which relates the elastic stress concentration factor to fatigue notch factor can be written as follows:

$$K_f = 1 + \frac{(K_t - 1)}{[1+(\rho^*/r)^{1/2}]} \qquad (7)$$

where

r = radius at the notch-root (weld-toe),

ρ^*=experimentally determined material parameter.

The value of ρ^* may be determined for steels based on the ultimate strength S_u of the material (Graham 1968) in millimeters

$$\rho^* = 0.0254(2070 \text{ Mpa}/S_u \text{ Mpa})^{1.8}$$

or in inches

$$\rho^* = 10^{-3}(300 \text{ ksi}/S_u \text{ ksi})^{1.8}.$$

Proper determination of the fatigue notch factor K_f is important for estimation of fatigue crack initiation life. The plot of fatigue notch factor K_f (Eq. (7)) and K_t (Eq.

(6)), elastic stress concentration factor as a function of weld-toe root radius "r",is shown in Fig.2.3. From Fig.2.3 it is seen that with a decrease in "r" K_t always increases but K_f approaches a constant value of 2.0. For a conservative estimate of fatigue crack initiation life K_f should be taken at that maximum. Extending Neuber's hypothesis (Eq.(1)) to fatigue loading for the low and intermediate life region, where local yielding can occur, K_f was substituted for K_t (Eq.(3)) which gives the influence of notch-root in fatigue life.

The difficulty in selecting the K_f value arises because the notch root radius is not known precisely and thus weld toes could be considered to have any possible value of notch-root radius. The value of "r" should be decided in accordance with the value of fatigue notch factor K_f. In this study a root-radius of r=0.001in (0.0254mm) was considered corresponding to a K_f value of 1.851 which is very close to the K_f maximum value of $\cong$2.0. The value also gives a reasonable estimate of the elastic stress concentration factor K_t (Fig.2.3).

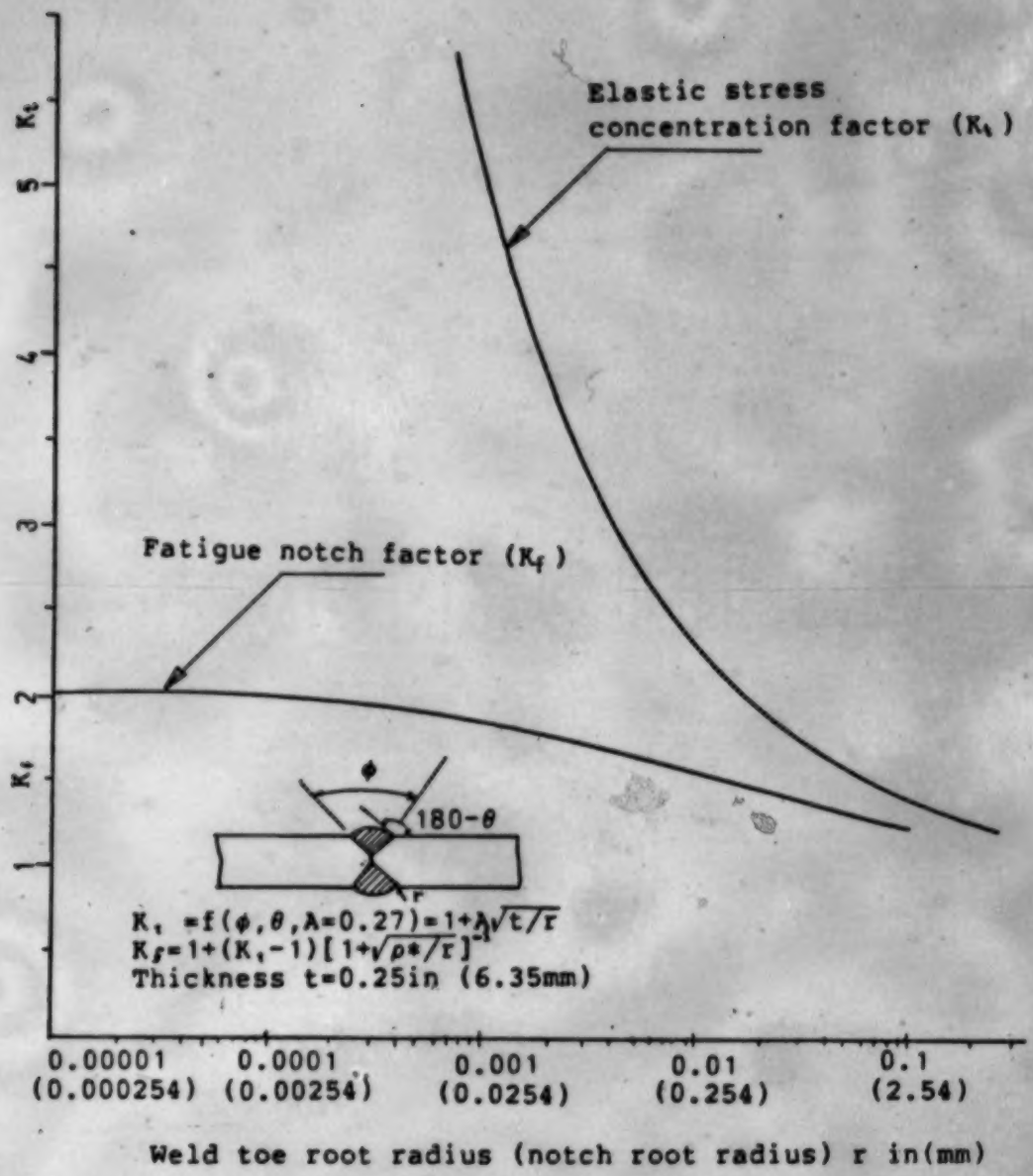

Figure 2.3 Fatigue notch factor & elastic stress concentration factor as a function of weld toe root radius.

2.1.5 Cyclic Stress-Strain Curve And Hysteresis Loops

Under dynamic loading conditions the local stress-strain curve at the weld toe follows the cyclic stress-strain curve. The stress-strain space (starting point of the hysteresis loop) is found from the intersection of Neuber's hyperbola and the cyclic stress-strain curve. While unloading it follows the hysteresis loop shape which is discussed below.

The cyclic stress-strain properties and hysteresis loop shape are determined by testing a smooth specimen under axial cyclic strain-controlled conditions. Landgraf & others (1969) defined the cyclic stress-strain curve as the locus of the tips of the stable hysteresis loops from several companion specimen tests at completely reversed constant strain amplitudes. They pointed out that this curve could be considered as a measure of steady cyclic deformation resistance of a material.

The equation for the cyclic stress-strain curve (Fig. 2.4)is given by,

$$\epsilon = \sigma/E + (\sigma/K')^{1/n'} \qquad (8)$$

where

ϵ = local strain,

σ = local stress,

K′=cyclic strength coefficient,

n′=cyclic strain hardening exponent.

It has been found (Wetzel 1968) that the hysteresis loops can be represented by a power function. Assuming the same exponent n′ the equation for the hysteresis loop can be found from the following conditions. One point on the cyclic stress-strain curve ($\Delta\epsilon/2$, $\Delta\sigma/2$) corresponds to the tip of the loop. Substituting these values for stress and strain in the above equation yields,

$$\Delta\epsilon/2 = \Delta\sigma/2E + (\Delta\sigma/2K')^{1/n'}. \qquad (9)$$

This represents the equation for the hysteresis loop. It is the same curve (cyclic stress-strain) except that the stress and strain are divided by a factor of two. The outer traces of separate loops have the same mathematical shape as the cyclic stress-strain curve. A point on a cyclic stress-strain curve and the tip of the hysteresis loop is shown in Fig.2.4. The monotonic and cyclic responses are not usually the same.

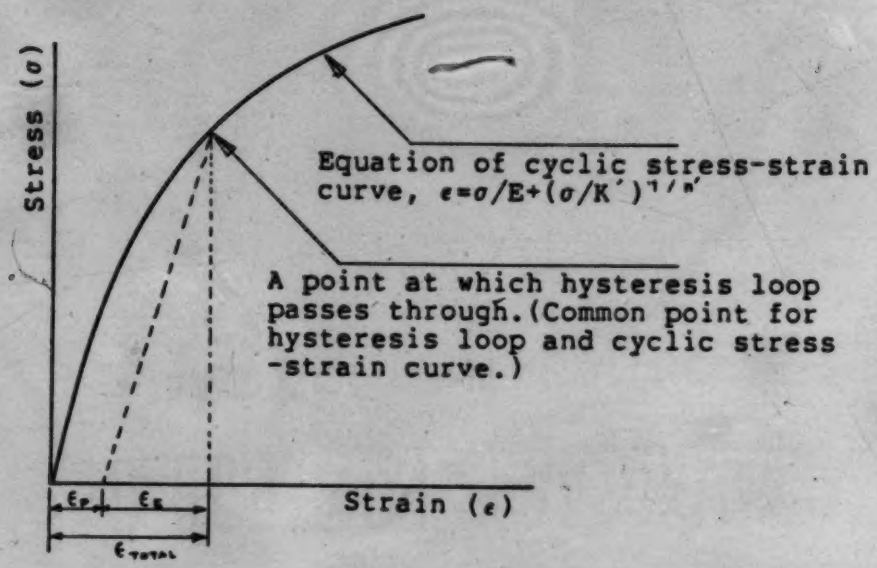
Stress (σ)
Equation of cyclic stress-strain curve, $\epsilon=\sigma/E+(\sigma/K')^{1/n'}$
A point at which hysteresis loop passes through.(Common point for hysteresis loop and cyclic stress -strain curve.)
Strain (ε)
ϵ_p
ϵ_e
ϵ_{total}

A point on a cyclic stress-strain curve.

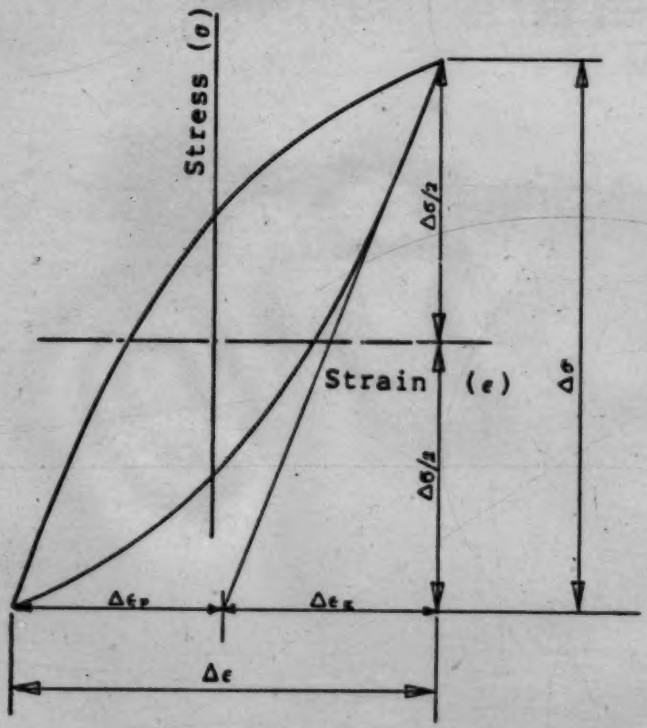

Figure 2.4 Tips of hysteresis loop and points on cyclic stress-strain curve.

2.1.6 Local Strain Analysis With Residual Stresses

In order to apply Neuber's idea which relates nominal stress-strain to local stress-strain (Neuber 1961) to the case of a weld with residual stresses it is necessary to determine $\Delta\sigma$, the local stress range and $\Delta\epsilon$, the local strain range. The simulation of the notch root stress-strain behaviour with initial residual stress at the weld toe $\sigma_{r,i}$, a nominal mean stress S_m, and a nominal stress range ΔS is shown in Fig. 2.5 (Reemsnyder 1981).

It is assumed that the notch root stresses and strain begin at some initial point "o" (Fig.2.5) representing the state of initial residual stress . At maximum stress S_{max}, σ and ϵ are established by the intersection of the cyclic stress-strain curve and the Neuber's hyperbola, C_a, i.e., point "a" in Fig. 2.5. Neuber's Rule (Eq. (5)) at S_{max} is

$$\sigma_{max}\,\epsilon_{max} = C_a$$

where

$$\sigma_{max} = K\sigma\, S_{max} + \sigma_{r,i},$$

$$\epsilon_{max} = K\epsilon\, e_{max} + \epsilon_{r,i}.$$

Evaluating,

$$C_a = K_f^2\,[S_{max} + \sigma_{r,i}/\,K\sigma]^2/E.$$

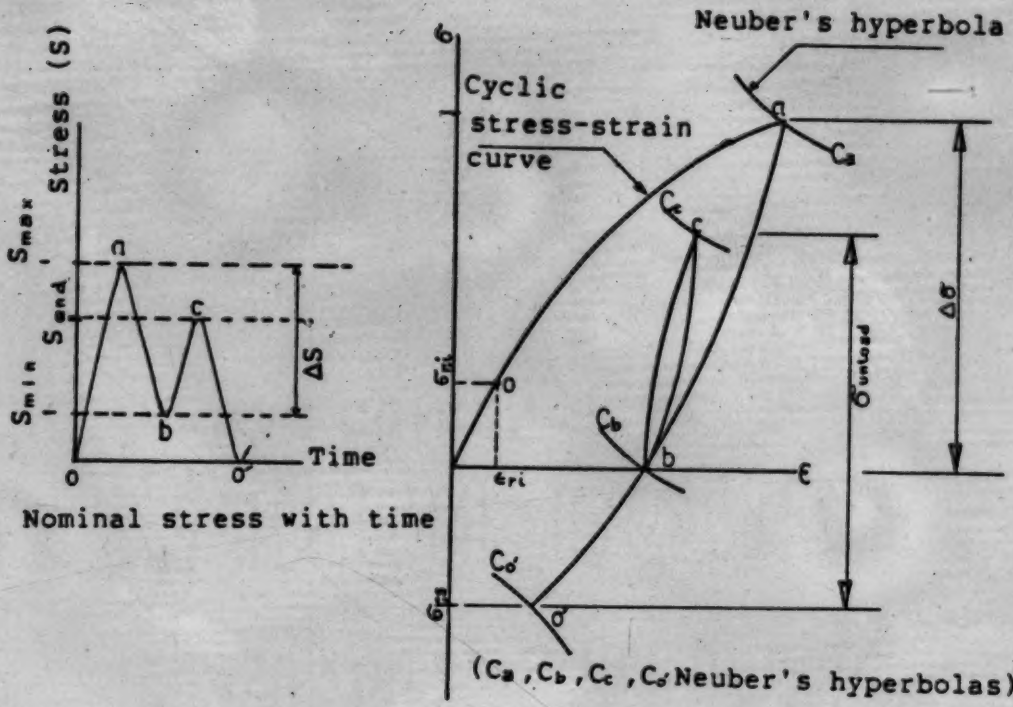

Figure 2.5 Notch-root stress and strain, $S_{end} > S_{min}$.

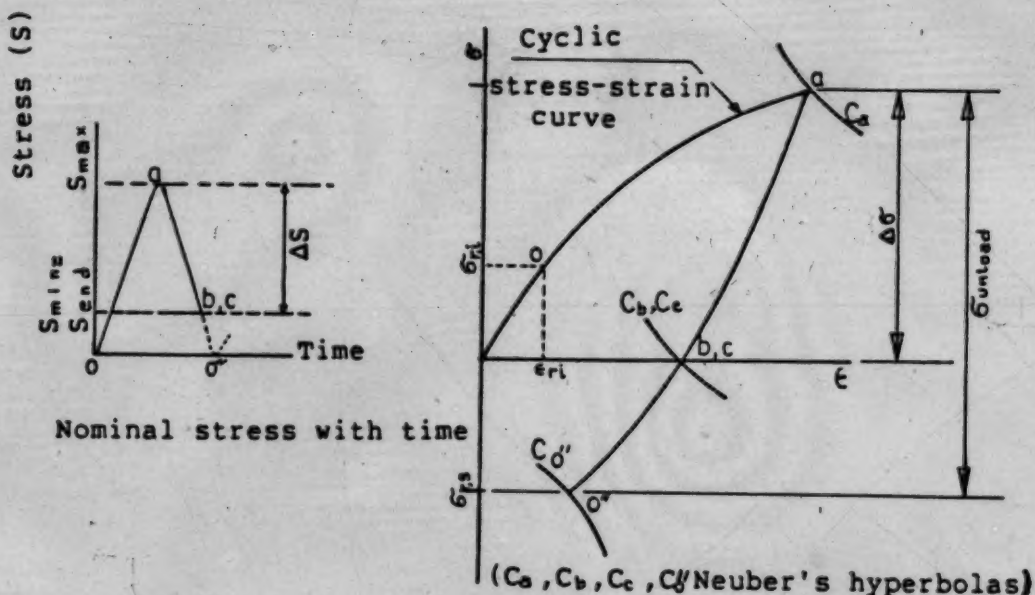

Figure 2.6 Notch root stress and strain, $S_{end} = S_{min}$.

Assuming linear elastic behaviour it can be found that

$$S_{max} + \sigma_{r,i} / K\sigma = E\,[e_{max} + \epsilon_{r,i} / Ke].$$

Combining the above equations and the equation for cyclic stress -strain (Eq.(8)) the following equation relating K_f and $K\sigma$ was developed:

$$K_f = \frac{K\sigma\, S_{max}\,[1+E/(K')^{1/n'}\{(K\sigma\, S_{max})^{(1-n')/n'}\}]^{0.5}}{[S_{max}+\sigma_{r,i}/K\sigma]} \quad . \qquad (10)$$

Equation (10) determines the value of $K\sigma$ from the known values of material properties, applied maximum stress range and K_f value. An accurate value of $K\sigma$ is important for the determination of local notch-root stress σ from the applied nominal stress. Reemsnyder (1981) determined the following relationship for K_f and $K\sigma$ which gives a value of local notch root stress less than the applied nominal stress from the basic definition of $K\sigma$ (i.e. $K\sigma=\sigma/S$).

$$K_f=K\sigma[1+\{E/(K')^{1/n'}\}\{K\sigma S_{max}+\sigma_{r,i}\}^{(1-n')/n']^{1/2} \qquad (10*).$$

Equation (10) can be solved for $K\sigma$ numerically by using Newton-Raphson's iterative technique. Once $K\sigma$ is known Ke can be computed from Eq.(3). The coordinates of point "a" (Fig.2.5) i.e (σ_{max}, ϵ_{max}) can be found by using the above expressions relating σ_{max} and ϵ_{max} respectively.

As the nominal stress S decreases, σ and ϵ follow the $\Delta\sigma$-$\Delta\epsilon$ curve (Eq.(9)) with origin at point "a". At S_{min}, σ and ϵ are obtained by the intersection of the $\Delta\sigma$-$\Delta\epsilon$ curve and the Neuber's hyperbola C_b. Using (Eq.(5)) at point "b"

and using Eq.(9) for the hysteresis loop (Eq.9), Reemsnyder (1981) obtained the following relationship:

$$K_f^2(\Delta S)^2/E=(\Delta\sigma)^2/E+(2)^{(n'-1)/n'}[(\Delta\sigma)^{(n'+1)/n'}/(K')^{1/n'}] \quad (11)$$

which can be solved numerically for $\Delta\sigma$.

The notch root residual stresses at the end of one stress cycle can be estimated using local-strain analyses. When the nominal stress at the end of a cycle S_{end} is greater than the nominal minimum stress S_{min}, the notch root stresses and strains follow the $\Delta\sigma$-$\Delta\epsilon$ curve (Eq.(9)) with origin at point "b" and then intersecting Neuber's hyperbola C_c at point "c" (Fig.2.5). Using Neuber's rule (Eq.(5)) at point c i.e.,

$$\sigma_{end}\,\epsilon_{end} = K_f^2\,[S_{end} - S_{min}]^2/E$$

and the hysteresis loop Eq.(9) it can be found that (Reemsnyder 1981),

$$K_f^2(S_{end}-S_{min})^2/E=[\sigma_{end}]^2/E+2^{(n'-1)/n'}\left[\frac{(\sigma_{end})^{(n'+1)/n'}}{(K')^{1/n'}}\right] \quad (12)$$

which can be solved iteratively for σ_{end}.

The notch residual stress subsequent to cyclic loading $\sigma_{r,s}$ can be determined by unloading the notch to zero nominal stress (see nominal stress-time curve Fig.2.5). The notch stress and strain follow the $\Delta\sigma$-$\Delta\epsilon$ curve (Eq.(9)) with origin at point "c" until they intersect the Neuber's hyperbola C_o' at point "o'"(Fig.2.5). Using Neuber's Rule (Eq.(5)) at point o', i.e

$$\sigma_{unload}\,\epsilon_{unload} = K_f^2\,(S_{end})^2$$

and Eq.(9) yields (Reemsnyder 1981):

$$K_f^2[S_{end}]^2/E=[\sigma_{unload}]^2/E+2^{(n'-1)/n'}\left[\frac{(\sigma_{unload})^{(n'+1)/n'}}{(K')^{1/n'}}\right] \quad (13)$$

which can be solved iteratively for σ_{unload}.

The notch residual stress subsequent to cyclic loading $\sigma_{r,s}$ can then be found as:

$$\sigma_{r,s} = \sigma_{max} - \Delta\sigma + \sigma_{end} - \sigma_{unload} \quad (14)$$

for the case when $S_{end} > S_{min}$.

For the case where $S_{end} = S_{min}$ the notch stress and strain during unloading follow the $\Delta\sigma$-$\Delta\epsilon$ curve (Eq.(9)) with origin at point "a" from "b" to point "o''" (Fig.2.6). Combining Neuber's rule (Eq.(5)) at point "o''" i.e.,

$$K_f^2\,(S_{max})^2/E = \sigma_{unload}\,\epsilon_{unload}$$

and Eq.(9) yields (Reemsnyder 1981),

$$K_f^2[S_{max}]^2/E=[\sigma_{unload}]^2/E+2^{(n'-1)/n'}\left[\frac{(\sigma_{unload})^{(n'+1)/n'}}{(K')^{1/n'}}\right] \quad (15)$$

which can be solved iteratively for σ_{unload}. The residual stress subsequent to cyclic loading is given by

$$\sigma_{r,s} = \sigma_{max} - \sigma_{unload} \quad (16)$$

for the case when $S_{end} = S_{min}$.

From the preceding sections the change of initial residual stress ($\sigma_{r,i}$) to residual stress subsequent to

cyclic loading ($\sigma_{r,s}$) is known. By simulating the effect of residual stress at the weld toe on the nominal load ΔS, Neuber's Eq.(5) can be modified to give the actual local stress-strain conditions at the weld toe.

Gurney (1979), Morrow & others (1959) have suggested that residual stresses from the welding processes may be treated as mechanical prestressing. The residual stress acting in a transverse direction on an element of material at the weld toe was measured experimentally and it was found that it varies from nearly a half to the full yield strength of the base metal. It is also assumed that the HAZ and WM which are often of higher strength than the base metal cannot be subjected to residual stresses higher than the yield strength of the base metal.

The residual stresses at the weld toe may be simulated as shown in Fig.2.7 considering an infinitely long weld to avoid the triaxial stress pattern at the ends. A nominal stress of (σ_r / K_t) is then remotely applied to produce a local stress equal to the residual stress σ_r from welding. The nominal stress range ΔS is then added to give (ΔS + σ_r/K_t) which is equivalent to the remote stress range ΔS in Neuber's Eq.(5).

Considering the initial residual stress $\sigma_{r,i}$ the first cycle is bounded by:

$$K_f^2 \, [\Delta S/(1-R_{eff})+\sigma_{r,i}/K_t]^2/E = \Delta\sigma \, \Delta\epsilon \qquad (17)$$

where R_{eff} is the effective stress ratio which accounts for

the effect of initial residual stress. It is assumed that after the first cycle the initial residual stress changes to $\sigma_{r,s}$ according to Eq.(14) or Eq.(16). For the subsequent cycle Neuber's equation (Eq.(5)) is considered as:

$$K_f^2 \, [\Delta S + \sigma_{r,s}/K_t]^2/E = \Delta\sigma \, \Delta\epsilon \qquad (18)$$

Equations (17) and (18) were derived in this study by modifying Neuber's equation(Eq.(5)).

The simulation of weld toe stress-strain behaviour in the presence of an initial residual stress $\sigma_{r,i}$, a nominal mean stress S_m, and a nominal stress range ΔS are shown in Figs. 2.5 & 2.6. The initial residual stress $\sigma_{r,i}$ at the weld toe does not remain constant, but changes in sign and/or magnitude to a new value $\sigma_{r,s}$ depending on the cyclic properties of the material and loading conditions after the nominal "set-up cycle" was applied (Figs. 2.5 & 2.6). Initial residual stresses subsequent to cyclic loading therefore, change due to weld toe notch-root plasticity.

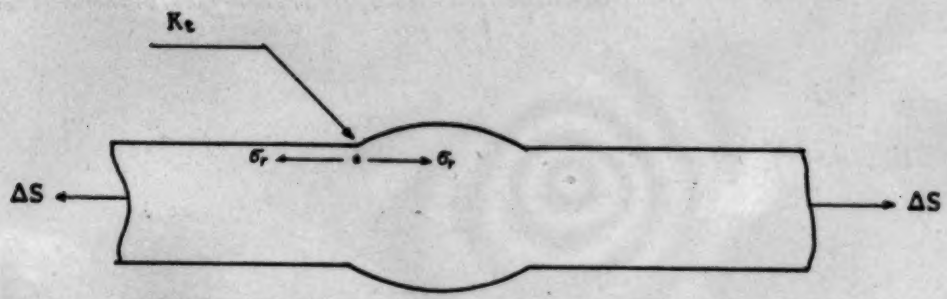

Residual stress (σ_r) and elastic stress concentration factor (K_t) at the weld toe.

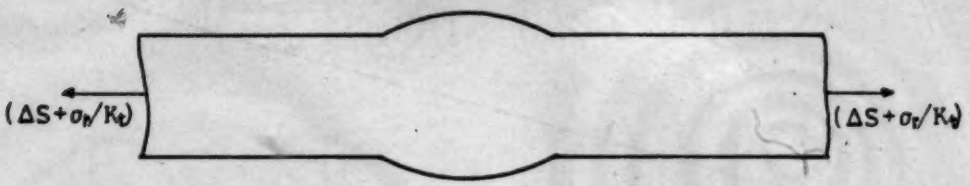

Nominal stress equivalent to σ_r/K_t applied at the end due to residual stress and elastic stress concentration factor. The total nominal stress at the end becomes $(\Delta S+\sigma_r/K_t)$.

Neuber's equation (Eq.(5)):

$$K_f^2\,[\Delta S + \sigma_r\ /K_t]^2/E = \Delta\sigma\ \Delta\epsilon$$

Figure 2.7 Simulation of residual stress at the weld toe by elastic superposition and Neuber's rule (Eq.(5)).

2.1.7 Strain-Life Relation

To calculate the crack initiation life the damage rule needs to be satisfied. To perform the damage calculation, four cyclic properties σ_f', ϵ_f', b and c along with the knowledge of $\Delta\sigma$ and $\Delta\epsilon$ are required. To obtain these properties experiments which establish strain-life ($\Delta\epsilon/2$ vs. $2N_f$) relations are required. These cyclic properties are obtained from smooth specimen tests.

The fatigue behaviour of a smooth specimen under reversed cyclic-strain can be characterized by four material properties that relates the strain amplitude to the fatigue life (Manson & Hirschberg 1964, Wetzel 1968 and Stadnick & Morrow 1972). Manson & Hirschberg (1964) have shown that the resistance of a metal to total strain cycling can be considered as the summation of its elastic and plastic strain resistances:

$$\Delta\epsilon/2 = \Delta\epsilon_e/2 + \Delta\epsilon_p/2$$

and

$$\Delta\epsilon/2 = \sigma_f'(2N_f)^b/E + \epsilon_f'(2N_f)^c \qquad (19)$$

where

σ_f' = fatigue strength coefficient,

ϵ_f' = fatigue ductility coefficient,

b = fatigue strength exponent,

c = fatigue ductility exponent,

$2N_f$ = number of reversals to failure.

When the mean stress σ_0 is present then Eq.(19) can be

corrected (Graham 1968) as shown below:

$$\Delta\epsilon/2 = (\sigma_f'-\sigma_0)(2N_f)^b / E + \epsilon_f'(2N_f)^c .$$

An additional useful index of the fatigue mechanism is the transition fatigue life $2N_{t,r}$ or transition strain $\epsilon_{t,r}$. The transition fatigue life is the life of a smooth specimen under strain control at which the elastic $\Delta\epsilon_e/2$ and plastic $\Delta\epsilon_p/2$ strain amplitudes are identical and are given as

$$2N_{t,r} = (\epsilon_f' E / \sigma_f')^{1/(b-c)}$$

and

$$\epsilon_{t,r} = \sigma_f'/E \left[(2N_{t,r})^b+\epsilon_f'(2N_{t,r})^c\right].$$

Once the five constants σ_f', b, ϵ_f', c and E are known for a material, a fatigue analysis can be performed if the data on the load spectrum is available. These constants are obtained from fatigue tests described in Chapter III. The experimental curve representing "strain - life" relations (Eq.(19)) is shown in Chapter IV.

2.1.8 Cumulative Fatigue Damage Analysis

Several cumulative fatigue damage rules are available to calculate the crack initiation life under constant stress or strain amplitudes (Manson 1964, Manson & others 1967, Thang & others 1971, Dowling 1972). For a cumulative damage calculation a knowledge of the elastic and plastic strain and mean stress for each cycle is necessary.

The damage in terms of elastic strain amplitude of a particular reversal is obtained from (Basquin 1910),

$$[1/2N_f]_\varepsilon = [\ (\Delta\sigma/2)/\ \sigma_f']^{-1/b}.$$

The damage in terms of plastic strain amplitude is given by

$$[1/2N_f]_p = [(\Delta\varepsilon_p/2)/\ \varepsilon_f']^{-1/c}.$$

If $(\sigma_{max} + \sigma_{r,1}) \geq \sigma_y'$, (cyclic yield stress) in the first cycle the plastic damage criterion is considered, otherwise elastic conditions prevail. The damage due to mean stress σ_o may be calculated according to Martin (1973)

$$[1/2N_f]_o = (\varepsilon_f')^{1/c}[\{(\Delta\sigma/2)/K'\}^{-1/n'c}][(1-\sigma_{o,2N}/\sigma_f')^{1/n'c}-1].$$

The mean stress relaxation criterion is taken according to Jhansale & Topper (1973),

$$\sigma_{o,2N} = \sigma_{o,1}(2N-1)^k \qquad (20)$$

where

$\sigma_{o,2N}$ = Mean stress at reversal 2N,

$\sigma_{o,1}$, initial mean stress $= \dfrac{(1+R)\ \Delta S/2}{(1-R)}$,

k = relaxation exponent which is dependent on strain amplitude.

For mild steel the relaxation exponent k can be taken as (Higashida & others 1978)

$$k = -4625\ [\frac{\Delta\varepsilon_p/2}{E\ \varepsilon_{tr}}]\ \text{ksi}^{-1}. \qquad (21)$$

The total damage per reversals $D_{i,t}$ can be calculated as,

$$D_{i,t} = [(1/2N_f)_t \text{ or } (1/2N_f)_p] + [1/2N_f]_o. \qquad (22)$$

The crack initiation life is assumed to end when the linear cumulative damage rule (Palmgren 1968, Miner 1945) is satisfied, i.e.,

$$\sum_{i=1}^{2N_I} D_{i,t} = 1.0 \qquad (23)$$

where $2N_I$ is the number of reversals necessary to initiate a crack.

2.2 Fatigue Crack Propagation Life For A Weld

The successful application of fracture mechanics concepts enables an estimation of the remaining crack propagation life of the welded structures (N_p). A large portion of the fatigue life of welded joints is spent in fatigue crack propagation from an initial flaw size a_i to a terminal flaw size a_f.

Many theories and empirical equations relating fatigue crack propagation rate (da/dN_p) to stress intensity factor range ΔK have been proposed by several researchers (Paris & Erdogen 1963, McEvily 1965, Forman & others 1967, Pelloux 1970, Throop & Miller 1970, Elber 1971) In this study, the fatigue crack propagation life for a butt-weld was estimated by using Forman's equation (1967) of crack propagation. This is an improved theory over the frequently used Paris' crack propagation law (1963). Forman's theory assumes that the crack tip stress-intensity factor range ΔK is the controlling variable for analyzing crack-extension rates. This also takes into account the effective load ratio R_{eff} and the instability when the stress-intensity factor approaches the fracture toughness of the material K_c. Forman's equation is written in the following form:

$$\frac{da}{dN_p} = \frac{C_R(\Delta K_{eff})^m}{(1-R_{eff})\,K_c - \Delta K_{eff}} \qquad (24)$$

where

a = half crack length,

N_p = fatigue crack propagation life,

K_c = critical stress intensity factor for fracture,

$K = YS\sqrt{\pi a}$ (fracture mechanics stress intensity factor),

ΔK = range of stress intensity factor ($K_{max} - K_{min}$),

m, C_R = crack growth exponent & coefficient respectively,

R_{eff} = fracture mechanics effective stress ratio,

Y = generalized correction factor (function of crack length and specimen geometry).

In Eq.(24) the effective stress ratio R_{eff} takes into account the effect of residual stresses in fatigue. The effective stress ratio R_{eff} can be described in terms of nominal loads and initial residual stress as shown in the following equation.

$$R_{eff} = K_{min} / K_{max} = \left[\frac{\sigma_{r,i} + S_{min}}{\sigma_{r,i} + S_{max}}\right].$$

From Eq.(24) the cycles required to propagate a crack of initial size a_i to a final crack length a_f are then:

$$N_p = \int_{a_i}^{a_f} \frac{(1-R_{eff})\, K_c - \Delta K_{eff}}{C_R(\Delta K_{eff})^m}\, da. \qquad (25)$$

Equation (25) can be integrated numerically to obtain the fatigue crack propagation life. The evaluation of the required parameters are discussed in the following paragraphs. Equation (25) also provides a satisfactory description of crack behaviour for the mid-range of crack growth rates. The complete variation of the rate of crack propagation (da/dN_p) with range of stress intensity factor (ΔK) is approximately sigmoidal in shape and bounded at the extremes by ΔK_{th} the threshold range of stress intensity

factor and critical stress intensity factor K_c. As ΔK is decreased below the ΔK_{th} the crack propagation rate diminishes rapidly. This implies that a crack may not propagate unless ΔK exceeds ΔK_{th}. Few empirical relations are available for the range of threshold stress intensity factor (Rolfe & Barsom 1977, Garwood 1978, Backlund 1982). Garwood (1978) proposed the following relationship:

$$\Delta K_{th} = (190-144R)\ Nmm^{-3/2} \text{ or, } 5.46(1-0.76R)\ ksi\sqrt{in}.$$

The initial crack length a_i is taken as the crack size when the initiation life N_i is complete. The initial crack length for welds may be taken as the length of some pre-existent weld defect or flaw but a_i should not be smaller than the threshold crack size a_{th}. The threshold crack length a_{th} may be estimated from the threshold range of stress intensity factor ΔK_t and the stress range ΔS (Mattos & Lawrence 1977)

$$a_{th} \geq [1/(\Pi A^2)]\ [\frac{\Delta K_{th}}{\Delta S}].$$

By knowing ΔK_{th} and ΔS an approximate result can be obtained for a_{th} and consequently a_i. The initial crack length can also be approximated by the following relationship (Lawrence & others 1981),

$$a_i = \frac{0.1878\ \sqrt{t}}{A\ Su}\ (ksi).$$

Estimations of the total fatigue life from propagation theory alone assumes that there exists a small initial

defect resulting from the fabrication process at the weld toe. This, however, may require a_i less than a_{th} especially for long fatigue lives.

In order to carry out a fracture mechanics analysis of a crack at the weld toe it is necessary to know the relevant values of the stress intensity factor. For a butt-weld with remote axial and bending stresses, along with the effect of residual stress intensity factor K_R, the stress intensity factor was obtained by superposing all the above effects.

$$\Delta K = \Delta K_A + \Delta K_B + K_R \qquad (26)$$

where

ΔK_A, ΔK_B = range of stress intensity factor for axial loading and pure bending stresses respectively.

Several researchers have studied the influence of weld geometry, material properties and loading conditions on propagation life (Lawrence 1973, Maddox 1974, Burk & Lawrence 1977, Gurney 1979). Maddox (1974) has considered the influence of crack shape, plate thickness and weld reinforcement shape for a weld through a series of corrections to the stress intensity factor range:

$$\Delta K = Y \, \Delta S \sqrt{\pi a} \, . \qquad (27)$$

Lawrence (1973) has used an elastic superposition method to study the influence of weld geometry, material properties and the combined effect of bending and axial loads which is written as:

$$\Delta K = \Delta S \sqrt{\Pi a}\ f(c/t,\ \theta\ ,\phi)$$

where the function $f(c/t,\theta,\phi)$ is a correction factor for weld geometry, loading type and thickness . The stress intensity factor for bending ΔK_B can be written in terms of ΔS_B nominal extreme fibre stress due to the bending component of load, coefficients of bending, plate thickness t and crack length:

$$\Delta K_B = \Delta S_B \sqrt{\Pi a}\ f(b/t,\theta,\phi).$$

Similarly,

$$\Delta K_A = \Delta S_A \sqrt{\Pi a}\ f(c/t,\theta,\phi)$$

where

ΔS_A = remote axial component of load and $f(c/t,\theta,\ \phi)$ represents the coefficients for axial loading, plate thickness and crack length.

The effect of residual stresses on the fatigue crack growth in welds under constant amplitude loading must be accounted for. Studies by Kapadia & Imholf (1977) and James (1973) have shown that welding residual stresses are responsible for higher or lower fatigue crack growth rates in comparison with unwelded base material. It has been shown that the crack growth rate in the HAZ and the WM are similar to what can be expected to occur in the base material (Maddox 1972, Parry & others 1972a).

For an estimation of the residual stress intensity factor K_R Kanazawa's (1961) formula in combination with the actual residual stress distribution near the weld toe σ_r is considered. In this study the actual residual stress distribution is obtained from the experimental stress measurements,

$$K_R = \int_{x=-a}^{x=a} \sigma_r(x)\, G(x)dx \qquad (28)$$

where

G(x) is a function of half crack length a and specimen shape. It is zero at x=-a and goes to infinity at a crack length of x=+a.

$$G(x) = \left[\frac{2\sin\pi(a+x)/W}{W \sin(2\pi a)/W \cdot \sin\pi(a-x)/W}\right]^{1/2}.$$

It was assumed that the distribution of residual stress at the weld toe is a cosine shape in the middle and sloping downwards at the ends (Fig.2.8) and remain unchanged under fatigue loading. These assumptions may overestimate the effect of residual stress because the residual stress redistributes after fatigue cycling.

Glinka (1979) and Nelson(1982) studied the effect of residual stresses on fatigue crack growth in steel weldments using Kanazawa's formula (1961) for constant and variable amplitude loadings. Three specimens (unwelded, transverse, and longitudinal butt-welds) were evaluated with the introduction of a stress raiser. Glinka (1979) used a simplified rectangular distribution instead of actual

residual stress distribution. It was concluded that the inclusion of the effect of residual stresses in the theoretical analysis permits a realistic prediction of the fatigue life of welded structures.

The following formulation for the distribution of residual stress (σ_r) was derived in this study. The actual shape of the distribution of the residual stress at the weld toe was obtained experimentally. The distribution of residual stress is shown in Fig. 2.8. This correlates closely with the actual shape found from experiments. Since the residual stress redistributes itself during fatigue cycling it is not possible to know the exact distribution. Therefore, the initial residual stress is taken for the propagation part of the model.

From Fig.2.8 the nondimensional term ϵps is written as:

$$\epsilon ps = [\ X + CDIFF\ ] / HPI$$

where

CDIFF = distance between centre of the specimen and centre of crack,

X = distance from centre of the crack to the intersection of the residual stress distribution,

HPI = a constant according to the distribution of residual stress.

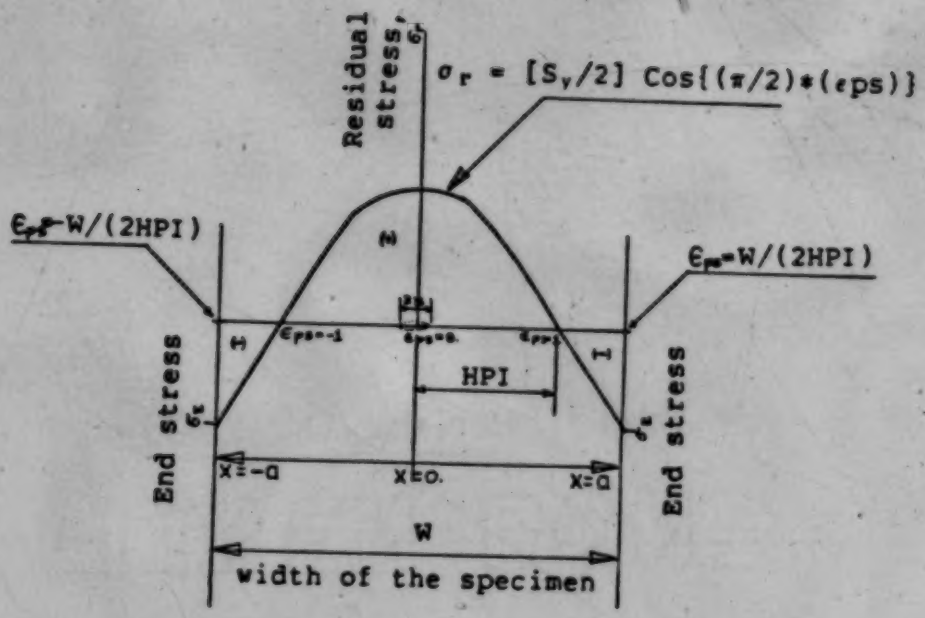

Figure 2.8 Distribution of residual stress at the weld toe.

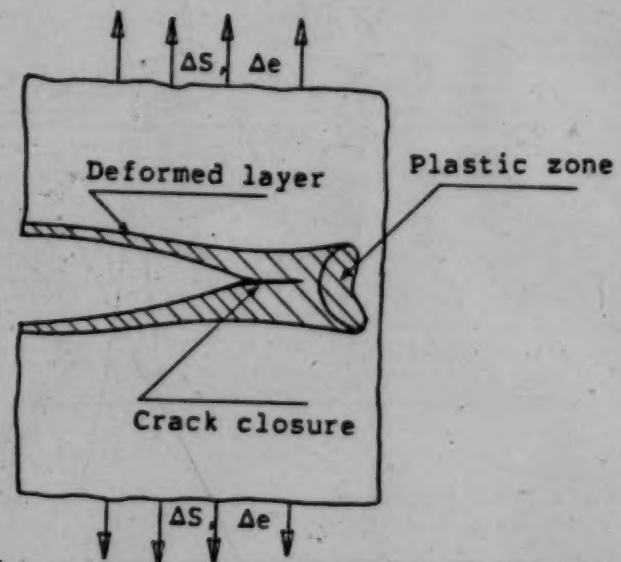

Figure 2.9 Fatigue crack closure concepts. Plastically induced crack closure.

The distribution of residual stress from ϵ_{PS}=-1 to ϵ_{PS}=+1 can be taken as:

$$\sigma_r = [S_y/2]\ \mathrm{Cos}\{(\pi/2)*(eps)\}. \qquad (29a)$$

For the straight line portion, that is ϵ_{PS}=+1 to W/(2HPI),

$$\sigma_r = (eps-1)*\left[\frac{-\sigma_E}{W/(2\ HPI)-1}\right] \qquad (29b)$$

and from ϵ_{PS}=-1 to -W/(2HPI),

$$\sigma_r = [eps+1]*\left[\frac{\sigma_E}{W/(2HPI)-1}\right] \qquad (29c)$$

where σ_E is the end stress (see Fig. 2.8).

The non-dimensionalized equations (Eqs.(29a),(29b), (29c)) which give the residual stress distribution along the toe of the butt-weld were derived in this study. The location of the crack could be considered anywhere along the weld toe. Numerical integration over the crack length was performed for the K_R by using Simpson's Rule as the crack propagates from the initial crack length a_i to a final crack size a_f. Combining the effect of axial, bending and residual stress intensity factors Eq.(26) for ΔK can be solved.

To evaluate the effective stress intensity factor ΔK_{eff} in Eq.(25) it is required to consider the influence of the crack opening factor C_f (Elber 1970, 1971, Barsom 1973, Socie 1975, and Bell & Wolfman 1976) The range of effective stress intensity factor can be written in terms of crack opening factor and the range of stress intensity factor as shown below:

$$\Delta K_{eff} = C_f \, \Delta K. \qquad (30).$$

The crack opening factor at any stress ratio $C_f(R)$ is a function of range of stress intensity factor and crack opening stress intensity factor. The crack opening factor, thus takes into consideration the loading condition, residual stress intensity factor and the crack opening stress S_{op}. The crack opening factor at any stress ratio $C_f(R)$ can be expressed as:

$$C_f(R) = \frac{\Delta K - \Delta K_{open}}{\Delta K} \qquad \text{when } \Delta K_{open} < \Delta K$$

$$= 0.4 \text{ to } 1.0 \qquad \text{when } \Delta K_{open} \geq \Delta K$$

$$C_f(R=0.0) \cong 0.5 \qquad \text{for steel,}$$

where

ΔK_{open} is the crack opening stress intensity factor range,

$$\Delta K_{open} = K_R + \Delta K_B + (S_{max} - S_{op}) \, f(c/t, \theta, \phi).$$

The crack opening stress (S_{op}) can be approximated as (Elber 1976):

$$S_{min} = 1.25 \, [\, (1.6 \, S_{max} \, S_{op} - 0.79 \, S_{max})^{1/2} - 0.1 \, S_{max}].$$

The above equation can be solved iteratively for S_{op}. Finally, the crack growth coefficient considering the crack opening concept can be found as (Socie 1975):

$$C_R = C \, [C_f(R)/C_f(R = 0.)]^m \qquad (31)$$

where C is crack growth rate constant for materials at the crack initiation sites.

In recent years a considerable amount of work has been done on the concept of crack opening (or crack closure) for fatigue crack growth. Various techniques for estimating crack opening have been employed which include surface measurements by displacement gauges, strain gauges placed across the crack surface and fractographic measurements. Experimental and analytical investigations have been shown that $K_{op}/K_{max} \cong S_{op} / S_{max} \cong 0.66$ for alloy steel when R=0 (Kobayashi & others 1981). The K_{op} represents the level of stress intensity factor where the opposing crack surfaces are no longer in contact. Elber (1971) has proposed this plasticity induced crack opening concept in fatigue crack growth as shown in Fig.2.9. It shows that a crack in a fatigue specimen is fully open for only a part of the load cycle even when the loading cycle is fully in tension. For the same material various techniques give different values of K_{op} / K_{max}. The reason is due to the fact that surface measurements may not reflect inner crack closure in the bulk of the material.

The fatigue crack propagation properties K_c , m and C are assumed on the basis of material properties (see Appendix D). Finally, the crack propagation life (N_p) can be estimated by integrating Eq.(25) over the crack length.

2.3 Method Of Analysis For Fatigue Life

The total fatigue life of a butt-weld containing residual stresses was estimated based on the crack initiation and crack propagation models as described in this Chapter. The initiation life was based on the damage integral (Eq.(23)) which allowed the damage during cycling to vary as the mean stress relaxed. The influence of cyclic hardening and softening on mean stress was ignored in the analysis. The crack propagation life was calculated using Eq.(25)). Combining N_I and N_T gives the total life model.

The same model was also used to study the effect of mechanically or thermally induced compressive residual stresses on the fatigue life of transverse butt-welded specimens. For the estimation of the total fatigue life due to various mechanical and thermal treatment (i.e., annealing, tensile preloading, glass and steel shot-peening, single and multiple point hammer peening, and stress-peening) residual stresses along the weld toe were measured experimentally. The measured values of the residual stresses (with sign) were used in the estimation of initiation and propagation lives while assuming the initial residual stress due to welding as zero after the treatment.

In this study the effect of residual stresses are considered in both cases of crack initiation and crack propagation along with the effect of material properties, mean stress relaxation behaviour, weld geometry and the effect of bending stresses on the specimen. The concepts of

local stress-strain analysis are used which take into account the material properties of the critical locations, the severity of the notches, the initial residual stress and the remotely applied stress range. Figure 2.10 schematically illustrates the fatigue analysis for the calculation of total fatigue life. Comparisons of the total fatigue life prediction with actual data are made by testing Columbium-50 steel welded specimens.

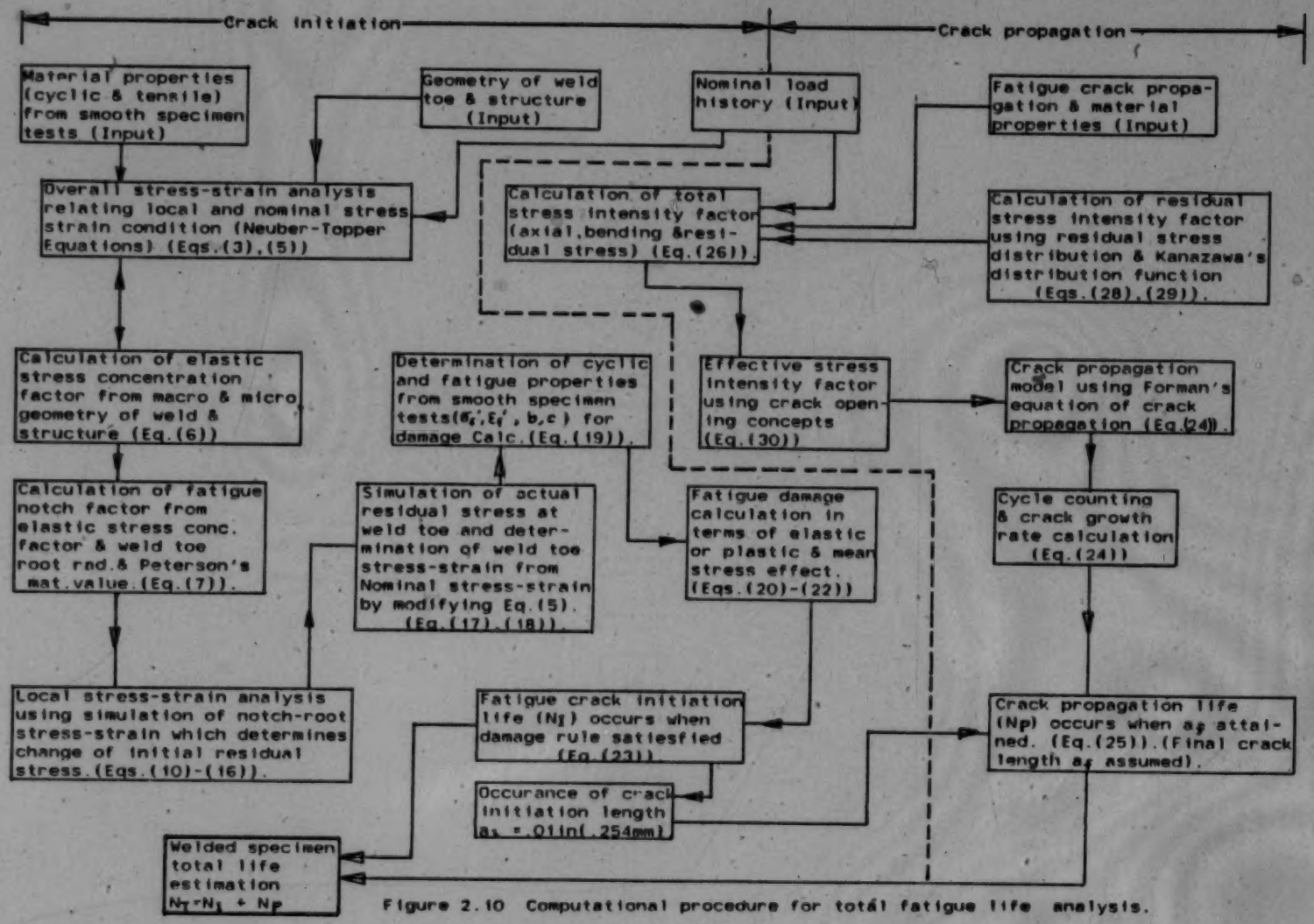
Crack initiation
Crack propagation
Material properties (cyclic & tensile) from smooth specimen tests (Input)
Geometry of weld toe & structure (Input)
Nominal load history (Input)
Fatigue crack propagation & material properties (Input)
Overall stress-strain analysis relating local and nominal stress strain condition (Neuber-Topper Equations) (Eqs.(3),(5))
Calculation of total stress intensity factor (axial,bending &residual stress) (Eq.(26)).
Calculation of residual stress intensity factor using residual stress distribution & Kanazawa's distribution function (Eqs.(28),(29)).
Calculation of elastic stress concentration factor from macro & micro geometry of weld & structure (Eq.(6))
Determination of cyclic and fatigue properties from smooth specimen tests(σ_f',ε_f', b,c) for damage Calc.(Eq.(19)).
Effective stress intensity factor using crack opening concepts (Eq.(30))
Crack propagation model using Forman's equation of crack propagation (Eq.(24)).
Calculation of fatigue notch factor from elastic stress conc. factor & weld toe root rad.& Peterson's mat.value.(Eq.(7)).
Simulation of actual residual stress at weld toe and determination of weld toe stress-strain from Nominal stress-strain by modifying Eq.(5). (Eq.(17),(18)).
Fatigue damage calculation in terms of elastic or plastic & mean stress effect. (Eqs.(20)-(22))
Cycle counting & crack growth rate calculation (Eq.(24))
Local stress-strain analysis using simulation of notch-root stress-strain which determines change of initial residual stress.(Eqs.(10)-(16)).
Fatigue crack initiation life (N_i) occurs when damage rule satiesfied (Eq.(23))
Crack propagation life (Np) occurs when a_f attained. (Eq.(25)).(Final crack length a_f assumed).
Occurance of crack initiation length a_i =.01in(.254mm)
Welded specimen total life estimation $N_T=N_i + N_p$

Figure 2.10 Computational procedure for total fatigue life analysis.

3. EXPERIMENTAL PROGRAM

3.1 Scope Of The Experimental Investigation

The choice of the appropriate experimental method for evaluating the total fatigue life of welded structures depends on an accurate determination of the fatigue crack initiation and propagation lives. The traditional approach has been based on the "stress-life" curve. High cycle stress-controlled fatigue tests are used for the region where the strain remains essentially elastic. Low-cycle ($<10^4$ cycles and at relatively high stress) strain controlled fatigue tests are used for the crack initiation life in the region where the strain is mainly plastic. High cycle fatigue tests were performed to study the effect of residual stresses on the fatigue life of welded joints. Low cycle strain-controlled tests were performed on the base material for the determination of cyclic and fatigue properties. These properties were used in the calculation of crack initiation life of the welded structures.

For a welded joint it is necessary to calculate the cyclic stress-strain and fatigue properties of the WM and the HAZ materials for accurate determination of total fatigue life. These properties are obtained from the micro-hardness readings in these regions using the empirical relationship (Graham 1968, Landgraf 1970, and Chang & Lawrence 1981) established from the micro-hardness readings. The equations necessary to calculate these properties are

shown in Appendix C. More accurate determination of these properties requires the proper simulation of the HAZ microstructures. This can be done by uniformly reproducing the weld thermal cycle in the specimens. The specimens should be of large enough size for normal method of fatigue testing. This was not possible at the present time, due to lack of proper facilities.

Experiments were designed to obtain the base material properties for the prediction of total fatigue life and to obtain the experimental data ("S-N" curve) for mechanically and thermally treated welded joints. High cycle, pulsating tension tests were performed for a "stress-life" curve and to study the effect of residual stresses. Determination of the base metal properties are discussed in the following section.

3.2 Determination Of Material Properties

The crack initiation life ends when the cumulative damage criterion is satisfied. To determine the damage criteria and the cyclic behaviour of the material under the influence of a mean stress the cyclic and tensile properties of the base metal are needed. Cyclically stabilized stress-strain curves are an important characterization of the cyclic response of the material as the tensile properties of the material are not the same as the cyclic properties due to the formation of cyclic plasticity during the fatigue loading. To study both properties, base material

cylindrical specimen were used for cyclic and fatigue properties while base metal flat specimens were used for the tensile material properties.

3.2.1 Tensile Test

For the monotonic tension tests a 2000 lbs (8895N) Instron, open loop, servocontrolled, axial, hydraulic test system was used. A MTS clip-on extensometer with a one inch (25.4mm) gauge length was used on a rectangular shaped specimen (Fig. 3.1). The transducer signals (load and strain) were recorded on an X-Y plotter. Strain was controlled before necking and then stroke was controlled to failure. The material properties were then calculated from the plot of the load-strain curve and the dimensions of the specimen before and after the tests. True strains and true stresses were calculated from the engineering strains and nominal stresses respectively. The results obtained are discussed in Chapter IV.

3.2.2 Cyclic Strain-Controlled Test

For the determination of cyclic stress-strain and fatigue properties Columbium-50 base metal cylindrical specimens were cut and carefully machined from 0.25 inch (6.35mm) thick plate to form cylindrical specimens. After machining the specimens were mechanically polished with three successively finer grades of emery paper to the final dimension and geometry shown in Fig. 3.2.

Cyclic stress-strain properties were determined by testing smooth polished specimens under axial cyclic strain-controlled conditions. The cyclic stress-strain curve was obtained from the locus of the tips of stable true stress-strain hysteresis loops obtained from companion test specimens (several specimens were tested and stabilized hysteresis loops were taken) and are shown in Figs. 3.3 and 3.4.

Testing was conducted on a MTS closed-loop servo-controlled hydraulic test system using a 0.5 inch (12.7mm) gauge length clip-on extensometer for the measurement of strains under strain-controlled conditions. Proper axial alignment was critical for this small specimen to prevent bending or complete buckling of the specimen during the compressive portion of the loading cycle. Amplified signals from the extensometer and load-cell were recorded at predetermined intervals on an X-Y recorder to determine cycle-dependent changes in stress and plastic strain amplitudes. Tests were conducted at frequencies from 0.1 to 5 Hz at room temperature. In order to maintain isothermal conditions during the tests, tests were run at these lower frequencies. For zero mean strain condition and for stress ratio R=-1 a full sine wave form was used whereas for non zero mean strain a "Haver Sine" wave form was used. The cylindrical shaped specimens were cycled to failure at essentially a constant strain range to determine cyclic stress-strain properties. Because of the limitation in the

size of the specimen the maximum strain amplitude was 0.009. The data obtained from these tests were used to determine the "strain-life" curve which in turn determined the fatigue properties (σ_f', ϵ_f', b and c). Experimental data from a few of the specimens were also used to study the cyclic hardening and softening behaviour of the base metal. The results obtained are shown in Appendix B.

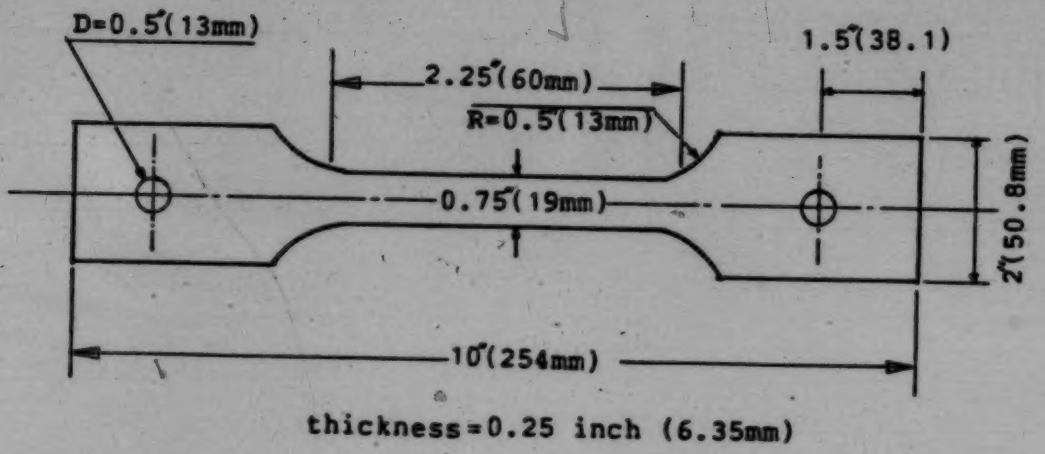

Figure 3.1 Specimen geometry for tensile test.

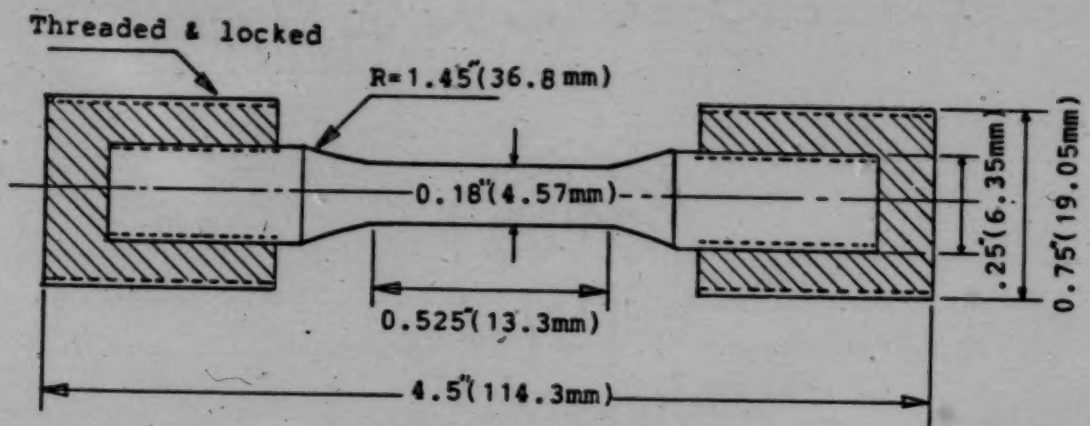

Figure 3.2: Specimen geometry for cylindrical specimen.

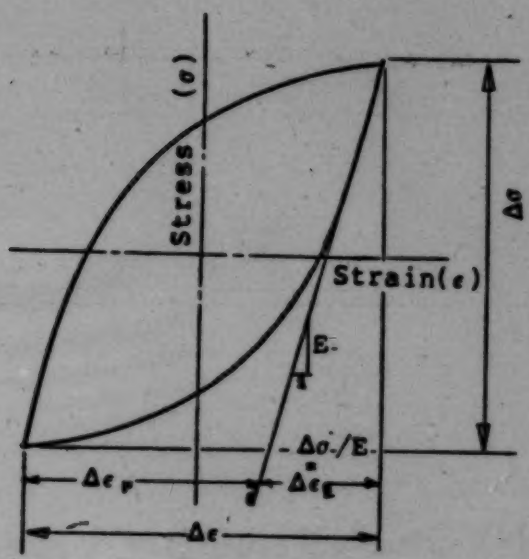

Figure 3.3 Stable hysteresis loop for fully reversed condition.

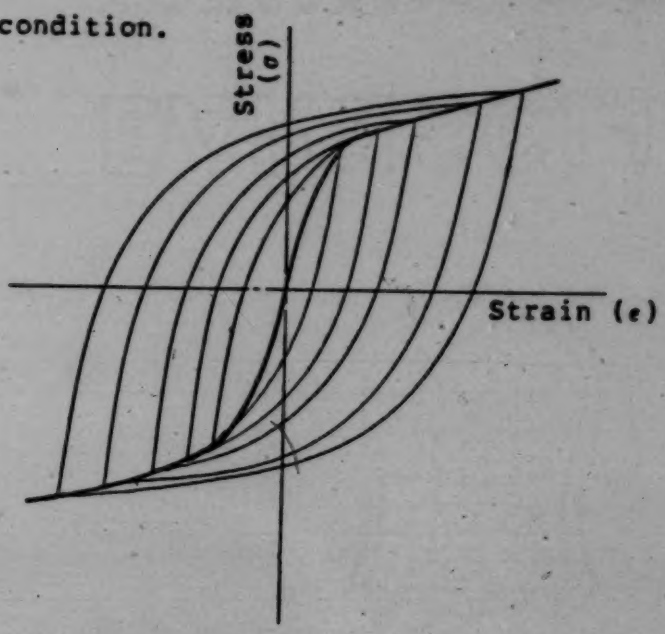

Figure 3.4 Cyclic stress-strain curve drawn through stable hysteresis loop tips.

3.2.3 Cyclic Relaxation Test Of Mean Stress

For a fully reversed condition (when R=-1) either mean stress (σ_0) or mean strain (ϵ_m), or both simultaneously are zero. In the case where the loading is not fully reversed (e.g. zero to tension loading) some mean stress or mean strain or both is normally present. The mean stress or strain changes in the same cycle dependent fashion as do the stress or strain amplitudes. This cycle dependent stress relaxation is defined as a decrease in the absolute value of the mean stress (σ_0) under constant strain amplitude cycling. All of these changes are caused by cyclic plasticity. The effect of mean stresses is such that the tensile mean stress reduced and compressive mean stress increased the fatigue life at a given amplitude of loading. The general observation was that under loading that produces cyclic plastic strains the mean stress tends to become smaller as cycling progresses (Morrow & Sinclair 1958).

According to the concepts developed in Chapter II, Fig. 3.5 shows that for Columbium-50 steel weldments under zero to tension fatigue loadings an initial tensile residual stress ($\sigma_{r,1}$) changed to residual stress subsequent to first cycle ($\sigma_{r,s}$). Upon loading, the mean stress (σ_0) does not remain constant but relaxes during the fatigue cycling. The criteria for the relaxation of mean stresses was necessary for the prediction of crack initiation life (Eqs. (20) and (22)).

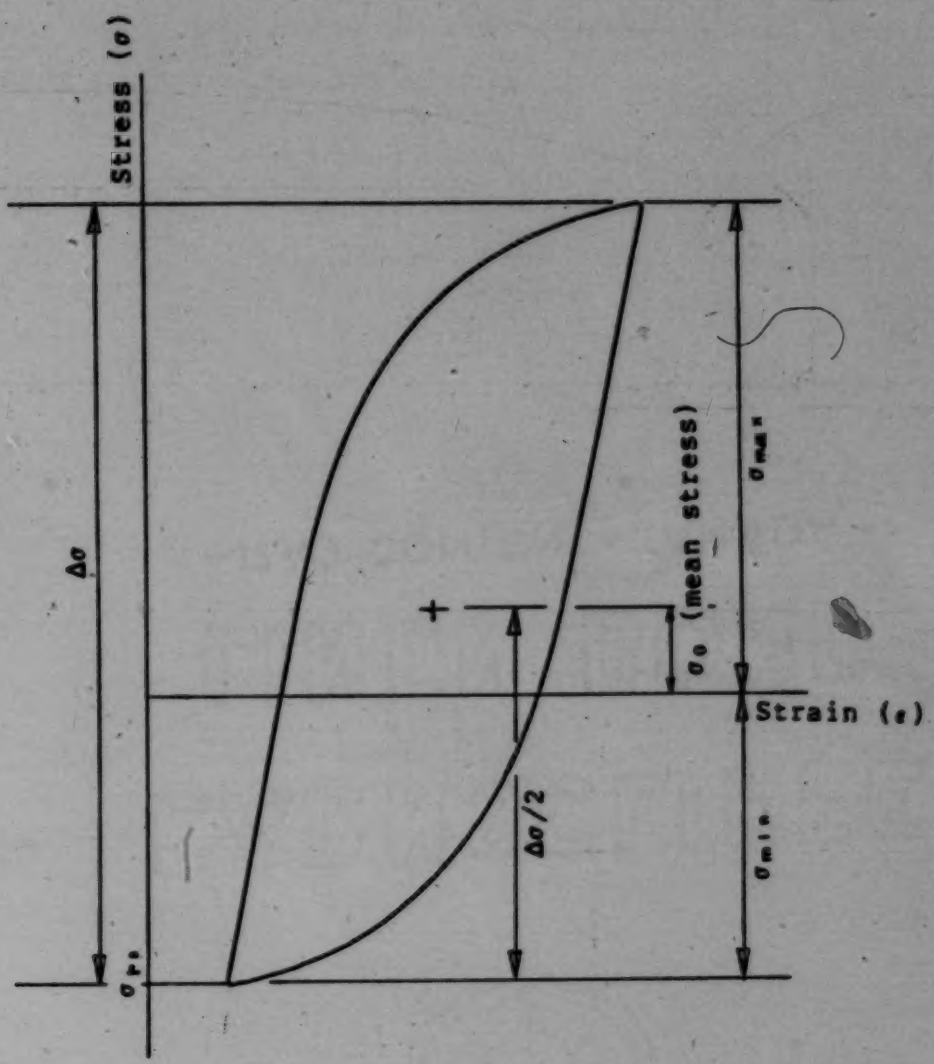

Figure 3.5 Local (notch-root) hysteresis loop subsequent to first cycle under zero to tension fatigue loading of welded structures.

The criteria chosen were according to Jhansale & Topper (1973) (Eq.(20)) and Higashida & others (1978) (Eq. (21)) which was discussed in Chapter II. The mean stress relaxation criteria in the calculation of damage due to mean stress (σ_0) (Eq.(22)) was correlated by using the results from the tests of base material cyclindrical specimens. The following experiments were performed to determine whether the damage criteria due to mean stress ($\sigma_{0,zH}$, Eq.(20)) and the relaxation exponent (k, Eq.(21)) used was applicable for Columbium-50 steel.

Two cases of mean stress relaxation tests were conducted. In the first case, mean stress relaxation data were obtained by axially loading the material to a predetermined mean strain (ϵ_m) but constant strain amplitude ($\Delta\epsilon/2$) and then peak stresses were calculated at certain intervals as the mean stress relaxed. Three specimens were tested at constant strain amplitude but variable mean strains. In the second case only one specimen was used at constant mean strain but three different strain amplitudes. The concept of Jhansale & Topper (1973) was applied to a single specimen to ensure stabilization of the hysteresis loop before inducing a mean stress. Figure 3.6 illustrates a typical strain block sequence used for the study of mean stress relaxation in the material which was cyclically stabilized prior to testing. This eliminated any transient cyclic hardening or softening interactions with the mean stress relaxation response. The data for tensile and

compressive peak stresses were recorded at specific intervals as the mean stress relaxed. After the mean stress relaxed the stress and strain were returned to zero. A stabilizing mean stress wash-out block (wash-out block removes the memory of the previous straining, see Fig.3.6) was then employed which allowed further mean stress relaxation testing with the same specimen. The next mean stress was induced and relaxed with a different strain amplitude.

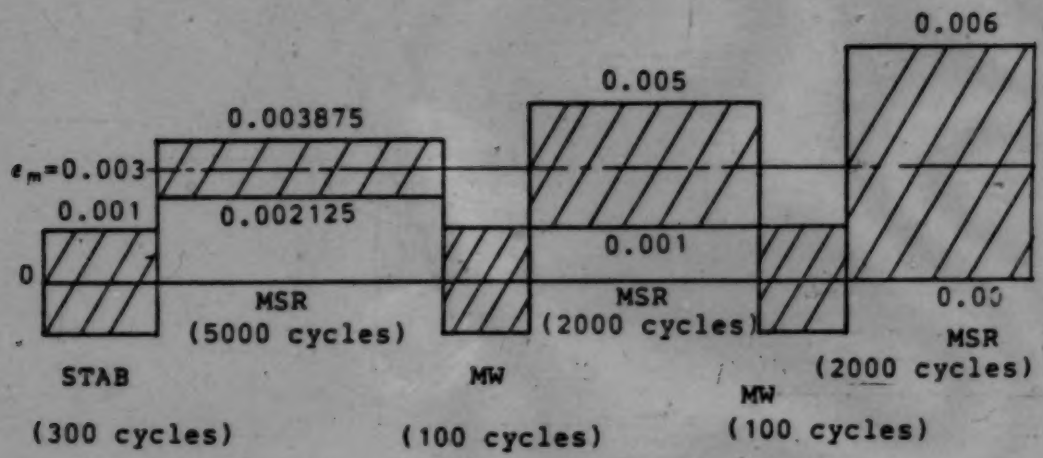

STAB: Stabilization block, 300 cycles.

MSR: Mean stress relaxation block.

MW: Mean stress wash-out block, 100 cycles.

Figure 3.6 Block sequence of the mean stress relaxation tests on the base material.

3.3 Experiments On Welded Structures

The experiments were performed on Columbium-50 / Oxweld#36 welded joints to obtain fatigue ("stress-life") curves for high cycle tests. The tests on the welded joints were of pulsating tension (stress level varied from zero to tensile). Fatigue tests performed on mechanically and thermally treated welded specimens are discussed in the later part of this section where the program of high cycle fatigue testing on the welded specimens is described.

3.3.1 Preparation Of High Cycle Fatigue Specimen

The high cycle fatigue specimens were made by welding two five inch (127mm) wide 0.25 inch (6.35mm) thick plates of as-rolled low carbon Columbium-50 (C-Mn) steel. This steel was selected as it has good weldability and relatively high yield strength. The plate edges were machined straight and the edges bevelled at 45° degrees to a depth of about 1/16 inch (1.59mm). An automatic submerged arc-welding process was used for double-vee butt welding the plates. The welding electrode Oxweld#36 rod was used in the preparation of the weld. The chemical composition of the base and filler metals and the welding parameters employed are given in Appendix D. The welds were all fluroscoped to check for flaws, slag inclusions or any other welding defects and then sawed into three inch (76.2mm) wide strips with the weld axis transverse to the saw cut. A few of the specimens were tested ultrasonically.

Both "dog-boned" shaped (Fig.3.7a) and rectangular shaped specimens (Fig.3.7b) were used. It was observed that (Bellow & Faulkner 1979) for the same maximum tensile load and cross-sectional width there was no significant difference in fatigue results between these two types of specimens. Therefore, most of the specimens tested were of the rectangular type which reduced the amount of machining for specimen preparation. Some of the fatigue specimens were made from the as-welded condition. The rest of the specimens were treated mechanically and thermally before the fatigue testing. The methods used for surface treatment are discussed in the next section.

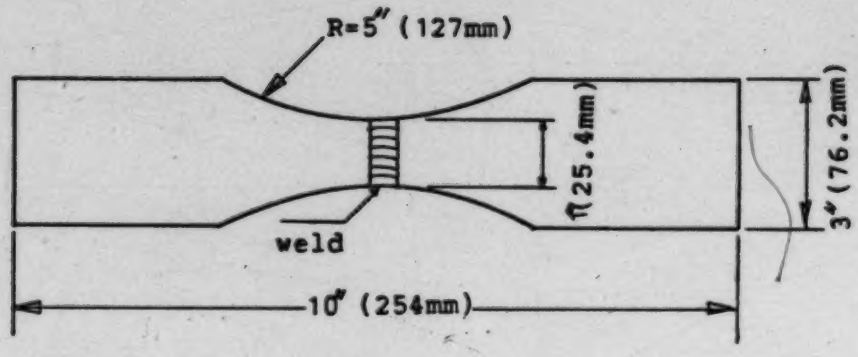

(a) "Dog-bone" shaped specimen.

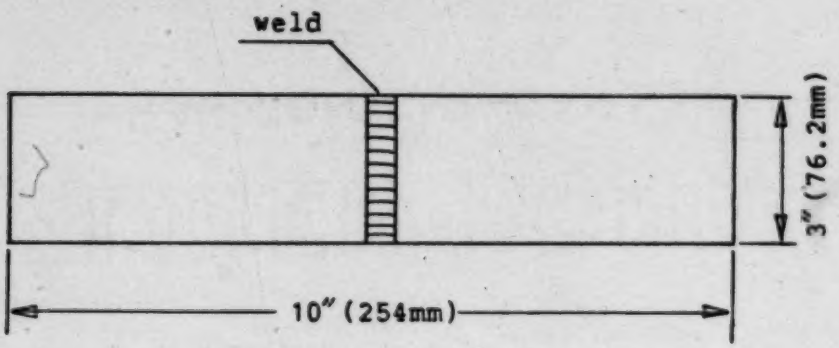

(b) "Rectangular" shaped specimen.

Figure 3.7 High cycle fatigue specimens.

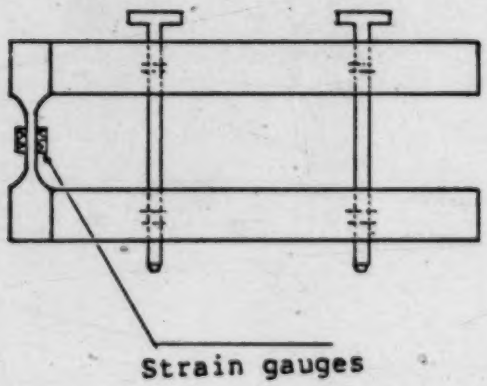

Figure 3.8 Bending stress jig.

3.3.2 Generation Of Compressive Residual Stress By Mechanical And Thermal Treatment

In order to examine the effects of induced residual stresses four different peening processes were applied to the transverse butt-welded specimens. These were:

(1) A single point hammer of 0.25 inch (6.35mm) diameter,

(2) a multiple point hammer using flat needles of 1/8 inch (3.18mm) diameter. The time of peening of each of these processes was 25 to 35 seconds per square inch (6.45 sq.cm.) of surface area tested,

(3) Glass bead shot peening of bead sizes of 0.007 inch (0.18mm) to 0.012 inch(0.31mm) in diameter. Peening was done in and around the weld toe for five to six minutes. The angle of impingement was approximately 45° degrees.

(4) Steel shot peening with shot sizes of 0.025 inch (0.635mm) to 0.045 inch (1.14mm) with a velocity of impingement approximately 250 ft/sec (76.2m/sec) were used to cover the complete area of the specimens for about eight minutes.

In all these cases visual checks were made to insure that the coverage of peening near the weld toe and the surrounding region was uniform. For a few of the specimens from each batch an ultra-violet sensitive coating (magnaflux penetrant and developer) was applied to the surface in the region of the weld toe and the surrounding area before the

peening. Full coverage of the surface during peening removed the coating so that incomplete coverage was detected by directing ultraviolet light on the surface. Also visual examinations of the weld toe regions did not reveal any indication that the profile had been altered significantly by shot peening.

The intensity of peening was measured by standard Almen strips. As this does not always give a reasonable indication of the peening intensity (Horger & Neifert (1944) and Fuchs (1981)), the actual depth of work-hardening was evaluated by the method used by Faulkner & Bellow (1972). The specimen near the weld toe was cut at an angle of approximately 10 degrees to the peened surface of the specimen. The small piece of the material was moulded in Bakelite powder and prepared as a smooth and polished specimen for micro-hardness tests. The hardness versus the depth was measured on this inclined surface using a Knoop indentor with a 300 gm. load. The depth of the work hardening was obtained by plotting the hardness measurements versus the actual depth and estimating the depth at which the hardness approached that of the parent material.

(5) The technique of tensile preloading was used for the generation of compressive residual stresses in the butt-welded specimen near the weld toe. This technique was used to verify the fatigue life predictions made for welds with initial compressive residual stresses. The welded specimens were preloaded to a value slightly less than 90 -

92 percent of the yield strength of the base metal. To verify that the material away from the weld toe remained elastic two strain gauges were fixed to the specimen 1/2 inch (12.7mm) away from the weld toe. Load-strain plots were made during the preloading. To control the limit and speed of the loading a one inch (25.4mm) clip on extensometer was used along with a ramp generator. The rate of preloading was 1700 lbs/minute (7.5 kN/minute). Stress measurements were taken by using X-ray diffraction method near the weld toe before and after the preloading to measure the changes in the nature of the residual stress.

(6) Stress-Peening

(a) Stress-Peening, preloaded first and then peened:

Two types of stress-peening were considered. In the first case welded specimens were preloaded and then peened at this stress level using a multiple rod hammer. Ultraviolet sensitive coatings were applied to the surface to check the coverage of peening. The specimen was then unloaded slowly after the peening was completed.

(b) Stress-Peening, Peening first and then preloaded once: In this case the specimen was first peened after gripping into the machine using a multiple rod hammer. It was then preloaded to the same level as above and then unloaded slowly. The coverage of peening near the weld toe was checked by ultraviolet sensitive coatings. In both the cases stress measurements were taken before and after the

treatment.

(7) The process of annealing was used for residual stress relieving in the welded specimen and to study the effect of annealing on fatigue life. The specimens were annealed in an oven at 1020°F (550°C) for 30 minutes and cooled slowly for five to six hours. Stress measurements were taken before and after the annealing treatment.

All welded specimens were fatigue cycled to obtain the "stress-life" plots. The method of fatigue testing is discussed in the next section.

3.3.3 High Cycle Fatigue Testing Of Welded specimen

Fatigue testing of the welded specimens was performed in the stress-controlled and zero to tensile loading conditions. The testing was controlled for a programmed mean and dynamic load. The peaks of the dynamic load were controlled within ±10 percent of the peak load. Control was set so as to stop the machine as soon as a very small crack initiated. The initiated crack was checked with liquid penetrant and ultraviolet light. The test was then run again until the specimen broke completely to obtain the total fatigue life of the specimen. Care was taken to ensure that the loading was as near uniaxial as possible. The specimen was gripped in hardened serrated clamps.It was noticed that slight tightening of these grips could result in bending stresses which were as high as 30 to 40 percent of the axial load. To help eliminate this bending a special jig (Fig.

3.8) was designed to fit smoothly on both sides of the specimen. With the proper tightening sequence the variation of bending stress was kept within approximately 10 percent of the axial load. This was checked by attaching strain gauges on a welded specimen and comparing with the "bending stress jig" readings.

3.4 Measurement Of Residual Stress

In order to theoretically predict the crack initiation and the crack propagation lives of welded joints the distribution and redistribution of the residual stresses are necessary. It is also necessary to know the amount of imposed surface compressive stresses caused by various treatments so that an estimation of fatigue life under these situations can be obtained.

The accurate determination of the residual stresses near the weld toe is crucial for the study of the effect of residual stresses on the fatigue life. All the relevant stress measurements were performed by using the "Thomas Method-B" double exposure X-ray diffraction technique. The details of the X-ray technique, calibration and the other methods used for measuring residual stresses are discussed in Appendix A. To calibrate the X-ray diffraction method a semi-destructive (blind-hole drilling) and a destructive method (sectioning) were used as well as calibrating against strain-gauge readings and strain measurements by using an extensometer. A close correlation was obtained among the

various methods which are shown in Appendix A. The percentage errors at 20 ksi (138 MPa) (X-ray stress) between upper and lower ranges of scattered data from the line of calibration was found to be 26.5%. Before fatigue testing the residual stresses were determined in areas as close as possible to the toe of the weld. Additional stress measurements were made for a few specimens at the end of fatigue cycling. Residual stress measurements were also taken for peened and inclined cut specimens. To improve the accuracy and to compensate for the selective action of the X-rays at least three exposures of each setting were taken.

3.5 Hardness Test

Information regarding the cyclic and fatigue properties of the WM and the HAZ materials were established from the empirical relations and micro-hardness readings in those areas (Appendix C). Hardness measurements were also necessary to study the variation of hardness due to surface treatments.

Hardness tests were carried out on both peened and unpeened welded specimens. The peening intensity in terms of surface hardness and the depth of work hardening were measured with a Knoop indentor. Micro-hardness tests were conducted on untreated welded specimens near the critical locations using Vicker's hardness indentor and a 300 gm. load. The position of the critical locations are shown in the Fig.3.9 (Chang & Lawrence 1981). Micro-hardness tests

were also performed on polished specimens of the base metal, the WM and the HAZ area.

Cyclic stress-strain and fatigue properties of the WM and the HAZ materials were calculated from the data obtained from micro-hardness measurements at these locations and using the empirical relationships (Graham 1968, Landgraf 1970, Chang & Lawrence 1981). Usually the test data on the HAZ and the WM were difficult to obtain experimentally but approximate values were measured.

Both hardness and stress measurements were also taken on a welded specimen cut at a small inclined angle (three to five degrees) along the width of the specimen from the weld toe. This was to correlate any changes in surface hardness with changes in surface residual stress.

The material properties and the distribution of residual stresses necessary to calculate the crack initiation and crack propagation lives of welded joints were obtained from the experiments described above. This data was used in the theoretical models to estimate the fatigue life discussed in Chapter II.

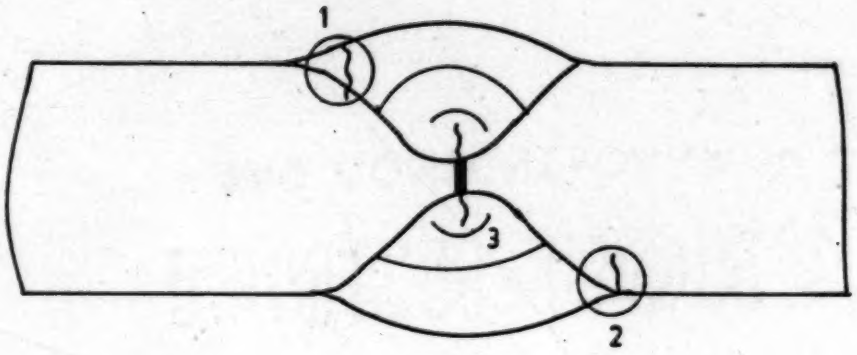

(1) Represents highly diluted, untempered weld metal

(2) Represents grain coarsened HAZ close to fusion line

(3) Represents tempered weld metal zone.

Figure 3.9 Typical locations of fatigue crack initiation in a butt-weld.

4. RESULTS AND DISCUSSION

4.1 Introduction

In this Chapter the results of both the experimental and theoretical development are presented. The experimental findings include the results of the static and dynamic material properties, fatigue life tests and residual stress measurements. The theoretical development includes the results for prediction of both the initiation and propagation phases of the fatigue process. The final analysis compares these predictions to the experimental results.

4.2 Experimental Results

The laboratory results include the determination of the static and cyclic properties of the parent material, the WM and the HAZ metal. As well the residual stresses existing in the butt-welded joints are measured. The effect of various mechanical treatments on these residual stresses and the hardness variation also is given.

4.2.1 Properties Of Columbium-50 Steel Material

Monotonic And Cyclic Stress-Strain Behaviour:

The static and cyclic stress-strain properties of the base metal, the WM and the HAZ materials are listed in Tables 1 and 2 respectively.

Table 1.

Mechanical properties of base, weld and HAZ materials for
for Columbium-50 steel / Oxweld#36 weld metal / HAZ metal.

Material Properties	Base Metal	Weld Metal	HAZ Metal.
Modulus of Elasticity, $EX10^3$,ksi(MPa)	29000.0(200.0x10^3)	30000.0(207.0x10^3)	30000.0(200.0x10^3) **
Average Upper Yield Strength, ksi (MPa)	41.0 (283.0)	-----	-------
Average Lower Yield Strength, ksi (MPa)	37.0 (255.0)	-----	--------
0.2% Offset Yield Strength, S_Y ksi (MPa)	39.0 (269.0)	75-90(517-620) x	75-90(517-620) **
Ultimate Tensile Strength, S_U ksi (MPa)	64.0(441.0)	98.0(676.0) +	98.0(676.0) **
True Fracture Strength, σ_f ksi (MPa)	123.0 (848.0)	148.0(10190) ++	137.0(943.0) ++
True Fracture Ductility, ϵ_f	0.96	0.75 ***	0.90 ***
Percent Reduction in Area, %RA	62.0	57.0 +	57.0 **
%Elongation over 2in (50.8mm) gauge length	11-14%	20-30% x	20-30% **
Strain Hardening Exponent, n	0.245	0.12 ***	0.145 ***
Strength Coefficient, K, ksi (MPa)	111.0(765.0)	153.0(1055) xx	139.0(958.0) xx
Average Hardness (BHN)	187	221.5	199.5

***:Dependent on hardness values for C-Mn steels (Higashida & others 1978)
++: $\sigma_f = \sigma_f'$ (Graham 1968)
+ :Dependent of %C in steel (Alloy Rods Div.,Chemetron Corp. Hanover, PA 17331, USA.)
x :(Faulkner & Bellow 1972)
xx :(Raske & Morrow 1969)
** : Values approximated as same as that of Weld metal

Table 2

Cyclic and fatigue properties of base, weld and HAZ materials for Columbium-50 steel /Oxweld# 36 weld metal /HAZ metal.

Material Properties	Base Metal	Weld Metal	HAZ Metal.
0.2% Cyclic Yield Strength, σ'_{ys} ksi(MPa)	34.3(237.0)	44.0(303.0)	38.0(261.0)
Cyclic Strength Coefficient, K' ksi(MPa)	183.0(1262.0)	268.0(1845.0)	273.0(1887.0)
Cyclic Strain Hardening Exponent, n'	0.278	0.306	0.334
Fatigue Strength Coefficient, σ'_f ksi(MPa)	130.5(900.0)	148.0(1019.0)	137.0(943.0)
Fatigue Strength Exponent, b	-0.127	-0.121	-0.125
Fatigue Ductility Coefficient, ϵ'_f	0.21	0.105	0.094
Fatigue Ductility Exponent, c	-0.435	-0.395	-0.375
Average Hardness (BHN)	187	221.5	199.5
Transition Fatigue Life $2N_{tr}$ Reversals	26×10^4	25×10^4	25.7×10^4

* Properties of Weld and HAZ Materials were obtained from Empirical Relations and Correlations (Appendix C).

The properties of the WM and the HAZ metal were calculated from the empirical relationship using the hardness values measured (Appendix C, Eqs. (C.1) to (C.8)). A few of the properties which could not be derived from the empirical relations for the HAZ and the WM were taken to be the same as those of the base metal (see Table 1). The properties of the base material determined from the experiments were compared with the empirical relations and found to be close. The empirical formulas which relate hardness values to material properties (Eq.(C.1) to (C.4)) were obtained by Chang & Lawrence (1981) from a wide range of data. This emphasizes that the empirical formulas (Eq. (C.1) to (C.4)) are approximate. For parent material the static and cyclic true stress strain responses are shown in Fig. 4.1. Figure 4.1 shows the cyclic stress-strain curve determined by companion specimens (i.e. stable hysteresis loops taken from several specimens). From Fig. 4.1 it is observed that the material below the yield strength is cyclically softened and the material above the yield strength cyclically hardened since the monotonic and cyclic stress-strain curves intersect each other. Like other mild steels Columbium-50 steel exhibits an upper and lower yield point (Fig. 4.1).

True plastic strain as a function of true stress is plotted in Fig. 4.2. The static strength coefficient (K) and the strain hardening exponent (n) were determined as shown in Fig. 4.2. A single straight line fit of these data would not be appropriate for all the data points, therefore, the

stress-strain curve was divided into two parts.

Figure 4.3 shows the plot for the determination of cyclic strength coefficient K' and the cyclic strain hardening exponent n'. These were determined by plotting the true plastic strain amplitude $\Delta\epsilon_p/2$ versus the true stress amplitude $\Delta\sigma/2$. The plastic strain amplitudes and the stress amplitudes were obtained from the stabilized hysteresis loops of smooth specimen strain-controlled tests.

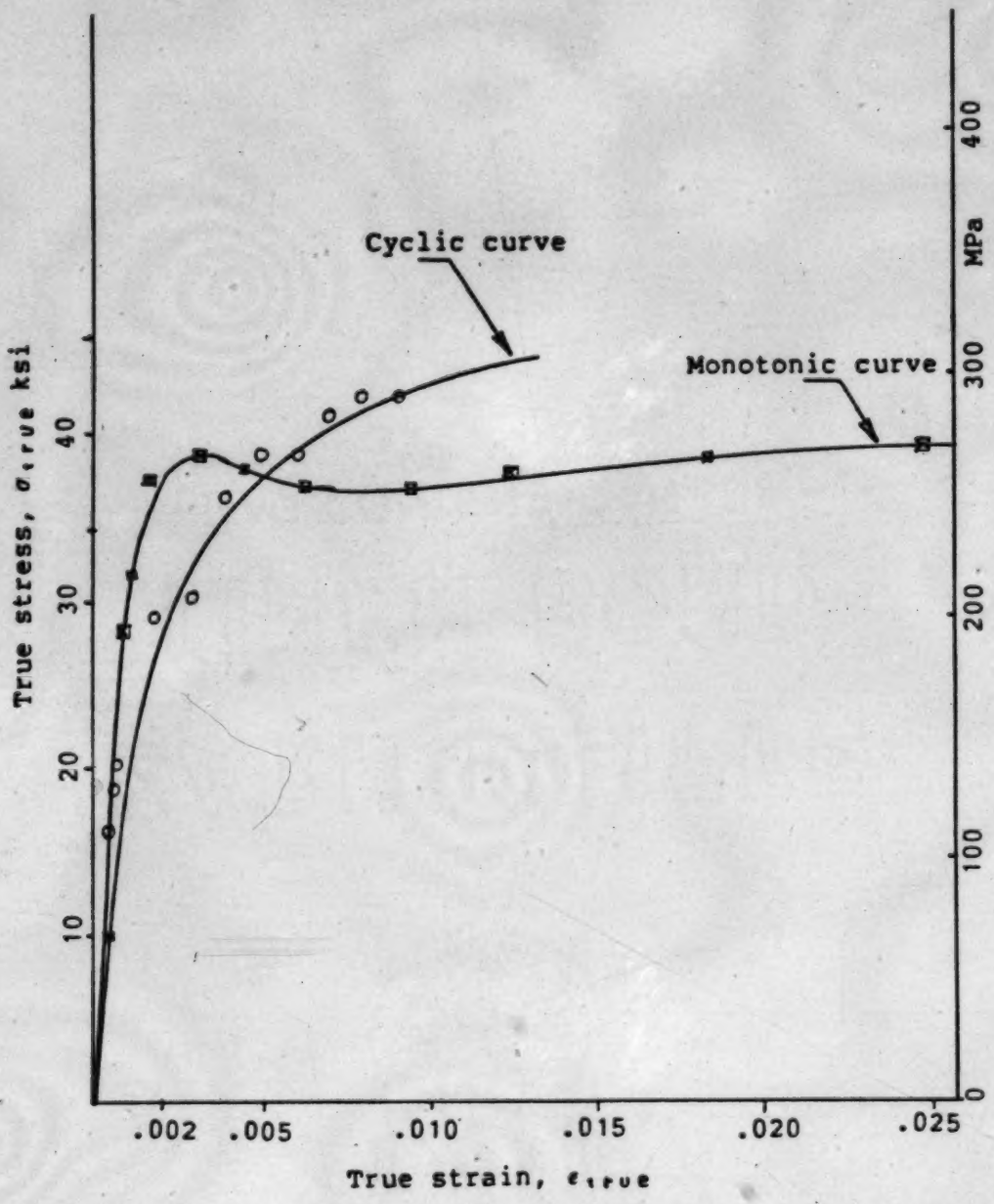

Figure 4.1 The Cyclic and monotonic stress-strain curves for Columbium-50 steel base material.

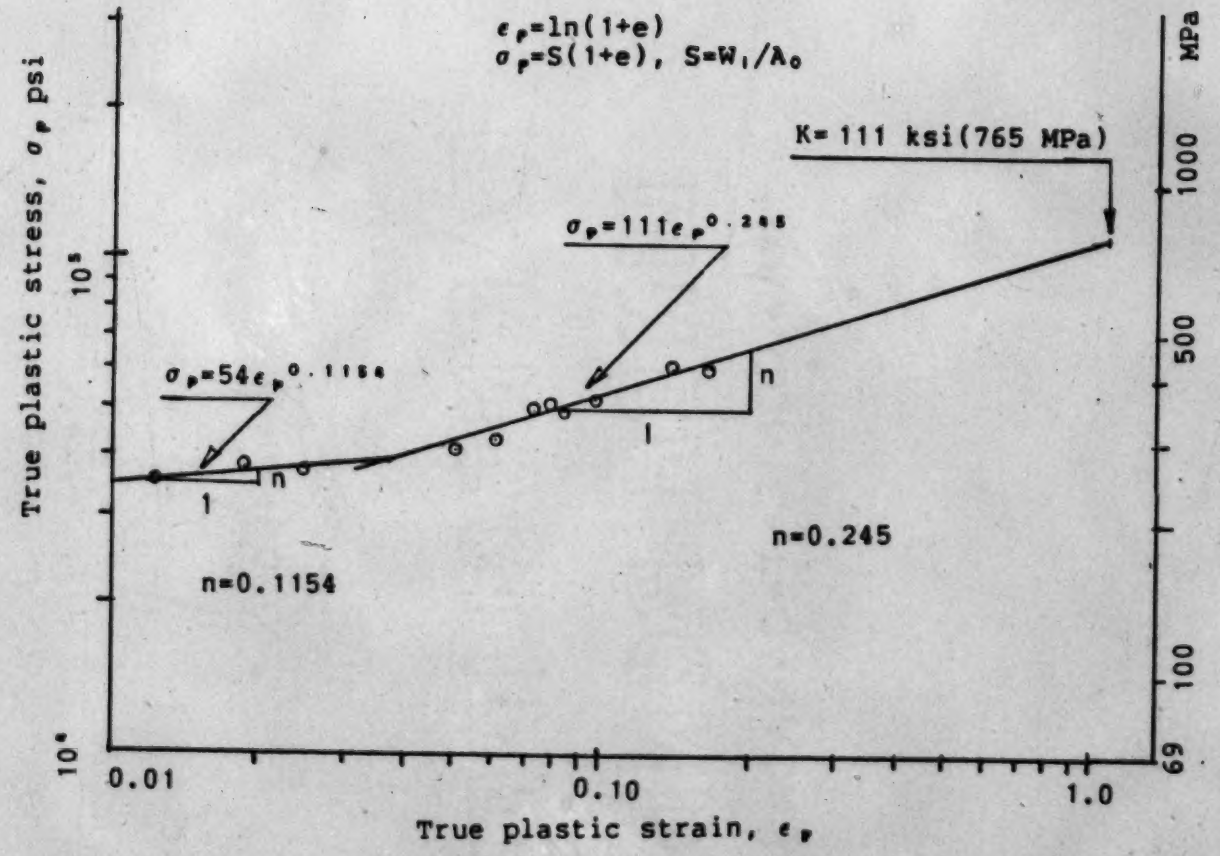

Figure 4.2 Determination of static strength coefficient and strain hardening exponent from true plastic strain and true plastic stress.

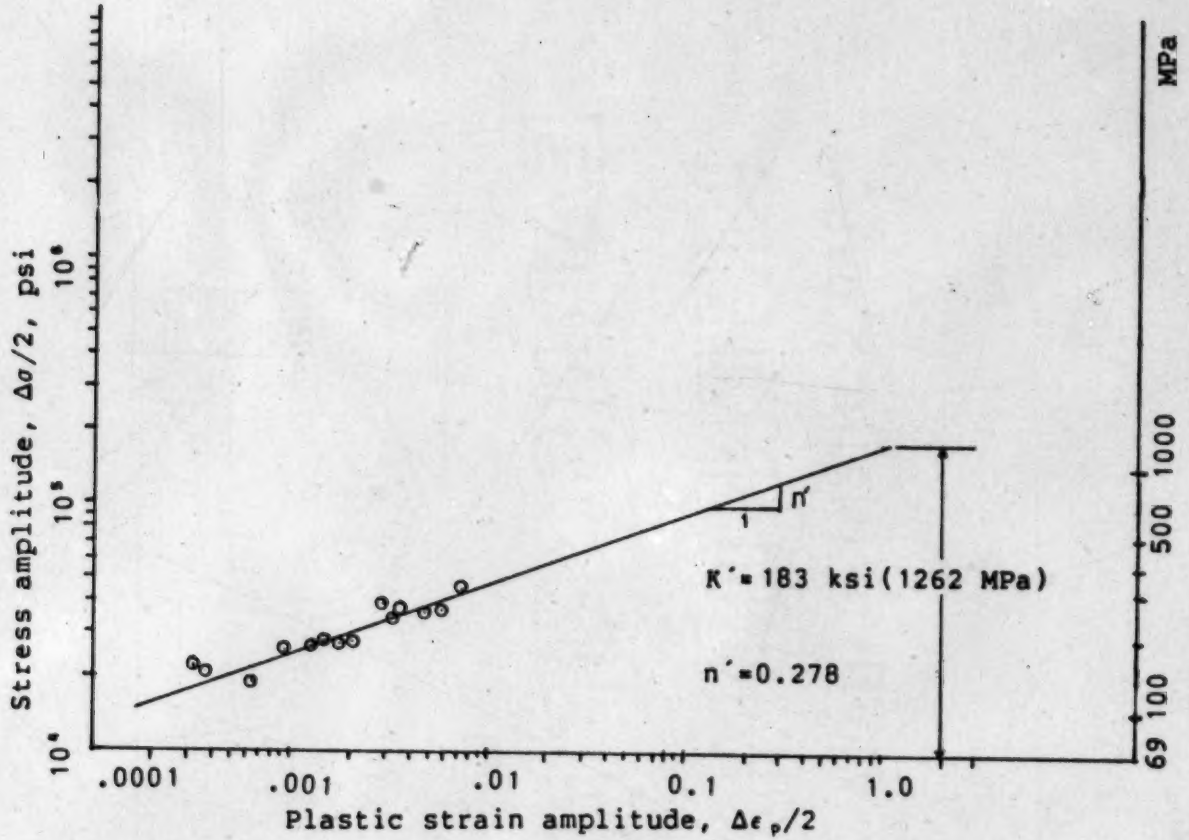

Figure 4.3 Determination of cyclic strength coefficient and cyclic strain hardening exponent from plastic strain and stress amplitudes measured from hysteresis loops.

4.2.2 Results Of Smooth Specimen Fatigue Behaviour

The results of the completely reversed strain-controlled fatigue tests for the Columbium-50 base material are summarized in Table 3. The stress and strain amplitudes were taken from a half-life stable hysteresis loop for each test. Both elastic ($\Delta\epsilon_e$) and plastic ($\Delta\epsilon_p$) strains were calculated from the stable hysteresis loops (Fig.3.3). The fatigue strength coefficient (σ_f') and exponent "b", the fatigue ductility coefficient (ϵ_f') and exponent "c" were calculated by least squares method to fit the data for elastic and plastic strain-life results. Figures 4.4 and 4.5 show the results of these tests in terms of stress / strain and reversals to failure. Due to the limitations of the available size for Columbium-50 steel plate material the diameter of the smooth polished specimen was small (d=0.18 inch, 4.572mm.) and the maximum strain amplitude tested was 0.009.

Manson & Hirschberg (1964) argued that the fatigue resistance of a material subjected to a given strain range could be estimated by superposition of elastic and plastic strain components. The total strain amplitude ($\Delta\epsilon/2$) is given by Eq.(19). It would be expected that the "total strain-life" curve would approach the "plastic strain-life" curve at large strain amplitude whereas the "total strain-life" curve would approach the "elastic strain-life" curve at low strain amplitudes (Fig. 4.4). In high cycle fatigue tests on the weld the strain (stress) amplitudes are

usually low and therefore, the total strain-life curve approaches the "elastic strain-life" curve. The fatigue damage is caused by cyclic plastic strain and the only significant difference between various life ranges is the amount of cyclic plasticity due to fatigue cycling.

The four cyclic fatigue properties σ_f', b, ϵ_f' and c found from the experiments were used in the calculation of fatigue crack initiation life of the weld as described in Chapter II. From Fig. 4.4 it can be seen that the transition fatigue life $2N_{t}$, of Columbium-50 steel is 26×10^4 cycles which falls within the range of medium strength steels. The transition fatigue life is defined as the life at which elastic and plastic amplitudes are equal.

Table 3.

Experimental results for low-cycle fatigue strain-control tests of Columbium-50 steel base metal (Fully reversed tests).

Total Strain Amplitude $\Delta\epsilon/2$	Total Stress Amplitude ksi(MPa) $\Delta\sigma/2$	Elastic Strain Amplitude $\Delta\epsilon_E/2$	Plastic Strain Amplitude $\Delta\epsilon_P/2$	$2N_f$ .Reversals to failure
0.009	42.7	0.00129	0.0057	628
0.009	43.0	0.00145	0.0062	762
0.007	38.0	0.0017	0.0058	1960
0.006	34.6	0.0015	0.0048	4878
0.005	36.0	0.0012	0.0036	7264
0.0045	35.0	0.00155	0.0045	13270
0.004	39.50	0.0014	0.0030	12638
0.003	27.20	0.00105	0.0020	36392
0.0025	26.80	0.001	0.0019	38436
0.002	26.10	0.00095	0.00135	84534
0.0015	26.50	0.00076	0.00095	347340
0.0015	19.70	0.00086	0.00064	383956
0.0010	21.30	0.00062	0.00037	1833490
0.0010	21.80	0.00068	0.00033	1874322

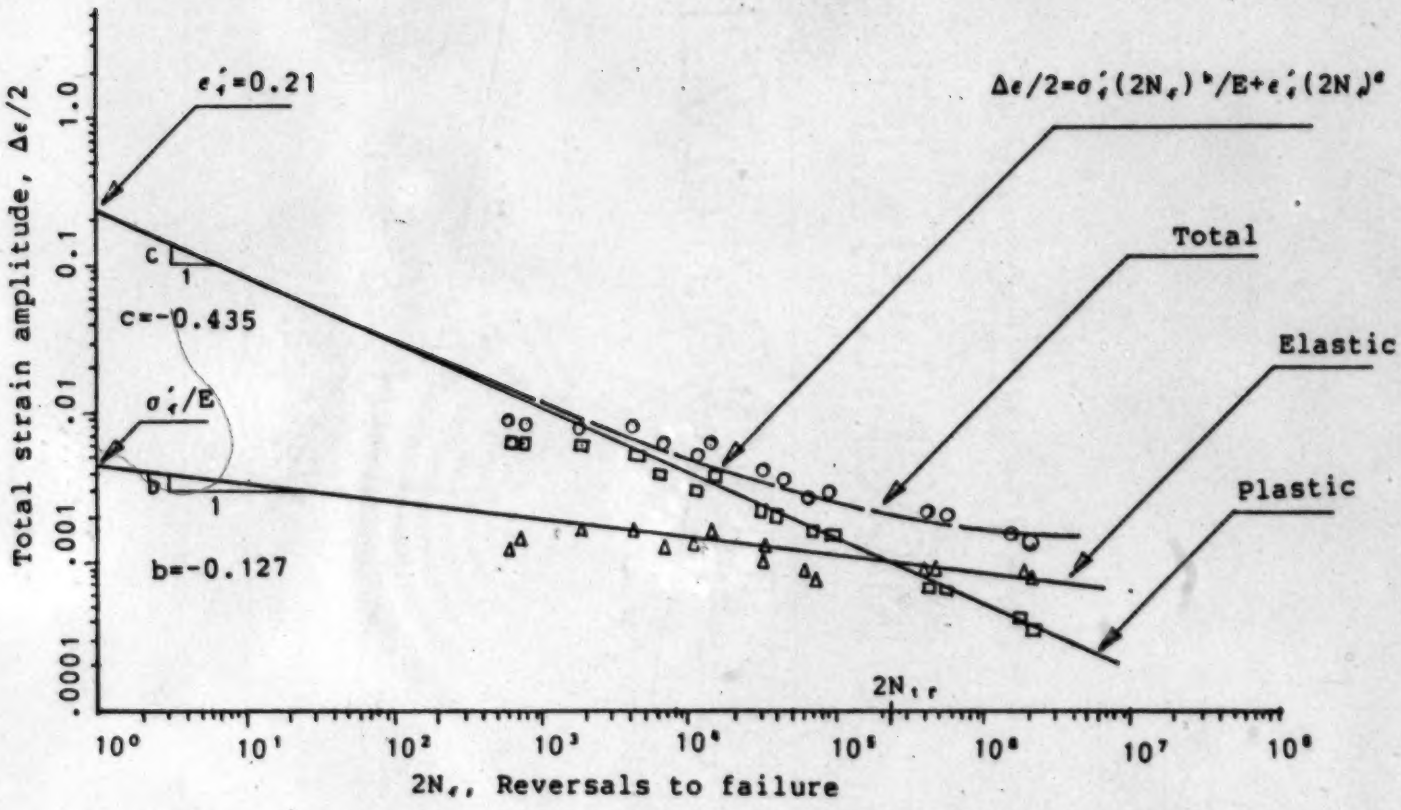

Figure 4.4 Fatigue properties from total strain amplitudes and reversals to failure using smooth specimens fully reversed strain-controlled tests.

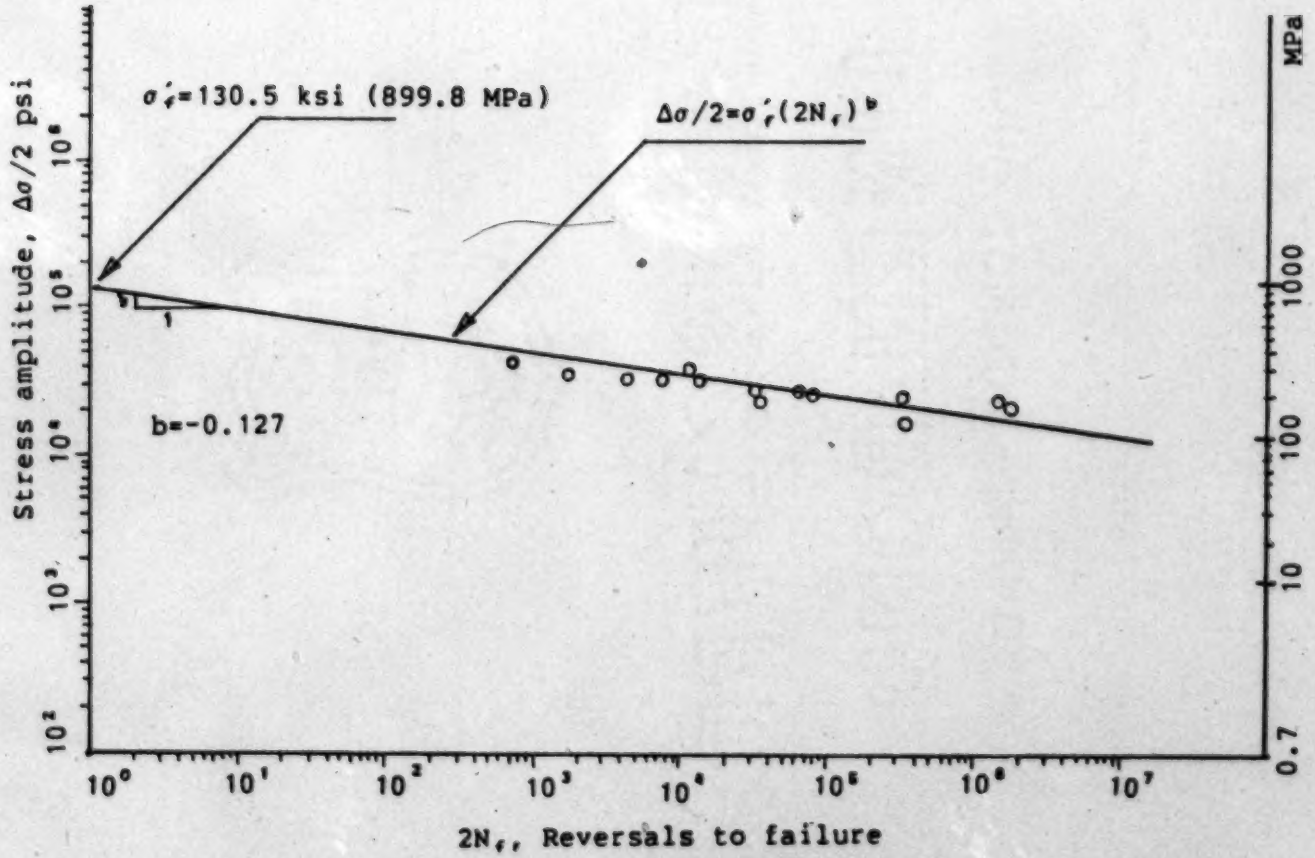

Figure 4.5 Fatigue strength coefficient from stress amplitudes and reversals to failure using smooth specsmens strain-controlled tests.

4.2.3 Cyclic Mean Stress Relaxation

Figure 4.6 shows the result of the tests conducted at constant strain amplitude ($\Delta\epsilon/2 = \pm 0.001$) and positive mean strains ($\epsilon_m = +0.002$, $+0.003$ and $+0.004$). Figure 4.7 shows the result of constant positive mean strain ($\epsilon_m = +0.003$) and three strain amplitudes ($\Delta\epsilon/2 = \pm 0.000875$, ± 0.002 and ± 0.003) respectively. These results show that for constant strain amplitude and variable mean strain the stress amplitude changes very little in the range from 1 to 10^4 cycles. This shows that a negligible damage in softening or hardening. The mean stress was measured as an average of two stress peaks. Results from Fig. 4.7 show that the rate of relaxation of mean strain is higher for constant mean strain and variable strain amplitudes. The cyclic relaxation of mean stress depends on mean strain, strain amplitudes and number of cycles. For higher mean strain (Fig. 4.6, $\epsilon_m = +0.004$) and higher strain amplitudes (Fig. 4.7, $\Delta\epsilon/2 = \pm 0.003$) Columbium-50 steel showed the tendency of higher rate of mean stress relaxation in the range of 10^4 cycles. (Tables of the experimental data are shown in Appendix D).

Figure 4.8 shows the results of the tests conducted on Columbium-50 steel at a constant value of mean strain ($\epsilon_m = +0.003$) and three strain amplitudes ($\Delta\epsilon/2 = \pm 0.003$, ± 0.002 and ± 0.000875). The data shown in Fig. 4.8 were replotted in terms of dimensionless values of the mean stress (expressed as ratios of the current mean stress $\sigma_{0,2N}$ to the initial mean stress $\sigma_{0,1}$ which is the mean stress

corresponding to the first reversals) and Reversals-1, i.e. (2N-1). The straight lines were drawn for data up to 10^4 reversals assuming the power law relation suggested by Jhansale & Topper (1973) (Eq.(20), Fig. 4.8). From Fig. 4.8 the mean stress relaxation exponent (k) for a given test at a constant strain amplitude ($\Delta\epsilon/2$) can be obtained. The mean stress at particular reversals ($\sigma_{0,2N}$) can be calculated by knowing the relaxation exponent and initial mean stress. The larger the absolute value of "k" is, the more rapidly the mean stress diminishes with reversals (2N-1). The straight lines drawn from the experimental data points in Fig. 4.8 shows that the complete relaxation of mean stress can be obtained as the number of reversals increases. But by simply joining the data points it can be observed that the complete relaxation is not possible i.e. $\sigma_{0,2N}/\sigma_{0,1}$ will not become zero as the number of reversals increases. This can be observed in Fig. 4.6 and 4.7 that the mean stress relaxes to a very small value as the number of reversals increases.

The relationship (Eq.(21)) for the relaxation of mean stress exponent (k) for medium and high strength steels can be adequately used for Columbium-50 steel. This can be observed from Fig. 4.9. The relaxation exponent (k) is plotted as a function of modulus of elasticity (E), transition strain (ϵ_{tr}) and the plastic strain amplitude ($\Delta\epsilon_p/2$). The plastic strain amplitudes were calculated from the measured values of stress amplitudes ($\Delta\sigma/2$), cyclic strength coefficient (K') and cyclic strain hardening

exponent (n′). Also for a few of the data points the plastic strain amplitudes were obtained from the hysteresis loops under the condition of mean strain and strain amplitudes. The straight line drawn from the theory (Eq.(21)) shows that the correlation between the experimental points and the theory is quite good, although only over a short interval and Eq.(21) can be used as a relaxation criteria for Columbium-50 steel.

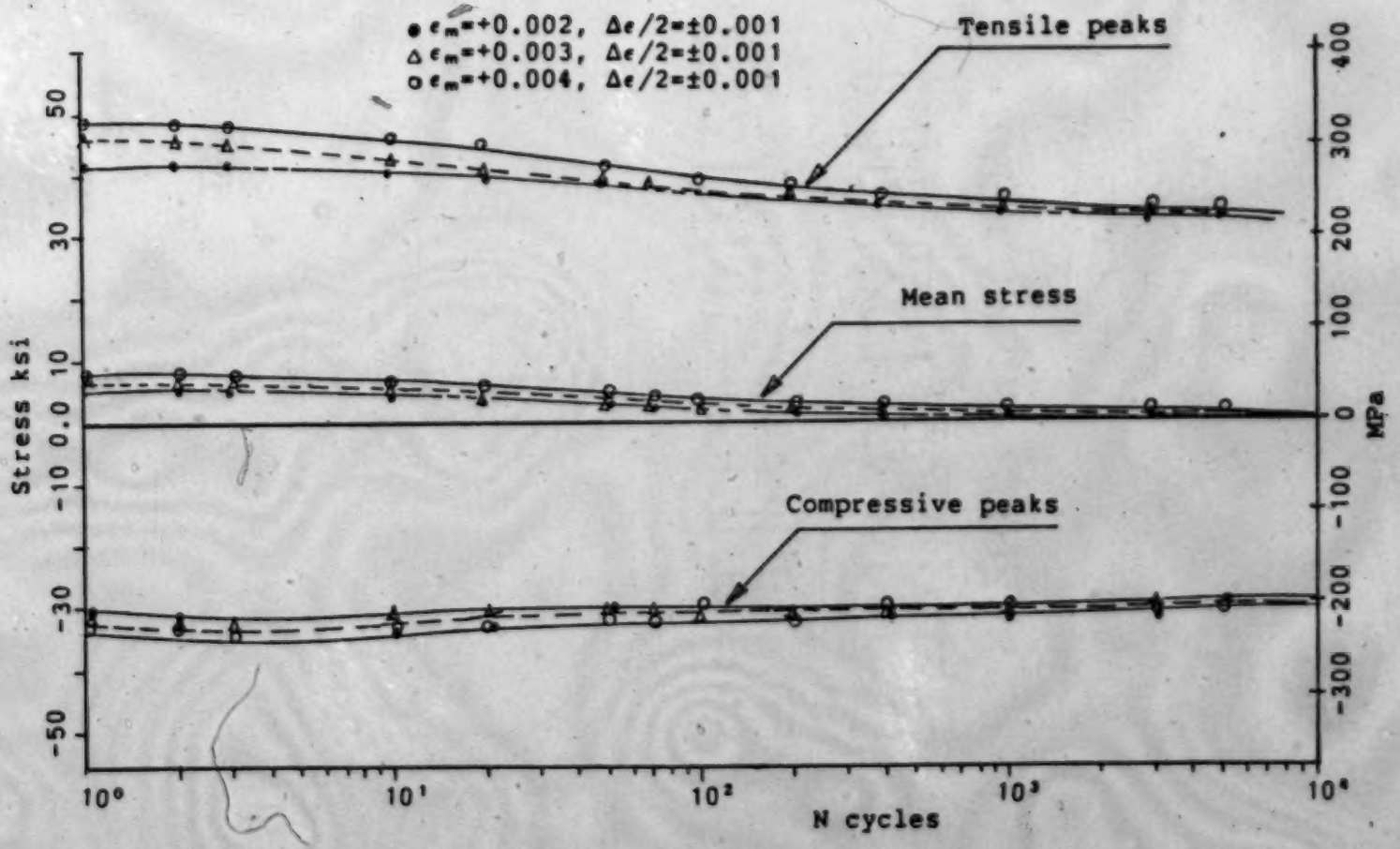

Figure 4.6 Mean stress relaxation tests using three mean strains and constant strain amplitude.

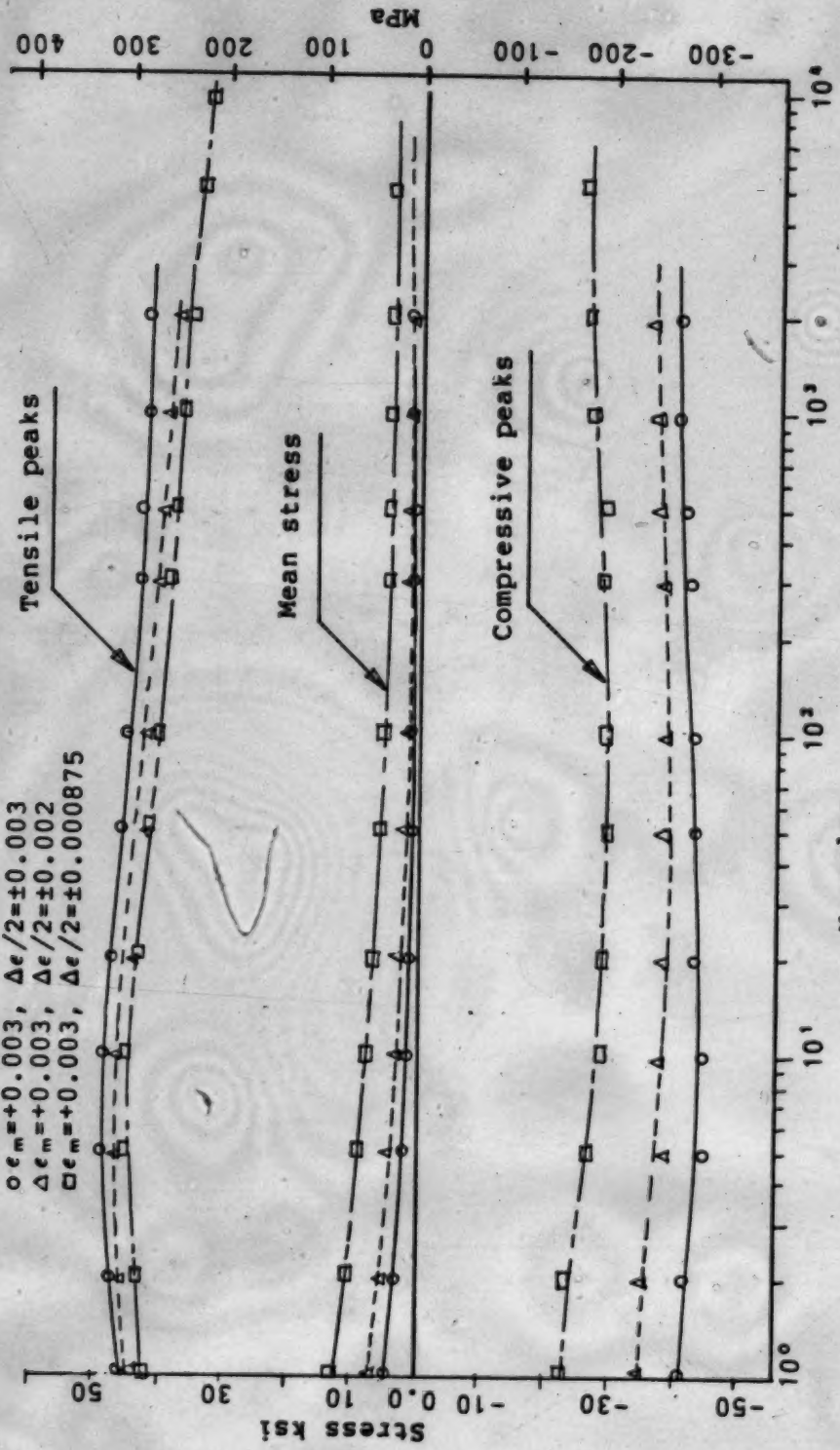

Figure 4.7 Mean stress relaxation tests for constant mean strain and three strain amplitudes.

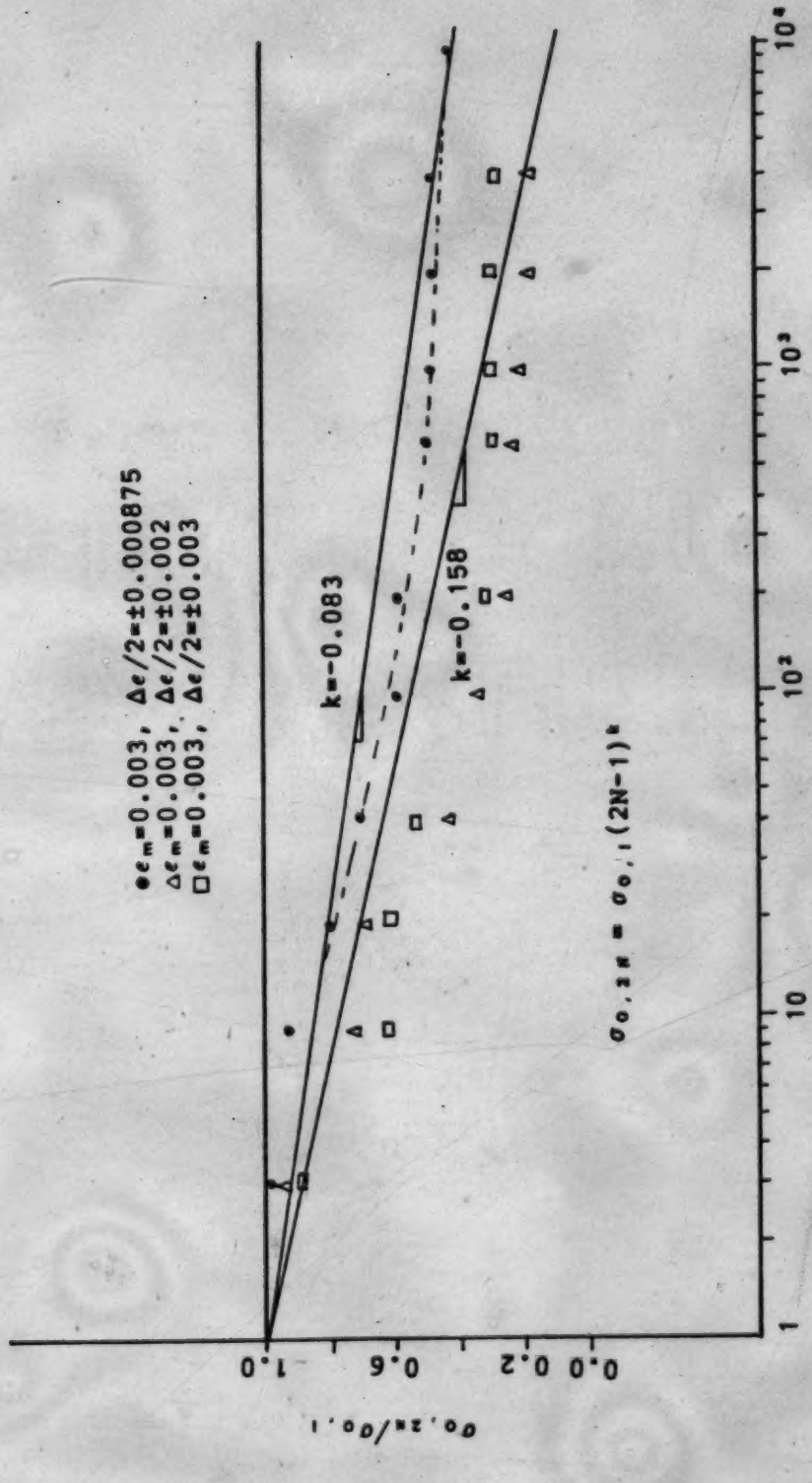

Figure 4.8 Normalized mean stress relaxation behaviour of Columbium-50 steel.

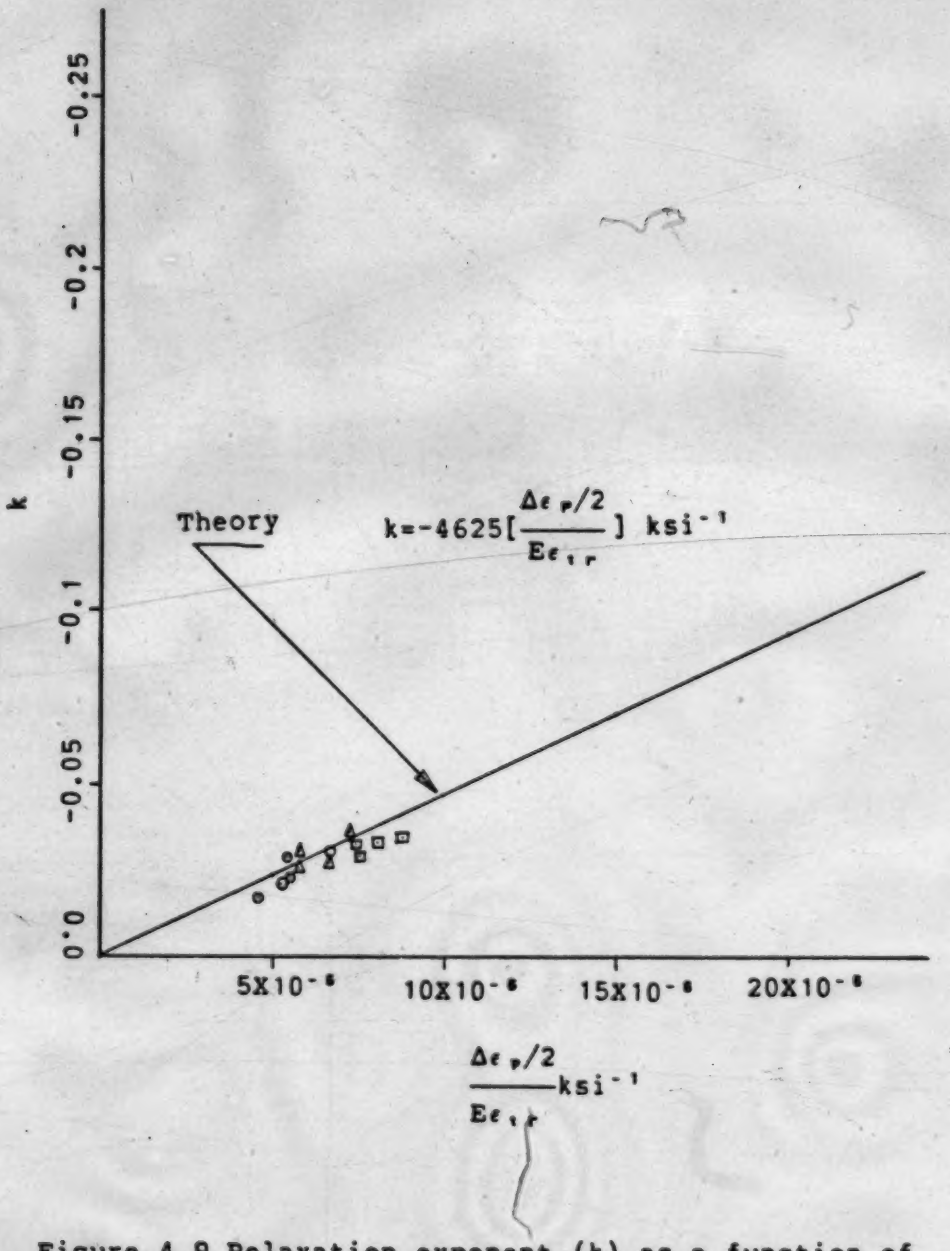

Figure 4.9 Relaxation exponent (k) as a function of modulus of elasticity, transition strain and the plastic strain amplitude.

4.3 Experimental Verification Of The Welding Residual Stresses

4.3.1 Introduction

Experimental stress measurements were made along the toe of the weld before fatigue cycling of the specimens to show the presence of the welding residual stresses. A few of the specimens were measured before and after fatigue cycling to demonstrate the redistribution of residual stresses. Stress measurements were also taken across the thickness of both the parent material and transverse butt-welded specimens to examine the presence of a stress gradient due to welding. All these stress measurements were made using the X-ray diffraction method.

Several mechanical treatments for the improvement of weld fatigue life and a thermal method (annealing) were studied. Stress measurements on the surface of these treated specimens showed that there was a variation of compressive stress level due to each method of treatment. Centre line average readings were noted to study the smoothness of the surface after the peening operation. Hardness measurements were taken across the weld and on a glass shot peened specimen to show the variation of surface hardness due to peening and that due to the welding. Surface hardness was measured on a glass peened specimen to show that the cyclic properties of the material might change due to peening on the surface. Hardness readings were taken across the

thickness of the mechanically treated specimens to measure the depth of work hardening. Hardness readings taken on the WM and the HAZ metal to establish the static and cyclic properties of the weld and HAZ metals are shown in Tables 1 and 2. Usually the crack initiated in the critical regions of the untempered WM, the HAZ metal close to the fusion and the WM zone (Fig. 3.9). Thus the cyclic properties of the WM and the HAZ metal could be used to determine the fatigue crack initiation life.

Axial fatigue tests were performed on the base material specimens, welded and treated specimens to obtain "stress-life" curves for each specimen type. The theoretical predictions of total fatigue life were obtained as a combination of crack initiation and crack propagation life for each case using the analysis discussed in Chapter II. The experimental results were then compared with the theory.

4.3.2 Distribution Of Welding Residual Stresses

Residual stresses near the weld toe in welded joints were assumed to be the cause of the reduction in fatigue strength of the welded joints. Consequently, the distribution of welding residual stresses near the weld toe was investigated and are shown in Figs. 4.10 and 4.11. It was observed that away from the weld toe the residual stresses decreased abruptly. This indicated that residual stresses due to welding exist very close to the weld toe. A tensile residual stress of 20 (138 MPa) to 25 ksi (172 MPa)

was observed to exist in the middle near the weld toe and a compressive stress of -13 (-90 MPa) to -17 ksi (-117 MPa) was obtained at the end of the specimen. Because of the preparation of the specimen the residual stress may not have been the original stress present in the specimen. There could be a slight change in the residual stress pattern at the ends due to the machining stresses. The effect of this positive tensile residual stress was considered in the evaluation of theoretical fatigue life. In the actual fatigue testing of the welded joint it was found that the fatigue crack originated in the "second pass" side of the weld. Therefore, most of the stress measurements were performed on this side of the weld.

A few of the welded specimens were stress cycled between 0 to 21 ksi (145 MPa), 0 to 24 ksi (165 MPa) and 0 to 38.5 ksi (265 MPa) in the as-welded condition. Residual stress measurements at several locations were performed before and after fatigue cycling at various ranges of cycles.

From Fig. 4.11 it can be seen that the magnitude of the initial residual stresses are the same whereas the residual stress pattern changed considerably after cycling. This shows that the residual stress redistributes during fatigue cycling but its pattern is not well known or predictable.

Two welded specimens in the as-welded condition were used to perform the stress measurements through the thickness as shown in Fig. 4.12. The specimens were milled

out at an angle of three degrees along the width from the weld toe. The milling operation was performed very slowly and in small increments. Care was taken not to introduce extra machining stresses by allowing sufficient cooling time between operation. The results showed that a sharp stress gradient exists through the thickness. The maximum stress near the weld toe exists mainly on the surface and up to a depth of 0.005 in (0.127 mm). During fatigue cycling these surface stresses play an important role in the reduction of fatigue life of welded structures. Measurements of residual stresses through the thickness were also performed at the end of the "second pass" side of the welded joints. It can be seen from Fig. 4.13 that the compressive end stress existed only up to a depth of $\cong$ 0.003 in (0.076 mm). Figures 4.14 and 4.15 show that there existed a compressive surface stress of 3000 (21 MPa) to 5000 psi (35 MPa) on the surface of the base metal specimens. Figure 4.15 showed the measurement of surface stresses of parent material by the sectioning method. The plot was obtained by noting the strain changes versus the shim thickness as the small blocks of the material were milled out from the middle of the thickness to become thin shims.

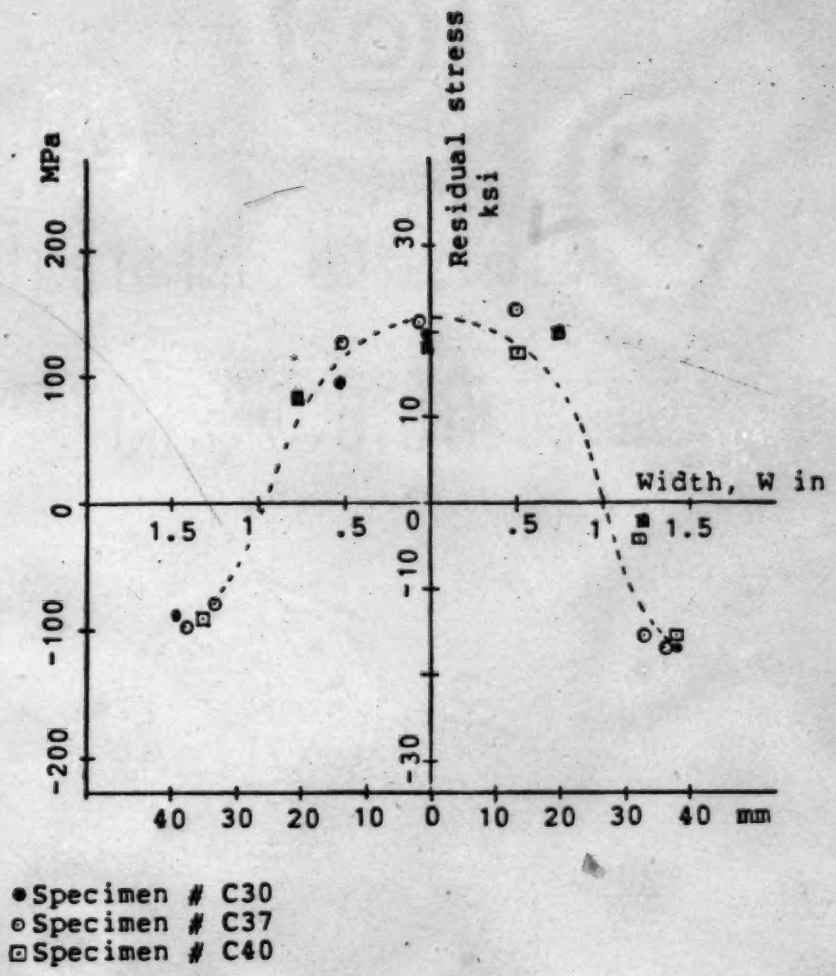

Figure 4.10 General residual stress distribution near the weld toe of Columbium-50 / Oxweld #36 butt-weld.

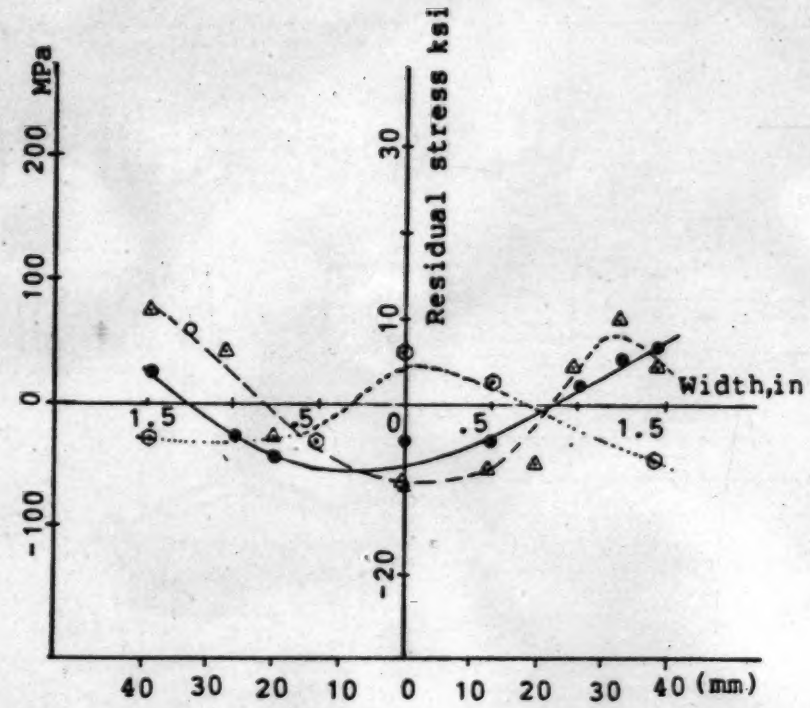

● Specimen # 163, Stress(21 ksi, 144.8 MPa), 57200 cycles
▲ Specimen # 55, Stress(38.5 ksi, 265.5 MPa), 100300 cycles
⊙ Specimen # 131, Stress(24 ksi, 165.5 MPa), 1200 cycles

Figure 4.11 Distribution of residual stresses after fatigue cycling.

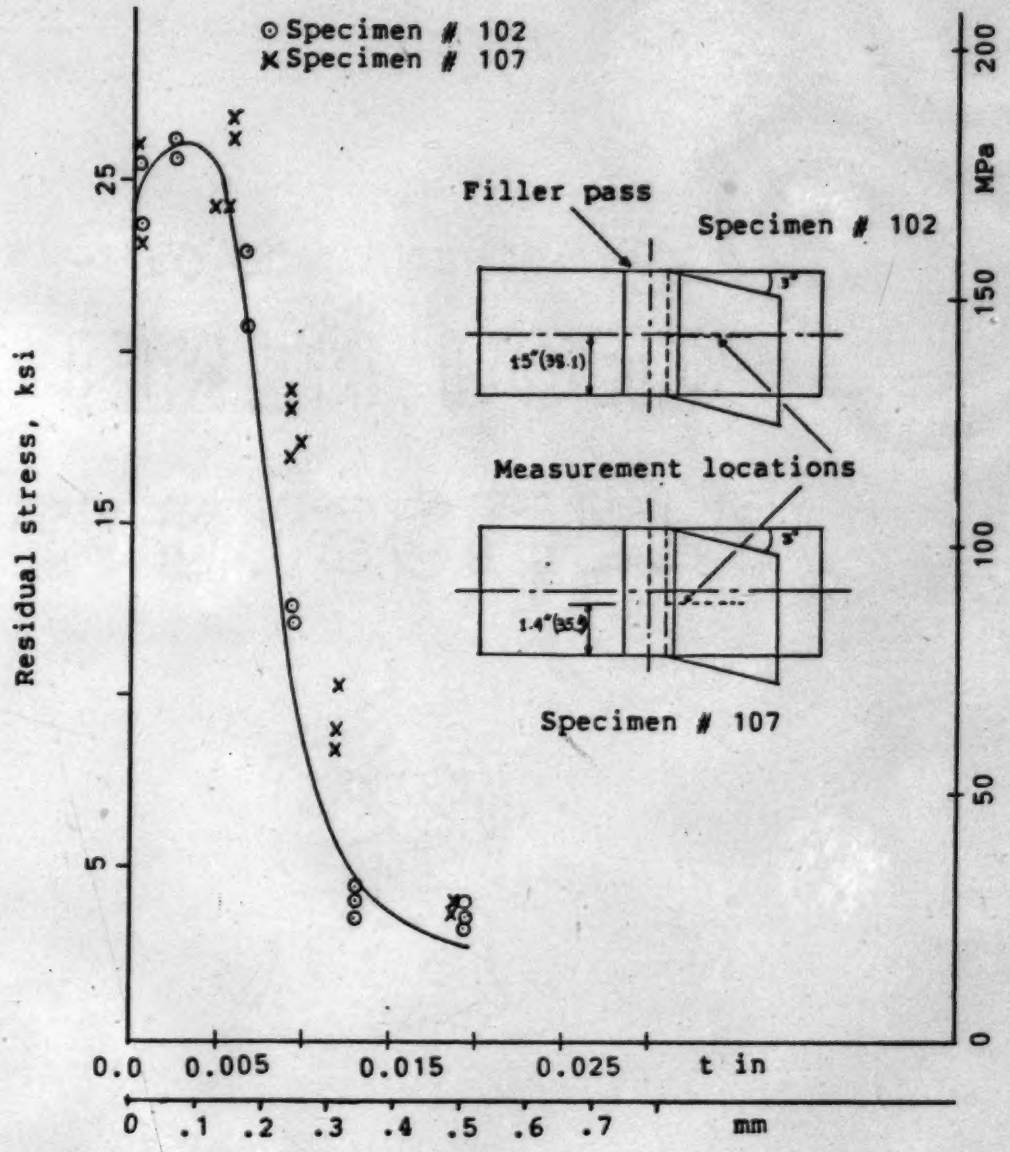

Figure 4.12 Measurement of residual stress along the thickness on the middle of the width of the specimen.

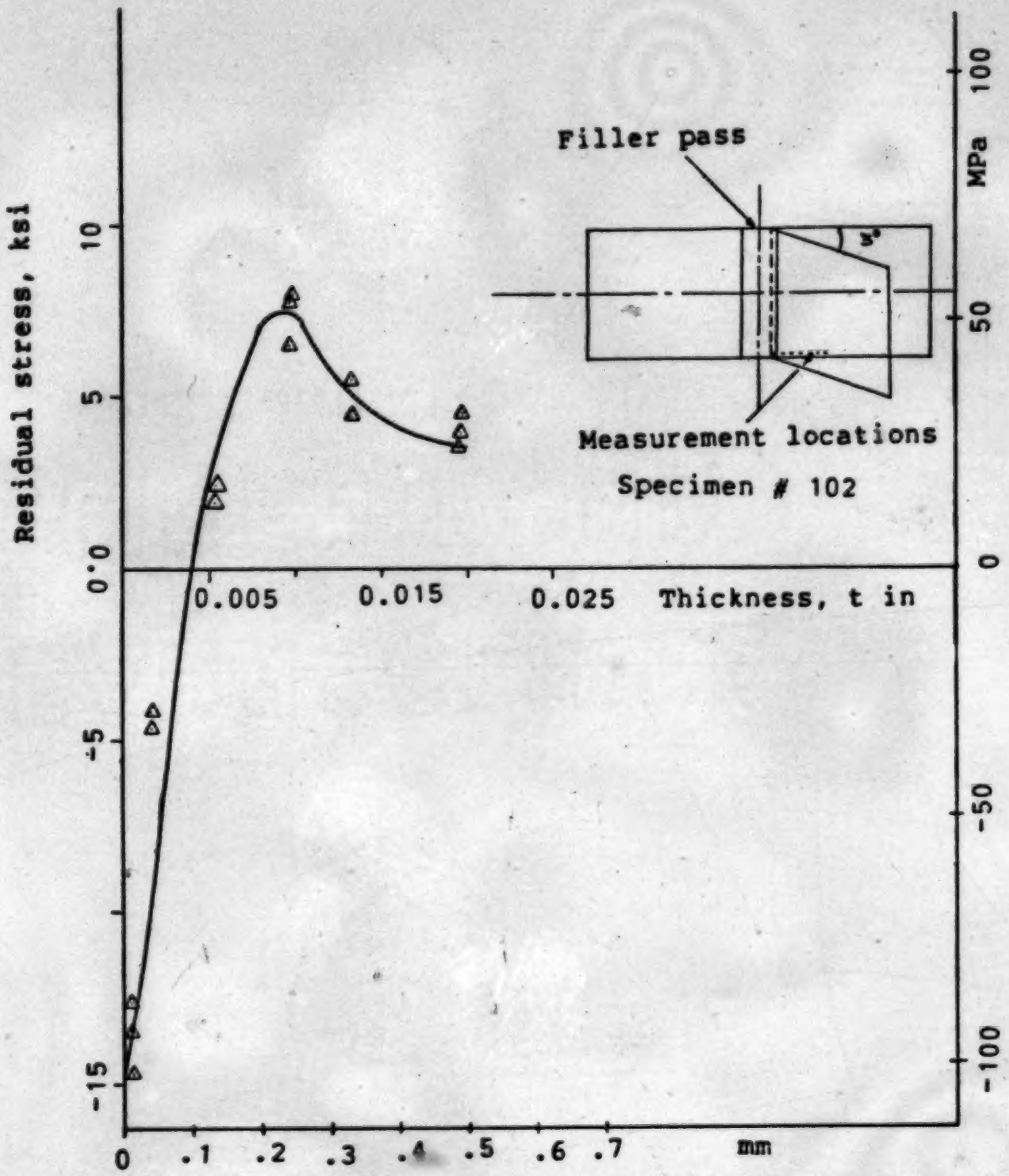

Figure 4.13 Measurement of residual stress through the thickness on the end along the width of the specimen.

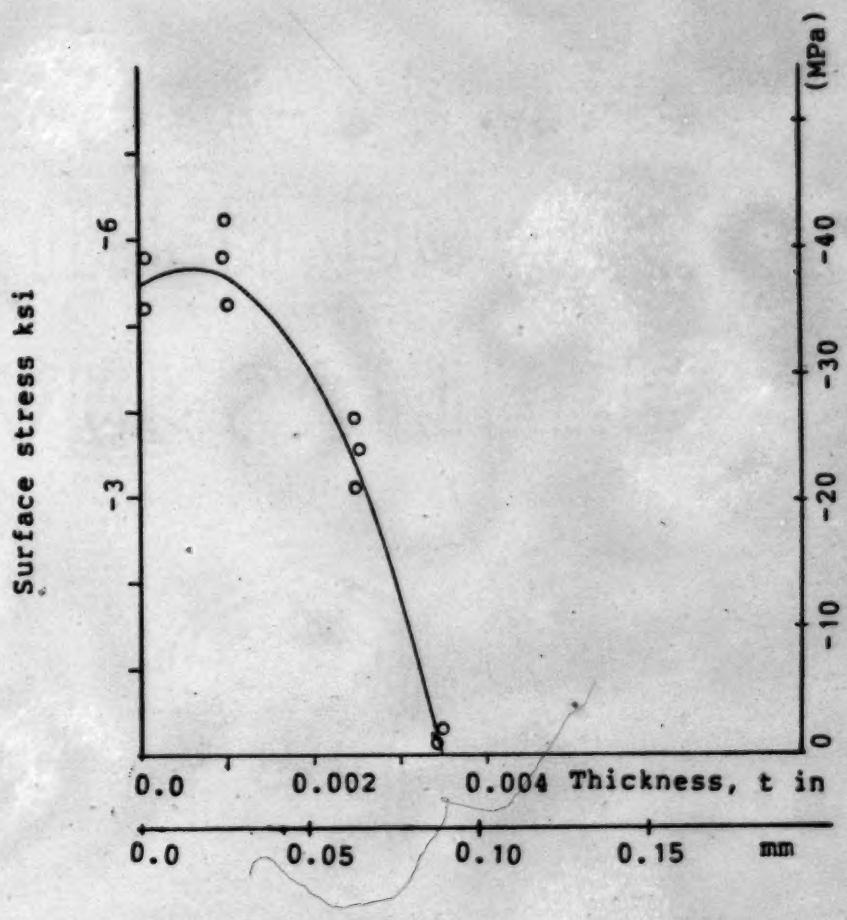

Figure 4.14 Measurement of stress across the thickness of the parent material.

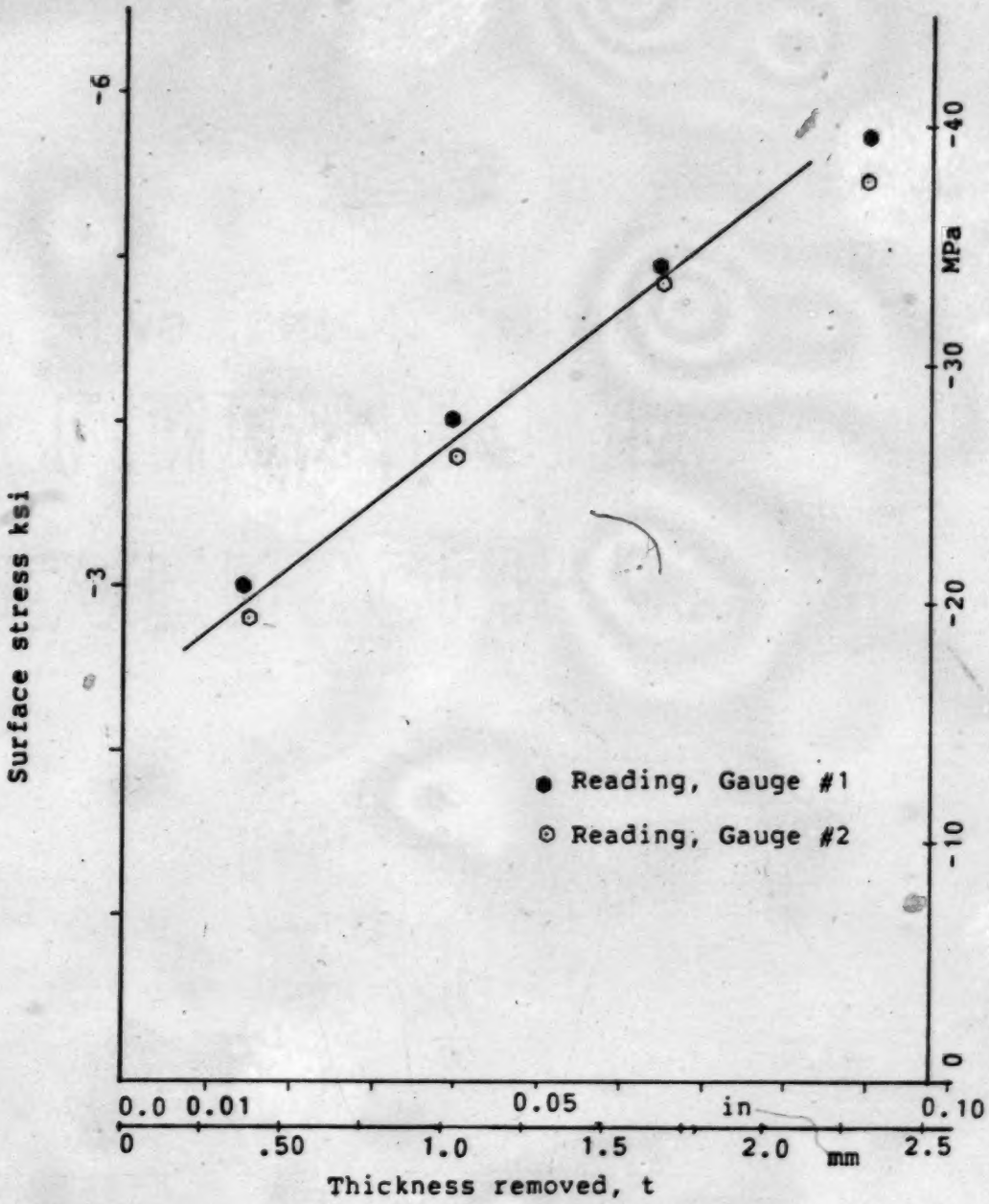

Figure 4.15 Measurement of surface stresses of base metal by sectioning method.

4.3.3 Surface Compressive Stress Measurements Of Treated Welded Specimens

The X-ray diffraction stress measurements were made near the weld toe for all of surface treatments studied. For the annealed specimen the stress level varied from 0 to 3000 psi (21 MPa). For the case of tensile preloading stress measurements were taken near the weld toe before and after the application of preload. The preload was controlled by the ramp generator settings of the testing machine and described in Chapter III. Figures 4.16 to 4.18 show the data obtained by an application of a single preloading. It can be seen that the initial residual stresses were redistributed and a compressive residual stress of approximately 7 ksi (-48 MPa) was imposed near the weld toe. By comparing Figs. 4.16 to 4.18 it can be observed that although the initial tensile residual stress changes to compressive values at the toe of the weld the stress pattern after the preloading was not consistent. The method of tensile preloading introduces the compressive residual stresses at the weld toe without the modification of the weld toe root radius (r).

X-ray diffraction stresss measurements were also made on the glass and steel shot peened multiple and single point hammer peened and stress peened specimens. The results obtained are plotted in Figs. 4.19 and 4.20. It was observed that glass shot peened introduced approximately -9 ksi (-62 MPa) compressive surface residual stress whereas steel shot peened, -16 ksi (-110 MPa); single -point hammer peened, -22

ksi (-152 MPa); and multiple point hammer peening and stress peening produced a surface compressive stress level of -25 ksi (-172 MPa). Figure 4.20 shows that the two types of stress peening introduced almost the same level of residual stresses.

The forgoing levels of surface residual stresses were used to calculate the total fatigue life of the welded treated specimens. The method of analysis of fatigue life which included these surface compressive residual stresses are described in Chapter II.

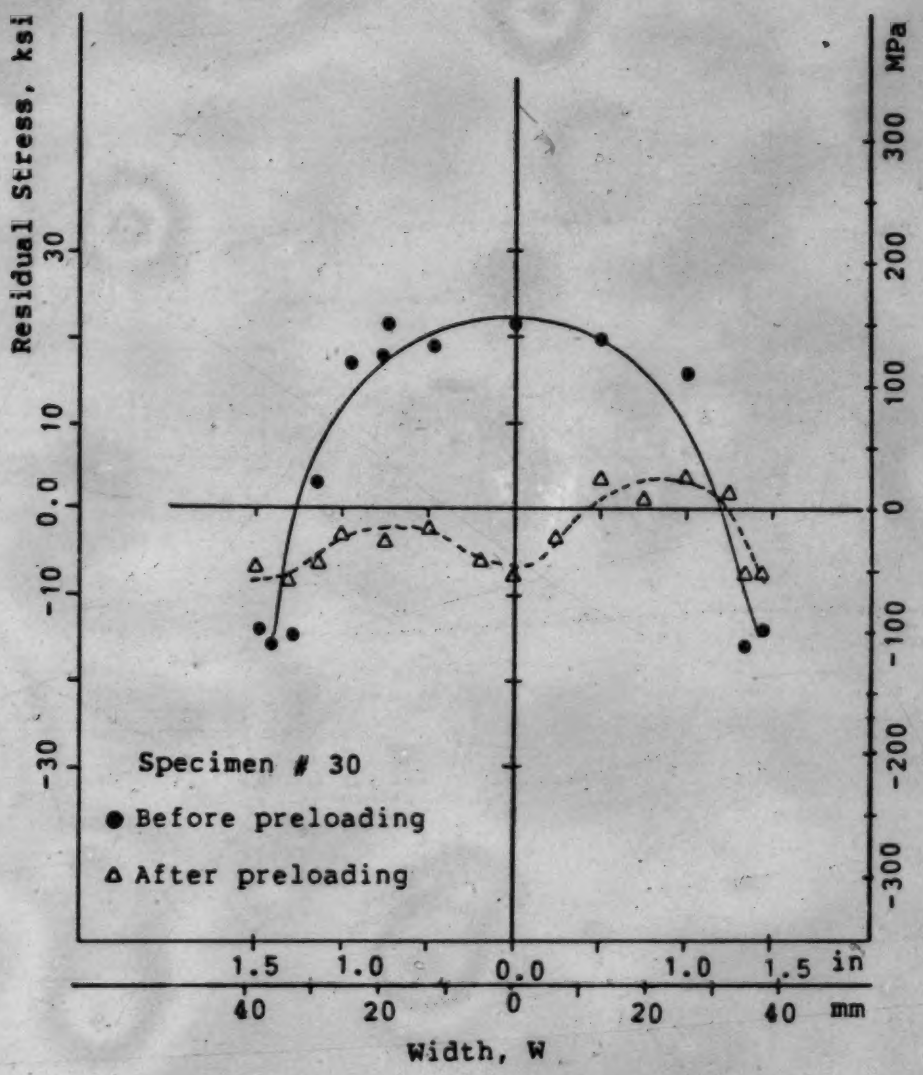

Figure 4.16 Change of residual stress pattern after preloading.

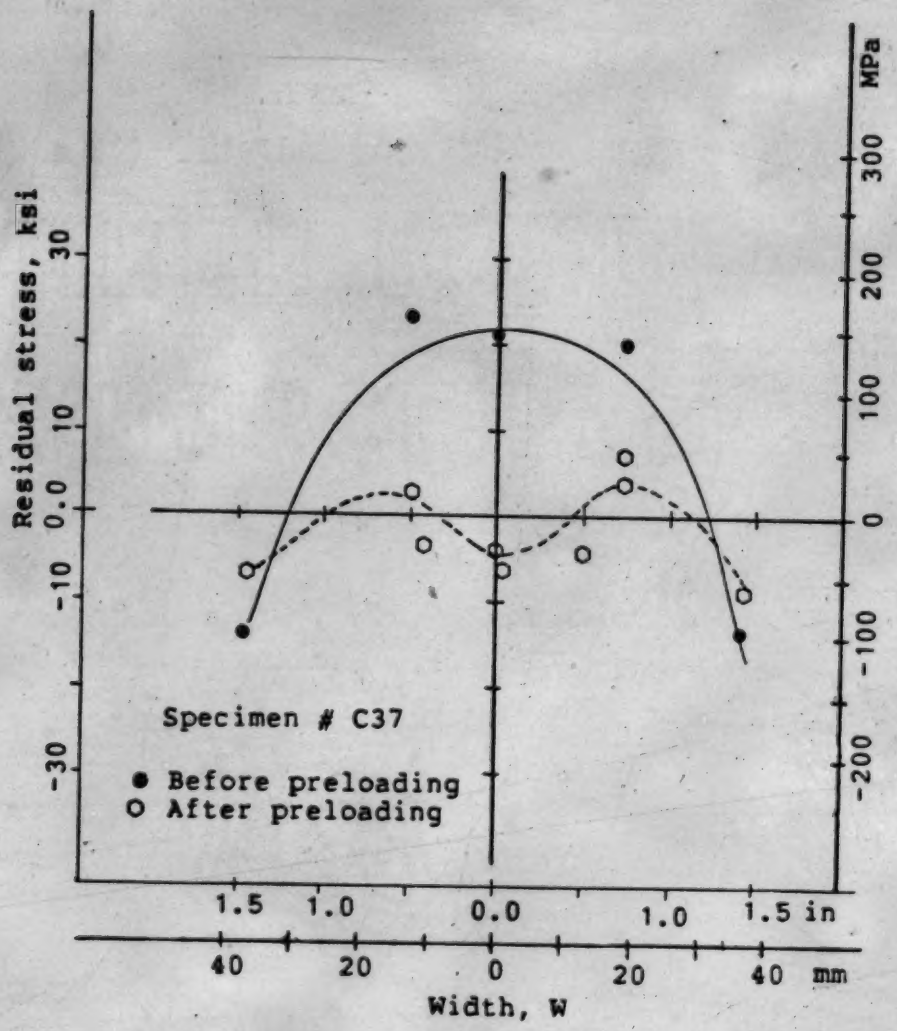

Figure 4.17 Change of residual stress pattern after preloading.

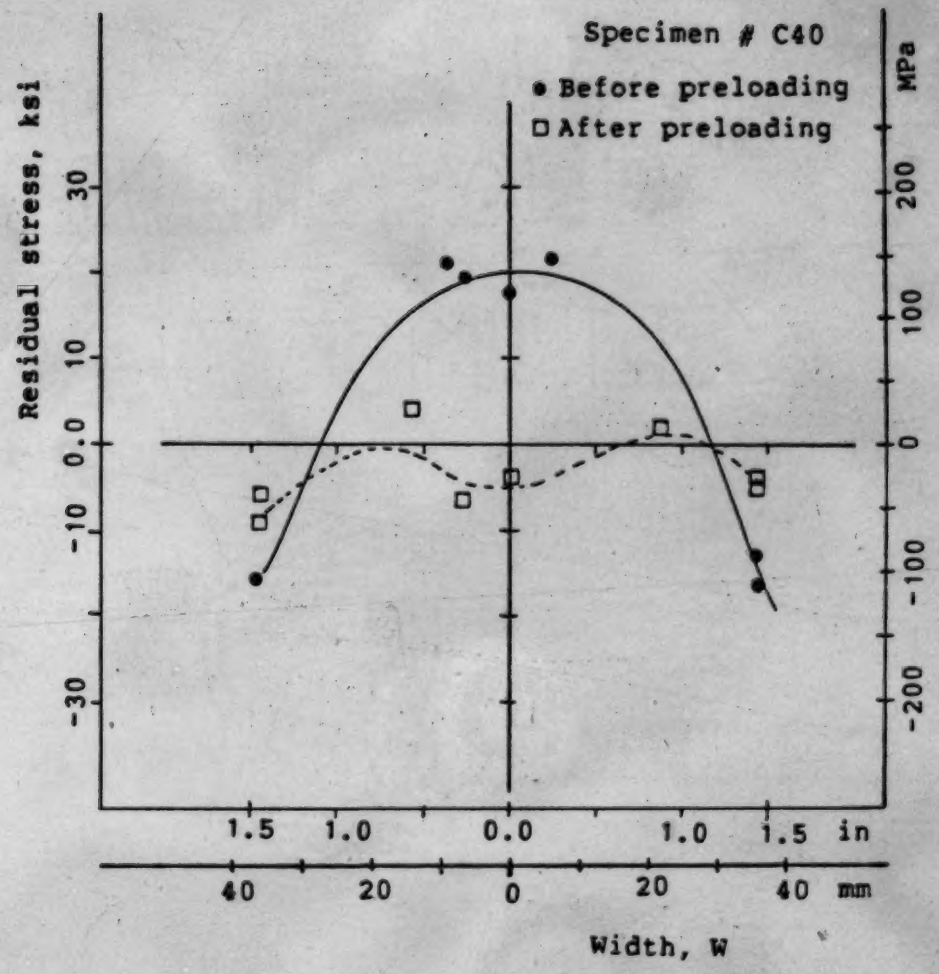

Figure 4.18 Change of residual stress pattern after preloading.

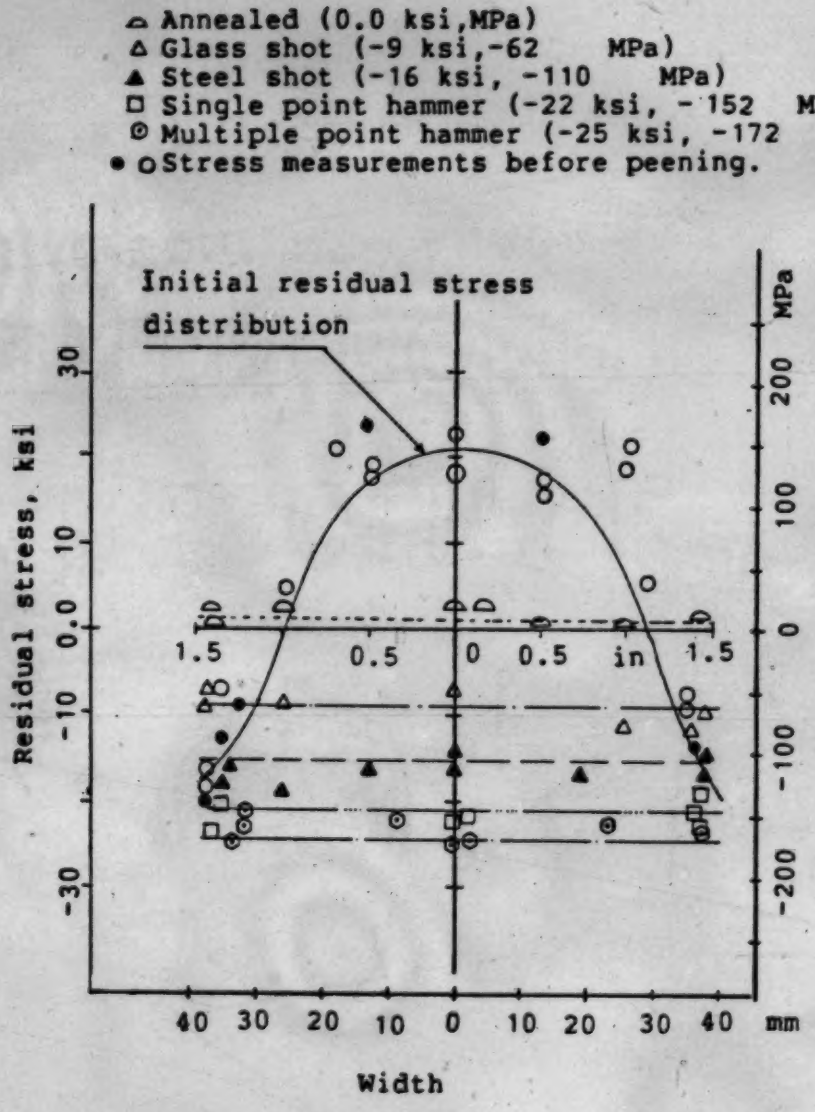

Figure 4.19 Introduction of compressive peening stresses by various mechanical / thermal methods.

○ Stress peening (peening first & then preloaded) (-25 ksi,-172 MPa)
▲ Stress peening (preloaded first & then peened) (-25 ksi, -172 MPa)

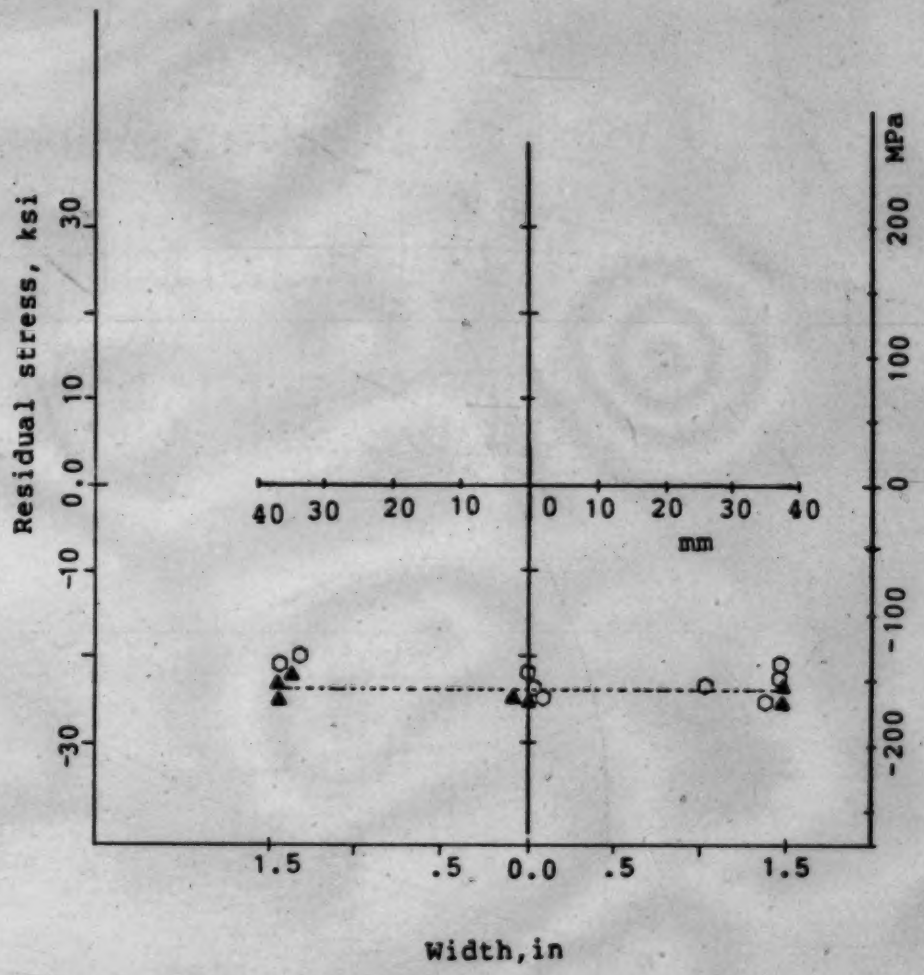

Figure 4.20 Introduction of compressive stresses by stress-peening

4.4 Fatigue Testing, Methods Of Stress Relief And Their Effectiveness

The data obtained from the fatigue tests were plotted in Figs. 4.21 to 4.23 for "stress-life" curves for each of these cases mentioned above. The tests were discontinued with the appearence of a very small crack in the specimens. The levels of the applied dynamic peak stresses decreased with the appearence of a crack whereupon the machine shut off automatically. Usually four to six specimens were tested at a particular stress level and the curve was drawn through the mean values. A specially designed bending stress jig (Fig. 3.8) was used to minimize the effect of bending stresses while gripping the specimens in the testing machine. A considerable amount of scattering showed in the data particularly at intermediate and lower stress levels. For single point hammer peened specimens scattering was found even at large stress ranges. This may be due to the fact that the weld toe could not be peened smoothly with the single point hammer and there could have existed sharp stress raisers due to the non-uniform peening effect. The origins of the scatter of data may be due to the variations in the preparation of the specimen surface, alignment of the test specimens, metallurgical variables and variations in stress concentrations. In most of the cases it was noted that the crack started on the surface and near the weld toe, the HAZ or in the weld metal and at the highly stressed "second pass" side. It was observed that for few of the

multiple point hammer peened and stress-peened specimens it did not break near the toe or weld region but in the base metal part of the specimens. The specimens which "ran out" are shown by a special notation ($o\rightarrow$) to indicate that they do not represent the actual number of cycles to failure.

From the results of the fatigue tests (Figs. 4.21 to 4.23) it can be seen that the fatigue strength at 2×10^6 cycles of the base metal was 49 ksi (338 MPa) and the as-welded specimen was 21 ksi (145 MPa) i.e. 43% of the parent material. The fatigue strengths for the other cases mentioned above lie within the range of 43% to 100%. The fatigue strength improved up to 50% (24.5 ksi, 169 MPa) for tensile preloading, 49% (24 ksi, 165 MPa) for annealing, 59% (29 ksi, 200 MPa) for glass and 72.5% (35.5 ksi, 245 MPa) for steel shot peened, 74.5% (36.5 ksi, 252 MPa) for single point and 77.5% (38 ksi, 262 MPa) for multiple point hammer peening, and 83% (40.5 ksi, 279 MPa) for stress peening. From the data it was observed that the two cases of stress peening (first the specimen was preloaded to less than the yield stress of the base metal and then the surface was peened and secondly the specimen was peened first and then preloaded as above) resulted in a considerable amount of increase in the fatigue strength of the weld. A clear difference in the improvement of stress-peening between the above mentioned two methods was not observed for this medium strength steel. The data showed that the improvement of fatigue strength at stress level greater than 35 ksi (241

MPa) or at life less than 5 x 10^5 cycles glass and steel shot peened specimens were small in comparison to the long life regime.

The total fatigue life N_T obtained for all the above cases are compared with the theoretical predictions later in this Chapter.

Figure 4.24 shows the percentage improvement in fatigue strength over the as-welded butt-joints as a function of the difference in induced stress from the initial residual stress of 22 ksi (152 MPa) due to welding. The difference in induced stress was calculated as the absolute value of the initial residual stress at the weld toe minus the induced compressive stress due to various forms of post-welding treatment. The fatigue strength was taken at $2x10^6$ cycles. A fourth order polynomial curve fit was obtained and the equation of the curve was shown in Fig. 4.24 which showed the trend of the improvement due to mechanical and thermal treatment (annealing, tensile preload, glass and steel shot, single and multiple point hammer and stress-peening). A maximum improvement of 93% was obtained due to stress peening. Thermal stress relieving (annealing) produced an improvement of only 14%. Multiple point hammer peening and stress peening introduced the same amount of surface compressive stresses (-25 ksi ,-172 MPa). The difference in improvement on fatigue strength between multiple point hammer and stress peening is approximately 12%. Therefore, the surface residual stress measurements alone may not give

the justification for improvements in fatigue strength.

The following observation was made from Fig. 4.24:

(I) A close fit (correlation coefficient r.=0.965) was obtained assuming the curve did not pass through the origin for a straight line. This states that for residual stresses less than about 20 ksi (138 MPa) no beneficial effect can be expected in fatigue life.

(II) Assuming that any residual stress, no matter how small, will improve fatigue life then a fourth order polynomial fit which was almost linear for residual stresses in excess of 30 ksi (207 MPa) showed that for residual stresses less than 20 ksi (138 MPa) the beneficial effects to increase fatigue life were less than 10%.

(III) In support of the assumptions in (II) it was found that the fatigue life could be improved in butt-welded specimens when mildly peened with glass shot beads.

It has been reported by various researchers that the maximum amount of compressive stresses that can be induced on the specimen surface is of the order of 0.4 to 0.6 S_u, where S_u is the ultimate tensile strength of the material. It can be concluded that by severe peening on the surface the improvement on fatigue strength will not increase considerably (by large percentage) rather it may damage the surface. Severe surface roughness due to peening may give rise to very localized variations in stress which, in turn, may be harmful in improving the fatigue life.

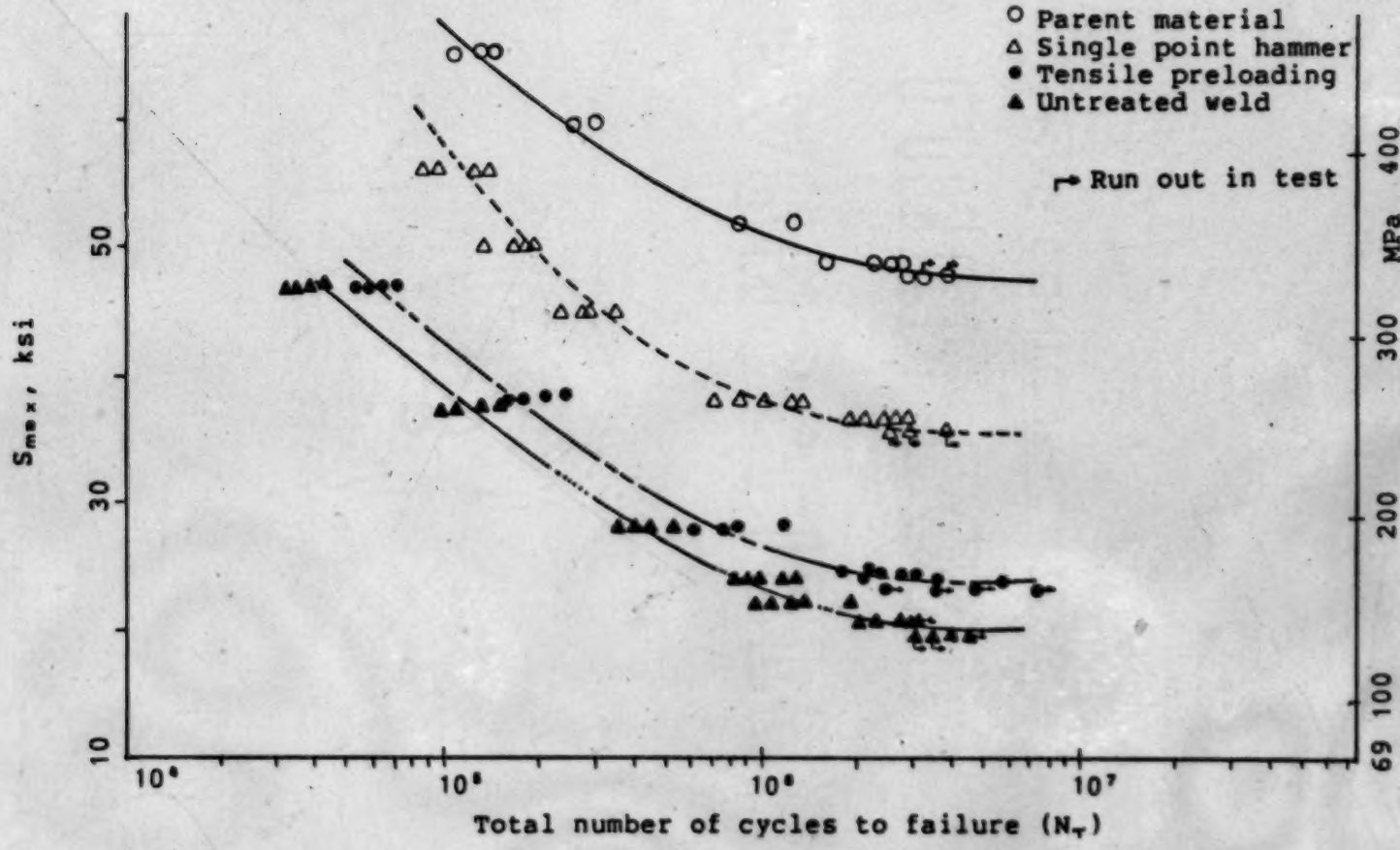

Figure 4.21 Experimental fatigue tests results of parent material, single point hammer peened, tensile preloading and untreated welded specimens.

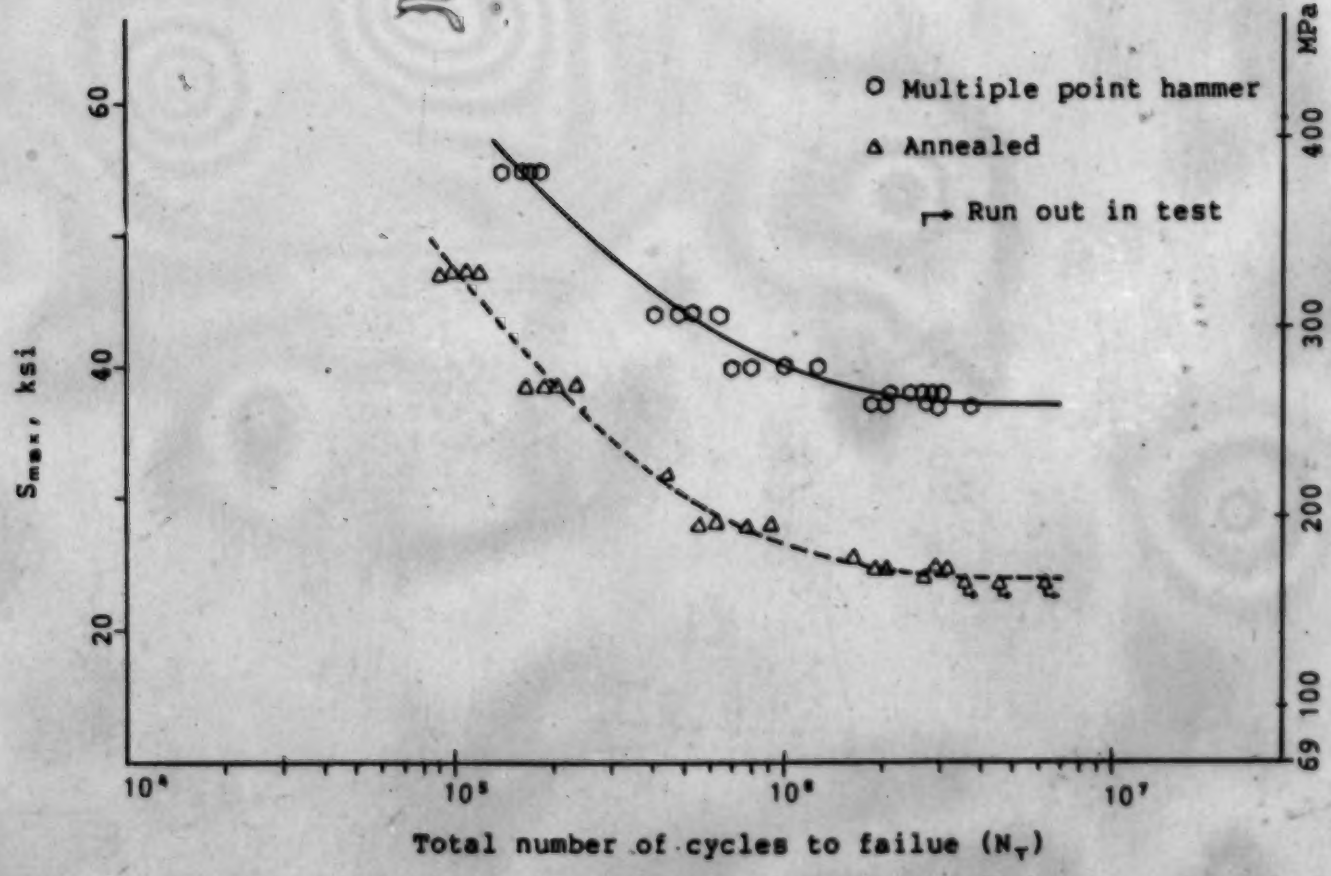

Figure 4.22 Experimental fatigue tests results of annealed and multiple point hammer peened specimens.

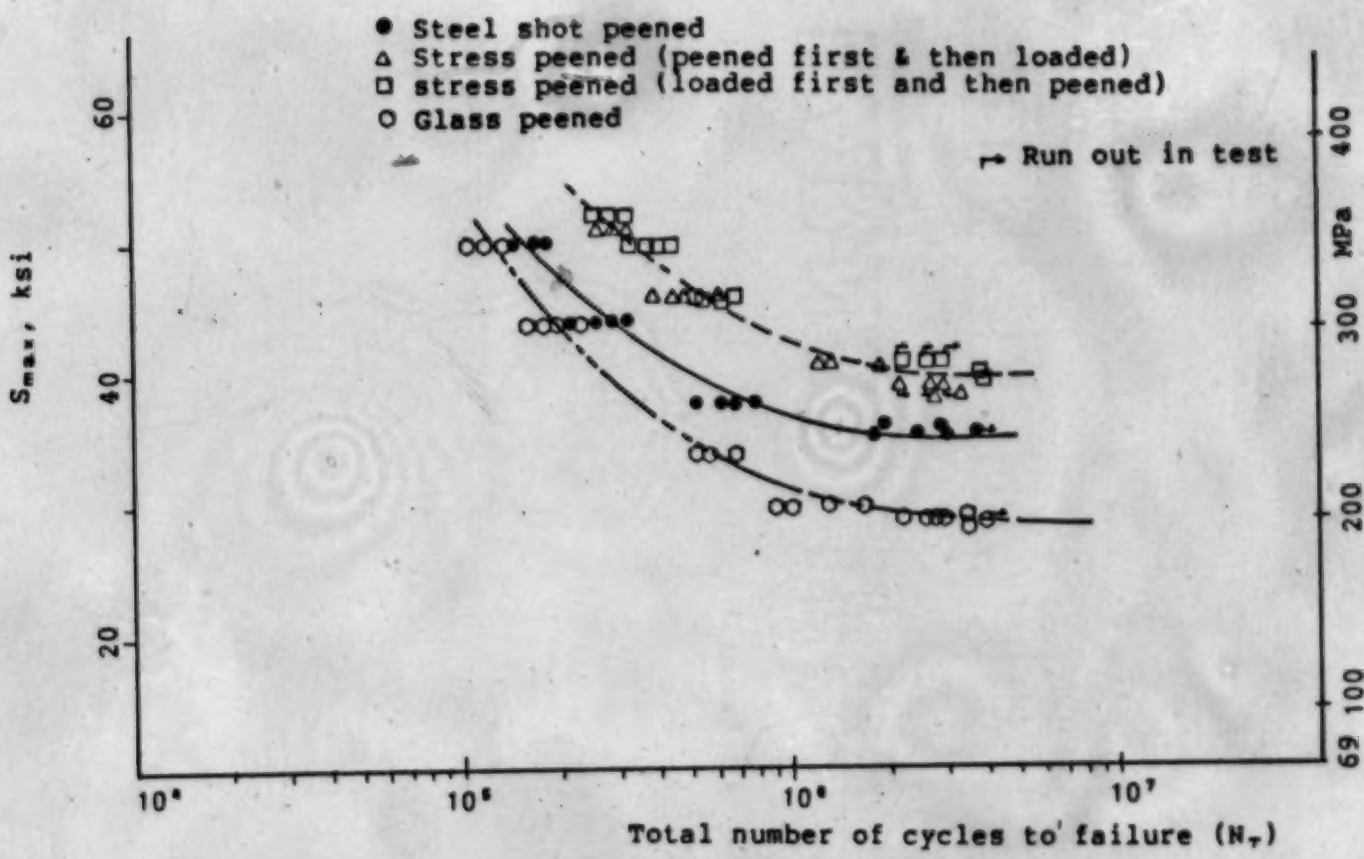

Figure 4.23 Experimental fatigue tests results of glass peened, steel shot peened and stress peened specimens.

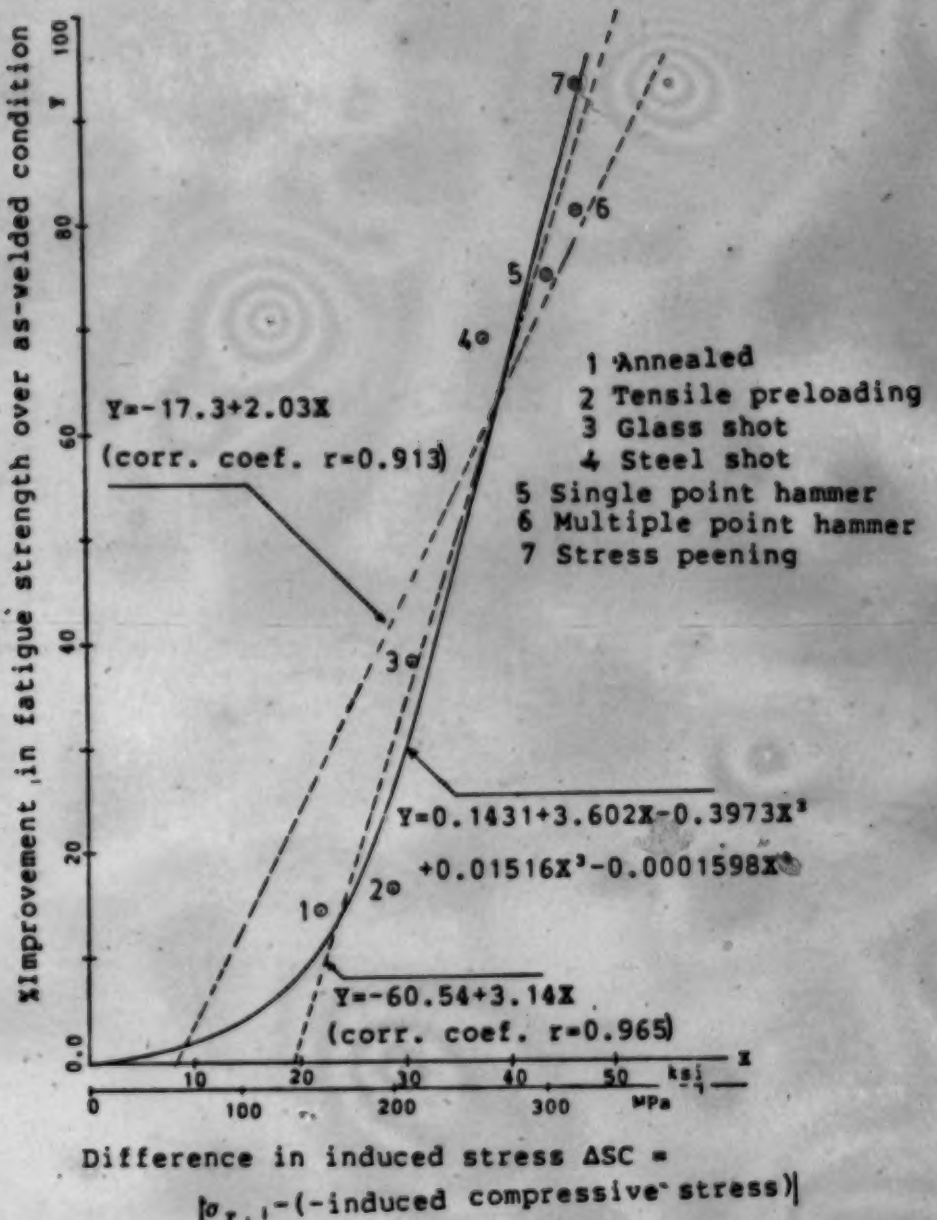

Figure 4.24 Percentage improvement in fatigue strength and difference in induced stress.

To study the depth of work-hardening Knoop hardness readings using a 300 gm. load across the depth of work-hardened area were taken. The data showing the hardness versus the depth are plotted in Figs. 4.25 to 4.27. The glass shot peening produced a depth of work-hardening of 0.008 in (0.203 mm), steel shot peened 0.017 in (0.432 mm), multiple point and single point hammer peening 0.027 in (0.686 mm) and 0.030 in (0.762 mm) respectively and the both forms of stress-peening produced a depth of work-hardening of 0.028 in (0.711 mm). Figure 4.28 shows the plot of surface residual stresses as functions of Almen strip readings and the depth of work-hardening. A consistent trend was found between the residual stress levels and the depth of work-hardening. Although the depth of work hardening was slightly more for single point hammer peening than that of multiple point hammer peening the improvement on fatigue strength by multiple point hammer peening was greater. This may be because when these two peening processes were investigated by using an ultra-violet sensitive coating (magnaflux penetrant and developer) it was observed that the toe of the weld was not uniformly and completely peened in the case of single point hammer peening. The compressive residual stress level was higher in the multiple point hammer peening than that of the single point hammer peening. Consequently, multiple point hammer peening produced an increase of 7.2% improvement in fatigue strength over the single point hammer peening.

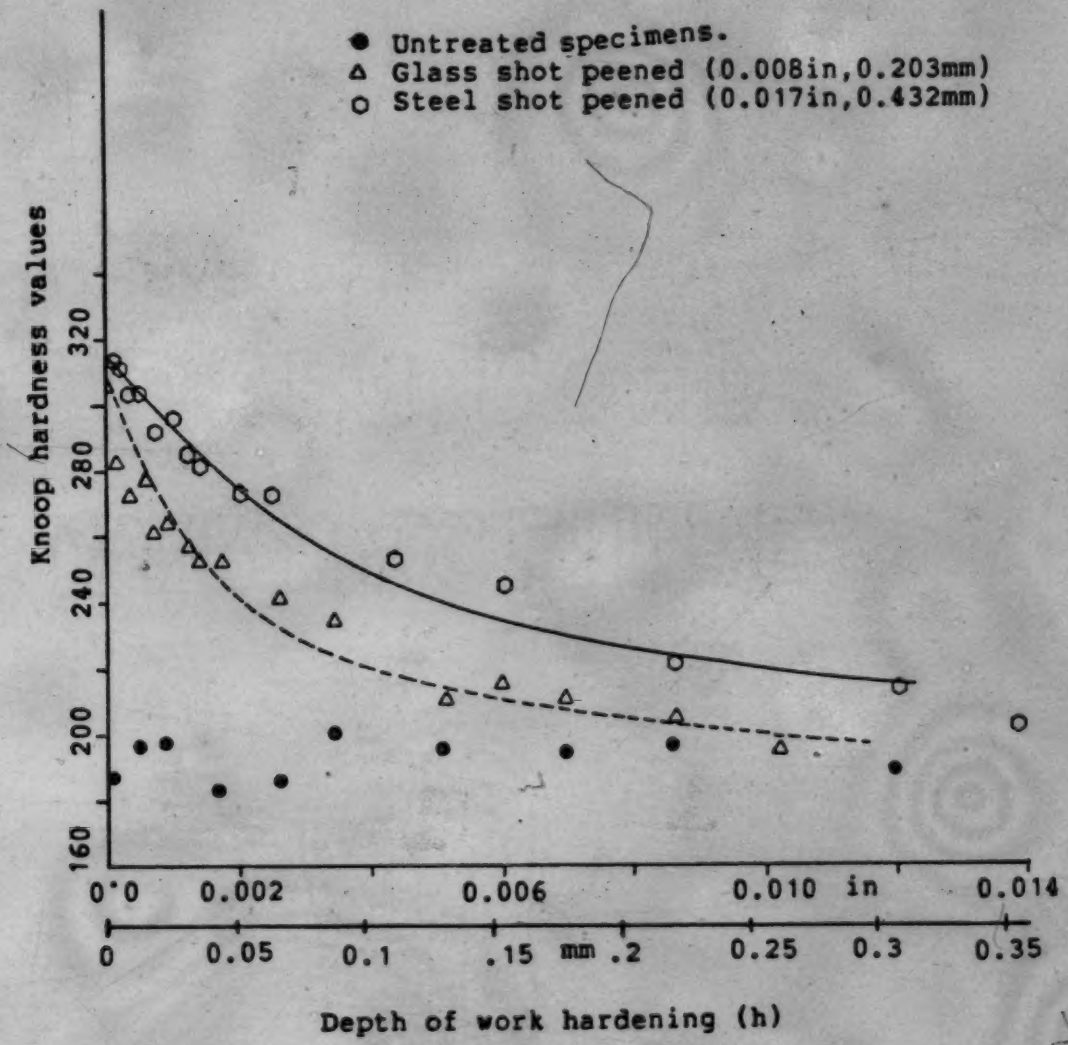

Figure 4.25 Knoop hardness values vs. depth of work hardening of glass and steel shot peened and untreated welded specimens.

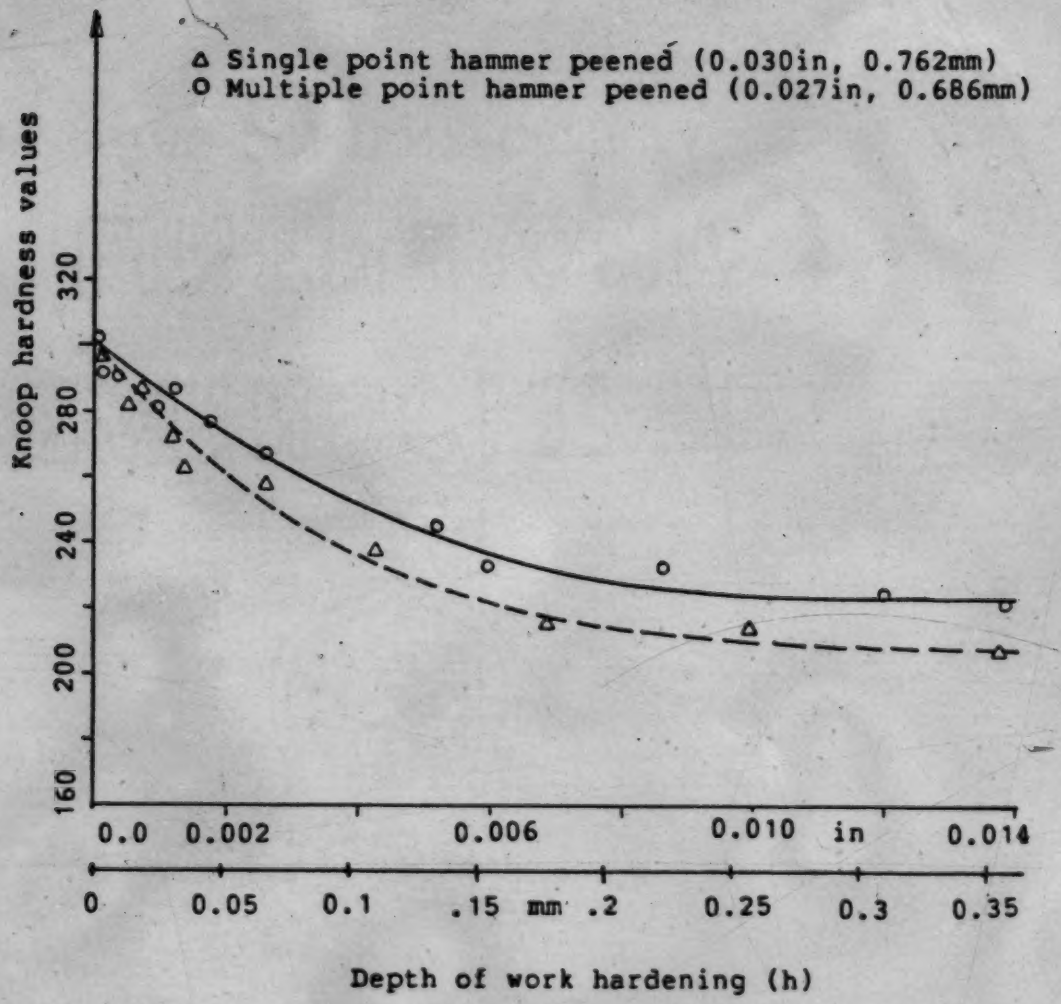

Figure 4.26 Knoop hardness values vs. depth of work hardening for multiple and single point hammer peening.

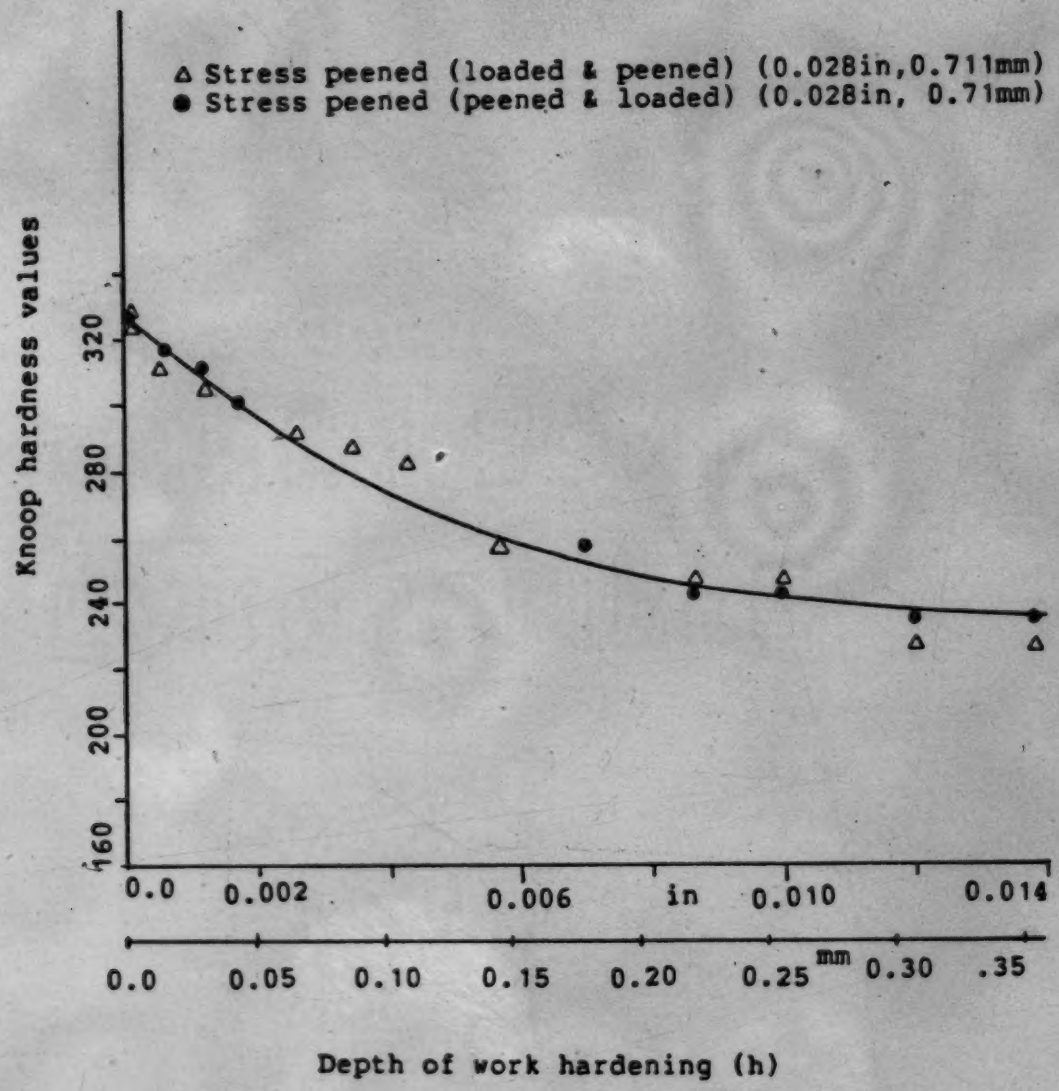

Figure 4.27 Knoop hardness values vs. depth of work hardening for two cases of stress-peening.

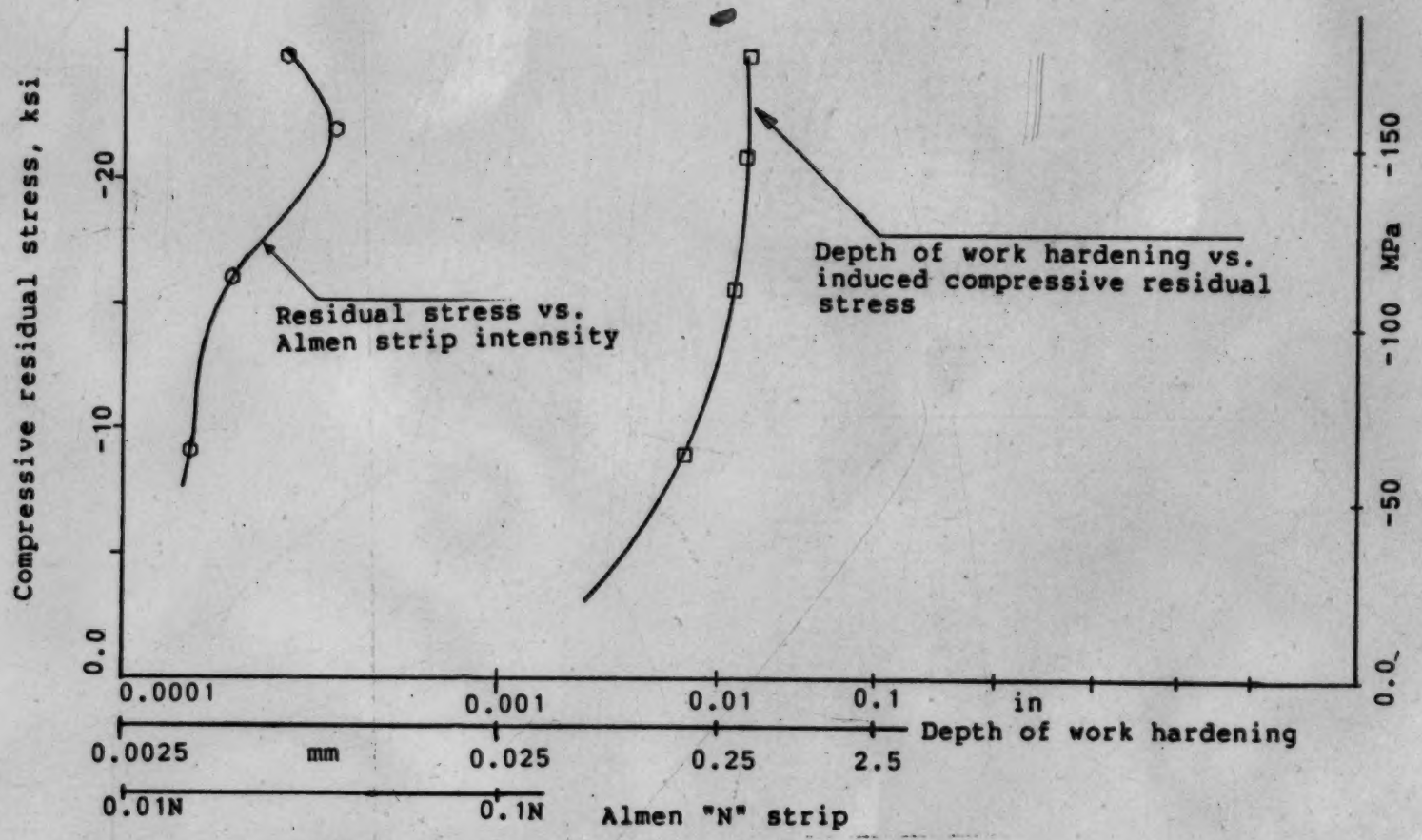

Figure 4.28 Depth of work hardening and Almen strip intensity vs. induced compressive residual stresses by various methods.

From Fig. 4.28 it was seen that the Almen strip readings did not give a consistent indication as a function of surface compressive stresses.

Surface peening produces the work hardening of the surface metal. Figures 4.29 & 4.30 show the difference in Rockwell B hardness values on the base metal, the weld metal, the HAZ metal and across the thickness for an untreated ground flat welded specimen and a glass peened specimen. It can be seen that there is considerable change in hardness values in the weld and the HAZ material areas. Micro-hardness measurements require the smooth and highly polished surface finish. It was not possible to use micro-hardness measurements on the large specimen and glass peened surface because of the size and surface roughness of the specimen. Therefore, Rockwell hardness measurements (1/16 in (1.6 mm) ball, 100 Kg. load) were taken for the measurement of hardness on glass shot peened specimens (Figs. 4.29 and 4.30). Micro-hardness readings using a 300 gm. load and Vicker's hardness test on the critical locations of the weld also showed that there were differences in hardness readings at those critical locations. From the average of about 10 readings the HAZ had a hardness of VHN 170. The highly diluted and untempered weld metal had a hardness of VHN 205 and the tempered weld metal zone measured VHN 206 (Fig. 3.9).

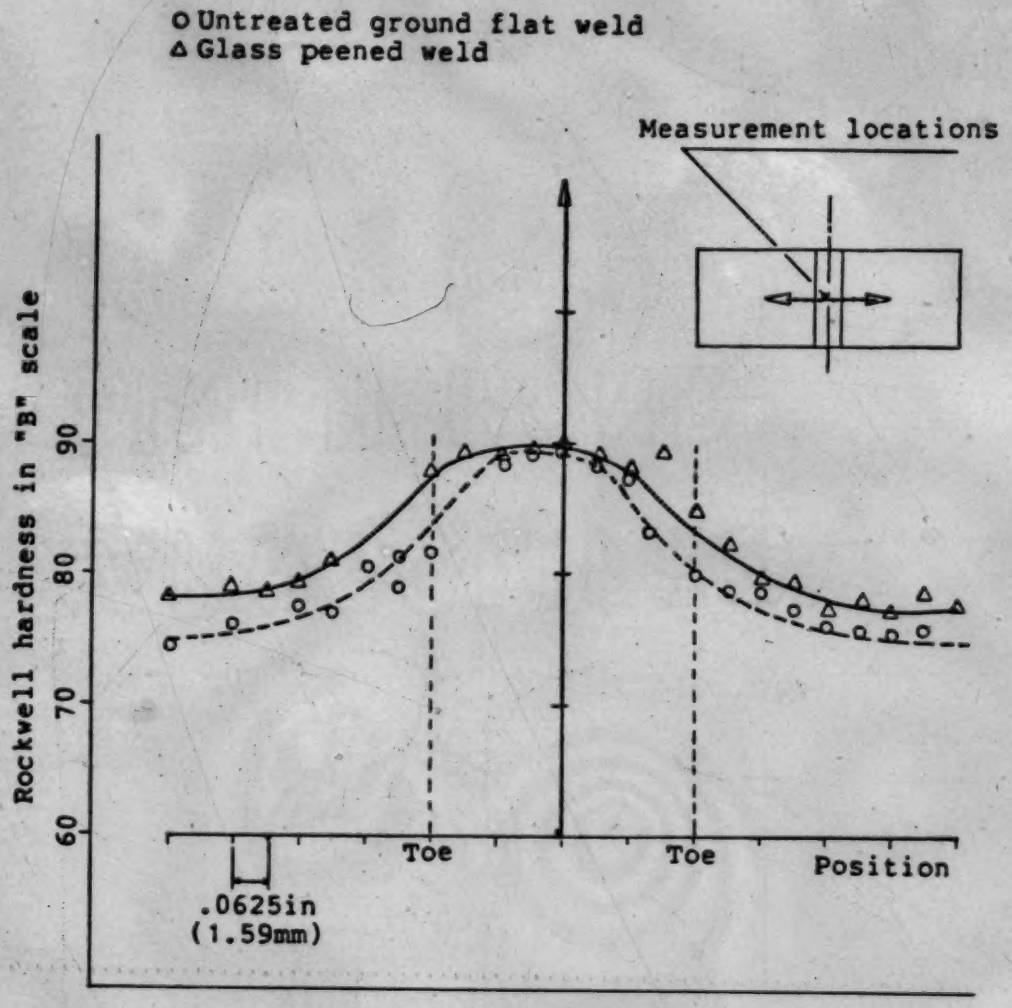

Figure 4.29 Hardness on the surface across the weld, the HAZ and the base metal

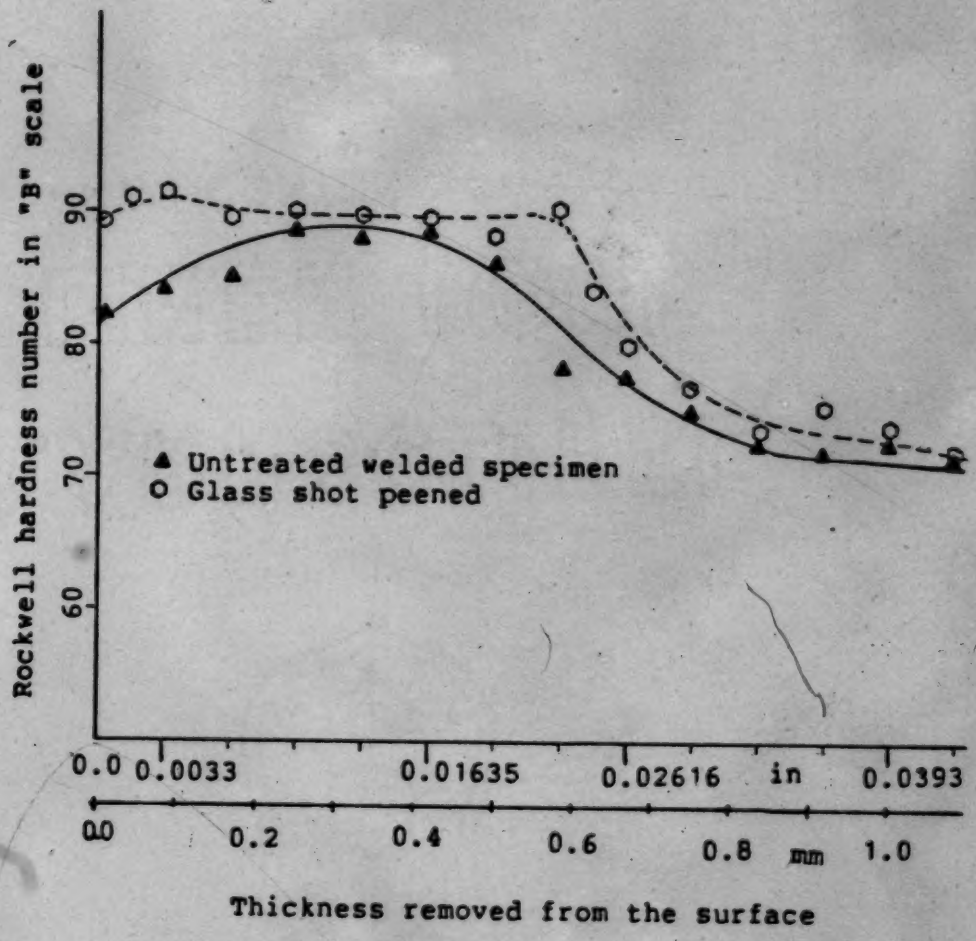

Figure 4.30 Hardness readings across the thickness of untreated weld and glass shot peened specimens.

4.5 Theoretical Results, Correlations With Experiments And Discussion

4.5.1 Introduction

This section correlates the experimental results to the theoretical prediction of fatigue crack initiation and crack propagation. This section also examines the suitability of the experimental measurements and the assumptions used in the theoretical analyses in predicting the total fatigue life of butt-welded joints.

Fatigue lives of weldments were estimated by using the theoretical model discussed in Chapter II. The K_f value was computed based on Neuber's equation (Eq.(7)), the weld geometry (edge preparation angle θ=90°, flank angle ϕ=45°) and the weld toe root radius (r). The theoretical stress concentration factor K_t was computed by using Eq.(6) taking the value of A=0.27. The weld toe root radius (r) as a function of K_f and K_t were discussed in Chapter II (Fig.2.3). The parametric study showed that the crack initiation life was sensitive to the weld toe root radius. With the increase of "r" the fatigue life improves. The crack initiation life (stress range ΔS=25 ksi (172 MPa), residual stress σ_r=22 ksi (152 MPa)) improved by an ammount of 63% for an increase of "r" value from 0.001 in (0.0254 mm) to 0.01 in (0.254 mm) while the crack initiation life increased by 44% due to an increase in root radius from r=0.0001 in (0.00254 mm) to 0.001 in (0.0254 mm). The values

of $K\sigma$ and $K\epsilon$ were obtained for each individual level of S_{max} by using Eq.(10) and Eq.(1). Modified Neuber's Equations (Eqs. (17) & (18)) were used to compute the effect of residual stresses initially and subsequent to the first cycle. The damage in terms of elastic, plastic and mean stress effects were calculated on a cycle by cycle basis until the cumulative damage law (Eq.(23)) was satisfied which calculated the crack initiation life of a weld. For the calculation of fatigue crack propagation life the crack growth rate constant C and crack growth rate exponent m and fracture toughness stress intensity factor K were assumed for the base metal, the HAZ and the WM which were chosen on the basis of material strength and properties (Table 10). The total fatigue life was estimated by summing the crack initiation and crack propagation lives.

Equation (10) which determines the value of $K\sigma$ from material properties, loading condition and K_f value was developed in this study. Reemsnyder (1981) also derived a different relationship between K_f and $K\sigma$ as shown in Eq.(10*). Equation (10) is an important equation to determine the local notch-root stress from the applied nominal stress. This local notch-root stress is important in the estimation of crack initiation life. For a value of K_f=1.851 Eq.(10) produces a value of $K\sigma$=1.521; whereas Eq.(10*) produces $K\sigma$=0.85 (at nominal stress S=25 ksi (172 MPa), E=29000 ksi (200X10^3 MPa), n'=0.278, $\sigma_{r,1}$=22 ksi (152 Mpa), K'=183 ksi (1262 MPa)). Using the basic definition of

$K\sigma$ (i.e. $K\sigma=\sigma/S$), Eq. (10) produces a local notch-root stress σ=38 ksi (262 MPa) which can be expected due to the stress concentration at the local notch-root. For the same case, Reemsnyder's (1981) Eq.(10*) produces a local notch-root stress σ=21 ksi (145 MPa) which is even less than the applied nominal stress S=25 ksi (172 MPa). This stress condition at the notch-root may not be possible. Therefore, Eq.(10) derived in this study calculates local stress condition more accurately than Eq.(10*).

4.5.2 Predictions Of Total Fatigue Life And Experimental Results

The comparisons of predicted and measured fatigue life are given in Figs. 4.31 to 4.40. This includes the results for the as-welded specimens as well as those for the various surface treatments described above.

Figure 4.31 showed the plot of stress range versus total number of cycles to failure for the theories and experimental data points for the as-welded condition. The theories were based on parent material, weld material and the "adjusted weld-parent interface material properties". The "adjusted" weld-parent interface material properties were taken as the average values of the parent and weld material properties (Table 4). From Fig. 4.31 it can be observed that the theory based on the parent material properties predicts a higher total life than that obtained experimentally. The percentage error in the applied stress

range between theoretical predictions based on parent material and experimental results at $2x10^6$ cycles was approximately 16%. The percentage error in stress range at $2x10^6$ cycles between the theories based on parent and weld material properties for the as-welded conditon was approximately 25%.

It was observed (Fig. 3.9) that the critical locations of the fatigue crack initiation in butt-welds are in the weld metal and the 'weld-parent' interface material close to the fusion line. Figure 4.31 also showed the prediction of total life based on WM proerties. The weld metal properties were obtained from the empirical relations using hardness readings. It was observed that the WM estimates the total life less than the experimental results. The percentage error in stress range at $2x10^6$ cycles was approximately 8% from the experimental results.

To obtain a more accurate prediction of total life the actual 'weld-parent' interface material properties are needed. These material properties can only be obtained from the standard size specimens made from the actual 'weld-parent' interface materials. This would have been difficult due to the small area of the interface. To overcome this difficulty and to obtain a better correlation between the experimental results and the theoretical predictions adjusted 'weld-parent' interface material (as mentioned above) properties were obtained by averaging between the WM and base metal. It can be seen from Fig. 4.31

that the adjusted material properties correlated closely with the experimental results. The percentage error in stress range at 10^6 cycles between the experimental results and the theory based on the adjusted material properties was 5%.

Before considering the correlation between experimental results and the theoretical predictions the discrepencies due to the following reasons should be considered. These discrepencies may be (i) in the measurement of initial residual stresses, (ii) difference in taking the exact weld-toe root radius, (iii) effect of initial residual stress distribution which was considered in the calculation of crack propagation life, (iv) difference in the values of actual cyclic material properties than that found from experiments, (v) the applicability of linear cumulative damage rule for Columbium-50 steel, (vi) in the assumptions of initial and final crack length of 0.01 in (0.254mm) and 0.05 in (0.2t, 1.27 mm) respectively and (vii) localized variations in stress due to surface roughness. There are various types of discontinuities other than geometric discontinuities which may be considered stress-raisers. Surface roughness may give rise to very localized variations in stress particularly in the case of peened specimens. The effect of surface roughness was not considered in this study. Also, the experimental data showed a wide range of scattering in the low and intermediate ranges of life.

Table 4

Adjusted material properties ("weld-parent" interface material properties taken as average of the weld and parent material properties).

Material properties	Base metal	Weld metal	Adjusted ("weld-parent" interface)
0.2% cyclic yield strength σ'_{ys} ksi(MPa)	34.3(237)	44(303)	39(270)
Cyclic strength coeff., K' ksi(MPa)	183(1262)	268(1845)	226(1555)
Cyclic strain hardening exponent, n'	0.278	0.306	0.292
Fatigue strength coeff., σ'_f ksi(MPa)	130.5(900)	148(1019)	139(960)
Fatigue strength exponent, b	-0.127	-0.121	-0.124
Fatigue ductility coeff., ε'_f	0.21	0.105	0.158
Fatigue ductility exponent, c	-0.435	-0.395	-0.415
Transition fatigue life, $2N_{tr}$ reversals	262333	249467	255900
Modulus of Elasticity, $Ex10^3$ ksi(MPa)	29000($200x10^3$)	30000($207x10^3$)	29500($203X10^3$)
0.2% offset yield strength, Sy ksi(MPa)	39(269)	78(538)	58.5(403)
Ultimate tensile strength, Su ksi(MPa)	64(441)	98(676)	81(558)

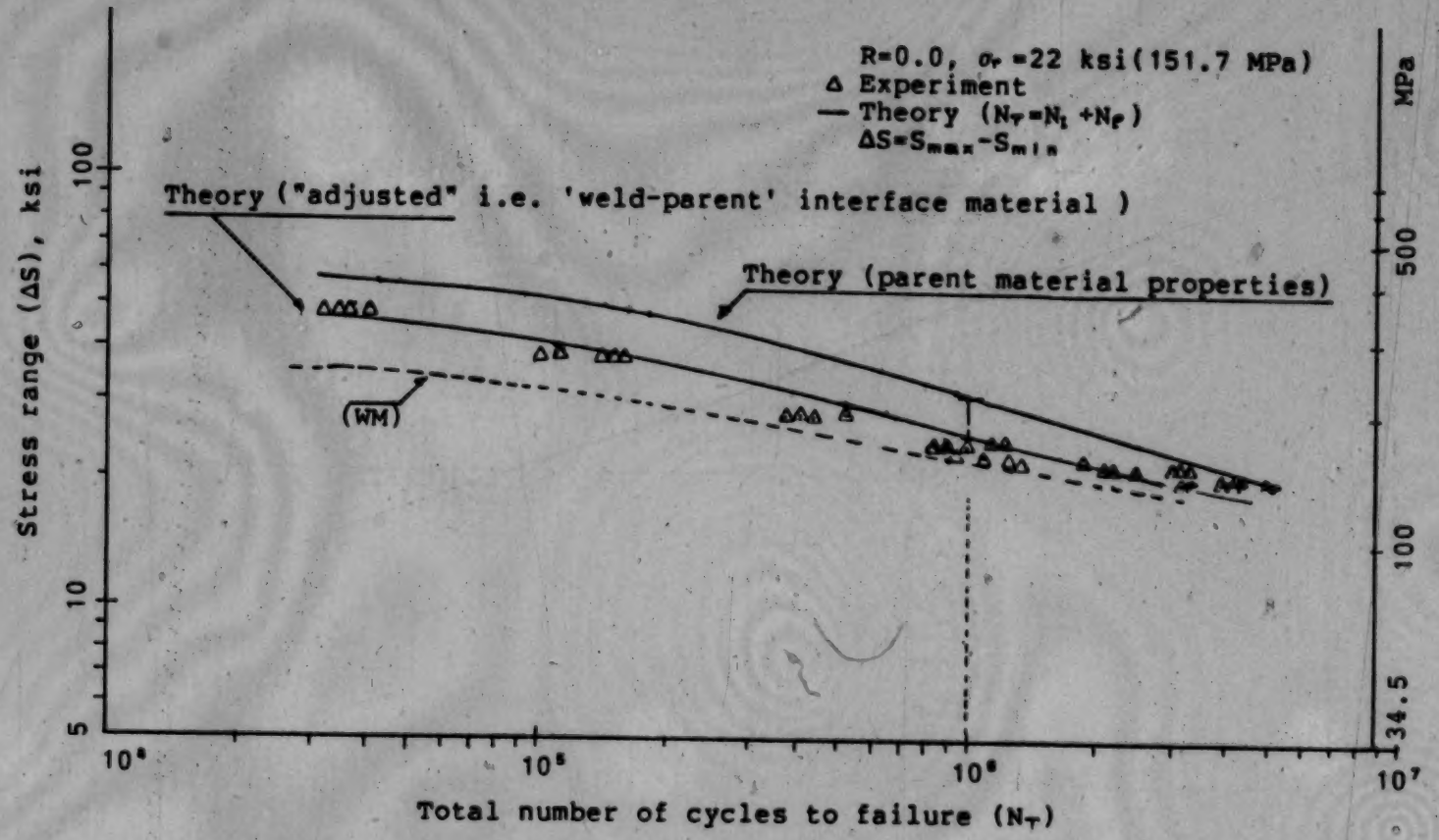

Figure 4.31 Experimental results and theoretical predictions of as-welded specimens.

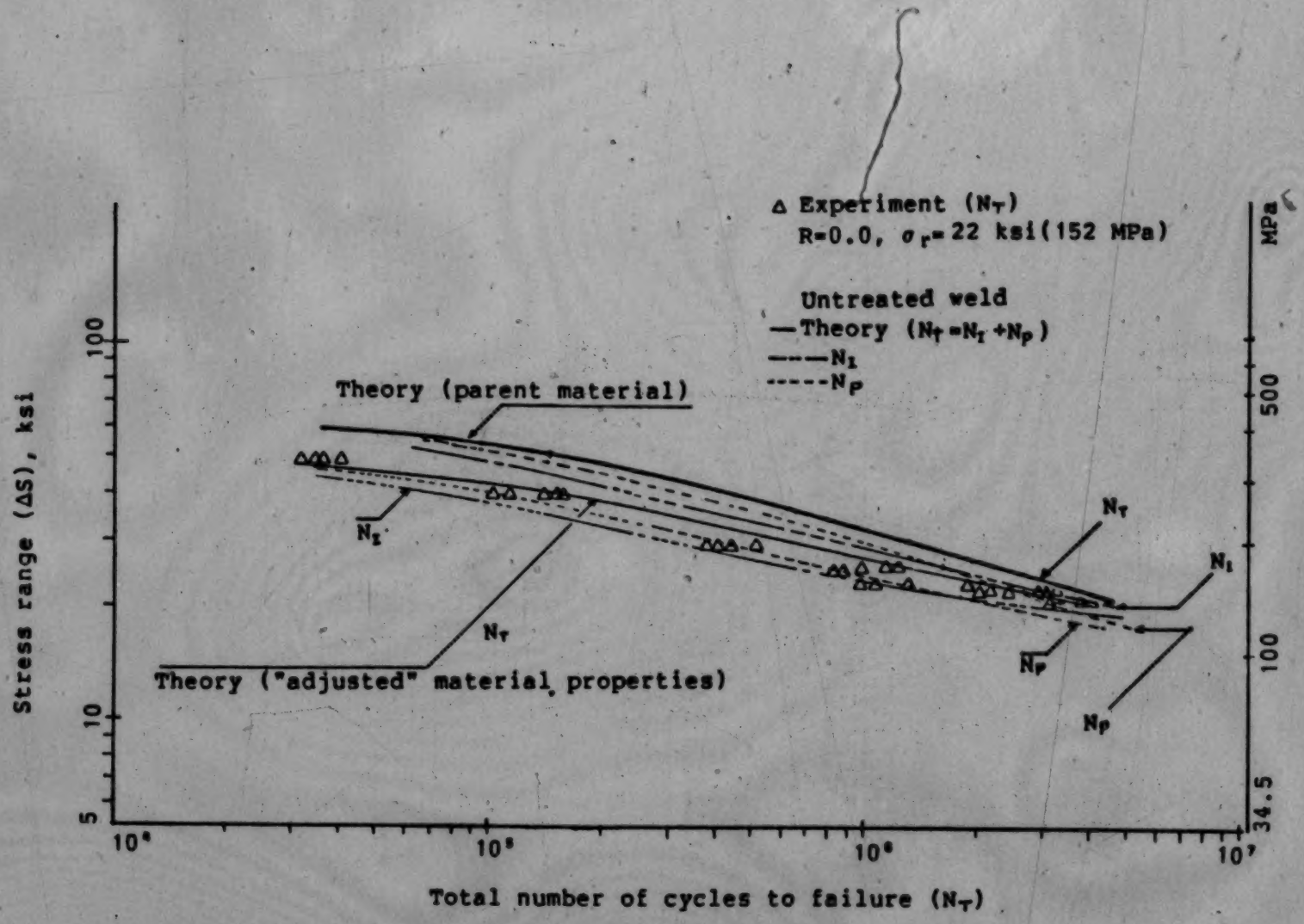

Figure 4.32 Experimental results and theoretical predictions for crack initiation, crack propagation and total fatigue life of the butt-welded joints.

All the tests were performed at room temperature but because of the high frequency of the tests (approximately 87 Hz) an isothermal condition did not prevail. However, from all the above considerations it can be concluded that the theoretical predictions based on the adjusted material properties is in good agreement with the experimental data. Either the actual "weld-parent" interface material properties should be obtained experimentally or approximately the average values of the weld and parent material properties should be considered for the prediction of total fatigue life.

Figure 4.32 showes the predictions (parent material) of initiation , propagation and total lives of as-welded butt-welds with the experimental data. It can be seen that life beyond 1.5×10^6 cycles (i.e. at low stress ranges) initiating a crack takes the larger part of the total life for the same range of nominal stress ΔS; whereas at higher stress ranges and at a life less than 1.5×10^6 cycles propagation life predominates.

Figure 4.32 also showes the predictions (based on the adjusted material properties) of initiation, propagation and total lives of as-welded butt-welds. It can be observed that lives $>1.7 \times 10^6$ cycles required larger part of the total life as the crack initiation life for the same stress range; whereas lives $<1.7 \times 10^6$ cycles propagation life predominates.

Figure 4.33 showed the theoretical predictions (adjusted material properties) and the experimental results

of total fatigue life for the annealed specimens. It was found that the variation in percentage stress range was ≅ 8%. The percentage error in stress range at $2x10^6$ cycles between the theories based on parent and weld material properties for the annealed specimens was approximately 23%. It was obtained experimentally (Fig. 4.19) that the initial residual stress at the weld toe after annealing was about 2 ksi(14 MPa). For annealing, there could be a slight modification of the material properties at the weld toe. The degree of prior cold-working of the parent material was not known accurately and therefore, the annealing temperature (1020°F (550°C)) which was used might have caused a slight recrystallization or grain growth in the HAZ material. For medium cold-working a lesser annealing temperature is required.

Figure 4.34 showed the theoretical predictions (adjusted material properties) and the experimental results for the tensile preloaded cases. It was observed that the percentage error in stress range between the predictions and the experimental results was 14%. The percentage error in stress range at $2x10^6$ cycles between the theories based on parent and weld material properties for tensile preloaded specimens was 27%. For the tensile preloaded case almost no modification of the weld toe root radius occurred during the generation of compressive residual stresses.

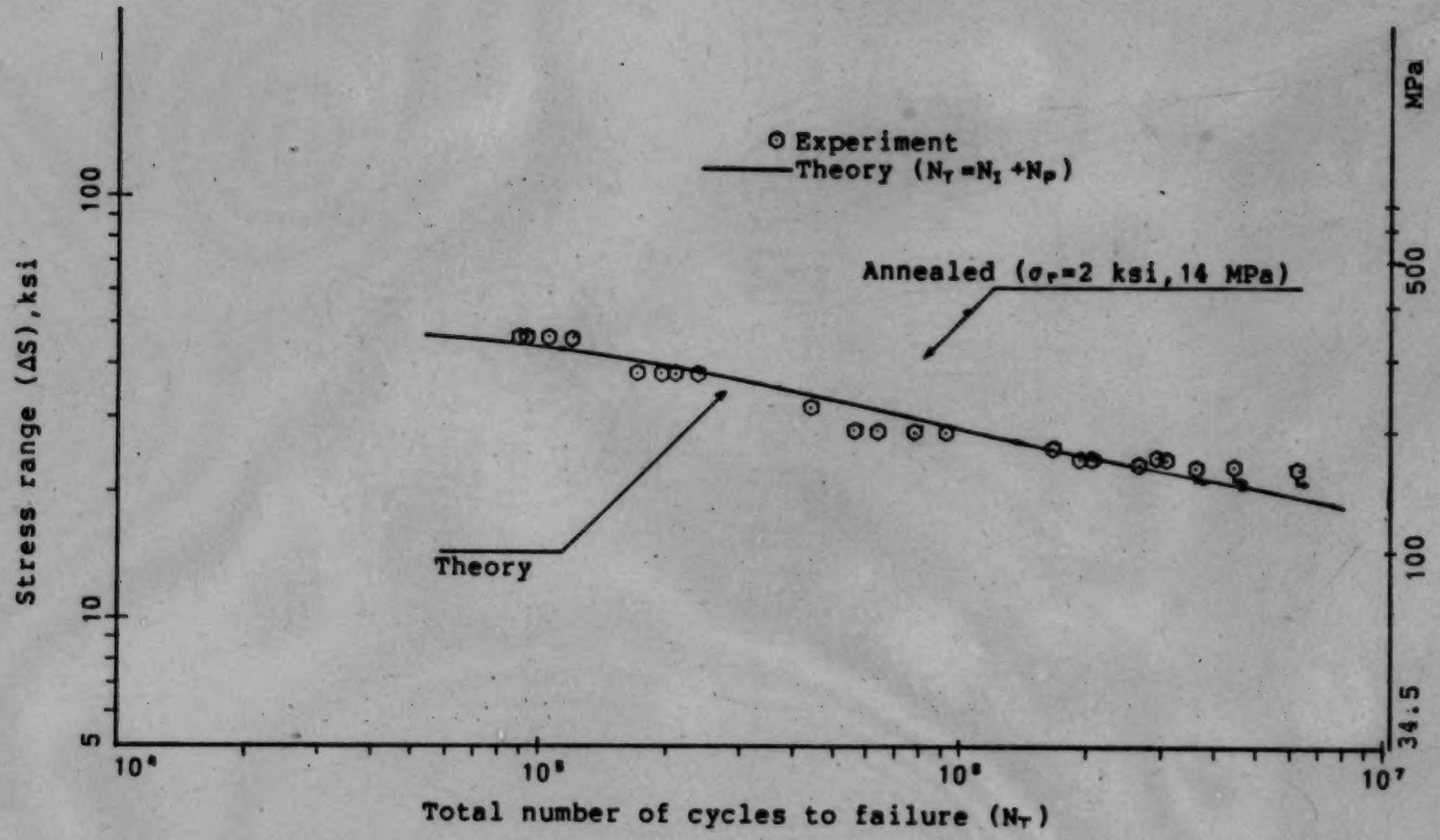

Figure 4.33 Experimental results and theoretical predictions for annealed specimens

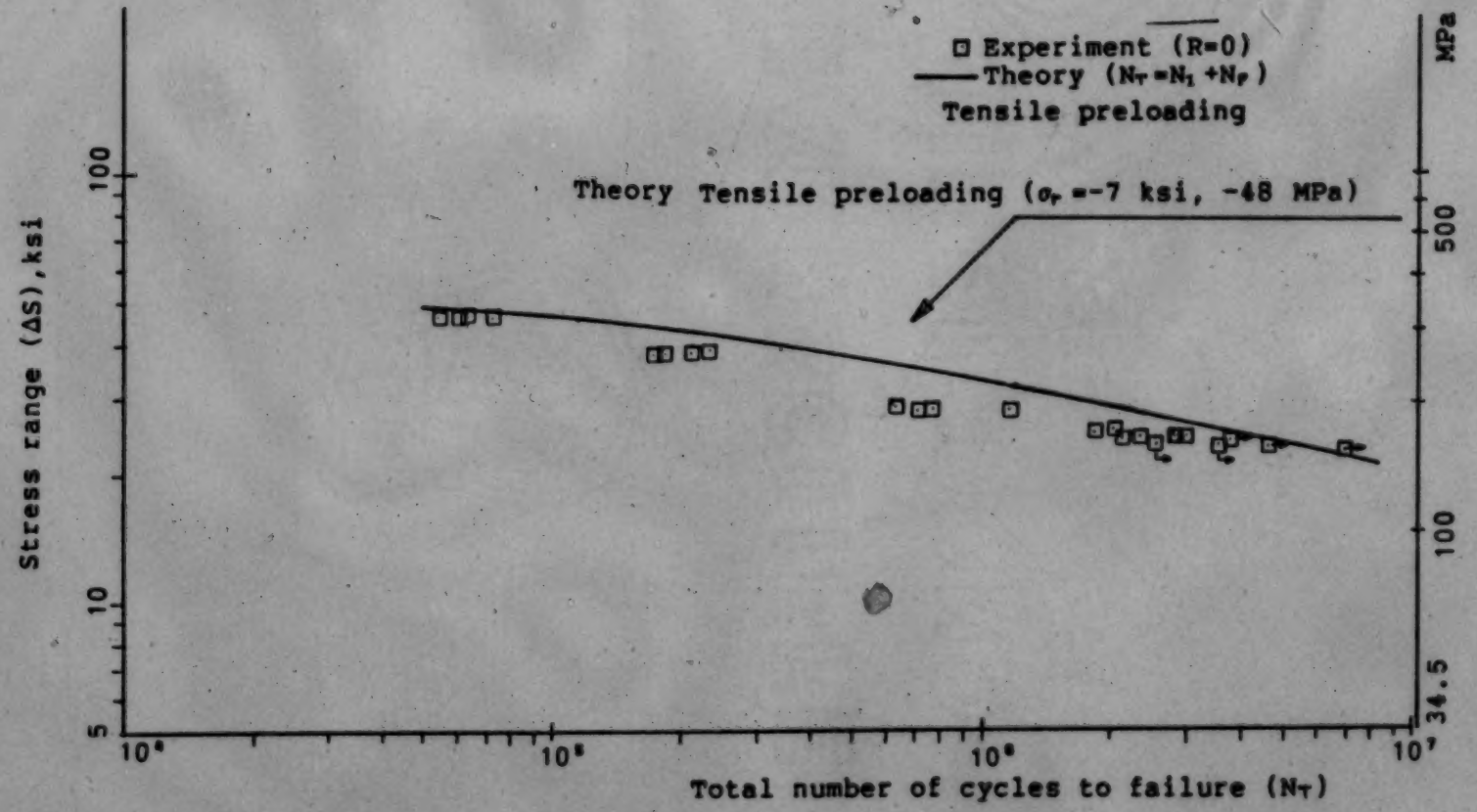

Figure 4.34 Experimental results and theoretical predictions for tensile preloaded specimens.

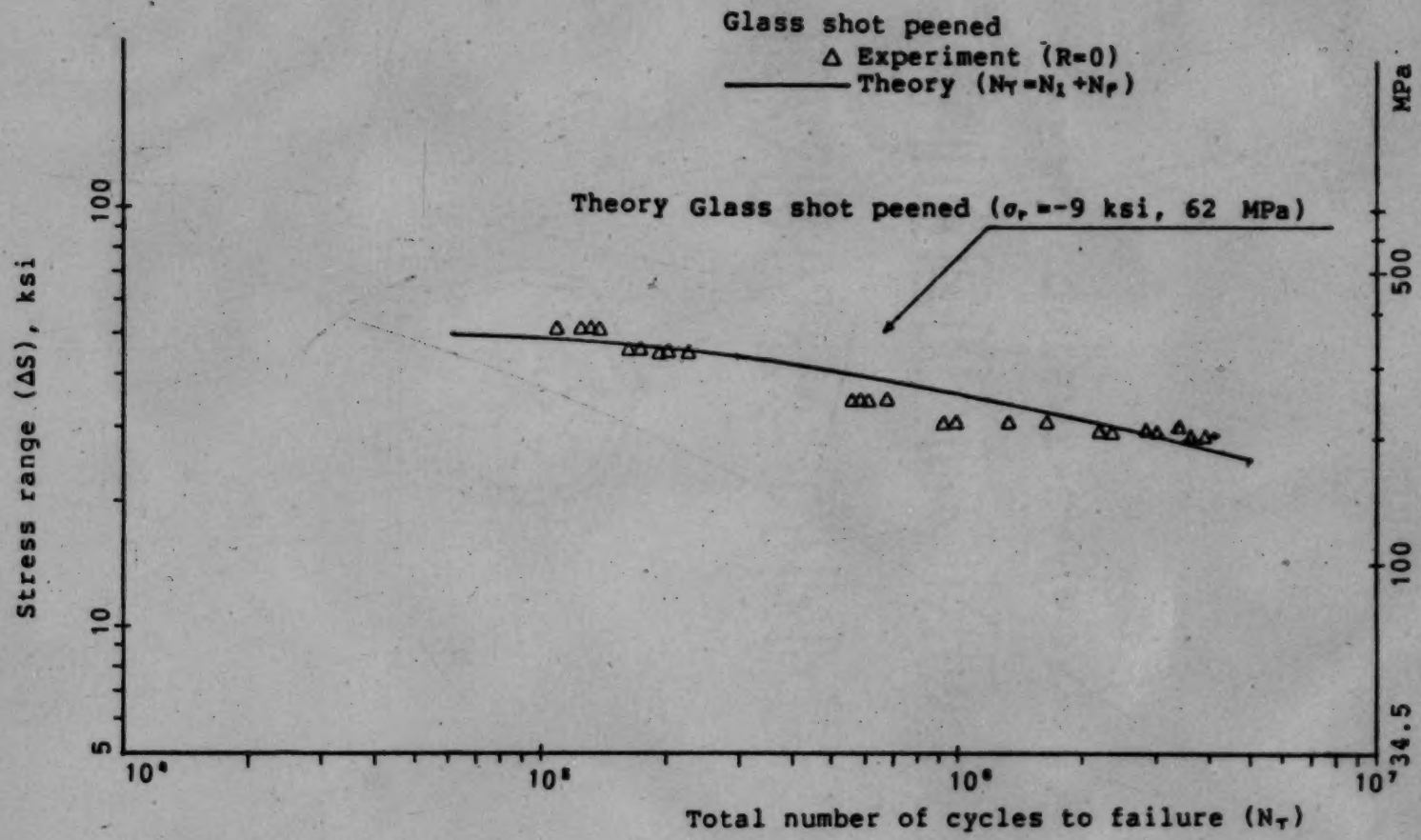

Figure 4.35 Experimental results and theoretical predictions of glass shot peened specimens.

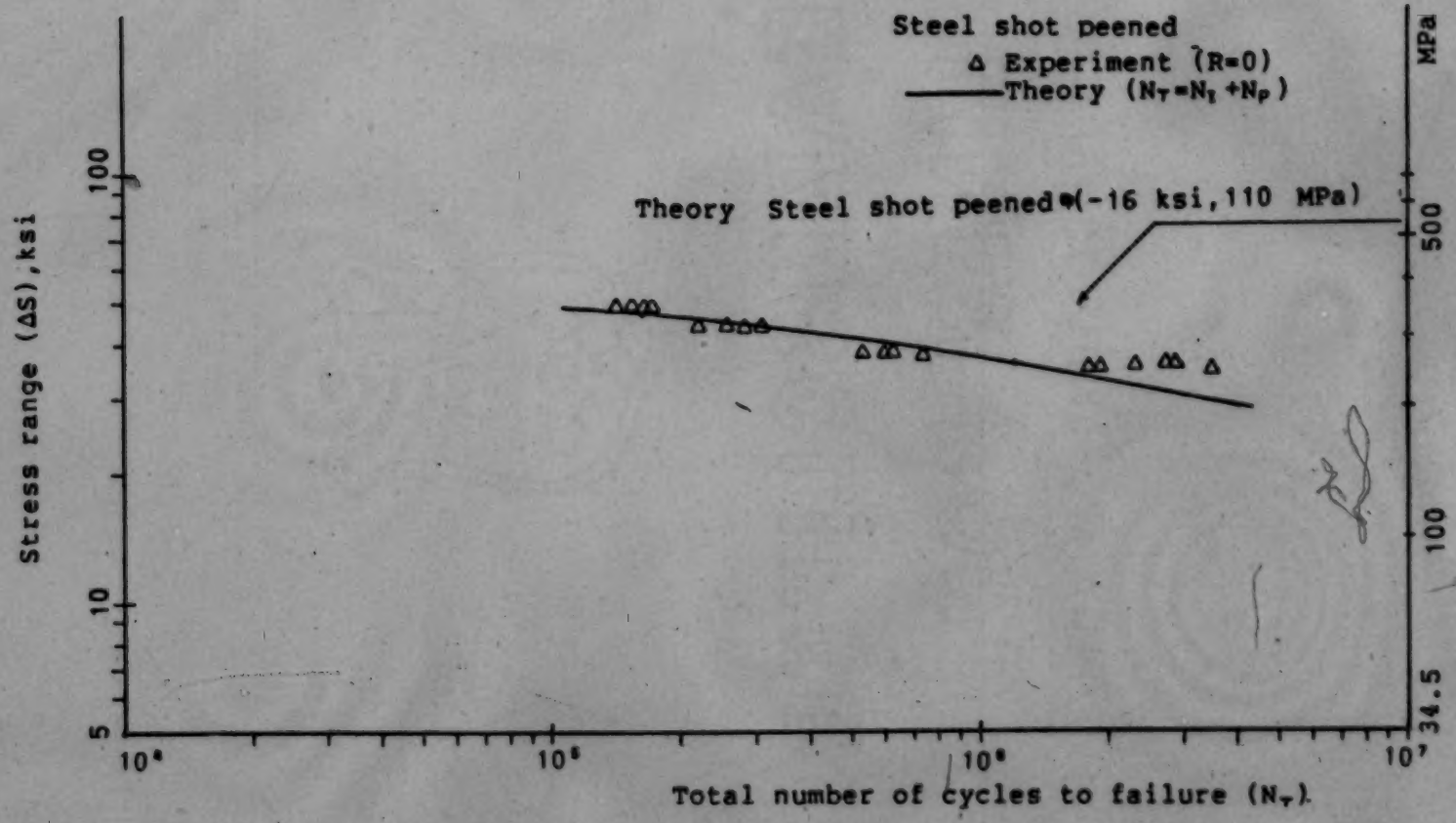

Figure 4.36 Experimental results and theoretical predictions of steel shot peened specimens.

But this generation of compressive residual stress was found to be not uniform throughout the weld toe region which was evidenced from the stress measurements shown in Figs. 4.16 to 4.18. This non-uniform distribution of initial tensile residual stress due to preloading might have caused the discrepency between theory and experiments.

Experimental results from the glass shot peened specimens and the theoretical predictions were shown in Fig. 4.35. The percentage error in the applied stress range between predictions and the experimental results was about 14%. The percentage error in stress range at $2x10^6$ cycles between the theories based on parent and weld material properties for the glass shot peened specimens was 23% For the prediction of fatigue life the smooth specimen material properties along with the measured value of the surface compressive stresses due to peening were used. The actual material properties of the peened surface may be different from that of the smooth specimen due to the work hardening and roughness of the peened surface. Although, there may be a small change to the weld toe root radius the work hardening due to peening, which increases the hardness and strength, could have caused this difference. Increase in hardness near the HAZ and weld toe due to peening was evidenced and shown in the Figs. 4.29 and 4.30. Also it was assumed in the prediction that stresses due to peening was uniform throughout the peened area

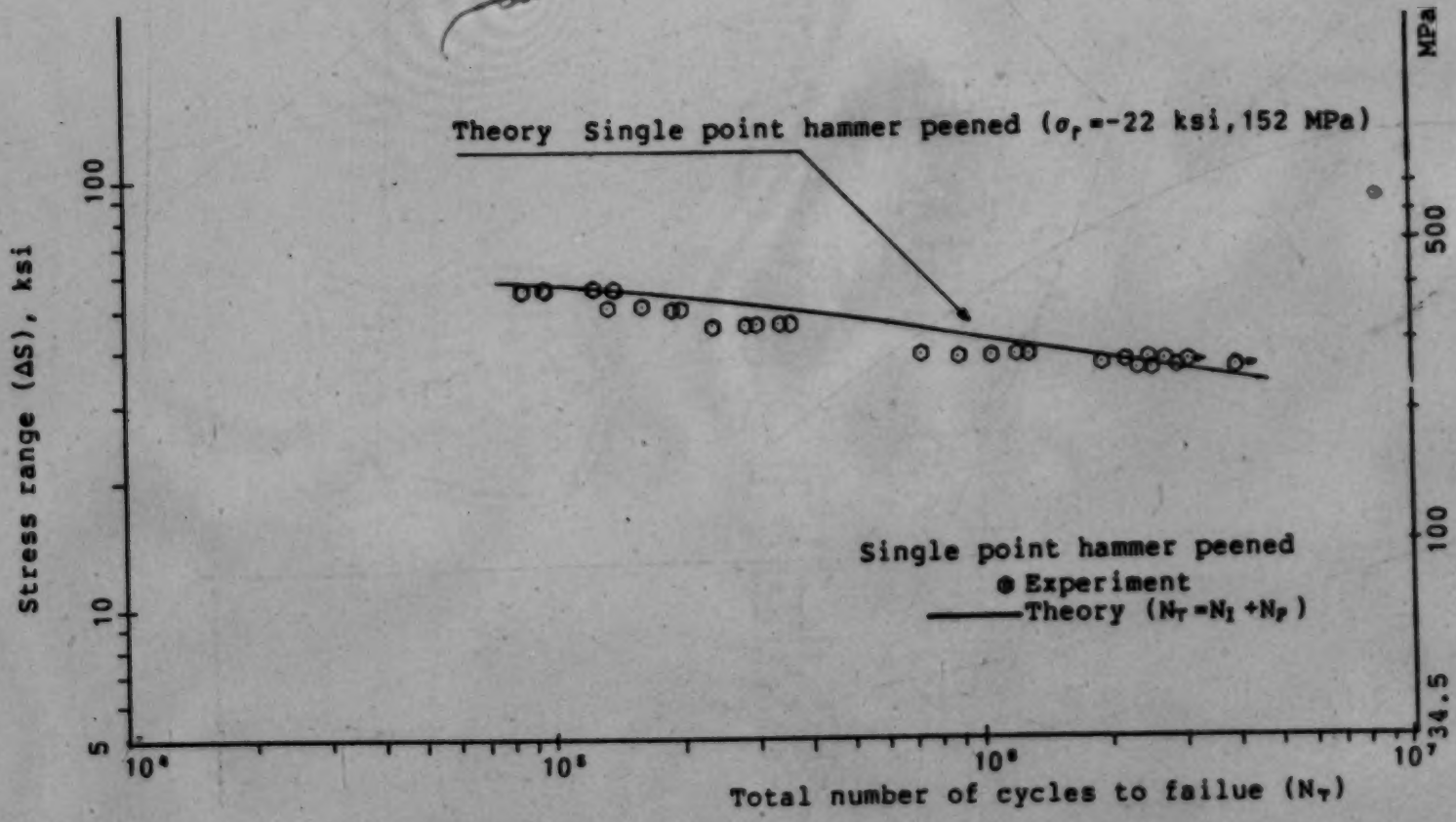

Figure 4.37 Experimental results and theoretical predictions of single point hammer peened specimens.

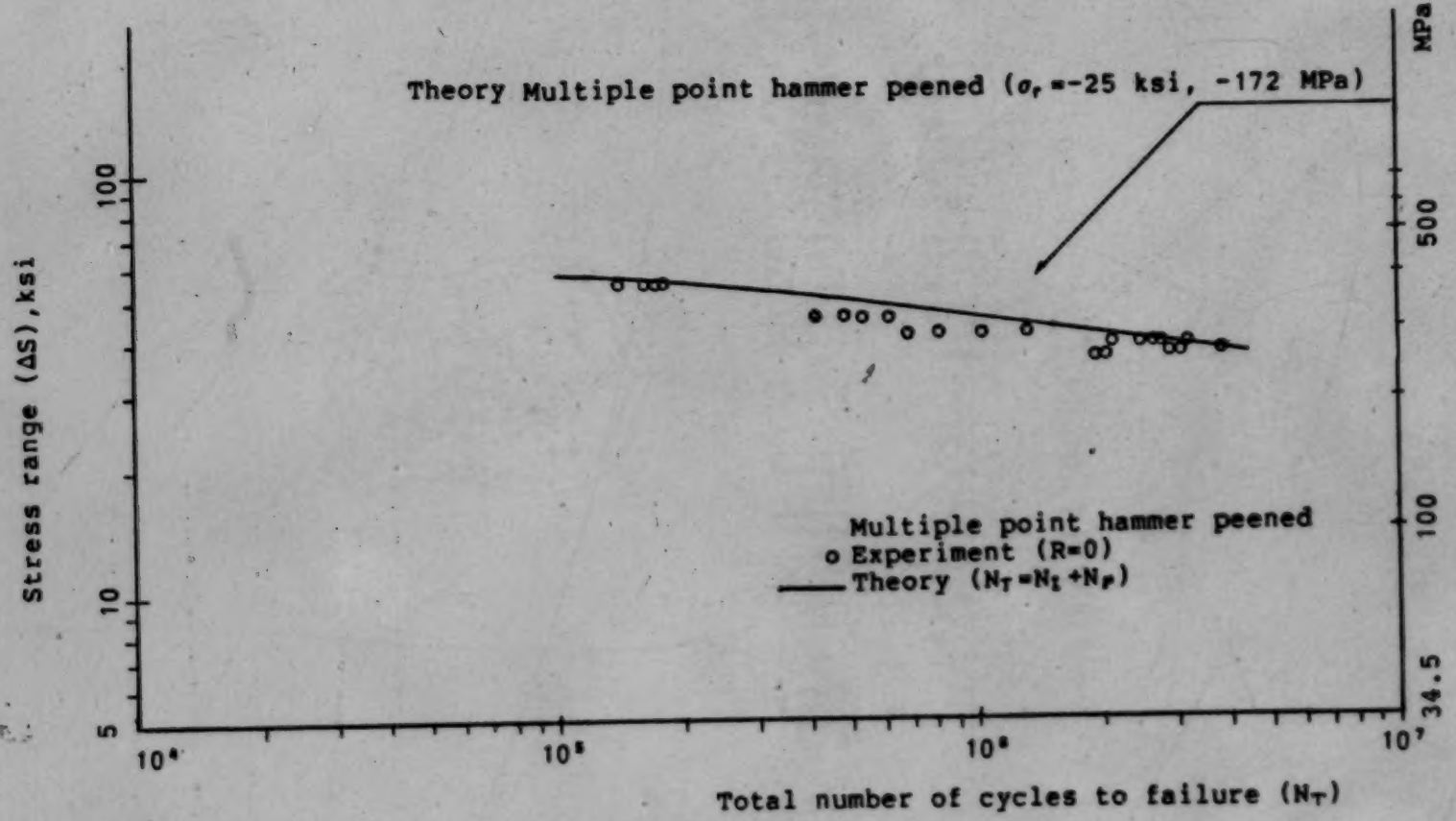

Figure 4.38 Experimental results and theoretical predictions of multiple point hammer peened specimens.

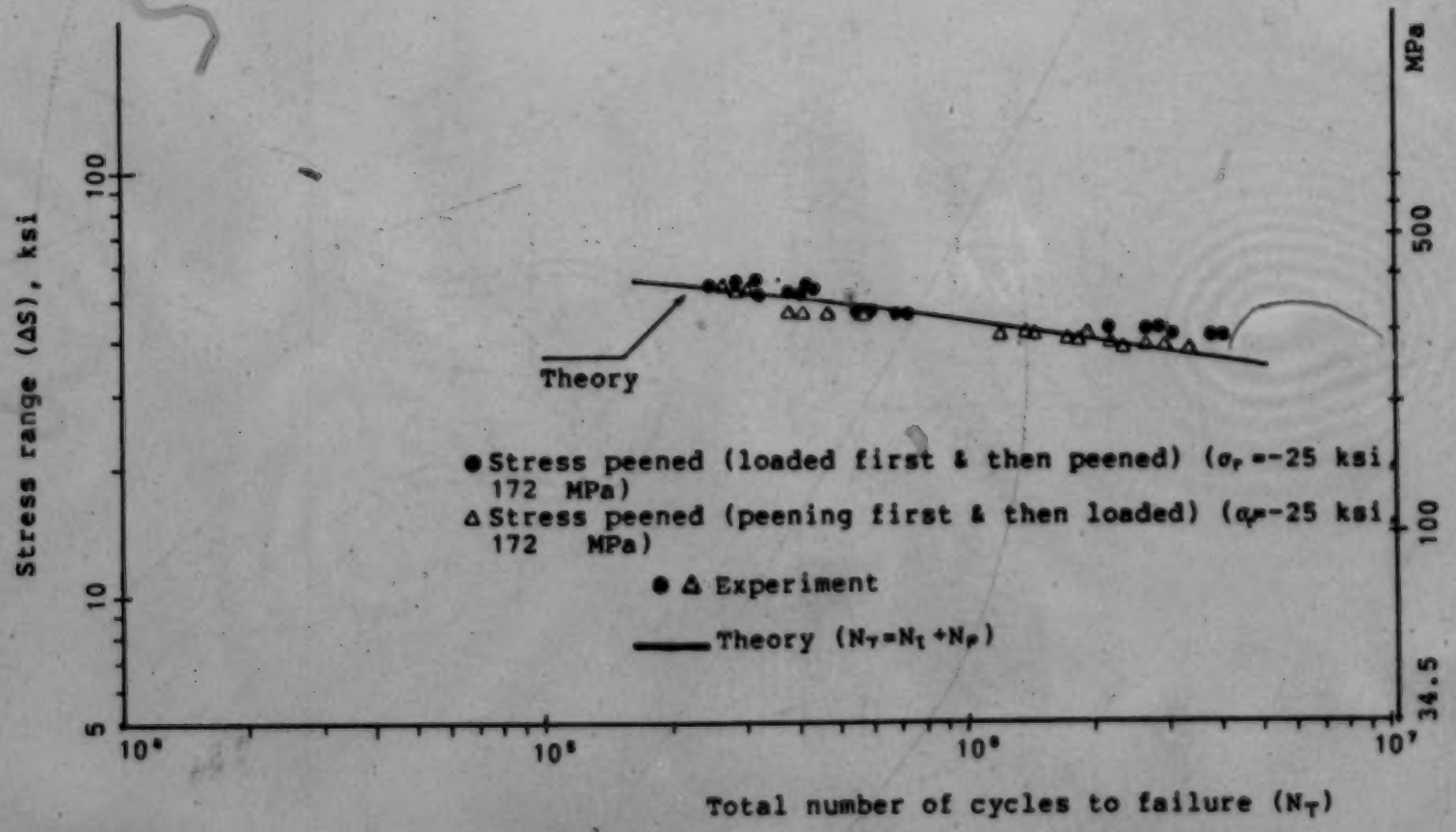

Figure 4.39 Experimental results and theoreical predictions of stress-peened specimens.

but the measurements (Fig. 4.19) showed that there was variation in the surface compressive stress levels due to peening.

Comparisons of theoretical predictions (adjusted material properties) of total fatigue life with experimental data for steel shot, single and multiple point hammer and stress peening were shown in Figs. 4.36 to 4.39. The percentage errors in the applied stress range between theoretical predictions and experimental results were 5%, 6%, 9% and 4% for steel shot, single point hammer, multiple point hammer and stress peened specimens respectively. The percentage errors in stress range at 2×10^6 cycles between the theories based on parent and weld material properties for steel shot, single point, multiple points and stress-peened specimens were approximately 19%, 21%, 22% and 22% respectively.

In the case of multiple and single point hammer peening some work-hardening and modification of the weld toe root radius might have occurred. The crack initiation life is sensitive to the weld toe root radius as mentioned earlier.

Figure 4.40 shows the plot of nominal stress range ΔS as a function of total life N_T for all the cases mentioned above. The predictions indicate that the induced surface compressive residual stress only influenced total fatigue life in excess of 10^5 cycles. Various techniques (annealing, tensile preload, glass and steel shot, single and multiple point hammer and stress peening) are predicted to be most

effective at low stresses or at long lives. For example, the percentage improvement in applied stress range over the as-welded condition due to multiple point hammer peening at $2x10^6$ cycles was 45% whereas at 10^5 cycles it was only 20%. This trend was found to be consistent with the experimental work done in this thesis (Figs. 4.21 to 4.23)

Figure 4.41 showed the predictions based on WM and HAZ properties and the experimental results for the as-welded condition. The WM and the HAZ material properties were obtained from the empirical relations and micro-hardness readings. These empirical relations (Appendix C) give only the approximate values. The percentage errors in stress range at $2x10^6$cycles were 6% and 8% for WM and the HAZ material respectively.

The percent of total life spent (N_i / N_T) for initiation for the base metal, the WM and the HAZ materials are shown in Fig. 4.42. It can be seen that the base metal takes about 30 to 50%, the weld metal 20 to 60% and the HAZ material 25 to 50% of the total life in the range of 10^5 to 5×10^6 cycles. The percent of total life spent in crack initiation is dependent on the cyclic material properties and stress ratios. It can be seen from Fig. 4.42 that Columbium-50 steel weldments takes about 46% of the total life in pulsating tension (i.e. R=0) as the crack initiation life at $2x10^6$ cycles.

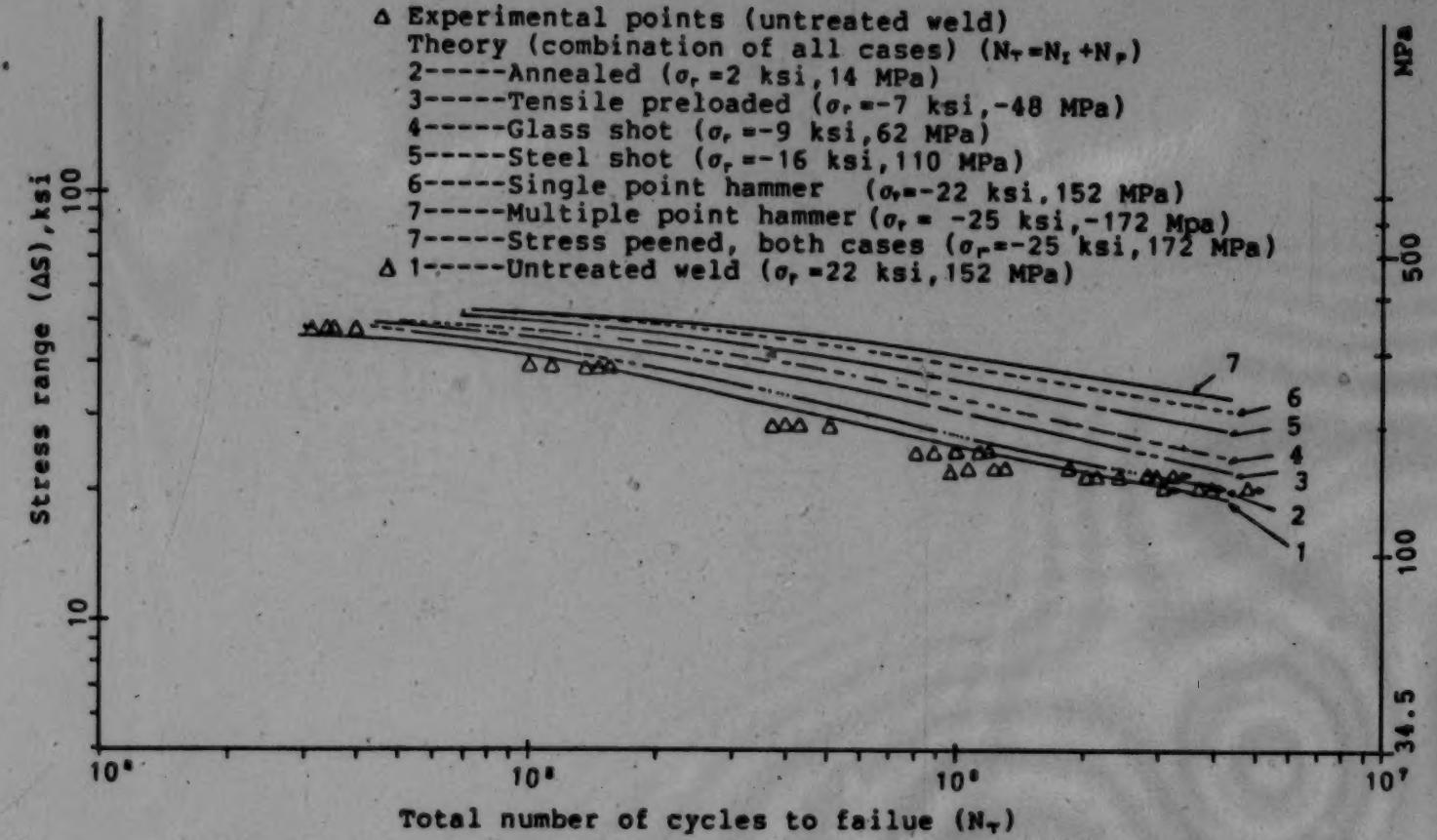

Figure 4.40 Experimental results of untreated weld and theoretical predictions of all cases of mechanical / thermal treatments.

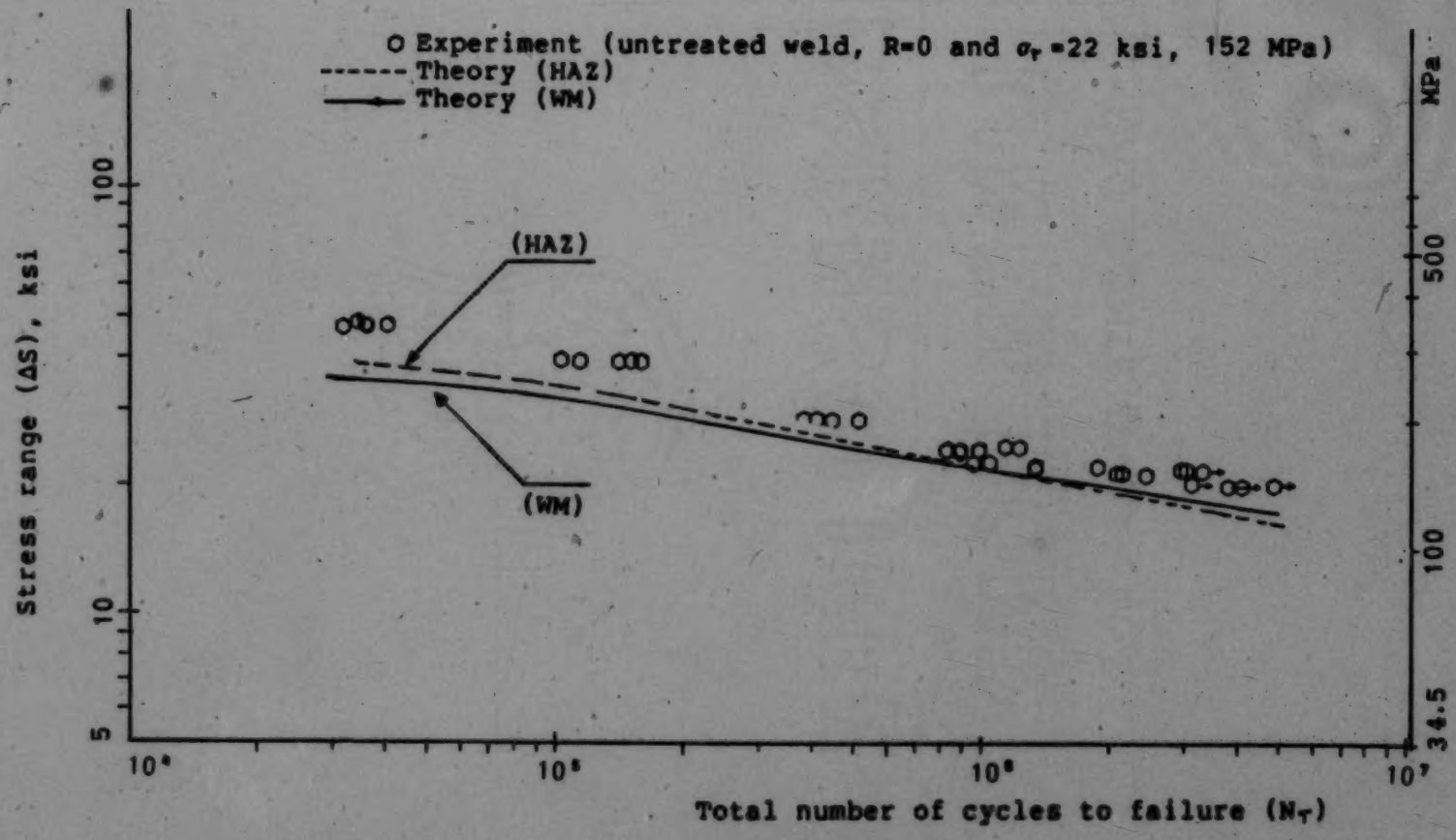

Figure 4.41 Experimental results of untreated weld and theoretical predictions using the HAZ and the weld metal properties.

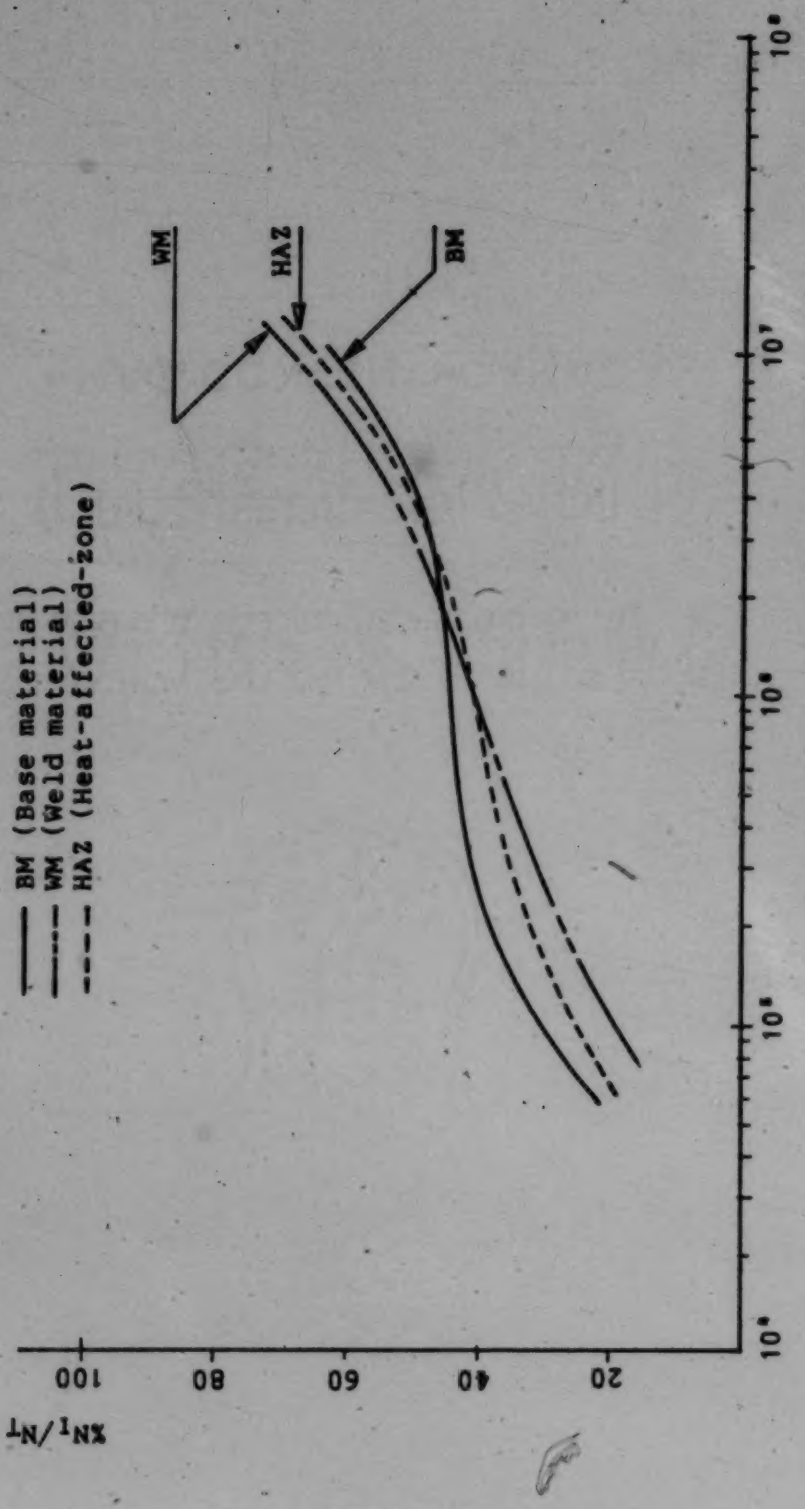

Figure 4.42 Percentage of total life needed to initiate a crack for the base, the weld and the HAZ materials.

4.5.3 Observations On The Total Life Model

The theoretical total life model applied in this study was found to predict with reasonably good accuracy the fatigue behaviour of transverse butt-welds of Columbium-50 steel with residual stresses.

Theoretical work on the damage rate model proposed by Socie (1977) indicates that the initial crack size (a_i) is in the range of 0.01 inch (0.254 mm) for mild steel plates with holes as crack initiation sites.

The initiation period was more difficult to measure or to predict. The duration of this period depends upon the cyclic stress-strain behaviour of the material, stress-history, residual stresses and the geometry of the defect. Furthermore, there are no exact theories available which allow a correct quantitative estimates of the crack initiation life. It is often conservatively assumed that the initiation period does not exist and all the life is spent in crack propagation. However, this assumption is not justified on the basis of observed data by various researchers (Lida 1972, Lawrence & Munse 1973, Rolfe & Barsom 1977, Abtahi & others 1976, Klensil & Lukas 1976). This present study also confirms that the crack initiation period cannot be neglected and it should be considered for the estimation of total fatigue life for a transverse butt-welded joints. This is especially true in the high cycle and low stress ranges of fatigue life.

The percentage of total life devoted to initiation (or un-detected propagation) appears to vary considerably depending on the material properties, loading histories, level of observation of crack and to some extent on the definition of crack initiation. It was found (for example, see Fig. 4.42) that at short lives (higher stresses) the percentage of life devoted to initiation was smaller than for longer lives (low stresses).

5. MODEL PREDICTIONS FOR CRACK INITIATION AND CRACK PROPAGATION

5.1 Introduction

A theoretical study was made on the crack initiation life showing the influence of residual stresses and stress ratios on fatigue life and the effectiveness of stress relieving. The theoretical study also includes the crack propagation phases of fatigue life. This shows the behaviour of crack length and crack propagation life, changes of crack growth rate and stress intensity factor and the effect of residual stress intensity factor on the rate of crack propagation.

5.2 Influence Of Residual Stresses, Stress Relieving And Stress Ratios On Fatigue Life

The theoretical model was used to illustrate the interaction of initial residual stress ($\sigma_{r,i}$), nominal stress range ($\Delta S = S_{max} - S_{min}$) and the nominal stress ratio ($R=S_{min} / S_{max}$) on the fatigue life of Columbium-50 steel weldments. The influence of complete stress relief, the tensile residual stresses, and the effect of stress ratios (R=-1, 0.0 and 1/2) on fatigue life of butt-welds was investigated.

The crack size (a_i) at the end of the initiation life was assumed to be 0.01 in (0.254mm). This could be assumed to be a reasonably sized "small" crack which will exist at

some early stage in the fatigue life of a weld. It is assumed that smaller cracks (≅ 0.0001in) (0.00254 mm)) pose no problems for the analytical procedures described in this work. However, the behaviour of smaller cracks may not be properly described by the crack propagation power law (Eq. (24)). The distribution of initial residual stress developed, the crack opening stress concept and the influence of effective stress ratio were considered for the crack propagation life.

The influence of cyclic hardening and softening were not included in this study . For long life fatigue (>10^5 cycles) cyclic hardening and softening effects can usually be ignored and generally stabilized conditions may be assumed. The results of the experiments performed for the cyclic softening and cyclic hardening are shown in Appendix B. The results showed that Columbium-50 steel exhibits very little softening or hardening behaviour.

The predicted influence of stress-relief and stress ratios are shown in Figs. 5.1 and 5.2 for the pulsating tension (R=0), alternating (R=-1) and half-tensile (R=+1/2) cases. These are commonly reported stress ratios for fatigue testing. From the stress difference ΔS vs. N_T (Fig. 5.1) and ΔS vs. N_I (Fig. 5.2) it can be seen that both stress relief and stress ratios have a marked influence on the fatigue lives of Columbium-50 butt-welds greater than 10^5 cycles. From Fig.5.1 it can also be seen that for alternating cycles (R=-1) the stress relief is not very helpful.

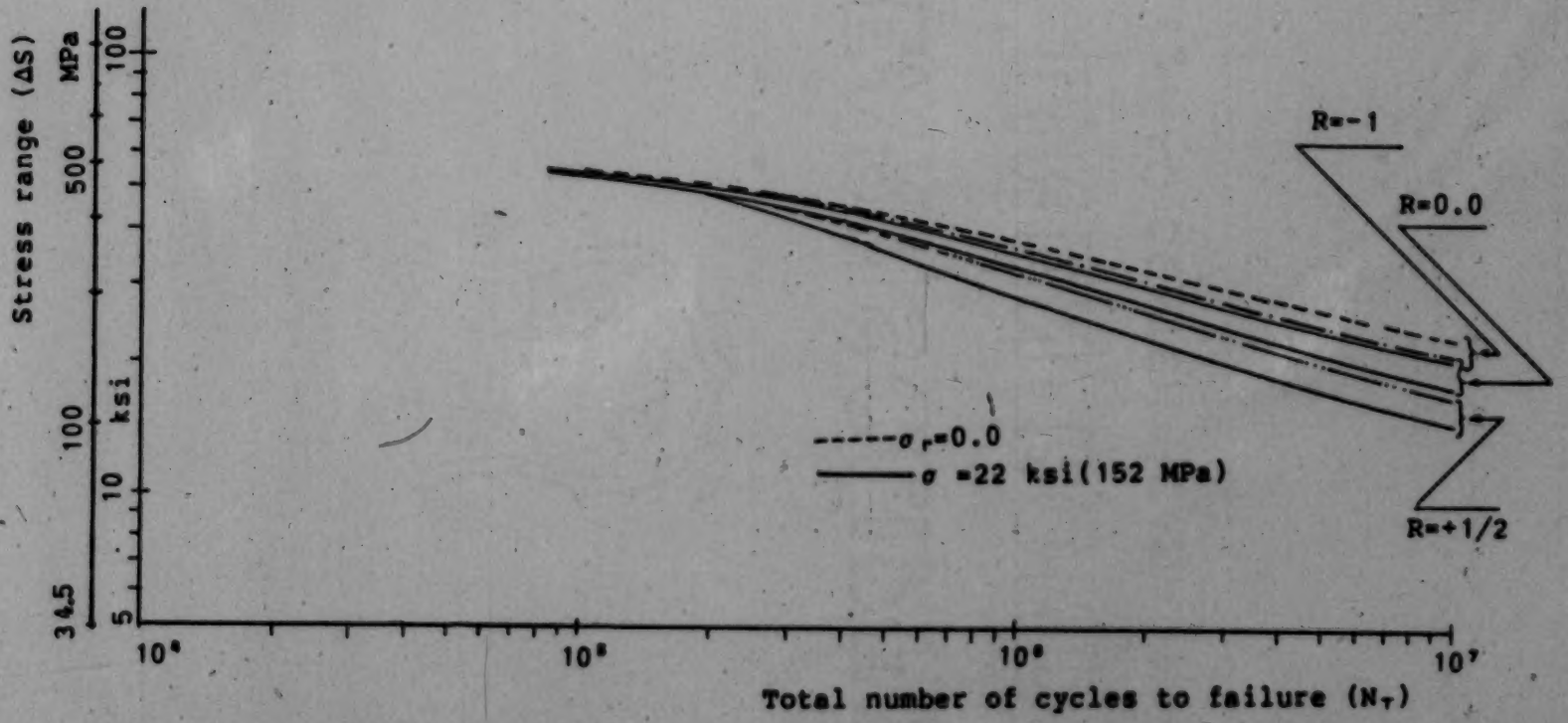

Figure 5.1 Theoretical predictions showing the influence of stress ratios and stress relieving for the total fatigue life of butt-welded joints.

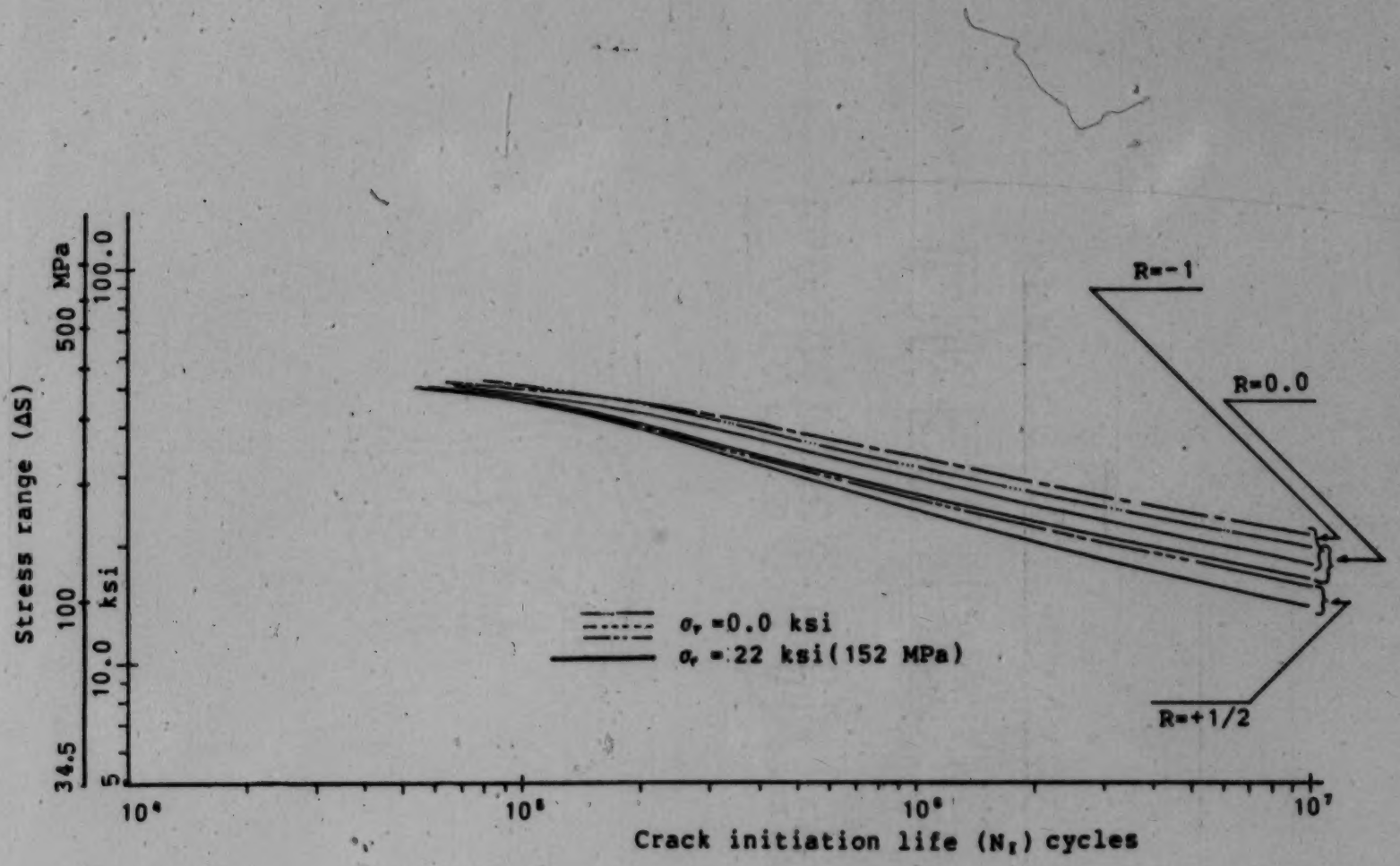

Figure 5.2 Theoretical predictions showing the influence of stress ratios and stress relieving for the crack initiation life of butt-welded specimens.

Figure 5.3 shows the modified Goodman diagram for as-welded condition (σ_r=22 ksi, 152 MPa) and complete stress relieved condition (σ_r=0). The modified Goodman diagram shows the dependence of the maximum and minimum applied stresses (S_{max} , S_{min}) on mean stress (S_{mean}). For each value of mean stress there is a different value of the limiting range of stress (S_{max}-S_{min}) which can be withstood without failure. The stress relieved (dotted lines) and as-welded condition (solid lines) show the improvement of stress relieving of Columbium-50 butt-welds at particular fatigue lives of 10^6, $2x10^6$ and 10^7 cycles. The modified Goodman criterion predicts the fatigue resistance of the welded joints when subjected to both varying mean stress and the stress amplitude under fatigue cyclic conditions.

The theoretical predictions for percentage of total life spent (N_i / N_T) in crack initiation for Columbium-50 butt-welds as a function of total life N_T is shown in Fig. 5.4 for both as-welded and stress-relieved conditions and three stress ratios of R=0, +1/2 and -1. From Fig. 5.4 it can be seen that crack initiation occurs faster when the stress cycle passes through zero (i.e. R=-1) and requires a larger percentage of total fatigue life to initiate a crack when the stress cycle is completely tensile (i.e. R = 1/2). For R = 1/2 the percentage of crack initiation life should dominate total fatigue lives greater than 10^5 cycles.

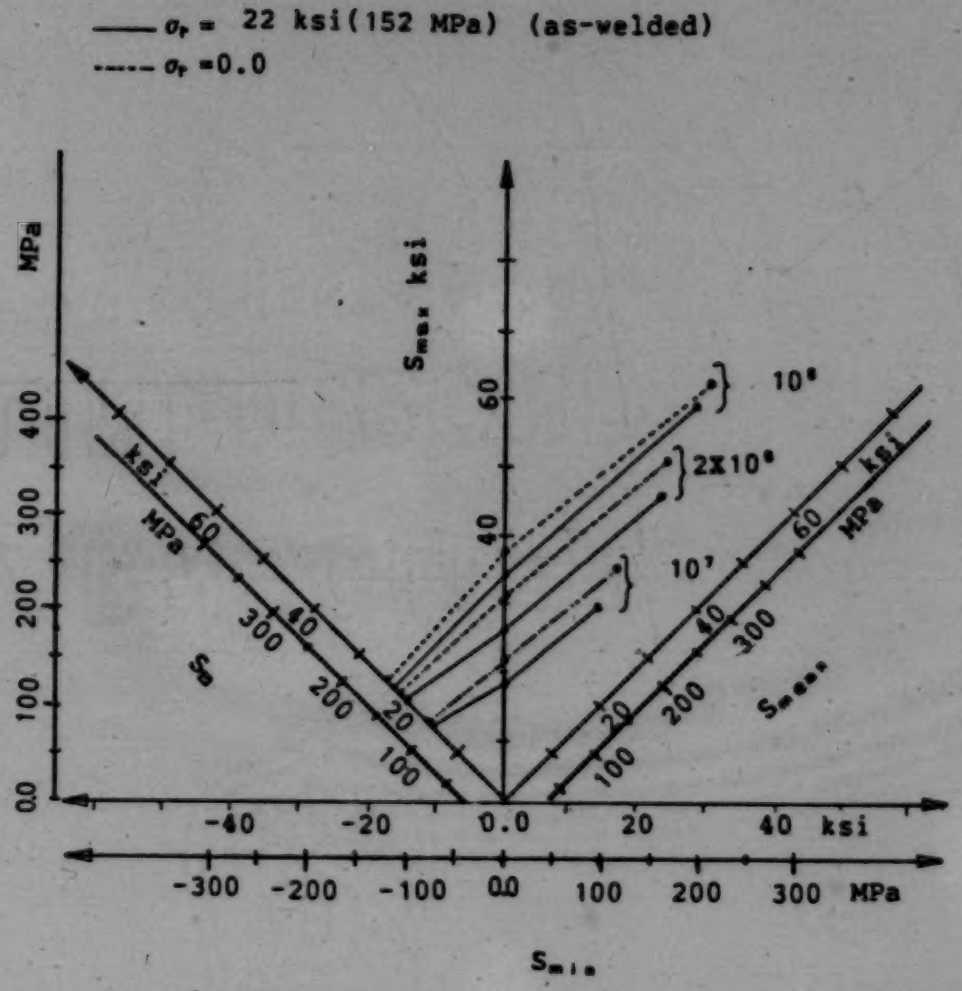

Figure 5.3 Modified Goodman diagram showing the as-welded (solid lines) and stress relieved (dotted lines) conditions.

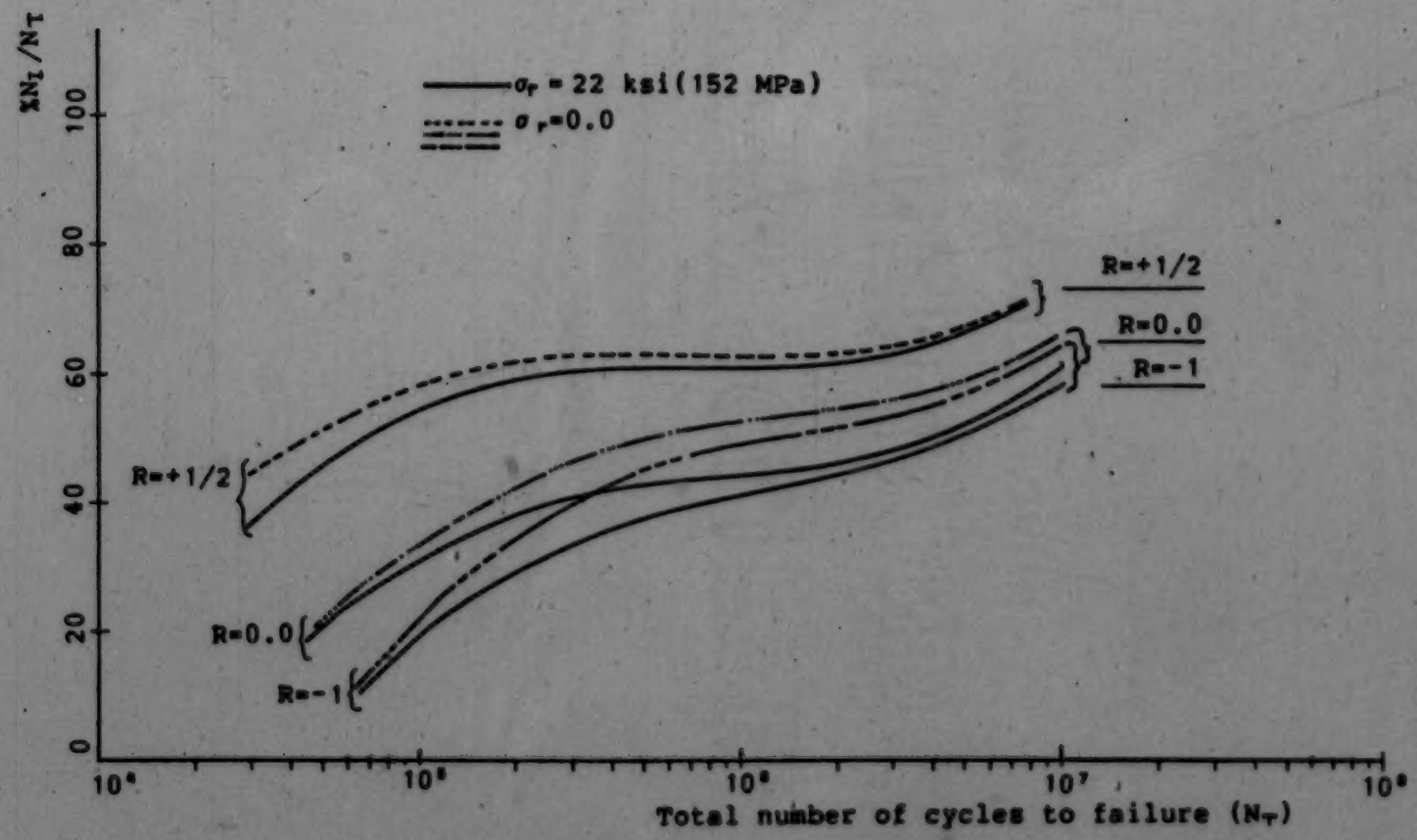

Figure 5.4 Theoretical predictions showing the percentage of total life needed for initiation of a crack for three stress ratios in as-welded and stress-relieved conditions.

It can also be seen that the percentage of total life spent in crack initiation was increased due to stress relief (σ_r=0) for lives greater than 10^5 cycles. It is also noted that as the stress ratio increased the percentage of life spent in crack initiation also increased.

5.3 Results Of Theoretical Study From The Crack Propagation Model

The theoretical predictions on the study of crack propagation life of a butt-weld was made according to the analysis developed in Chapter II. Forman's equation (Eq.(24)) for rate of crack propagation with the effective stress ratio and crack opening stress concepts were taken into consideration for the numerical integration of the crack propagation life N_p. The effect of axial loading, bending stresses due to gripping the specimen and of the effect of residual stresses were incorporated for the determination of the range of the stress intensity factor. To find the effective stress intensity factor assumptions were made for the crack opening factor. This crack opening (or crack closing) concept confirms the recent experimental study reported by Harrison (1981). He found that crack closure always occurred towards the bottom of the tensile part of the cycle while the applied stress was still tensile. Initial residual stress distribution was taken for the calculation of residual stress intensity factor. A distribution which approximates the shape of the actual

residual stress distribution was developed in Chapter II. It was observed that the residual stress redistributes itself after the fatigue cycling starts but no constant shape of distribution was found experimentally (see Fig. 4.11). From Fig. 4.11 it was also observed that the shape of the redistribution of the residual stresses changes in a certain fashion but it did not remain constant after the initial few cycles. The initial distribution of residual stresses was the shape that was considered in this study. It is also assumed that a crack can occur anywhere along the strained region (toe of the weld) due to the application of tensile residual stress. To apply compressive stresses for peening, the negative compressive stresses were superimposed on the applied stresses taking the initial residual stress as zero.

Figure 5.5 shows the predictions of the half-crack length "a" as a function of crack propagation life N_p for three stress ratios of R=-1/2, 0.0 and +1/2. It was observed that for the same crack length the propagation life increased as the stress ratio increased. It can also be seen that with the increase of stress range ΔS the crack propagation life decreased for the same crack length.

The effect of the range of stress intensity factor (ΔK) as a function of the fatigue crack growth rate (da/dN_p) are shown in Figs. 5.6 and 5.7. It shows that positive R values lead to slightly higher growth rates than does R=0.0 for the same value of ΔK. As R ratios become increasingly negative the growth rate drops because only stresses which open the

crack are capable of driving it. From this it could also be said that any compressive component in a stress cycle will be ineffective in driving the crack because it will cause the crack to close.

The effect of residual stress intensity factor on the rate of crack propagation (da/dN_R) are shown in Figs. 5.8 and 5.9. It was observed that the rate of fatigue crack propagation on the residual stress intensity factor depended on the applied stress ratio . Figures 5.8 and 5.9 also show the effect of three stress ratios R=-1/2, 0.0 and 1/2. It can be seen that the higher the applied stress range the lower the residual stress intensity factor for the same rate of crack propagation. This suggests that higher applied load caused greater relaxation of residual stresses. Figures 5.8 and 5.9 also show the tendency that as the residual stress intensity factor increased the rate of crack propagation almost becomes the same for the three stress ratios studied.

The behaviour of the range of stress intensity factor (ΔK) with the residual stress intensity factor (K_R) for the three stress ratios are shown in Figs. 5.10 and 5.11. For the same ΔK, the residual stress intensity factor was greater for positive R ratio. It can also be said that for the same residual stress intensity factor the range of stress intensity factor was largest for R=-1/2, therefore, crack propagation life decreased with negative stress ratio. On the other hand, stress ratio R=1/2 produced lower ΔK which in turn, increased the crack propagation life.

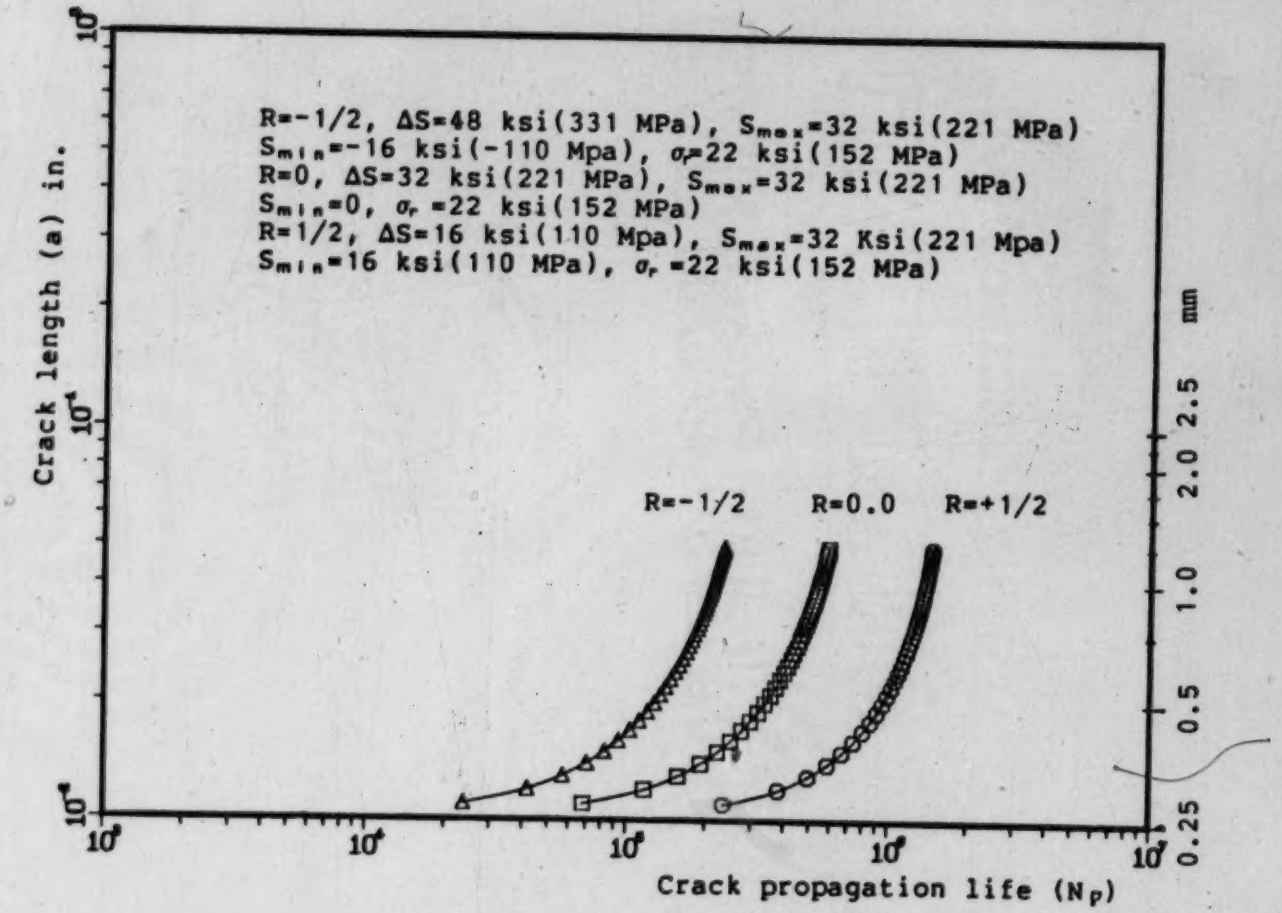

Figure 5.5 Theoretical predictions of crack propagation life and crack length.

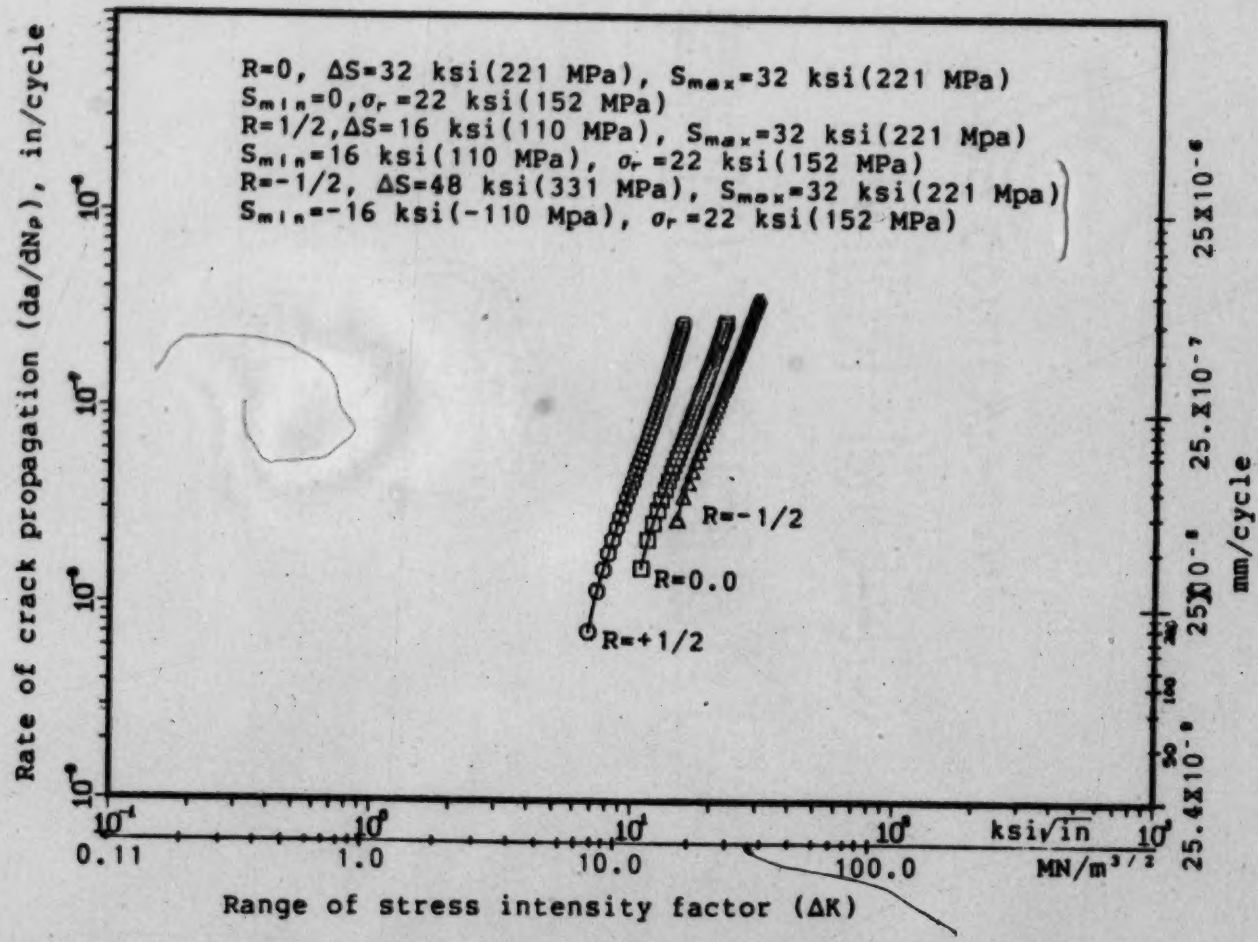

Figure 5.6 Calculated value of the range of stress intensity factor and the rate of crack propagation.

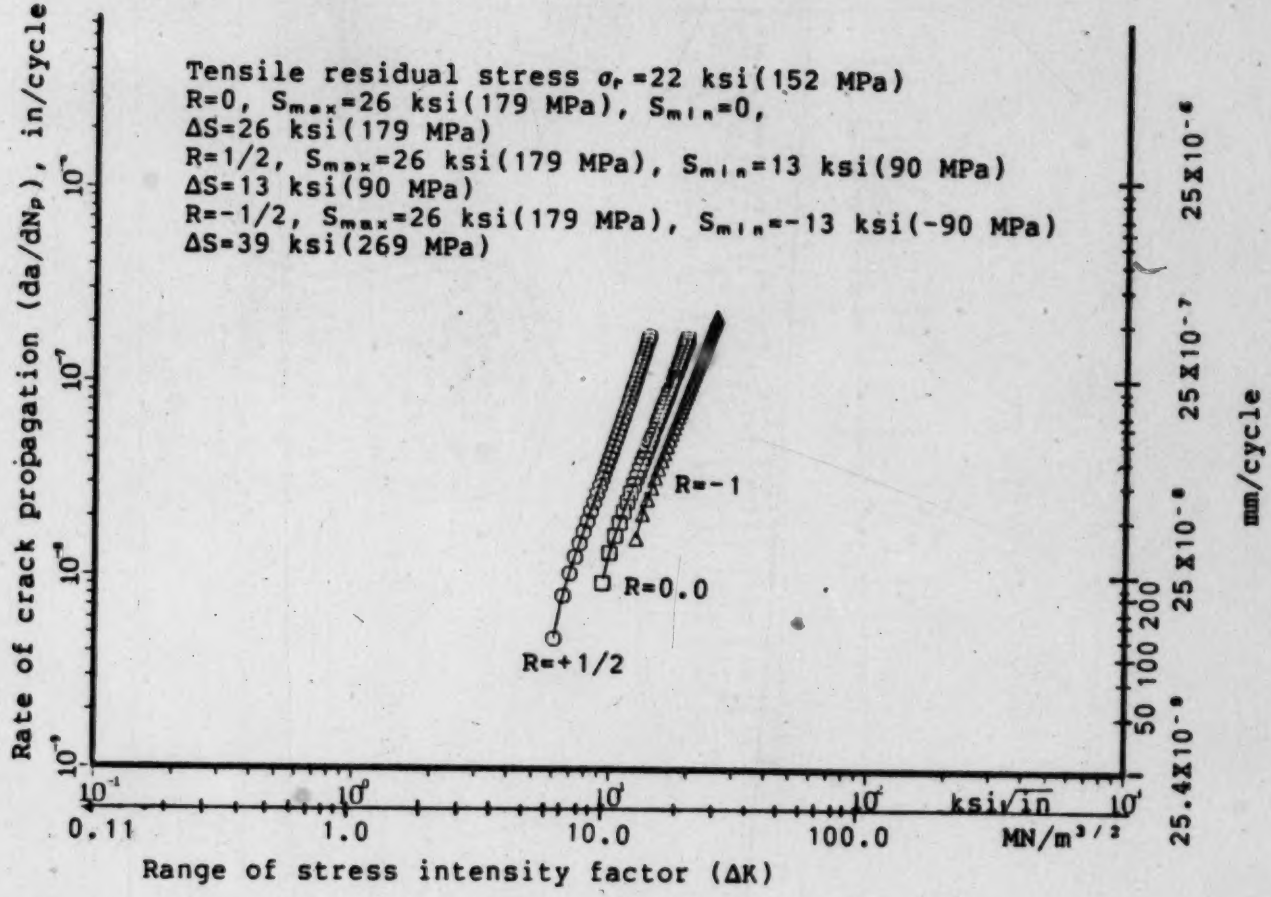

Figure 5.7 Calculated value of the range of stress intensity factor and the rate of crack propagation.

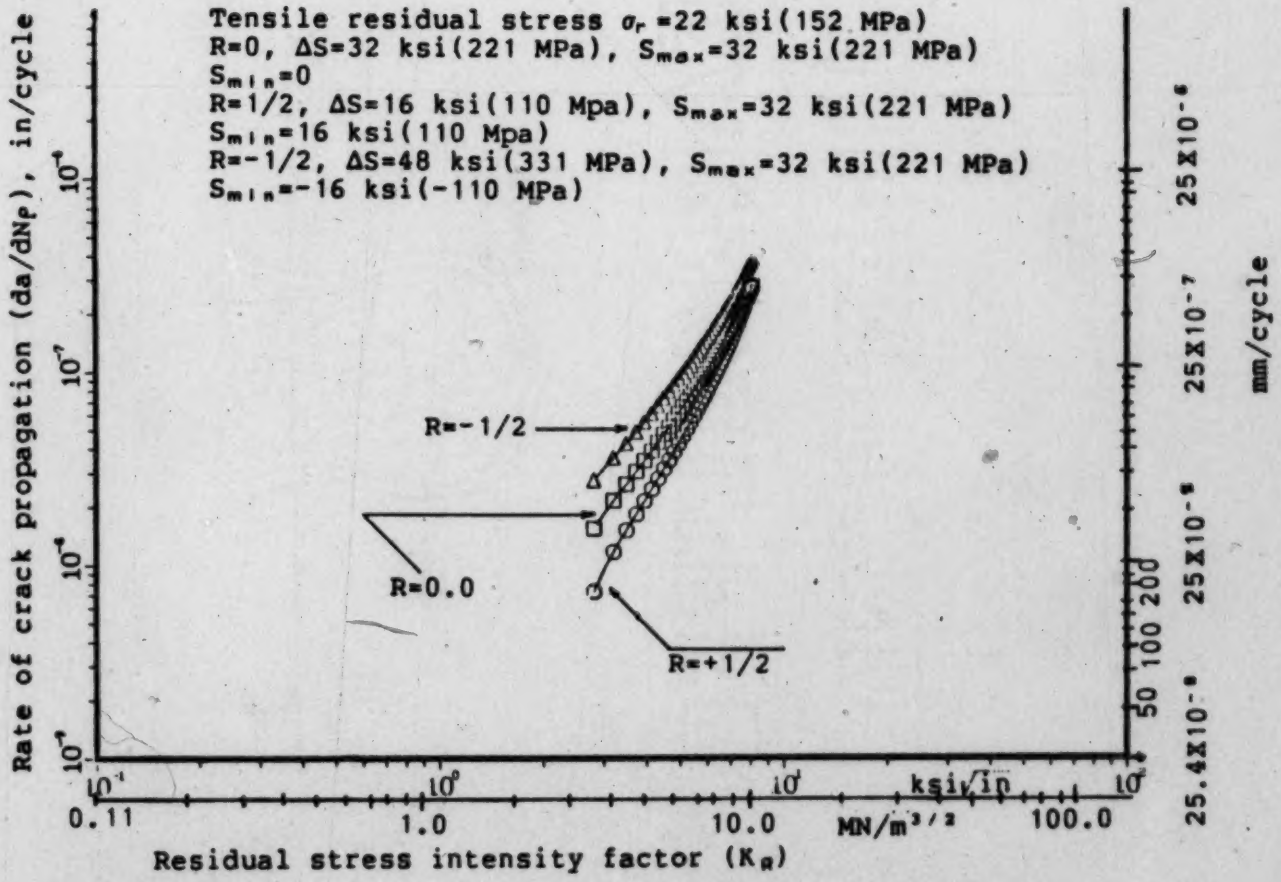

Figure 5.8 Calculated value of the residual stress intensity factor and the rate of crack propagation.

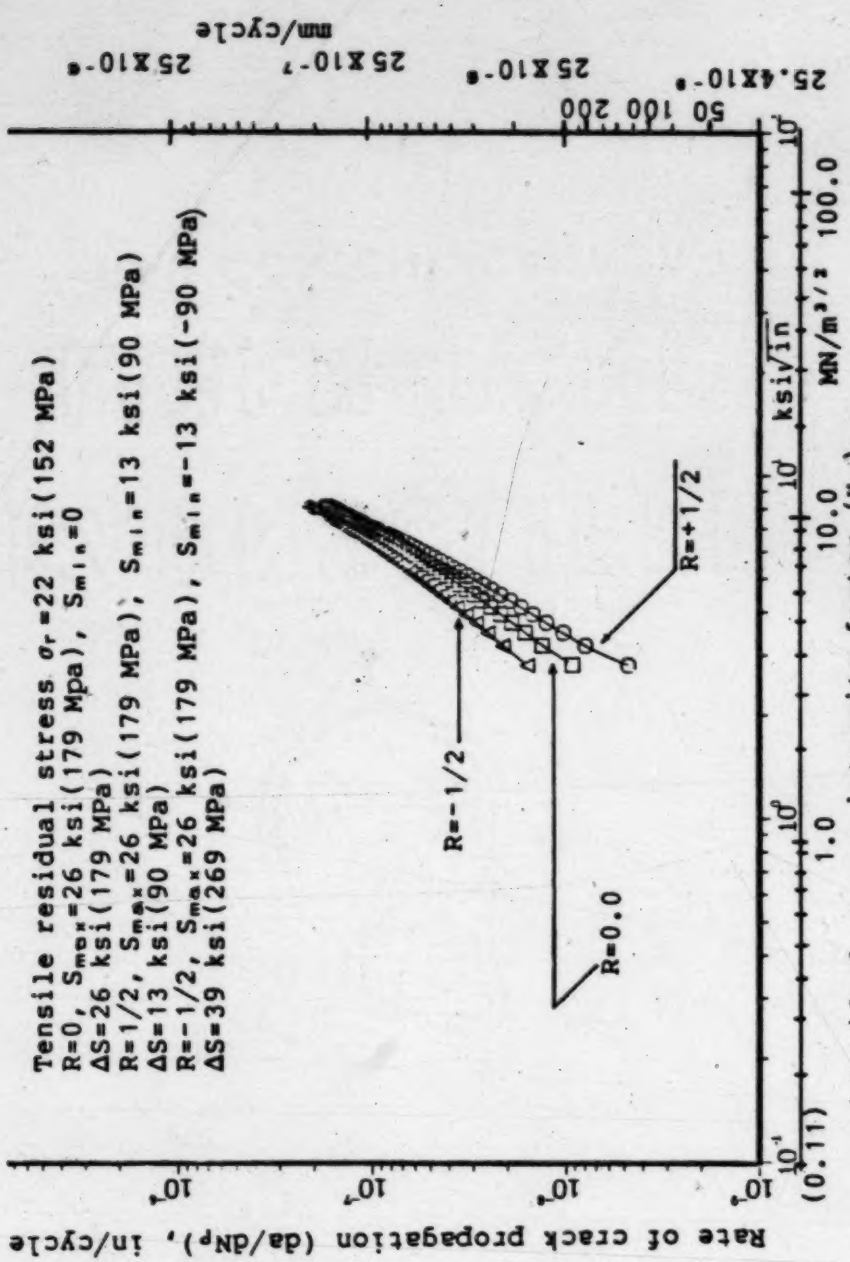

Figure 5.9 Calculated value of the residual stress intensity factor and the rate of crack propagation.

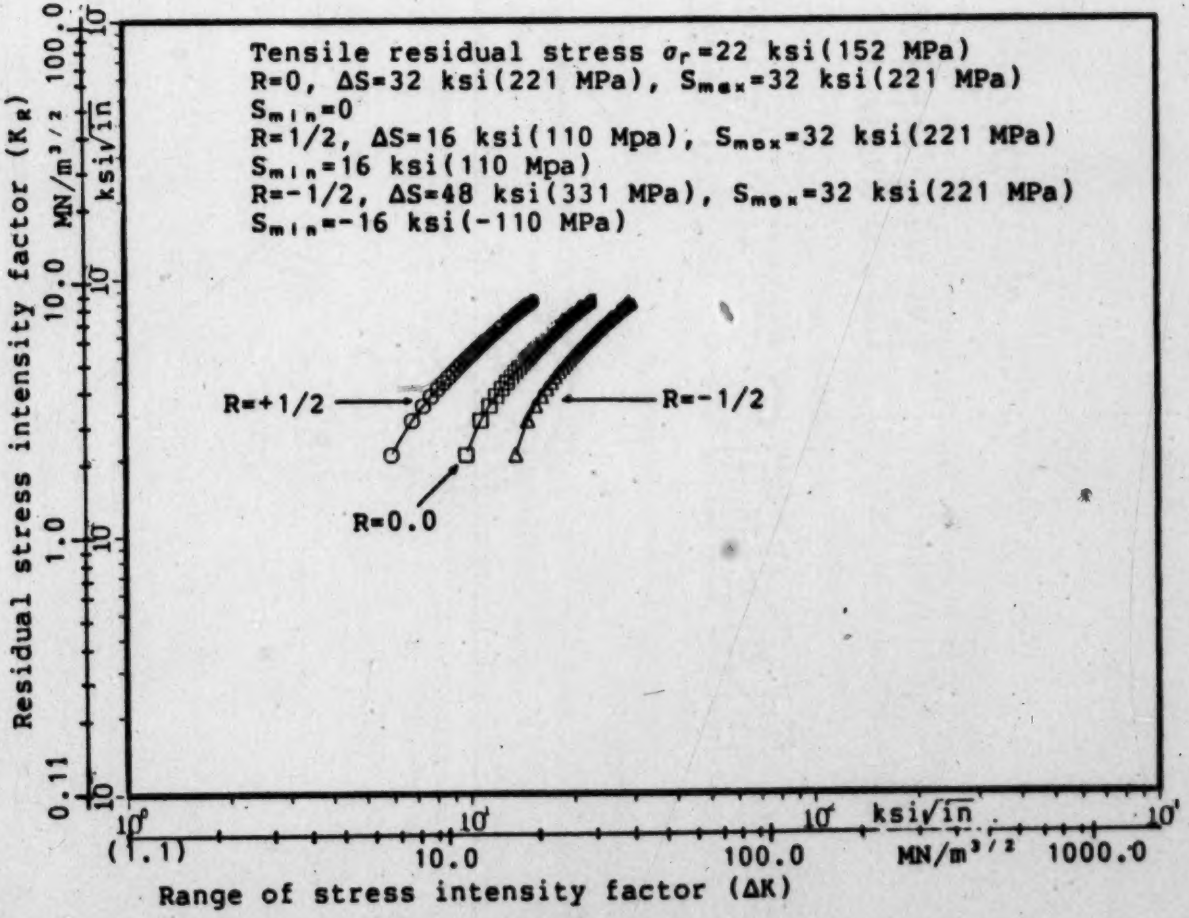

Figure 5.10 Calculated value of the range of stress intensity factor and the residual stress intensity factor.

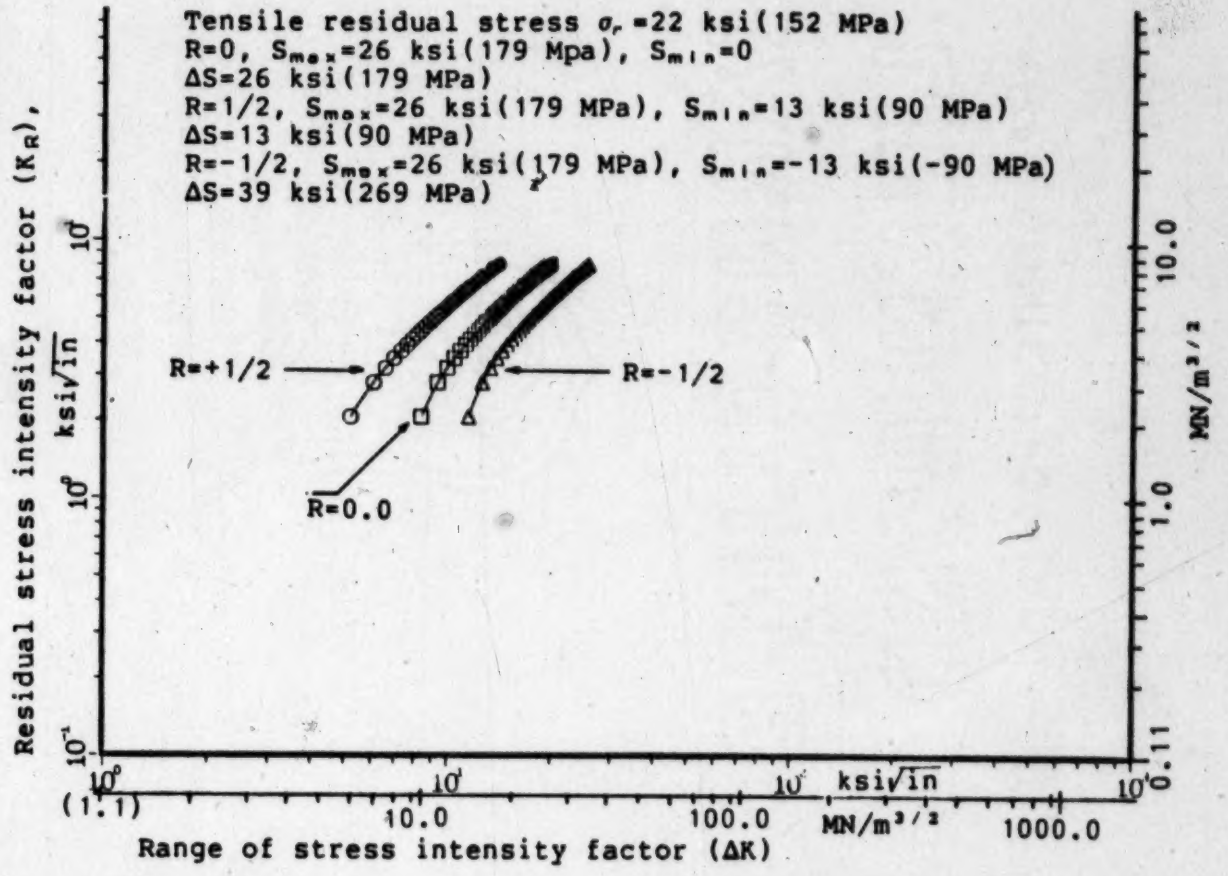

Figure 5.11 Calculated value of the range of stress intensity factor and the residual stress intensity factor.

Figures 5.12 and 5.13 show the effect of initial residual stress (σ_r = 22 ksi, 152 MPa), stress relieving (σ_r=0.0) and the induced compressive residual stress (σ_r = -5 ksi, -34 MPa) in a plot of ΔK and fatigue crack growth rate (da/dN_f). The effect of stress relieving on growth rate from tensile residual stress to the zero residual stress is comparatively more than that due to the application of surface compressive stresses. For the same fatigue crack growth rate the stress intensity factor range ΔK increases for the tensile residual stresses and therefore, the crack propagation life decreased. The improvement of fatigue crack propagation was small with the application of compressive residual stresses as can be seen from Figs. 5.12 and 5.13 for Columbium-50 steel.

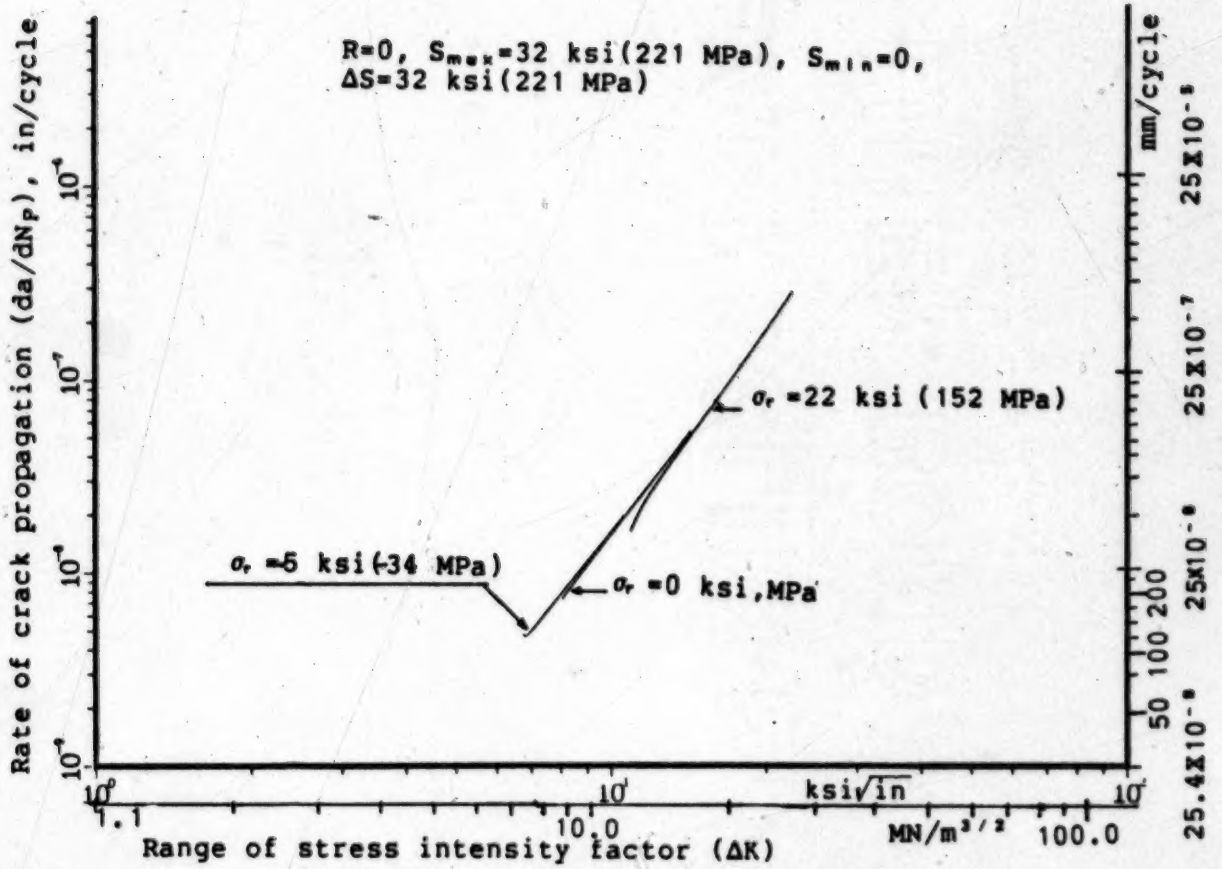

Figure 5.12 Calculated value of the range of stress intensity factor and the rate of crack propagation for as-welded, stress-relieved and induced compressive residual Stress.

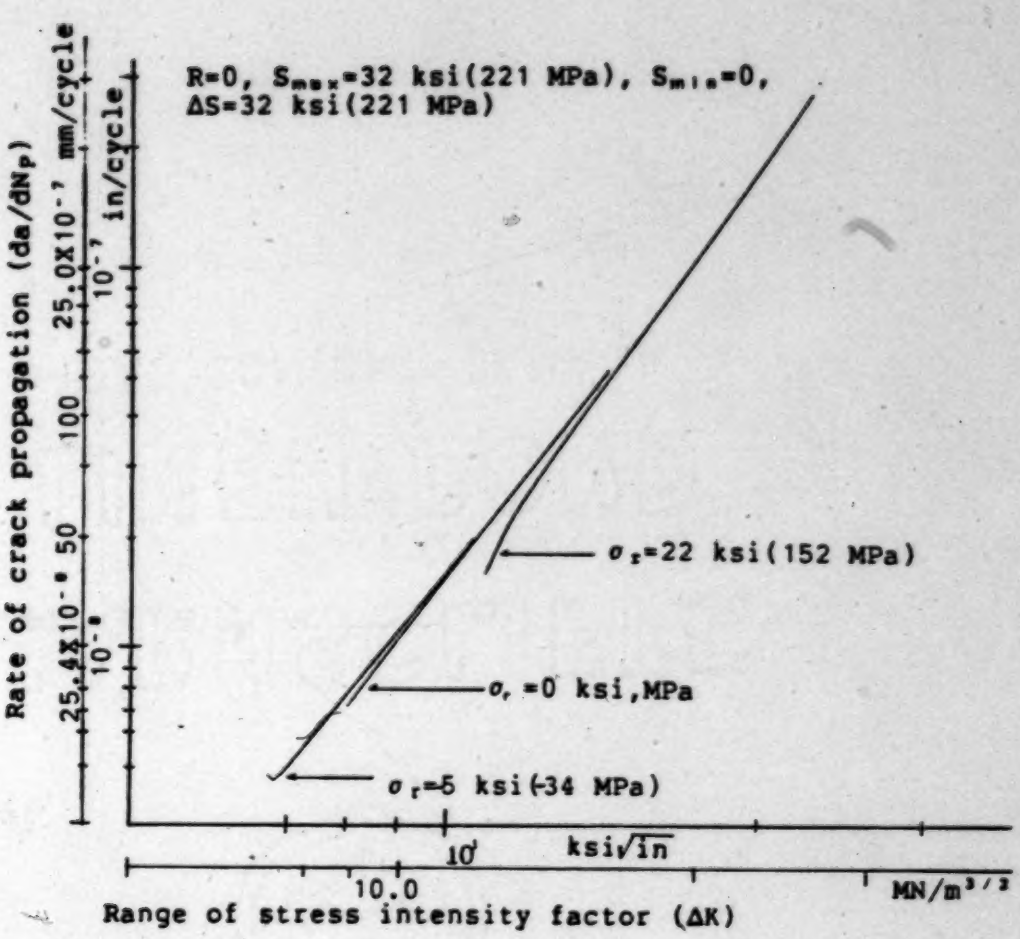

Figure 5.13 Enlarged view of Figure 5.12 showing the effect of stress relieving and induced compressive stress as a function of the range of stress intensity and the rate of crack propagation.

6. CONCLUSIONS & RECOMMENDATIONS FOR FUTURE WORK

6.1 Conclusions

The theoretical approach to the estimation of the fatigue crack initiation used Neuber's criterion and a cumulative fatigue damage analysis while the fatigue crack propagation phase used Forman's equation of crack propagation incorporated with the concept of crack opening stresses. The combined effects of axial loading, bending stress and residual stress were considered in the crack propagation phase. The results of these calculations were compared to experimental results for welds which have been mechanically and thermally treated and lead to the following conclusions:

(1) The influence of residual stresses on the fatigue life of welded structures may be treated by a notch-root stress and strain model which establishes the mean stress and predicts the weld-toe residual stress subsequent to cyclic loading. The effect of residual stress at the weld toe can be simulated by using elastic superposition of residual stress and elastic stress concentration factor and modification to Neuber's equation. The cumulative damage which allows for the mean stress relaxation determines the crack initiation life.

(2) The resulting total life predictions based on adjusted ('weld-parent' interface) material properties are in close

agreement with experimental results. The percentage error in stress range for as-welded condition at 10^6 cycles between predictions and experiments was within 5%.

(3) The influence of welding residual stresses varied as a function of the material properties. Material properties of the base metal, HAZ and the weld metal were found to significantly influence the effect of residual stresses on the weld fatigue life. The welding residual stress influenced the total fatigue life in the long-life regime.

(4) It was found that stress relieving or introduction of compressive stresses by mechanical means improved the fatigue life in the long life regime. The percentage improvement in applied stress range due to various surface treatment over the as-welded condition at long life (2×10^6 cycles) varied upto 45% whereas at life less than 10^5 cycles it was only 20%.

(5) Beneficial surface compressive stresses by tensile preloading, glass and steel shot peening, single and multiple point hammer peening, stress -peening and stress relief by annealing gave large improvements for lives exceeding 5×10^5 cycles with maximum improvement in the case of multiple point hammer peening and stress-peening. The single point hammer peening caused unacceptable surface damage and modification of the weld toe root radius.

(6) The ratio of crack initiation to total life was

dependent on the cyclic and fatigue properties of the material and on the range of fatigue life under consideration. It was found that approximately 44% of total life at $2x10^6$ cycles was spent as the crack initiation life.

(7) The theoretical study showed that the weld-toe root radius influenced the crack initiation life and hence, the total fatigue life of the weld. The crack initiation life increased by 44% as the root radius increased from 0.0001in (0.00254mm) to 0.001in (0.0254mm) and 63% for an increase from 0.001in (0.0254mm) to 0.01in (0.254mm).

(8) The depth of work hardening due to peening increased exponentially and approximated a constant value of 0.035in (0.89mm) as the surface compresssive residual stress of 25 ksi (-172 MPa) was attained.

(9) The improvement in fatigue strength over the as-welded condition can be represented by a least square fit (corr. coef. r =0.965) for the difference in induced stress by peening. A maximum improvement of 93% in fatigue strength over as-welded condition at $2x10^6$ cycles was obtained due to stress peening while annealing produced an improvement of 14%. It was found that for induced residual stresses less than about 20 ksi (138 MPa) no beneficial effect can be expected in fatigue life.

(10) Stress relieving was found to be more beneficial for zero or a positive stress ratio than under alternating

loading.

(11) The fatigue crack propagation life increased with an increase of stress ratio.

(12) For the same stress intensity factor range the fatigue crack growth rate of Columbium-50 steel increased with increase of stress ratio. Increase of growth rate was about 75-80% more for increase in stress ratio $0.0 \leq R \leq 0.5$ than for $-0.5 \leq R \leq 0.0$.

(13) The effect of residual stress on the rate of fatigue crack propagation depended on the applied stress range and the stress ratio. The tensile residual stress, stress-relieving and compressive surface residual stresses played a minor role in the propagation life regime more than for the initiation period.

6.2 Recommendations For Future Work

This investigation was limited to a study of the crack initiation life using the strain-controlled low-cycle fatigue behaviour of the base metal, theoretical calculation of crack propagation life and the experimental and theoretical predictions of the total fatigue life. This study also included the redistribution of surface residual stresses due to various mechanical and one type of thermal treatment. At the present time due to the lack of experimental facilities it was not possible to obtain cyclic and fatigue properties of WM and 'weld-parent' interface material from cyclic strain-controlled test. Determination of these properties will indicate more accurately the influence of the materials on the fatigue life of welded joints. Furthermore, the measurements of crack propagation rates as a function of stress intensity factor range will improve the prediction of fatigue crack propagation life.

The effect of mean stress relaxation on the low-cycle fatigue lives of actual welds is complex and should be further analyzed by experimental studies using smooth welded specimens and establishinig correlation with the results from the relaxation behaviour of the base material and computer simulation.

The local-strain analyses based on parent material properties overesimated the fatigue life of welded structures for Columbium-50 steel. Further research on the effect of surface roughness and a criterion for defining

crack initiation in smooth and welded specimens is recommended.

An attempt can also be made to extend the analytical model of the total fatigue life to include the variable amplitude or random loading histories using a statistical approach for the loading, because the random loading histories would reflect actual service situations.

REFERENCES

Abtahi,A., Albretcht,P., and Irwin,G.R., "Journal of the Structural Division," Proceedings of the American society of Civil Engineers, Vol.102, No. ST.11, pp 2103-2119, Nov., 1976.

Almen,J.O. & Black,P.H., "Residual Stresses and Fatigue in Metals., McGraw-Hill Book Company Inc., 1963.

Backlund,J., Blom,A.F., & Beevers,C.J., Edtrs: Fatigue thresholds, Proc. from Ist. International conf., Vol. 1 & 2, Enginnering Materials Advisory services Ltd., U.K., 1982.

Baron,H.G., & Brine,F.E., Commonwealth welding Conference, p 322, 1965.

Barsom,J.M., "Fatigue crack growth under variable amplitude loading in ASTM 514 grade B steel, ASTM, STP 536, Am. Soc. for testing & materials, 1973.

Basquin,O.H., Proceeding ASTM, 10:625, 1910.

Bathgate,R.G., "The collection, processing, and application of data obtained by the holedrilling technique," Fulmer Research Institute, April 23, 1974.

Beaney,E.M. & Procter,E., "A critical evaluation of the centre-hole technique for measurement of residual stresses," Strain, Jan., 1974.

Bell,P.D. & Wolfman,A., "Mathematical modelling of crack growth interaction effects," ASTM STP 595, Am. soc. for testing & materials, 1976.

Bellow,D.G. & Faulkner,M.G., "Influence of testing frequency on the fatigue of butt-welded steel joints." Weld. Res. Int., 9, pp 12-20, 1979.

Brine,E.E., Weber,D., & Baron,H.G., "Military Engineering Experimental establishment," Technical note # 5/68, England., 1968.

Buhler,H. & Buchholtz,H., "The effect of residual stresses on the dynamic bending strength," Mitt, Forsch. Inst. Dortmund, Vol.3, No.8, pp 235-248. September, 1933.

Burk,J.D. & Lawrence Jr.,F.V., "Influence of bending stresses on fatigue crack propagation life in butt-joint

welds," Welding Research Suppl., V.56, pp 61-66s, 1977.

Burk,J.D., "Predicted Effects of Residual Stresses on Butt-Weld fatigue life," Ph.D. Thesis, Univ. of Illinois, Urbana-Champaign, 1978.

Chadwick,M.D., Metal Const. & British Welding Journal, V.2, p 314, 1971.

Chang,Se-Tak & Lawrence Jr,F.V., "Predicting the effect of shot peening on weld fatigue life," First International Conf. on Shot Peening, pp 461-476, Paris, 1981.

Cullity,B.D., Elements of X-ray Diffraction Addison-Wesley Publishing Company, Inc., 1978.

De Garmo,E.P., "Preheat vs.low and high temperature stress-relief treatment, Ibid 31(5), Research suppl. 233s-237s, 1952.

Dixon,J.R. & Straunigan,J.S., "Effect of plastic deformation on the strain distribution around cracks in sheet materials," Jour. of Mechanical Engg. Science, V.6, No.2, p 132, 1964.

Dowling,N.E., "Fatigue failure predictions for complicated stress-strain histories," Journal of Materials, JMLSA, V.7, No.1, pp 71, March 1972.

Dowling,N.E., "Notched member fatigue life predictions combining crack initiation and crack propagation," Fatigue of Engineering Materials and Structures, V.2, pp 129-138, Pergamon press., 1979

Dugdale,D.S., "Effect of Residual Stresses on fatigue strength" Welding Research Supplement 45s to 48s, January 1959.

Elber,W., "Fatigue crack closure under cyclic tension," Engg. Fracture mechanics, pp 37-45, Vol.2, 1970.

Elber,W., "The significance of fatigue crack closure," ASTM, STP 486, Am. Soc. for testing & materials, pp 230-242, 1971.

Elber,W., "Equivalent constant-amplitude concept for crack growth under spectrum loading," Fatigue crack growth under spectrum loads, ASTM, STP 595, Am. Soc. for testing and materials, pp 236-250, 1976.

El-Haddad,M.H., Smith,K.N., & Topper,T.H., "Fatigue crack propagation of short cracks," Trans. ASME, Jour. of Engg., Mat. Tech. Vol.101, p42, 1979.

El-Haddad,M.H., Topper,T.H., Smith,I.F.C., "Fatigue life prediction of welded components based on fracture mechanics," Jour. of Test. & Eval., JTEVA, V.8, No. 6, Nov. 1980.

Faulkner,M.G. & Bellow,D.G., "Improving the fatigue life of butt-welded medium strength steels," Symposium on Application of Solid Mechanics, Univ. of Waterloo, June 26 & 27, 1972.

Forman,R.G., Kearney,V.E., & Engle,R.M., "Numerical analysis of crack propagation in cyclic loaded structures," Journal of Basic Engineering, Trans. of ASME, pp 459-464, Sept., 1967.

Frank,K.H., "The fatigue strength of fillet welded connections," Ph.D. Thesis, Lehigh University, 1979.

Fried Lima,E.Yu., "Influence of annealing on residual stresses and mechanical properties of welded joints in Magnasium alloys. MA2-1, VMD-3, Srar Prioz, No. 12, 1971.

Fuchs,H.O., "The strength of shot peened parts, design calculation, and specifications," Discussions on fatigue steels, Ist International Conf. on shot peening, pp 731-739, Paris, 1981.

Garwood,S.J., "Cumulative damage of Welded structures," Welding Institute Report# 3477/8/78, January, 1978.

Glinka,G., "Effect of residual stresses on fatigue crack growth in steel weldments under constant and variable amplitude loads," Fracture mechanics, ASTM, STP 677, pp 198-214, 1979.

Graham,J.A., Editor: Fatigue Design Handbook, SAE, Advances in Engineering, Vol.4, Chapter 3.2, 1968.

Greene,T.W. & Holzbarr,A.A., "Controlled low temperature stress relieving," The welding Journal 25(3), research supplement, 171s-185s (1946).

Gruzd,A.A., "Rilief of stresses in welded pipe joints by low temperature heat treatment. Avt. Svarka No.2, 1972.

Guerra,U., British Welding Journal V.7, p513, 1966.

Gurney,T.R., "The influence of residual stresses on the fatigue strength of plates with fillet welded attachment," British welding Journal, June,1960.

Gurney,T.R.,British Welding Research Assoc. Report # E/12A/67., March, 1968.

Gurney,T.R. & Maddox,S.J., "A reanalysis of fatigue data for welded joints in steels," Welding Research International, V.3(4), pp 1-54, 1973.

Gurney,T.R., "Some recent work relating to the influence of residual stresses on fatigue strength," Welding Inst. Conf. on "Residual Stresses in Welded Construction and Their Effects." London 15-17, pp 151-163, Nov., 1977.

Gurney,T.R., "Stress intensity factors for cracks at the toes of the transverse butt welds," Welding Inst. Report # 88/1979, May, 1979.

Gurney,T.R., Fatigue of Welded Structures , Cambridge University Press., 1979.

Hammouda,M.M., Smith,R.A., & Miller,K.J., "Elastic-Plastic fracture Mechanics for Initiation and Propagation of Notch Fatigue life," Fatigue of Engineering Materials and Structures, V.2, pp 139-154, 1979.

Hardrath,H.F. & Ohman,L., "A study of elastic and plastic stress stress concentration factor due to notches and fillets in flat plates," NACA Technical note 2566, December, 1951.

Harrison,J.D., "Further fatigue tests on fillet welded specimens subjected to prior overloading," British Welding Journal, V.12(5), pp 258-60, 1965.

Harrison,J.D., "An analysis of fatigue behaviour of crucuform joints," British Welding Inst. Report # E/21/12/68, Cambridge, England, 1968.

Harrison,J.D., "The effect of Residual stresses on fatigue behaviour," Welding Inst. monograph on "Residual stresses and their effect," pp 9-16, 1981.

Hebrant,E., Louis,H., Soete,W., and Vinokiev,A., "The relaxation of welding residual streses by static and fatigue bending" Welding Research Abroad, 58 to 63, September, 1957.

Higashida,Y., "Strain-controlled fatigue behaviour of weld metal and Heat-affected base metal in A36 and A514 steel welds," Ph.D. Thesis, Univ. of Illinois, Urbana-Champaign,1976.

Higashida,Y., Burk,J.D., Lawrence Jr.,F.V., "Strain controlled fatigue behaviour of ASTM A36 and A514 Grade F steels and 5083-0 Aluminium weld materials. Welding Journal, 57, 334s-344s, Nov., 1978.

Horger,O.J. & Neifert, H.R., "Improving fatigue resistance

by shot peening," The Timken roller bearing Company. SESA, Vol.II, No.1, p 178-90, 1944.

Horger,O.J. & Neifert, H.R., "Shot peening to improve fatigue resistance," Timken roller bearing company. Soc., of Experimental Stress Analysis, pp 1-10, 1945.

Huang, W.C., "Theoretical Study of Stress Concentration of Circular Holes and Inclusions of Strain-hardening materials," Int. Jour. Solids Structures,Vol. *(2), pp142-192, Feb., 1972.

Irwin,G.R., "Fracture testing of high strength steel materials under conditions appropriate for stress analysis," NRL Report # 5486, 1960.

Jack, A.R. & Price, A.T., "The initiation of fatigue cracks from notches in mild steel plates," International Journal of Fracture Mechanics, V.6, No. 4, pp401, 1970.

Jack, A.R. & Price, A.T., "Effect of thickness on fatigue crack initiation and growth in notched mild steel specimens", ACTA Metallurgica, V.20, pp 857, July, 1972.

James,L.A., Journal of Testing and Evaluation, V.1, No.1, ASTM, pp 52-57, 1973.

Jelm,C.R. & Herres,S.A., "Steel castings and weldments---Residual stress relief," American Foundryman 10(3), pp 37-47, Sept., 1946.

Jhansale,H.R. & Topper,T.H., "Engineering Analysis of the Inelastic stress response of a structural metal under variable cyclic strains," ASTM, STP 519, Am. Soc. for Testing & Materials, pp 246, 1973.

Kanazawa,S., Ishigaro,T.,& Mizni,M., III-W Document, X-111-575-70, 1970.

Kanazawa,T., Oba,H., & Machida, S., "Soceity of Naval Architects of Japan Journal, No. 109, pp 359-369, 1961.

Kapadia,B.M. & Imhoff,E.J., "Fatigue crack propagation in Electroslag weldments," Publ. Symposium proceedings, 10th. National Symposium on Fracture Mechanics, 1976.

Kapadia,B.M. & Imholf,E.J., "in Flaw growth and Fracture," ASTM, STP 631, pp 159-172, 1977.

Kenyon,N., Morrison,W.B., Quarrell,A.G., British Welding Journal, V.13, p 123, 1966.

Knight, J.W., "Welding Institute Research report # 8/1976/E, March,. 1976.

Klensil,M & Lukas,P Fatigue of Metallic Materials., Materials science monographs #7., Elsevier scientific publishing company, New York, 1980.

Kobayashi,H., Nakamura,H., Nakazawa,H., "Mechanics of fatigue crack growth," AMD-Vol.47, Mechasnics of fatigue, The winter annual meeting of ASME, Nov. 15-20, pp 133-150, 1981.

Landgraf,R.W., Morrow,JoDean, & Endo,T., "Determination of the cyclic stress-strain curve," Journal of Materials, JMLSA, Vol.4, No.1, pp 176, March, 1969.

Landgraf,R.W., "The resistance of metals to cyclic deformation," In achievment of high resistance in metals and alloys, ASTM STP 467, Am. soc. for testing and materials, pp 3-36, 1970.

Lawrence Jr.,F.V. & Munse,W.H., "Fatigue crack propagation in butt-welds containing joint penetration defects," Weld. Jour. V.14, pp 221s, 1973.

Lawrence Jr.,F.V., "Estimation of fatigue crack propagation life in butt-welds," Weld. Jour. V.52, pp 212s, 1973.

Lawrence Jr,F.V., Ho,N.J., & Mazumder,P.K., "Predicting the fatigue resistance of welds." Ann.Rev. Material Science, 11: 401-425. 1981.

Lawrence Jr.,F.V., Burk,J.D., & Yung,J.Y., "Influence of residual stresses on the predicted fatigue life of weldments," ASTM, STP 776, pp 33-43, 1982.

Lida,K., "Crack initiation life in low-cycle fatigue ," Dept of Naval architecture, Univ. of Tokyo, NAUT, Report # 9003, April, 1972.

Lomacky,O., Ellingwood,B., & Gifford,L.N., "Analysis of low-cycle fatigue performace of welded structural joints," Trans. 3rd. Int. Conf. on Structural Mechanics in Reactor Technology, V.5, part L, L6/6, 1975.

Maddox,S.J., "Fatigue crack propagation data obtained from parent plate, weld metal, and HAZ in structural steels," British Welding Institute Report # E/48/72 , 1972.

Maddox,S.J., "Assessing the significance of flaws in welds subject to fatigue," Welding Journal research Suppl. 53(9), p 401s, 1974.

Maddox,S.J., "An analysis of fatigue cracks in fillet welded joints," Int. Journal of Fracture Mechanics, V.11(2), pp 221-43, 1975.

Maddox,S.J., "An investigation of the influence of applied stress ratio on fatigue crack propagation on structural steels," Welding Inst. Report# 72/1978/E, pp53, Sept.,1978.

Manson,S.S., "Interpretative report on Cumulative Fatigue damage in the low-cycle range," Welding Research Suppl., pp 344s, Aug., 1964.

Manson,S.S. & Hirschberg,M.H., "in Fatigue an Interdisciplinary Approach," Syracruse University press, Syracruse, N.Y. pp 1331, 1964.

Manson,S.S., Freche,J.C., & Ensign,C.R., "Application of double linear damage rule to cumulative fatigue," Fatigue crack propagation, ASTM, STP 415, Am. Soc. for testing & materials, pp 384, 1967.

Martin,J.F., "Fatigue damage analysis of irregular shaped structures subject to representative loads," Fracture control program, Report # 10, Univ. of Illinois, Urbana-Champaign, 1973.

Mattos,R.J., "Estimation of Fatigue Crack Initiation Life in Welds Using Low-Cycle fatigue Concepts," Ph.D. Thesis, Univ. of Illinois,Urbana-Champiign, 1976.

Mattos,R.J. & Lawrence Jr.,F.V., "Estimation of fatigue crack initiation life in welds using low cycle fatigue concepts." SP-424, SAE, 1977.

McEvily,A.I., Proceedings of the first international conference on Fracture, V.II., Japanese Soc. for strength and fracture of materials, Sendai, Japan, 1965.

McEvily,A.J. & Gregor,J., "On the threshold for fatigue crack growth," Fracture, ICFA, V.2, pp 1293-1298, 1977.

McHenry,M.I., Read,D.T., & Begley,J.A., "Fracture Mechanics Analysis of pipeline girth welds in elastic-plastic fracture," ASTM, STP 668, 1979.

McKinsey,C.R., "Effect of low temperature stress relief on stress corrosion cracking, Ibid. 33(4), Research supplement 161s to 167s, 1954.

Minear,M.A., "Cumulative Damage in Fatigue," Journal of Applied Mechanics, V.12, p A159, 1945.

Morrow,JoDean., & Sinclair,G.M., Cycle dependent stress relaxation," ASTM-STP 237, Am.soc. for testing & materials, pp 83-109. 1958.

Morrow,JoDean., Ross,A.S., & Sinclair,G.M., "Relaxation of

residual stresses due to fatigue loading," "TAM Report# 568, University of Illinois, Urbana-Champaign, 1959.

Morrow, JoDean, "Internal Friction, Damping, and Cyclic Plasticity," ASTM, STP 378, Am. Soc. for Testing and Materials, pp 45-84, 1965.

Morrow,JoDean. & Socie,D.F., "The evolution of fatigue crack initiation life prediction methods," Materials, Experimentation & Design in Fatigue, Proc. of fatigue , Warwick Univ., pp 3-20, March, 1981.

Munse,W.H., Fatigue of Welded steel structures, Welding Research Council, New York, 1964.

Mura,T. & Tanaka,K., "Dislocation dipole models for fatigue crack initiation," Mechanics of fatigue, AMD-Vol.47. The Winter Annual meeting of ASME, Washington, D.C., pp 111-131, Nov. 15-20, 1981.

Nedoseka A.Ya., "Effectiveness of methods for reducing residual welding stresses," Avt. Svarka, No.3, pp 61-63, 1974.

Nelson,D.V., "Effect of Residual Stress on Fatigue Crack Propagation," ASTM STP 776, Am. Soc. for Testing and Materials, pp 172-194, 1982.

Nelson,D.V. and Socie,D.F., "Crack Initiation and Propagation Approaches to Fatigue Analysis," ASTM STP 761, Am. Soc. for Testing and Materials, pp 110-132, 1982.

Neuber,H., "Kerbspannungslehre", Sringer-Verlag, 2nd. Edition, 1958.

Neuber,H., "Theory of stress concentration for shear strained prismatic bodies with arbitrary non-linear stress-strain law," Transactoin of the Am.Soc. of Mech. Engrs., Jour. of Applied Mechanics, pp 544-550, Dec., 1961.

Neuber,H., Theory of Notch Stresses, Translated by F.A.Raven, Edwards, Ann Arbor, Michigan. ,1968.

Niku-Lari,A., "Residual stress and surface finish in shot peened components and materials," Experimental technics., The soc. of Experimental stress Analysis, pp 30-36, Feb.,1983a.

Niku-Lari,A., "Influence of residual stress introduced by shot peening upon the fatigue life of materials," Experimental Techniques, The soc. of Exp. stress Anal., March, 1983b.

Palmgren,A., "Die Lebensdauer von Kugellagern," Veyein Deutcher Ingenieure, Zeitschrift, p339, 1968.

Paris,P. & Erdogan,F., "A critical analysis of crack propagation laws," Journal of basic Engg., Trans. of ASME, p 528-534, December, 1963.

Parker,E.R., "Stress-relieving of weldments," Supplement to the Welding Journal, Welding Research Supplement, pp 433s-440s, Octoder, 1957.

Parlane,A.J.A., "Origin and nature of residual stresses in welded joints," Monogram "Residual stresses and their effect," The welding Institute, pp 1-4, 1981.

Parry,M., Norderg, H., Hertzberg,R.W., "Fatigue crack propagation in ASTM Base plate and welded joints," Weld. Jour. V.51, pp 485s, 1972a.

Parry,M., Nordberg,H., Hertzberg,R.W., "Welding Journal, pp 485-490, Oct., 1972b.

Pelloux,R.M., Review of theories and laws of fatigue crack propagation," Proc. of the Airforce Conf. on Fatigue and fracture of Aircraft structures & materials, AFFDL TR 70-144, pp 409-416, 1970.

Peterson,R.E., "Notch sensitivity," Metal fatigue, Chapter 13, Sines,G. and Waisman,J.L. edited , McGraw-Hill Book Company Ltd., pp 293-306.,1959

Peterson,R.E., Stress Concentration Factors, Wiley & Sons, Inc., New York, 1974.

Pollard,B. & Cover,R.J., "Fatigue of steel weldments," Welding Journal, V.51, pp 544s, 1972.

Polmear,I.J., "Effect of peening on the fatigue performance of Aluminium alloy fillet welds" AWRA report # P3-18-79. Australian Welding Research, V.8, pp 28-32, Feb.,1980.

Puchner, O. "Fatigue strength calculation of weldments with residual stress considered," Welding Research Institute, Czechoslovia, Slovak Technical Univ.,Bratislava, 1963.

Raske,D.T. & Morrow,JoDean., "Mechanics of materials of low-cycle fatigue testing," ASTM, STP 465, American Soc. for Testing & Materials, 1969.

Redner,S., "Measurement of residual stresses by blind-hole drilling method, ---- principle and application," Photoelastic Inc., Bulletin TDG-5, May, 1971. Book Company Inc., 1963.

Reemsnyder,H.S., "Evaluating the effect of residual stresses on notched fatigue resistance," Materials. experimentations and design in fatigue, Proc. of Fatigue, pp 273-295, 1981.

Rolfe,S.T. & Barsom,J.M., "Fracture and fatigue control in structures," Applications of fracture mechanics, Prentice Hall, N.J., p224, 1977.

Rosenthal,D. & Norton,J.T., "A method of measuring triaxial residual stresses in plates," Journal of American welding society, Welding suppl., V.24, pp295-307, 1945.

Ross, M. "Experiments for the determination of the influence of residual stresses on the fatigue strength of structures," Welding Research BWRA, 4(5), 83r to 93r, October, 1950.

Sanders Jr.,W.W., British Welding Council Bulletin # 171, April, 1972.

Signes,E.G., Baker,R.G., Harrison,J.D., & Buedckiw,F.M., "Factor affecting the fatigue strength of welded high strength steels," British weld.Jour. V.14, pp 108, 1967.

Smith,K.N., El-Haddad,M., & Martin,J.F., "Fatigue life and crack propagation analysis of welded components containing residual stresses," Jour. Mat. & Eval., V.5, No. 4, pp 327, 1977.

Socie,D.F., "Estimating fatigue crack initiation and propagation lives in notched plates under variable loading histories," TAM Report# 417, Univ. of Illinois at Urbana-Champaign, 1975.

Socie,D.F., "Non-arbitrary crack initiation length," Paper presented at SAE fatigue design and evaluation committee meeting, April,1977.

Sproull, X-rays in Practice, Mcgraw-Hill Book Company., NewYork, 1946.

Stadnick,S.J. & Morrow,JoDean., "Techniques for smooth specimen simulation of the fatigue behaviour of notched members," in "Testing for prediction of material performance in structures and components," ASTM, STP 515, Am.Soc. for testing & materials, pp 229-252, 1972.

Stowell,E.Z., "Stress ans strain concentration at a circular hole in an infinite plate," NACA Technical note 1073, April, 1950.

Stowell,E.Z., "The calculation of fatigue life in the presence of stress concentrations", Nucl. Engg. Design,

8, pp 313-316, 1968.

Tall,L., "Residual Stresses in Welded plates-a theoretical study," Welding Research Supplement, pp 10s-23s, January, 1964.

Tanaka,K., Nakai,Y., and Yamashita,M., "Fatigue growth threshold of small cracks," Int. Jour. of Fracture, Vol. 17, 1981.

Thang,B.Q., Dubac,J., Bazergin,A., & Biron,A., "Cumulative fatigue damage under under strain controlled conditions," Journal of Materials, JMLSA, vol.6, No.3, pp 718, Sept., 1971.

Throop,J.F. & Miller,G.A., "Optimum fatigue crack resistance," Achievment of high fatigue resistance in metals and alloys, ASTM, STP 467, p 154, 1970.

Throop,J.F., "Fracture mechanics analysis of the effects of residual stress on fatigue life," Journal of testing and evaluation, JTEVA, V.11, No.1, pp 75-78, Jan.,1983.

Topper,T.H., Wetzel,R.M., & Morrow,JoDean, "Neuber's Rule applied to fatigue of Notched specimens," Journal of Materials, Vol.1,(4), pp 200-209, March 1969.

Topper,T.H. & Conle,A., "An approach to the analysis of the non-linear deformation and fatigue response of components subjected to complex service load histories," Proc. Int. Symp. of Experimental mechanics, Univ. of Waterloo.,p419-442, June, 1972.

Vinokurov,V.A., "Stress relaxation and recovery of plasticity of metal in high temperature tempering of welded structures," Int. Symposium, Heat treatment of welded steel structures, Leningrad, Mashgiz, 1967.

Weck,R., "Residual stress due to welding," Symposium on Internal stresses in metals and alloys. Inst. Metals.,pp 119-129, 1947.

Wetzel,R.M., "Smooth specimen simulation of the fatigue behaviour of notches," Journal of Materials, Vol.3, pp 646-657, 1968.

Zettlemoyer,N., "Stress concentration and fatigue of welded details," Ph.D. Thesis, Lehigh University, 1976.

7. APPENDIX A

7.1 Introduction: Calibration Of X-ray Diffraction Stress Measurements

To calibrate the measurement of residual stresses by X-ray diffraction techniques a semi-destructive (blind-hole drilling) and a destructive method (sectioning) were used. X-ray diffraction was calibrated using strain gauges and an extensometer.

The X-ray diffraction technique has two advantages: first, it is non-destructive and secondly, the measurement need not be in a reference condition of zero-stress (measurements on un-stressesd metal) which allows one to measure the applied stress, the residual stress or the combined effect of both. The method is based on the principle that changes in atomic spacing in a metal are proportional to applied loads. The X-ray method, other techniques and its calibration for measuring residual stresses are discussed in the following sections.

7.1.1 Calibration Of X-ray Stress Measurements

The experimental results obtained from various measurement techniques are plotted in Fig. A.6 and showed a good correlation between X-ray diffraction and other measuring techniques. The measurements of stress by X-ray diffraction at a very low stress range was not very accurate because of the small difference in "Debye-Scherrer" ring

diameter. The central hole drilling technique was assumed to be an accurate method of surface stress measuring technique. In comparison to the blind-hole drilling, the X-ray technique gave good results (variation of 5%-11%) as shown in Fig. A.6. The slight variation from different methods could result because of the misalignment of the point of irradiation in determining the film to specimen distance for X-ray stress measurements and measurements in the difference in "Debye-Schrrer" ring diameter or due to the selective action of the X-rays.

7.1.2 Measurements Of Stresses In Steel Parts By X-ray Diffraction

To measure the distribution of residual stress present in the Columbium-50 steel transverse butt-welded specimens a flat camera "Kristalloflex-2" (Siemens Ltd.) X-ray diffraction unit with AgCr3ö tube was used. Although many techniques of X-ray diffraction are available the technique used in this study was the double-exposure "Thomas method B" for its known better accuracy. Vanadium filtered chromium Kα radiation (35 KV, 18 ma) diffracted from the {211} crystallographic planes provided the sharp deflection lines on the photographic film. The developed negatives were then scanned with the microdensitometer (Joyce, Loebel & Co.) for the "Debye-Scherrer" ring diameters.

"Thomas method B" (Sproull 1946, Cullity 1978) requires two exposures at the same point "O" with different known

camera inclinations α_1 and α_2 to the normal "ON" as shown in Fig. A.1.

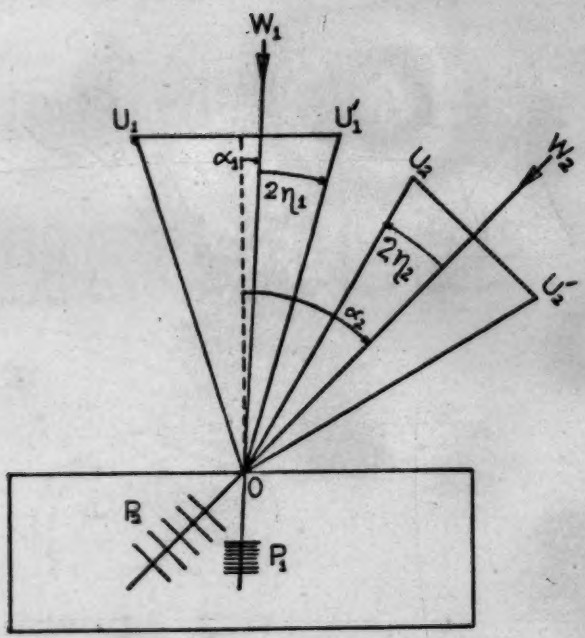

Figure A.1 "Thomas method B" X-ray diffraction stress measurements

If η_1 and η_2 are small angles the spacing computed from the diameter U_1U_1' may be taken as representative of the {211} planes for chromium radiation, planes P_1 normal to the primary beam W_1O and the spacing computed from the ring diameter U_2U_2' as representative of the same set of P_2 normal to the primary beam W_2O. Applying stress-strain relation and using elastic theory (Sproull 1946) the residual stress σ_r can be calculated from:

$$\sigma_r = \frac{E\,(U_1 - U_2)\,\tan\eta\,\mathrm{Cos}^2\,2\eta}{4D\,(1+\gamma)\,(\mathrm{Sin}^2\alpha_2 - \mathrm{Sin}^2\alpha_1)}$$

where

σ_r = stress at target location,

E = modulus of elasticity for steel,

γ = Poisson's ratio, 0.28 for steel,

η = 90° - Bragg's angle = 11.8025 degrees for Chromium radiation on steel,

D = film to specimen distance,

α_1 = normal exposure angle, 0 degree,

α_2 = inclined exposure angle, 45 degrees,

U_1 = stress ring diameter on normal exposure,

U_2 = stress ring diameter on inclined exposure.

Butt-welded specimens made from Columbium-50 steel were polished in areas close to the toe of the welds with 400/600 micron emery paper to remove any adhering tinder. It was then treated with 35 percent hydrochloric acid and greased lightly for preventing renewed oxidation. Calibration powders (Iron, Silver and Gold) were used with vaseline as a

thin coat on the specimen for determining the film to specimen distance, the film centroid and to compare the intensity of the diffraction lines. The true σ_r was calculated from the following relationship:

True stress = Indicated stress X (Measured distance)/Actual film to specimen distance.

$$D_{true} = D_{cal}/2 \tan\eta$$

where

D_{true} = the actual film to specimen distance,

D_{cal} = calibration ring diameter.

7.1.3 Measurements Of Residual Stresses By The Blind-Hole Drilling Technique

Residual stresses near the weld toe and on the surface of the specimens were also measured by the blind-hole drilling technique and used to compare with the X-ray diffraction measurement. A 45° rectangular strain rosette (Micro-measurement type EAXX-062RE (Fig.A.2)) was applied to the surface on which the residual stresses were to be measured. A small hole was drilled (0.0673 in dia., 1.71mm) at the rosette centre. This drilling relaxed the radial stresses at the edge of the hole and caused a local redistribution of the stresses. The resulting strain changes were detected by the gauges. These strain changes could be related to residual stresses in the material by an equation which was developed by Beaney & Procter (1974).

$$\sigma_{1,2} = -(E/2K_1)\left[\frac{\epsilon_1+\epsilon_3}{1-\gamma K_2/K_1} \pm \frac{1}{1+\gamma K_2/K_1}\sqrt{(\epsilon_1-\epsilon_3)^2+(2\epsilon_2-\epsilon_1-\epsilon_3)^2}\right]$$

and

$$\alpha = -(1/2)\tan^{-1}\left[\frac{\epsilon_1-2\epsilon_2+\epsilon_3}{\epsilon_1-\epsilon_3}\right]$$

where

$\sigma_{1,2}$ = principal stresses,

K_1, K_2 = constants,

E = Young's Modulus,

$\epsilon_1, \epsilon_2, \epsilon_3$ = relaxed strains,

γ = Poisson's ratio,

α = angle between gauge 1 and principle stress direction.

$1/K_1$ and $\gamma K_2/K_1$ can be found by measuring the relaxed strain in any known stress field.

Bathgate (1974) showed there was a good correlation between conventional gauges and hole drilling using milling cutters and standard loading equipment. Other researchers have also shown good results using an air-abrasion technique to drill the hole. But for this study a standard milling machine was used to drill the holes. To correct any error due to milling, one gauge was first applied to a specimen of known stress (annealed specimen) a hole drilled and relaxed strains recorded. This gave the stress due to the milling operation. Other gauges were then used to measure the stresses near the weld toe and at various points on the specimen and which were then corrected by the amount found from the first test.

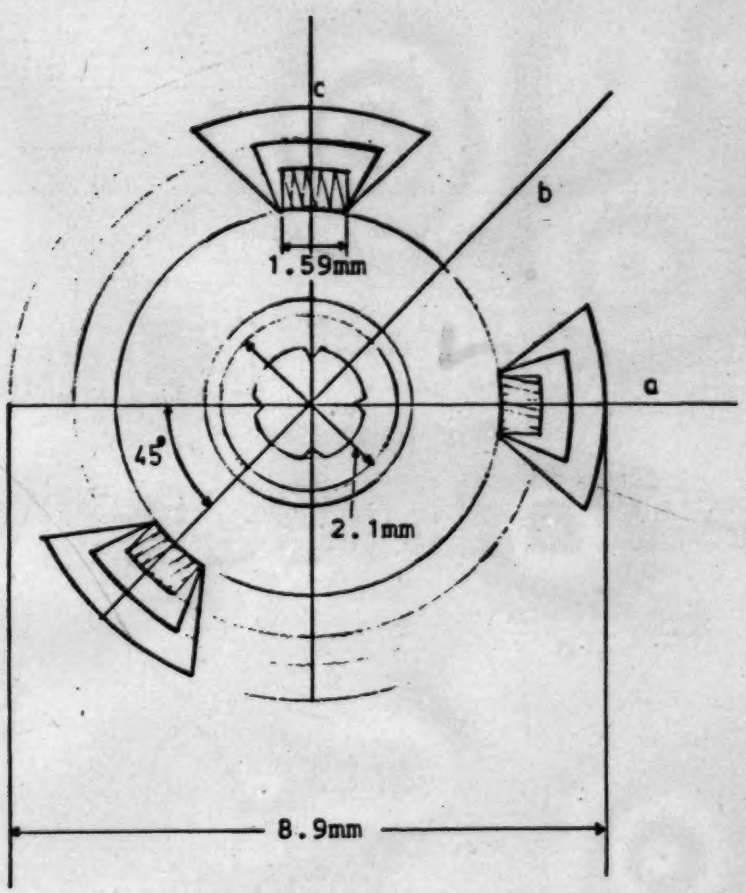

Figure A.2 Rectangular rosette for residual stress measurement (Micromeasurement type EAXX-062RE).

7.1.4 Stress Measurements By Sectioning

Residual stress measurements were made both on annealed and cold-rolled Columbium-50 steel base material by the sectioning method. Strain gauges were attached to the lower and upper surfaces of the cold-rolled flat plate specimen as shown in Fig. A.3a. Before sectioning initial strain readings were taken from the gauges. Following this, the bar was sawn across 1/2 inch (12.7 mm) away from the centre of the strain gauge grid and the length of the bar not supporting the gauge was discarded. The strain gauge readings were recorded. The gauge bearing block was removed from the bar as shown in Fig. A.3b and the thickness of the block was measured. Metal was then progressively removed from the inner block faces by careful milling and filing where necessary. This was done in small increments to avoid plastic bending of the remaining shim. Using a high speed cutting saw (112 teeth per inch, 4.5 teeth/mm) and a cutting speed of 175 ft/min (52.5 m/min) gave consistent strain readings. At each stage thickness and strain measurements were made.

This modified sectioning method of Rosenthal and Norton (1945) requires three sets of data to predict the complete residual stress pattern through the specimen thickness. The first was the change in gauge readings when the first and second cuts were made across the specimen on either side of the gauges. The second was the strain changes after making the longitudinal slit in the middle. The third was a plot of

strain changes versus shim thickness as the blocks were milled out to become thin shims.

For the second case of annealed specimens three strain gauges were mounted on the surface of the specimen and the first cut was made one inch (25.4mm) away from the gauges whereas the second and third cut were made 0.25 inch (6.35mm) away from the gauges (Fig. A.4). The changes in the strain readings were noted. Before the sectioning X-ray diffraction stress measurements were taken close to the strain gauges.

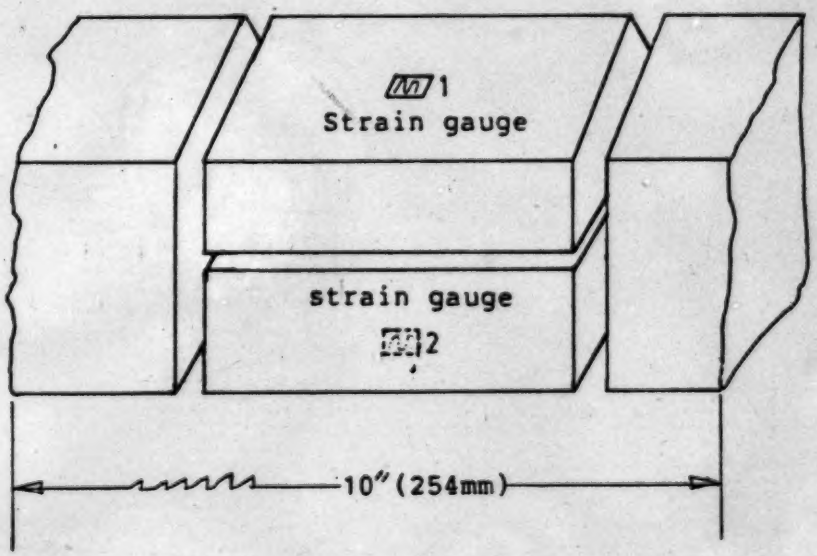

Figure A.3a Sectioned by sawing

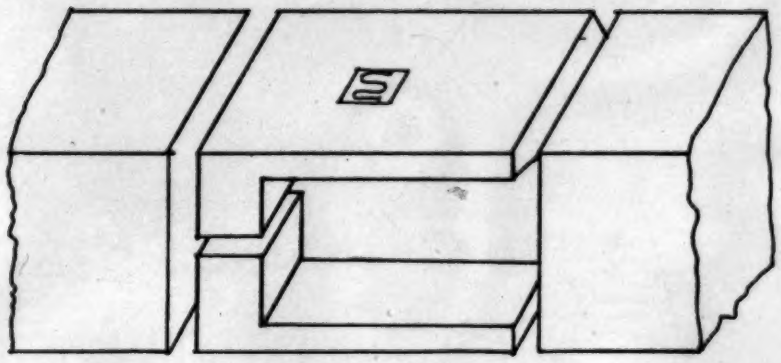

Figure A.3b Side view of base metal specimen showing sectioning method.

1, 2,3Strain gauges,G.F=2.08, Resistance=120Ω

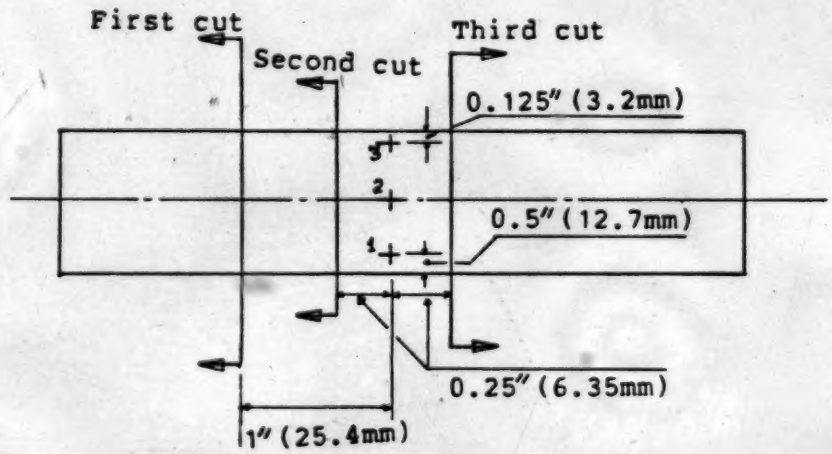

Figure A.4 Sectioning of annealed specimen.

7.1.5 Stress Measurements By A Strain Gauging

Calibration of X-ray stress measurements using a single strain gauge and a longitudinal bar of Columbium-50 steel are shown in Fig.A.5. The longitudinal bar was annealed for stress relaxation. It was sanded and cleaned with 35% HCl. A strain gauge was mounted after the surface preparation. Tensile forces were applied to the bar by a screw arrangement and strain gauge readings and X-ray stress measurements were taken.

It was assumed that the depth of penetration of X-rays was of order 0.001in (0.0254 mm), the stress was uniaxial and parallel to the longitudinal axis of the bar and was in pure tension. The stress along the thickness was zero as the stress is measured only on the top surface.

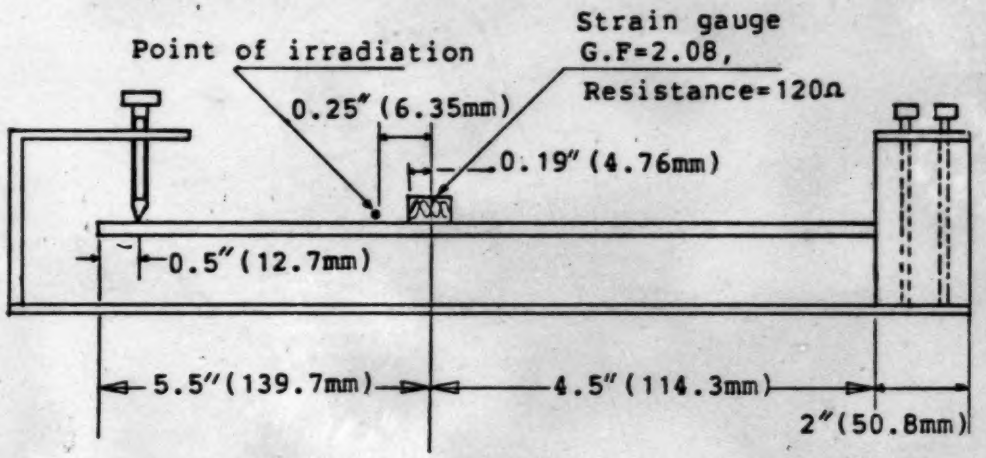

Figure A.5 Strain gauge and X-ray stress measurements.

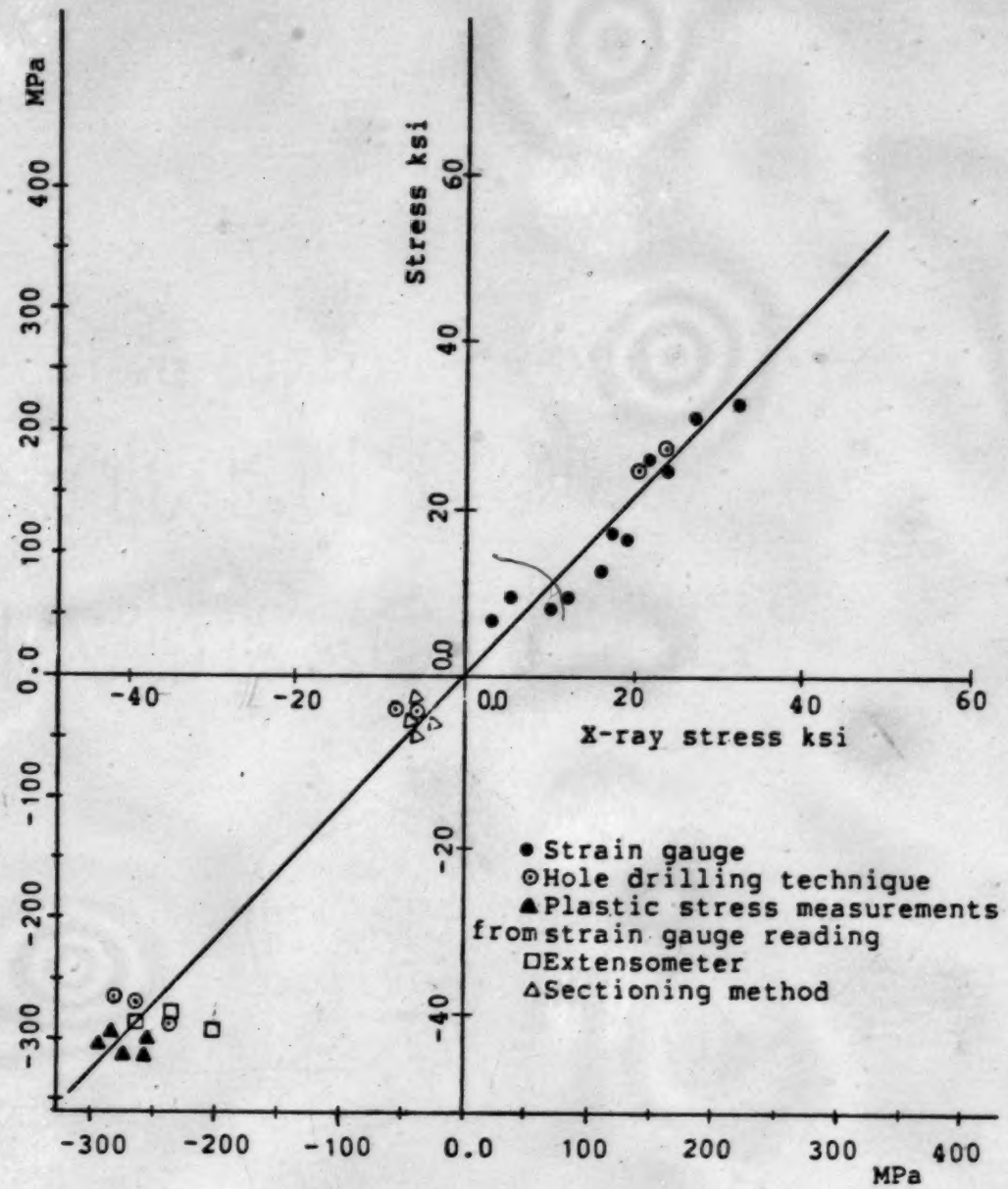

Figure A.6 Calibration of X-ray stress measurements vs. other methods.

7.1.6 Plastic Strain Measurements By Strain Gauging

The annealed specimens with two strain gauges mounted on the top and bottom surfaces were loaded slowly in the Instron testing machine and yielded to the plastic ranges of the material and then unloaded. Stress readings were taken by X-ray diffraction near the strain gauges of the specimen before gripping the specimen in the testing machine. Initial strain readings were also taken after gripping the specimen. After unloading X-ray stress measurements and strain gauge readings were noted. There was, however, no control on the amount of plastic strain after the yielding of the material.

7.1.7 Plastic Strain Measurements Using An Extensometer

The extensometer method in combination with hole-drilling method was used to calibrate the X-ray diffraction stress measurements. Base material specimens were loaded beyond the elastic limit and strains were measured using a one inch (25.4 mm) extensometer. From load and strain measurements and using stress-strain relationships in the plastic range (i.e., $\epsilon=(\sigma/E)+(\sigma/K)^{1/n}$) the amount of induced plastic stress was obtained. Later on, a special purpose 45° rectangular rosette was mounted on the yielded specimen and a hole was drilled at small increaments and the stress relaxion was noted. X-ray diffraction stress measurements were also taken before and after the yielding of the specimen.

8. APPENDIX B

8.1 Cyclic Hardening And Softening Behaviour Of Constant Strain Amplitude Tests

The laboratory results of cyclic hardening and softening behaviour of Columbium-50 steel base material are discussed in this section. It was observed experimentally that for fatigue cycles ($>10^5$) hardening and softening effects can usually be ignored and a generally stabilized condition may be assumed.

Figure B.1 indicates the variation of stress amplitudes for Columbium-50 steel during completely reversed constant-strain cycling for strain amplitudes of 0.001 and 0.0015 to 0.0070. The material cyclically softened for the lower strain amplitudes. Cyclic softening causes a decrease in stress amplitude or an increase in plastic strain amplitude with reversals. For higher strain amplitudes the material cyclically hardened. This caused an increase in stress amplitude or a decrease in plastic strain amplitude with reversals. While experiments could not be performed at very high strain amplitudes because of the limitations of specimen size, Fig. B.1 indicates that Columbium-50 steel has a tendency for both cyclically softening and cyclically hardening depending on strain amplitudes.

This was observed by Manson & Hirschberg (1964) in that cyclic hardening or softening depends on the ratio of static ultimate strength to 0.2% offset yield strength. When the above ratio is greater than 1.4 the material will usually harden and if it is less than 1.2 softening generally occurs.

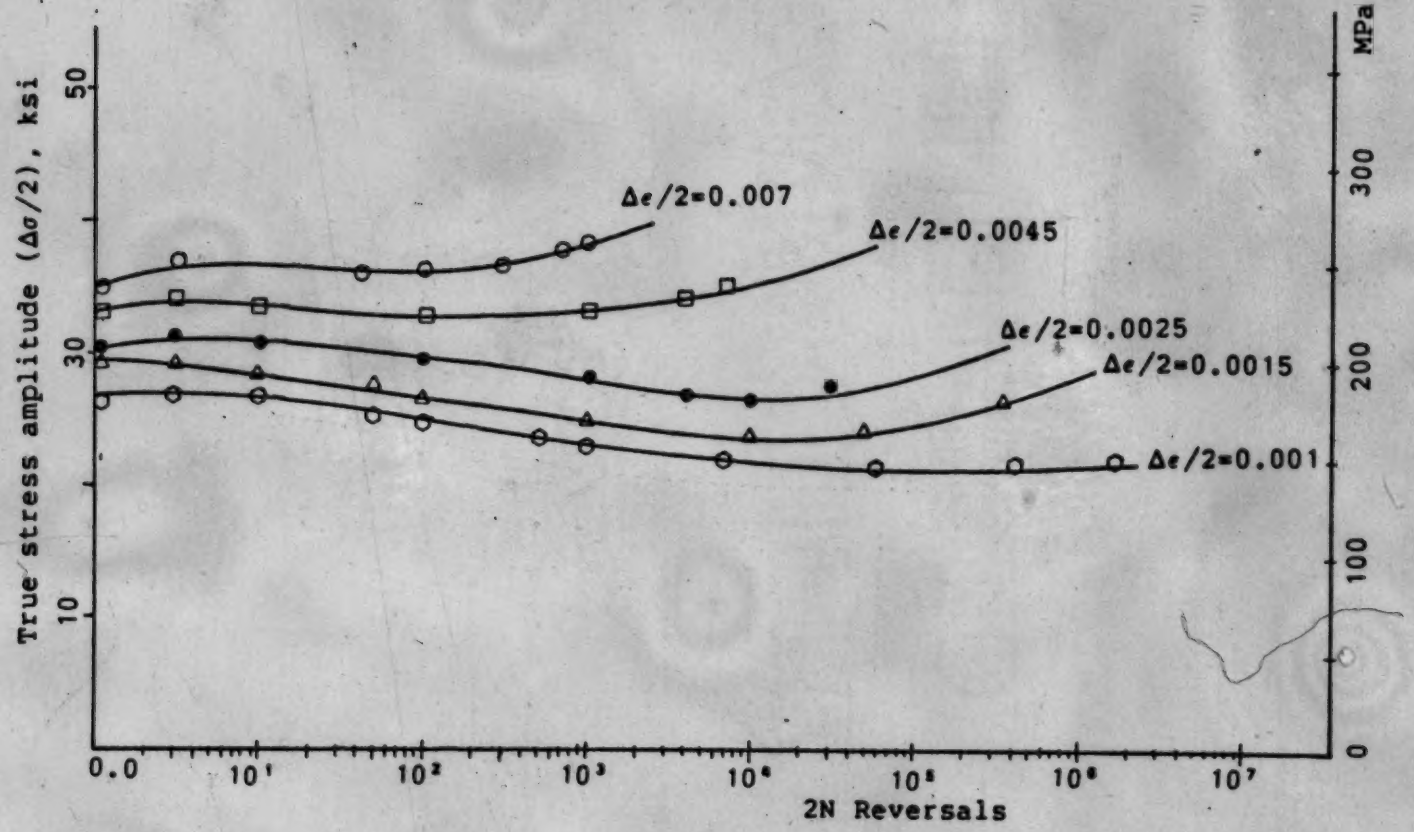

Figure B.1 Cyclic hardening & softening behaviour for constant amplitude and fully reversed strain-controlled tests on Columbium-50 smooth specimen.

9. APPENDIX C

9.1 Cyclic Stress-Strain Properties From Micro-Hardness Measurements

The cyclic and fatigue properties of the weld metal and the HAZ metal are estimated from empirical relationships and microhardness readings (Chang & Lawrence 1981, Morrow 1965, Landgraf 1970, Graham 1968). There was good agreement when the Columbim-50 base material properties were correlated with the empirical formulas.

The relationship showing the fatigue strength coefficient (σ'_f), fatigue strength exponent (b), cyclic yield strength ($\sigma'_{y,s}$) and transient fatigue life ($2N_{t,r}$) with hardness readings are shown in the following equations (Chang & Lawrence 1981):

$$\sigma'_f \cong (BHN/2)+50 \qquad (C.1),$$

$$b = -(1/6)\ \log[2(BHN+100)/BHN] \qquad (C.2),$$

$$\sigma'_{y,s} = (-21.5 + 0.331\ BHN) \qquad (C.3),$$

$$Log2N_{t,r} = (0.000633\ BHN + 5.463) \qquad (C.4).$$

The cyclic strength coefficient (K′) and cyclic strain hardening exponent (n′) can be approximated as (Morrow 1965):

$$K' = \sigma'_f\ /\ (\epsilon'_f)^{n'} \qquad (C.5),$$

$$n' = b/c \qquad (C.6).$$

A relationship showing the fatigue strength exponent (b) and fatigue ductility exponent (ϵ_f') can be obtained (Landgraf 1970, Graham 1968) as follows:

$$b = n' / (1+5\, n') \qquad \text{(C.7)},$$

$$\epsilon_f' = 0.002\, [\sigma_f' / \sigma_{y,}']^{1/n'} \qquad \text{(C.8)}.$$

10. APPENDIX D

10.1 Tables Of Experimental Data

This section contains experimental data obtained from the tests that were used in the theoretical calculation of crack initiation and crack propagation lives of transverse butt-welded joints of Columbium-50 steel. The data related to mean stress relaxation tests, cyclic hardening and softening behaviour, the welding parameters, percentage improvements in fatigue strength versus induced stress and material properties are also shown in the tables that follows.

Table 5.

Test data for mean stress relaxation tests
(Constant strain amplitude but variable mean strain)

N cycles	ϵ_m = 0.002 , $\Delta\epsilon/2$ = ±0.001			ϵ_m = 0.003 , $\Delta\epsilon/2$ = ±0.001			ϵ_m = 0.004 , $\Delta\epsilon/2$ = ±0.001		
	Smax ksi(MPa)	Smin ksi(MPa)	Mean Stress ksi(MPa)	Smax ksi(MPa)	Smin ksi(MPa)	Mean Stress ksi(MPa)	Smax ksi(MPa)	Smin ksi(MPa)	Mean Stress ksi(MPa)
2	42.4 (292.35)	-32.54 (-224.36)	4.93 (33.99)	46.21 (318.62)	-32.46 (-223.82)	6.87 47.37)	48.85 (336.82)	-32.94 (-227.12)	7.95 (54.81)
3	41.9 (288.90)	-32.24 (-222.29)	4.85 (33.44)	45.78 (315.65)	-33.15 (-228.57)	6.31 (43.51)	48.23 (332.54)	-33.5 (-230.98)	7.37 (50.82)
10	40.53 (279.45)	-32.47 (-223.88)	4.03 (27.74)	43.06 (296.89)	-31.41 (-216.57)	5.83 (40.19)	46.16 (318.27)	-33.05 (-227.88)	6.55 45.16)
20	39.36 (271.38)	-31.64 (-218.16)	3.86 26.61)	41.07 (283.17)	-31.04 (-214.02)	5.01 34.54)	44.91 (309.65)	-33.08 (-227.88)	5.91 (40.75)
50	38.28 (263.94)	-31.57 (-217.61)	3.36 (23.17)	38.48 (265.32)	-30.68 (-211.53)	3.87 (26.68)	41.05 (283.05)	-31.31 (-215.88)	4.87 (33.58)
70	38.03 (262.22)	-31.91 (-220.02)	3.06 (21.09)	38.15 (263.04)	-31.12 (-214.57)	3.52 (24.27)	39.05 (269.25)	-31.10 (-214.43)	3.97 (27.37)
100	37.82 (260.77)	-32.07 (-221.12)	2.87 (19.79)	38.05 (262.35)	-31.42 (-(216.64)	3.32 (22.89)	38.21 ((263.46)	-31.77 (-219.05)	3.22 (22.20)
200	36.83 (253.94)	-32.80 (-226.15)	2.01 (13.86)	37.80 (260.63)	-32.05 (-220.98)	2.87 (19.79)	36.36 (250.70)	-30.45 (-209.95)	2.96 (20.41)
400	36.00 (248.22)	-32.08 (-221.19)	1.96 (13.52)	36.03 (248.43)	-31.72 (-218.71)	2.15 (14.82)	36.01 (248.28)	-31.68 (-218.43)	2.16 (14.89)
1000	35.91 (247.59)	-32.19 (-221.95)	1.86 (12.83)	34.94 (240.91)	-30.86 (-212.78)	2.03 (13.99)	35.15 (242.36)	-31.13 (-214.64)	2.01 (13.86)
3000	34.23 (236.01)	-31.16 (-214.84)	1.54 (10.62)	33.78 (232.91)	-29.87 (-205.95)	1.96 (13.51)	35.01 (241.39)	-31.26 (-215.54)	1.87 (12.89)
5000	33.92 (233.88)	-31.22 (-215.26)	1.35 (9.31)	33.82 (233.18)	-30.75 (-212.02)	1.53 (10.55)	34.99 (241.25)	-31.16 (-214.84)	1.92 (13.24)
10000	33.41 (230.36)	-31.37 (-216.29)	1.02 (7.03)	33.40 (230.29)	-30.36 (-209.93)	1.52 (10.48)	34.08 (234.98)	-30.34 (-209.19)	1.87 (12.89)

Table 6.

Test data for mean stress relaxation tests
Constant mean strain but variable strain amplitudes
(Using method of stabilization blocks.)

N cycles	$\epsilon_m = 0.003$, $\Delta\epsilon/2 = \pm 0.00875$			$\epsilon_m = 0.003$, $\Delta\epsilon/2 = \pm 0.002$			$\epsilon_m = 0.003$, $\Delta\epsilon/2 = \pm 0.003$		
	Smax ksi(MPa)	Smin ksi(MPa)	Mean Stress ksi(MPa)	Smax ksi(MPa)	Smin ksi(MPa)	Mean Stress ksi(MPa)	Smax ksi(MPa)	Smin ksi(MPa)	Mean Stress ksi(MPa)
1	44.46 (306.55)	-24.20 (-166.86)	10.23 (70.54)	47.02 324.20	-35.30 -243.39)	5.86 (40.40)	48.62 (335.23)	-42.1 (-290.27)	3.26 (22.47)
2	44.06 (303.80)	-23.79 (-164.03)	10.13 (69.85)	46.34 (319.51)	-34.99 (-241.25)	5.67 (39.09)	47.93 (330.47)	-41.68 (-287.38)	3.12 (21.51)
5	45.26 (312.07)	-26.23 (-180.85)	9.52 (65.64)	47.19 (325.40)	-38.68 (-266.69)	4.26 (29.27)	48.35 (333.37)	-44.31 (-305.51)	2.02 (13.93)
10	45.22 (311.79)	-29.09 (-200.57)	8.06 (55.57)	46.03 (317.38)	-38.11 (-262.77)	3.96 (27.30)	48.14 (331.92)	-44.15 (-304.41)	1.99 (13.72)
20	43.71 (301.38)	-29.19 (-201.26)	7.26 (50.06)	44.37 (305.93)	-39.34 (-271.25)	2.52 (17.37)	47.22 (325.58)	-43.65 (-300.96)	1.78 (12.27)
50	41.87 (288.69)	-29.75 (-205.13)	6.06 (41.78)	43.06 (296.89)	-39.13 (-269.80)	1.96 (13.51)	46.01 (317.24)	-43.98 (-303.24)	1.01 (6.96)
100	41.05 (283.04)	-29.29 (-201.95)	5.87 (40.47)	42.00 (289.59)	-39.14 (-269.89)	1.44 (9.93)	45.87 (316.39)	-43.87 (-302.48)	1.00 (6.89)
300	39.05 (269.25)	-28.78 (-198.44)	5.13 (35.37)	41.66 (287.24)	-39.13 (-269.80)	1.26 (9.69)	43.96 (303.95)	-41.99 (-289.52)	0.98 (6.75)
500	38.14 (262.97)	-28.11 (-193.82)	5.01 (34.54)	40.36 (278.28)	-38.15 (-263.04)	1.10 (7.58)	43.35 (303.10)	-41.39 (-285.38)	0.98 (6.75)
1000	36.96 (254.83)	-26.96 (-185.88)	5.00 (34.48)	39.46 (272.07)	-37.44 (-258.15)	1.00 (6.90)	42.16 (290.69)	-40.18 (-277.04)	0.99 (6.83)
2000	35.77 (246.63)	-25.82 (-178.03)	4.97 (31.27)	37.96 (261.73)	-35.99 (-248.15)	0.98 (6.75)	42.02 (289.73)	-40.06 (-276.21)	0.98 (6.75)
5000	34.05 (234.77)	-25.32 (-174.58)	4.37 (30.13)	------	-------	----	-----	------	----

*: Value of Mean Stress at cycle 1 is the initial Mean stress.

Table 7.
Cyclic hardening and softening behaviour for constant amplitude fully -reversed strain-controlled tests on the base metal of Columbium-50 steel.

Total Strain Amplitude $\Delta\epsilon/2$	Total Stress Amplitude $\Delta\sigma/2$	2N Reversals.
0.001	26.4(182.0)	2
	27.0(186.1)	4
	26.5(182.7)	10
	25.2(173.7)	50
	25.0(172.3)	100
	23.9(164.8)	500
	23.0(158.6)	1000
	22.1(152.4)	7000
	22.0(151.7)	10000
	21.2(146.2)	15000
	21.0(144.8)	30000
0.0015	29.5(203.4)	2
	29.4(202.7)	4
	28.4(195.8)	10
	27.0(186.2)	100
	25.1(173.1)	1000
	23.6(162.7)	10000
	24.2(166.9)	50000
	24.5(169.0)	90000
	26.5(182.7)	205604
0.0025	30.5(210.3)	2
	31.0(213.8)	4
	30.8(212.4)	10
	29.8(205.5)	100
	28.0(193.1)	1000
	27.2(187.5)	4000
	26.4(182.0)	10000
	27.0(186.7)	30000
0.0045	33.2(228.9)	2
	34.0(234.4)	4
	33.5(231.0)	10
	33.2(228.9)	100
	33.0(227.5)	1000
	34.5(237.9)	4000
	35.8(246.8)	10000
0.007	34.2(235.8)	2
	37.2(256.5)	4
	36.2(249.6)	10
	36.0(248.2)	100
	37.0(255.1)	300
	38.0(262.0)	700
	38.5(265.5)	1200

Table 8.

(i)Improvement in fatigue strength vs. amount of induced stress
(ii)Induced stress vs. depth of work-hardening & Almen strip intensity.

Type of Treatment	Fatigue Strength ksi(MPa)	Induced Stress ksi(MPa)	Difference in Induced stres ksi(MPa)	%Improvement in Fatigue strength	Depth of Work-hardening in(mm)	Almen "N" strip Intensity
Untreated butt-weld	21(145)	22(152)	0.0	0.0	0.001(0.025)	----
Annealed	24(166)	0.0	22(152)	14.3	--------	-----
Tensile Preloaded	24.5(167)	-7(-48)	29(200)	16.7	-------	-----
Glass shot Peened	29(200)	-9(-62)	31(214)	38.1	0.008(.203)	0.0132N
Steel shot Peened	35.5(245.0)	-16(-110)	38(262)	69	0.017(.432)	0.0215N
Single pt. Hammer peened.	36.5(252.0)	-22(-152.0)	44(303)	73.8	0.0297(.756)	0.0495N
Multiple pt. Hammer peening	38(262)	-25(-172)	47(324)	81	0.027(.691)	0.033N
Stress Peening	40.5(279)	-25(172)	47(324)	93	0.0281(.713)	0.033N

Table 9.

Theoretical stress concentration factor, K_t and fatigue Notch factor, K_f as a function of weld toe-root radius., r.

ϕ = Edge preparation angle=90 degree.
θ = Flank angle =45 degree.
t = Specimen thickness=0.25in(6.35mm).

Root radius, r, in(mm)	K_t	K_f
0.00001(0.000254)	43.69	2.037
0.00005(0.00127)	20.09	2.006
0.00009(0.00229)	15.23	1.988
0.0001(0.0254)	14.50	1.904
0.0005(0.0127)	7.04	1.857
0.0009(0.0229)	5.5	1.859
0.001(0.0254)	5.269	1.851
0.003(0.0762)	3.464	1.7424
0.01(0.254)	2.35	1.595
0.025(0.635)	1.85	1.47
0.05(1.27)	1.60	1.383
0.1(2.54)	1.42	1.30

Table 10

Peterson's ρ^* value and assumed crack growth rate constants for materials at the crack initiation site.

Material at initiation site.	Su, ksi(MPa)	ρ^* in(mm)	C, in/cycle(mm/cycle)	m	K., ksi$\sqrt{in}$(MN/$m^{3/2}$)
Columbium-50	64(441)	0.01613(0.410)	1.018×10^{-10} (2.586×10^{-9})	3.0	45(49.5)
Weld material	98(676)	0.0075(0.190)	1.018×10^{-8} (2.586×10^{-7})	3.3	45(49.5)
HAZ material	98(676)	0.0075(0.190)	1.018×10^{-8} (2.586×10^{-7})	3.3	45(49.5)
"Adjusted" material	81(558)	0.01056(0.268)	1.018×10^{-9} (2.586×10^{-8})	3.15	45(49.5)

Table 11.

Chemical composition of the base metal and welding electrodes.

Material	%C	%Mn	%P	%S	%Si	%Columbium
Columbium-50 Steel	0.20	1.20	0.04	0.05	---	0.005
Oxweld # 36, Rod	0.14	2.00	0.017	0.024	0.050	-----

Welding Parameters

1. Welding Process--- Automatic submerged arc welding, double side using flux back-up.
2. Number of welding wires--- two, tandem.
3. Welding wire--- Linde, Oxweld #36, 1/8inch (3.18mm) diameter.
4. Flux--- Linde, Oxweld 585
5. Tip height--- 7/8 inch (22.3 mm) from work piece.
6. Distance between electrodes--- 5/16 inch (8 mm).
7. Speed--- 56 inch/minute (1.42 m/minute)